MODELING AND ROBUST CONTROL OF LARGE FLEXIBLE SPACE STRUCTURES

by

Benoit Boulet

A thesis submitted in conformity with the requirements
for the degree of Doctor of Philosophy
Graduate Department of Electrical and Computer Engineering
University of Toronto

Abstract

In this thesis, we consider the problem of robust control of large flexible space structures (LFSS). Dynamic models of LFSS are characterized by their high order and their significant number of highly uncertain, lightly-damped, clustered low-frequency modes. We propose the use of a left-coprime factorization (LCF) of LFSS dynamics in modal coordinates for robust control design. The plant uncertainty is described as stable perturbations of the coprime factors. The structure of the LCF allows us to transform easily modal parameter uncertainty into an unstructured description of the uncertainty as stable norm-bounded perturbations in the factors. The resulting set of perturbed LCFs is guaranteed to include all perturbed plant models produced by variations in the modal parameters within their bounds. Uncertainty in the coprime factors can also represent unmodeled modes and actuator dynamics. Closed-loop robustness to perturbations of the modal parameters within a priori bounds is guaranteed provided that the ∞-norm of a certain closed-loop sensitivity matrix can be made less than one with a stabilizing controller. Two multivariable $\mathcal{H}_\infty$ designs and two μ-synthesis designs for an LFSS experimental testbed are presented together with simulation and experimental results to illustrate the technique.

Once a family of perturbed LCF models has been derived from the LFSS model in modal coordinates, it is often desirable to test if it is consistent with a set of experimental data obtained on the plant. The objective is to reduce plant model uncertainty. The model/data consistency problem for coprime factorizations considered here is this: Given some possibly noisy frequency-response data obtained by running open or closed-loop experiments on the system, show that these data are consistent with a given family of perturbed factor models and a noise model. The results given are applicable to a large class of systems admitting coprime factorizations in $\mathcal{RH}_\infty$. A theorem on boundary interpolation in $\mathcal{RH}_\infty$ is a building block that allows us to devise computationally simple necessary and sufficient tests to check if the perturbed coprime factorization is consistent with the data. The cases of noise-free and noisy open-loop and closed-loop frequency-response data are treated.

Acknowledgments

The completion of this thesis would not have been possible without the help and insightful guidance of Professor Bruce Francis, my supervisor. Thanks Bruce for your mathematical rigor, your support, your patience, and your friendship. Thanks for listening to me and trusting my judgment. I will remember those three years spent working with you as some of the best in my life.

Some people at UTIAS deserve my gratitude for helping me run the experiments on Daisy. I thank Professor Peter Hughes for offering me the possibility to work on this fascinating LFSS testbed. His graduate students Tony Hong, Regina Sun Kyung Lee, Robert Zee, and the system manager Vince Pugliese all patiently explained to me the intricate details involved in running control experiments on Daisy.

I thank all my friends in the Systems Control Group for their support and friendship. In particular, Alireza Langari and Gary Leung inspired me and helped me understand some key ideas in robust control as I was beginning my PhD at the University of Toronto. Mike Michez provided me with a model of a flexible robot and experimental frequency-response data that were used in this thesis. I am also indebted to my friend Mark Lawford for introducing me to Linux and teaching me basic UNIX system administration.

I wish to express my gratitude to my parents and my brothers for their encouragement, love, and support over all these years of education that culminated into this thesis. It is difficult to find words to say just how much I appreciated the constant care, love, understanding, encouragement and support of my girlfriend Isabelle Lemay during the course of this work. It meant so much to me.

Finally, I gratefully acknowledge the financial support of the Natural Sciences and Engineering Research Council of Canada, the *Fonds pour la formation de chercheurs et l'aide à la recherche du Québec*, and the Walter C. Sumner Foundation.

This thesis is dedicated to the memory of Professor Jean-Charles Gille from Université Laval who introduced me to the wonderful world of automatic control. His great wisdom and passion for his work shall remain a source of inspiration for the rest of my life.

Contents

List of Tables

List of Figures

List of Acronyms

CCD	Charged Coupled Device
CF	Coprime Factorization
DC	Direct Current (it means *static*, or *frequency* 0)
DEOPS	Digital Electro-Optic Position Sensor
FE	Finite-Element
GCLD	Greatest Common Left-Divisor
LCF	Left-Coprime Factorization (Factor)
LFSS	Large Flexible Space Structure
LFT	Linear Fractional Transformation
LQG	Linear Quadratic Gaussian
LQR	Linear Quadratic Regulator
MIMO	Multi-Input, Multi-Output
NP	Nondeterministic Polynomial
PD	Proportional Derivative
PWM	Pulse-Width Modulation (Modulated)
RCF	Right-Coprime Factorization (Factor)
RP	Robust Performance
RSNP	Robust Stability and Nominal Performance
SISO	Single-Input, Single-Output
UTIAS	University of Toronto Institute for Aerospace Studies

List of Symbols

Signals and systems

Boldface	Used for transfer functions and transfer matrices
Lower case	Used for signals, scalar constants and transfer functions
Upper case	Used for constant matrices and transfer matrices
$\hat{v}$	Laplace transform of the signal v
$u \mapsto v$	mapping from u to v

Fields, Norms and Spaces

$\mathbb{R}$	Real numbers
$\mathbb{R} \cup \{\infty\}$	Extended real numbers
$\mathbb{R}_+$	Nonnegative real numbers
$\mathbb{C}$	Complex numbers
$\mathbb{C}_+$	Complex numbers with positive real parts (open right-half plane)
$\overline{\mathbb{C}}_+$	Complex numbers with nonnegative real parts (closed right-half plane)
$\overline{\mathbb{C}}_+ \cup \{\infty\}$	Extended complex numbers with nonnegative real parts (extended closed right-half plane)
$\mathbb{D}$	Open unit disk $\{z \in \mathbb{C} : \lvert z\rvert < 1\}$
$\mathbb{D}_{1+\epsilon}$	Open disk of radius $1+\epsilon$ $\{z \in \mathbb{C} : \lvert z\rvert < 1+\epsilon\}$

$\overline{\mathbb{D}}$	Closed unit disk $\{z \in \mathbb{C} \,:\, \lvert z\rvert \leq 1\}$
$\partial\mathbb{D}$	Unit circle $\{z \in \mathbb{C} \,:\, \lvert z\rvert = 1\}$
$\|x\|$	$:= (x^*x)^{\frac{1}{2}}$, Euclidean norm of $x \in \mathbb{C}^r$
$\|x\|_\infty$	$:= \max_{i=1,\ldots,r} \lvert x_i\rvert$, ∞-norm of $x \in \mathbb{R}^r$
$\|Q\|$	$:= \overline{\sigma}(Q)$, Spectral norm of $Q \in \mathbb{C}^{p\times q}$
$\|f\|_2$	$:= \left[\int_0^\infty \|f(t)\|^2 dt\right]^{\frac{1}{2}}$, $\mathcal{L}_2$ norm of $f : \mathbb{R}_+ \to \mathbb{R}^r$
$\mathcal{L}_2$	Space of Lebesgue measurable functions on $\mathbb{R}_+$ with finite $\mathcal{L}_2$ norm
$\|f\|_\infty$	$:= \operatorname{ess\,sup}_{t\in\mathbb{R}_+} \|f(t)\|$, $\mathcal{L}_\infty$ norm of $f : \mathbb{R}_+ \to \mathbb{R}^r$
$\mathcal{L}_\infty$	Space of Lebesgue measurable functions on $\mathbb{R}_+$ with finite $\mathcal{L}_\infty$ norm
$\mathcal{H}_\infty$	Hardy space of functions analytic in $\mathbb{C}_+$ and bounded on the imaginary axis, with norm $\|\boldsymbol{Q}\|_\infty := \sup_{\omega\in\mathbb{R}} \|\boldsymbol{Q}(j\omega)\|$
$\mathcal{RH}_\infty$	Space of real-rational functions in $\mathcal{H}_\infty$
$\mathcal{H}_\infty(\mathbb{D})$	Hardy space of functions analytic and bounded in $\mathbb{D}$ with norm $\|\boldsymbol{Q}\|_\infty := \sup_{\theta\in[0,2\pi)} \|\boldsymbol{G}(e^{j\theta})\|$
$\mathcal{RH}_\infty(\mathbb{D})$	Space of real-rational functions in $\mathcal{H}_\infty(\mathbb{D})$
$\mathcal{N}_L\{H\}$	Left-nullspace of H
$\mathrm{Ra}\{H\}$	Range of H
$\mathcal{B}\mathcal{X}$	Unit ball of the normed space $\mathcal{X}$

Miscellaneous

$[Q]_{ij}$	(i,j) entry of Q
Q^T	Transpose of Q
Q^*	Conjugate transpose of Q
$\sigma_i(Q)$	The i^{th} of the singular values of Q arranged in decreasing order.
$\overline{\sigma}(Q)$	Largest singular value of Q
$\underline{\sigma}(Q)$	Smallest singular value of Q
$\rho(Q)$	Spectral radius of Q

$Q^{\frac{1}{2}}$	Square root of positive semi-definite matrix Q, $Q^{\frac{1}{2}}Q^{\frac{1}{2}} = Q$
$\mathcal{F}_U(P,\, \Delta)$	Upper linear fractional transformation of P by Δ
$\mathcal{F}_L(P,\, K)$	Lower linear fractional transformation of P by K
N	Number of frequency-response measurements
$Q^\dagger$	$:= (Q^*Q)^{-1}\, Q^*$, Moore-Penrose left-inverse of Q
I_r	Identity matrix I of dimensions $r \times r$
$\boldsymbol{\tilde{M}},\ \boldsymbol{\tilde{N}}$	Left-coprime factors of nominal plant factorization
$\boldsymbol{\tilde{M}}_p,\ \boldsymbol{\tilde{N}}_p$	Perturbed factors of perturbed plant factorization
$\Delta\boldsymbol{M},\ \Delta\boldsymbol{N}$	Factor perturbations
$\widetilde{\Delta\boldsymbol{M}},\ \widetilde{\Delta\boldsymbol{N}}$	Factor perturbations normalized by $\boldsymbol{r}$
$\boldsymbol{\Delta}$	$:= [\Delta\boldsymbol{N}\ \ -\Delta\boldsymbol{M}]$, Factor perturbation
$\tilde{\boldsymbol{\Delta}}$	$:= \boldsymbol{r}^{-1}\boldsymbol{\Delta} = \left[\widetilde{\Delta\boldsymbol{N}}\ \ -\widetilde{\Delta\boldsymbol{M}}\right]$, Factor perturbation normalized by $\boldsymbol{r}$
$\Delta,\ \Delta_i$	Factor perturbation at frequency ω, ω_i respectively
$\tilde{\Delta},\ \tilde{\Delta}_i$	Factor perturbation at frequency ω, ω_i scaled by $\lvert\boldsymbol{r}(j\omega)\rvert$, $\lvert\boldsymbol{r}(j\omega_i)\rvert$ respectively
$\boldsymbol{r}$	Bound on the factor uncertainty ($\boldsymbol{r}$ is a unit in $\mathcal{RH}_\infty$)
$\mathcal{D}_r$	Set of factor perturbations in $\mathcal{RH}_\infty$ with $\lVert\boldsymbol{r}^{-1}\boldsymbol{\Delta}\rVert_\infty < 1$

LFSS Models

m	Number of inputs in LFSS model
p	Number of outputs in LFSS model
n	Number of modes in LFSS model;
	Noise signal in Chapters 3 and 4
M	Mass matrix of FE model of LFSS in Chapter 2;
	Bound on $\mathcal{L}_\infty$ norm of noise in Chapters 3 and 4
K	Stiffness matrix of FE model of LFSS
$\boldsymbol{G}$	$:= u \mapsto \eta$, Nominal plant model

q	Physical coordinates of LFSS in Chapter 2;
	Complex scalar $(\phi - V_{22})^{-1}$ in Chapters 3 and 4;
	Design parameter in Chapter 5
u	Torque/Force input signal
y	Measured angle/displacement output signal
z	Output signal whose norm is to be minimized
w	Input signal coming from the perturbation
E	Mode shape matrix of LFSS model
E_r	Matrix composed of columns of E corresponding to the modes kept in the model
η	Modal coordinates of LFSS
D	Diagonal damping matrix of modal model of LFSS
Λ	Diagonal matrix of squared modal frequencies
B_0	Input matrix of FE model of LFSS
C_0	Output matrix of FE model of LFSS
B_1	Input matrix of modal model of LFSS
C_1	Output matrix of modal model of LFSS
L_B	Matrix with nonnegative entries bounding the entries of perturbations of B_1
ζ_i	Damping ratio of i^{th} mode
ω_i	Natural frequency of i^{th} mode in Chapters 2, 5 and 6
	Frequency at which the i^{th} frequency-response measurement was made in Chapters 3 and 4
$J_1,\ J_2$	Diagonal scaling matrices computed from B_1
γ	Upper bound on norm of perturbation of scaled B_1
$s^2 + as + b$	Common Hurwitz denominator of $\tilde{\boldsymbol{M}},\ \tilde{\boldsymbol{N}}$
c_i	Upper bound on coefficient of s in numerator of $[\Delta \boldsymbol{M}_{rp}]_{ii}$
d_i	Upper bound on coefficient of s^0 in numerator of $[\Delta \boldsymbol{M}_{rp}]_{ii}$
c_{max}	$\max_{i=1,\ldots,n} \lvert c_i \rvert$
d_{max}	$\max_{i=1,\ldots,n} \lvert d_i \rvert$

$\boldsymbol{T}_a$	Diagonal transfer matrix of actuator dynamics
$\tilde{\boldsymbol{M}}_{rp},\ \tilde{\boldsymbol{N}}_{rp}$	Factors perturbed by variations in modal parameters
$\Delta\boldsymbol{M}_{rp},\ \Delta\boldsymbol{N}_{rp}$	Factor perturbations induced by variations in modal parameters
$\Delta\boldsymbol{M}_{rp0},\ \Delta\boldsymbol{N}_{rp0}$	Scaled factor perturbations induced by variations in modal parameters
$\boldsymbol{\Delta}_{rp0}$	$:= [\Delta\boldsymbol{N}_{rp0},\ -\Delta\boldsymbol{M}_{rp0}]$, Scaled factor perturbation
$\tilde{\boldsymbol{M}}_0,\ \tilde{\boldsymbol{N}}_0$	Scaled nominal left-coprime factors
$\tilde{\boldsymbol{\Delta}}_0$	Scaled factor perturbation normalized by $\boldsymbol{r}$

Model/Data Consistency Problem

g_ϵ	Conformal mapping defined by $g_\epsilon(z) := z/(1+\epsilon),\ z \in \mathbb{C}$
$\boldsymbol{T}$	Nominal model in general model/data consistency problem
$\boldsymbol{t}$	Perturbed closed-loop transfer function in closed-loop noisy SISO consistency problem
$\mathcal{K}$	Set of scalar transfer functions
$\mathcal{W}$	Set of noises
$\mathcal{D}$	Uncertainty set
$\mathcal{P}$	Set of perturbed plant factorizations
$\boldsymbol{J}$	Diagonal input scaling transfer matrix
C	Output matrix of factorization for LFSS
$\mathcal{N}$	Set of time-domain noises in $\mathcal{L}_\infty$ norm-bounded by M
A	Amplitude of noise-free sinusoidal output in frequency-response experiment
A_m	Measured magnitude of noisy output signal in frequency-response experiment
τ	time-delay between input and output sinusoids in noise-free frequency-response experiment
τ_m	Measured time-delay between output signal and input sinusoid at zero crossings.
$\phi,\ \phi_i$	Frequency-response datum in $\mathbb{C}$ obtained at frequency ω, ω_i respectively
$\Phi,\ \Phi_i$	Frequency-response datum in $\mathbb{C}^{p\times m}$ obtained at frequency ω, ω_i respectively
$\hat{\Phi},\ \hat{\Phi}_i$	Frequency-response datum in $\mathbb{C}^{p\times m}$ obtained at frequency ω, ω_i and scaled by $\boldsymbol{J}(j\omega),\ \boldsymbol{J}(j\omega_i)$ respectively

$\mathcal{U}$	Uncertainty set containing ϕ or an entry of Φ in $\mathbb{C}$
$\mathcal{W}_0$	Disk in $\mathbb{C}$ approximating $\mathcal{U}$
L_a	Bound on magnitude of additive complex noise perturbation
δ_a	Scalar additive complex noise perturbation
Δ_a	Matrix additive complex noise perturbation
β	Norm of minimum-norm perturbation $\tilde{\Delta}$ satisfying rank $\left[I - \mathcal{F}_L(P, \Phi^{-1})\tilde{\Delta}\right] \leq n$
$\Delta_{xi},\ \Delta_{yi}$	Fill-in perturbations at frequency ω_i in compromise open-loop noisy MIMO consistency problem; Also without subscript i at frequency ω
α_i	Bound on $\|[\Delta_{xi}\ \Delta_{yi}]\|$
$\tilde{\Delta}_{xi},\ \tilde{\Delta}_{yi}$	Fill-in perturbations at frequency ω_i scaled by α_i
$\hat{\Delta}$	Full $2p \times 2p$ perturbation in compromise open-loop noisy MIMO consistency problem
$\boldsymbol{P}$, $\boldsymbol{V}$, $\boldsymbol{H}$	Generalized plants
$\boldsymbol{k}_1$, $\boldsymbol{k}_2$	Finite-dimensional linear time-invariant SISO controllers
$\boldsymbol{d}$	Inverse of SISO sensitivity function (return difference)
$\boldsymbol{U}$, $\boldsymbol{U}_0$	Transfer matrices in sufficient condition for consistency with closed-loop data
$\boldsymbol{W}$, $\boldsymbol{W}_0$	Transfer matrices in sufficient condition for consistency with closed-loop data
$\tilde{\boldsymbol{M}}_H,\ \tilde{\boldsymbol{N}}_H$	Normalized left-coprime factors of a left factorization of $\boldsymbol{H}_{11}$
$\boldsymbol{N}_H,\ \boldsymbol{M}_H$	Normalized right-coprime factors of a right factorization of $\boldsymbol{H}_{11}$
$\boldsymbol{Q}$, $\boldsymbol{R}$	Free parameters in $\mathcal{RH}_\infty$ in the Youla parametrizations of all stabilizing controllers for $\boldsymbol{H}_{11}$ or $\boldsymbol{V}_{11}$
$\boldsymbol{p}$, $\boldsymbol{q}$	Weighting functions covering $\|R_i\|$ and $\|Q_i\|$ respectively on the imaginary axis

Robust Control Design

y	Measured angles/displacements
y_h	Attitude angles (component of y)

e	Angle/position errors
e_h	Errors in attitude angles
d	Input torque disturbance
r	Input reference
r_h	Hub angle references (component of r)
u_{sc}	Scaled force/torque input
$\boldsymbol{S}_d$	Sensitivity from d to y
$\boldsymbol{S}_{dh}$	Sensitivity from d to y_h
$\boldsymbol{S}_{dhp}$	Perturbed sensitivity from d to y_h
$\boldsymbol{S}_r$	Sensitivity from r to e
$\boldsymbol{S}_{rh}$	Sensitivity from r to e_h
$\boldsymbol{S}_{rhh}$	Sensitivity from r_h to e_h
$\boldsymbol{w}$	Weighting function for performance
$\boldsymbol{W}_q$	Weighting function for performance
$\boldsymbol{K}$, $\boldsymbol{K}_i$, $i = 1, \ldots, 4$	Finite-dimensional linear time-invariant MIMO controllers
$\boldsymbol{K}_{pi}$, $i = 1, \ldots, 4$	Unscaled controllers designed for Daisy
$\boldsymbol{K}_{pid}$, $i = 1, \ldots, 4$	Discretized unscaled controllers designed for Daisy
$D(A_d, T, axes)$	Double-pulse hub torque disturbance used in simulations and experiments
θ_{hx}, θ_{hy}, θ_{hz}	Daisy's hub angles around the x, y and z axes
Δ_s	Complex structured perturbation
$\tilde{\Delta}_s$	Normalized complex structured perturbation
Γ	Structured uncertainty set
Λ	Structured uncertainty set
Ω_0	Structured uncertainty set
$\mathcal{S}$	Set of structured perturbations in $\mathcal{RH}_\infty$
$\mathcal{Q}$	Set of Q-scales in μ theory
$\mathcal{A}$	Set of D-scales in μ theory
$\mu_\Gamma(Q)$	Structured singular value of Q with respect to the structured uncertainty set Γ

Chapter 1

Introduction

1.1 Characteristics and Uses of Large Flexible Space Structures

In the near future, large flexible space structures (LFSS) such as space stations or large communication satellites will be used in orbit around the earth to carry wide antennas, solar panels, scientific instruments, manned research laboratories, and so on. Because of their dimensions up to several hundred meters, LFSS must be assembled in space, and to reduce the cost of sending large payloads in orbit, they must be made of lightweight truss assemblies. As a result, these structures are highly flexible and their dynamics typically possess several low-damped, clustered low-frequency flexible modes. Some experimental testbeds featuring these characteristics have been built [49], such as Daisy [10] at the University of Toronto Institute for Aerospace Studies (UTIAS). A description of Daisy can be found in Chapter 5. An example of an LFSS is the International Space Station currently being built by the United States in partnership with Canada, Japan, Russia, and member nations of the European Space Agency. It will be assembled in space during the next seven years.

1.2 Modeling and Robust Control of LFSS

The dynamics of LFSS are characterized by their high order and their significant number of closely-spaced, lightly-damped, clustered low-frequency modes. They pose a challenging problem to the control system designer who must deal with those characteristics while ensuring a certain level of robustness in the face of significant model uncertainty. As Joshi puts it in

[26]:

> In order to achieve the required performance, it is of utmost importance to be able to control such structures in space with high precision in attitude and shape. Control of such structures is a challenging problem because of their special dynamic characteristics, which result from their large size and light weight.

Typical performance objectives for LFSS include tracking of a desired trajectory by the rigid part of the LFSS, attitude regulation, and vibration attenuation in the flexible part of the structure. These three objectives will be considered in this thesis. These objectives can be translated into more quantitative performance specifications such as desired shapes of the appropriate closed-loop sensitivity matrices in the frequency domain.

Mathematical linear dynamic models of LFSS are usually obtained using finite-element (FE) methods, but these models are known to be reasonably accurate only for a few of the most significant modes of the structure. Moreover, these models do not provide the modal damping ratios, hence they are originally undamped.

Model identification of LFSS is often impractical because such structures are assembled in space and cannot be easily tested on earth due to problems caused by the gravity field and the atmosphere. Thus it would be desirable to have a design procedure that would directly use an FE model and a natural description of the uncertainty to produce a controller that could be implemented on a real LFSS with good confidence. Nevertheless, some authors (e.g. [1], [9]) use identified models of LFSS experimental setups to design robust controllers.

Uncertainty modeling in LFSS is critical if one is to achieve acceptable robustness and performance levels with a practical controller. Some works [31], [1], [47] use norm-bounded additive or multiplicative perturbations of a nominal model in the frequency domain to account for uncertainty in the modal frequencies, damping ratios, and mode shape matrix of the model. Unmodeled modes of the structure and uncertain actuator dynamics can also be represented in this way [32].

Such approaches to uncertainty modeling in LFSS do not handle modal parameter uncertainty very well: Slight variations in either the mode frequencies or damping ratios usually cause the associated dynamic perturbations to be large in the ∞-norm sense. Indeed, additive or multiplicative perturbations may contain large peaks in their frequency responses because of the inherently low damping ratios in LFSS dynamics. At the limit, as the damping goes to

zero, undamped modes cannot have a representation as norm-bounded perturbations of these types. Covering unmodeled modes with such perturbations suffers from the same problem. As a result, one has to choose large weighting functions to bound perturbations which arise from small variations in the modal parameters. In an actual $\mathcal{H}_\infty$ controller design, this may lead to difficulties in making the closed-loop system robustly stable to all weighted perturbations of admissible ∞-norm while achieving some desired performance objective. Thus, in this case, the basic tradeoff between robust stability and nominal performance may be detrimental to the achievable performance level.

In this thesis, it is suggested to transform real parameter uncertainty in the modes into unstructured uncertainty without getting too conservative in the sense that the uncertainty set in $\mathcal{H}_\infty$ has to be kept relatively small. This is motivated by the fact that many results and practical controller design techniques are available for this kind of uncertainty whereas a useful frequency-based design method dealing explicitly with real structured perturbations with a large number of scalars in a high-order dynamic model has yet to be developed. So far, μ-synthesis has proven to be one of the most effective ways to deal with complex structured uncertainty, and some authors (e.g. [31]) have used it to model real parametric uncertainty. Recently the mixed real/complex μ problem has been studied [16] and design methods based on minimizing an upper bound on the mixed μ function, such as the so-called Popov controller synthesis [24], have been developed. An application to a flexible structure has been reported in [25].

These methods are attractive but they quickly become numerically difficult as the number of independent perturbations increase. As a matter of fact, just the calculation of the structured singular value μ for pure real or mixed real/complex uncertainty at one frequency is computationally complex as it has been shown to be NP-hard [5], i.e., at least as hard as the NP-complete problems (see [19] for a treatment of computational complexity and NP-completeness). It is generally accepted that a problem being NP-complete means that it cannot be computed in polynomial time in the worst case. Here, the recognition problem: *Given b and a complex matrix M, is $\mu(M) \geq b$?* cannot be solved in general in fewer steps than some polynomial function of, roughly, the number of real parameters. And this is true regardless of the algorithm used to solve the problem. Since robust control design techniques such as the Popov synthesis [24] attempt to minimize μ at all frequencies, it may be concluded that the design problem itself is no easier than the NP-complete μ recognition problem stated above. This strongly suggests

that such techniques become less useful as the plant's order and the number of independent perturbations increase. Some of these methods also suffer from controller inflation. Hence they are of limited use for high-order LFSS models when many real scalar perturbations are modeled as individual scalar blocks. Furthermore, an unstructured complex uncertainty block must still be added to account for unmodeled dynamics, and this block usually represents additive or multiplicative uncertainty. This means that the attainable performance may be severely limited as previously discussed.

Another approach to the robust control design problem for LFSS is to design controllers robust to variations in the plant state-space model (A, B, C, D). For example, this approach is used in [9] to design a decentralized controller for an LFSS, and also in [44] to design controllers for an earlier version of Daisy. This approach can lead to robustness for a special kind of uncertainty, i.e., real perturbations in the plant (A, B, C, D) matrices. But a design based on this type of uncertainty does not provide robustness to unmodeled dynamics which would change the order of the plant. Moreover, performance specifications in terms of sensitivity reduction are difficult to translate into regions of the complex plane where closed-loop poles should lie.

Yet another approach to the robust control of LFSS is the passivity approach [26]. It is well known that an LFSS with collocated rate sensors and force/torque actuators and with the same number of inputs and outputs has a positive-real transfer matrix model. Then if a strictly positive real controller is designed, it follows that the closed-loop will be stable for all modal perturbations, regardless of the number of unmodeled modes. Although this result is of great importance, it only applies to structures of rather restricted configurations. Moreover, one cannot use this result for controller design achieving robust performance. Recently, dynamic embeddings have been proposed to turn a nonsquare/noncollocated LFSS model into a positive real system [30]. Even though this approach seems promising, it is not yet clearly known how robust the embedding technique is, i.e., small perturbations in the original plant may destroy the positive realness property of the embedded plant.

It appears that a different description of the uncertainty is needed. Some authors have argued (e.g. [51]) that coprime factor descriptions in $\mathcal{H}_\infty$ of nearly unstable plants, such as LFSS, is a sound way to model these systems. This is the approach taken in this thesis. The loop shaping technique of McFarlane and Glover [34] involves modeling the plant as a normalized coprime factorization and it has been successfully applied to design controllers for

LFSS [34]. Similar to the loop shaping method is the weighted-gap optimization technique which was tested on LFSS experimental facilities by Buddie et al. [6]. These techniques show the potential of modeling LFSS dynamics using coprime factorizations, but they do not address the problem of converting known bounds on perturbations of the modal parameters into norm bounds on factor perturbations. The difficulty comes from the fact that these methods rely on *normalized* coprime factorizations which destroy the decoupled structure of the nominal modal state-space models.

Chapter 2 presents a very simple method to obtain a left coprime factorization (LCF) of LFSS dynamics in modal coordinates which preserves the decoupled structure. The plant uncertainty is described as stable perturbations of the coprime factors. The structure of the LCF allows one to go easily from modal parameter uncertainty to an unstructured description of the uncertainty as stable norm-bounded perturbations in the factors, as discussed in Section 2.3. This allows a better, less conservative description of the uncertainty and hence should lead to better closed-loop performance and guaranteed robustness.

Coprime factorizations (CF) can be derived directly from undamped FE models because factor uncertainty sets may include stable perturbations that change the number of closed right half-plane poles of the perturbed plant. This is one advantage of factor uncertainty models over additive or multiplicative uncertainty models. The use of a CF of the plant dynamics does not penalize the designer in terms of available theoretical results or design techniques: The problem can be formulated as a standard $\mathcal{H}_\infty$ or μ-synthesis design problem. Both of these design problems have been studied extensively in the past decade and well-developed solutions to them are available (see e.g. [14] for the $\mathcal{H}_\infty$-optimal control design problem and [2] for an introduction to μ-synthesis). The algorithms in [14] and [2] have been implemented in the software package Matlab^{TM}'s μ-Analysis and Synthesis Toolbox (μ-Tools).

1.3 The Model/Data Consistency Problem for CF Models

Uncertainty modeling is an important aspect of robust control theory. In the modeling process, the engineer is always faced with the fact that the choice of an uncertainty model is itself uncertain. But since the latter type of uncertainty is not modeled, it is highly desirable to reduce it using experimental data before an actual controller design is carried out. One way to do this is to check that the experimental data is consistent with the nominal plant model

and the plant uncertainty set. This is the model/data consistency problem. Based on these consistency checks, the engineer can modify the uncertainty set (without making it too large) until all data are consistent with the model.

This issue of consistency of uncertain models with experimental data has been overlooked for some time in the development of robust control, although some recent work has dealt with this problem for time-response data [39], [33], [48], [28]. This is somewhat surprising because one might argue that the problem of uncertainty modeling should not be determined only by how tractable the robustness problem gets with a given model, but also from the possibility of performing experimental consistency checks and by the feasibility of constructing bounds for the uncertainty sets from experimental data. Related works on identification in $\mathcal{H}_\infty$ use frequency-response data [22], [3], [7], and in particular, [22] and [7] use Nevanlinna-Pick interpolation theory to obtain their results.

For noisy time-domain input-output data, Smith [48], [47] developed a method based on optimization to answer this question. His method applies to a general structured uncertainty description where the structured uncertainty block is connected as a feedback around a generalized plant. Since coprime factor uncertainty fits this description, the method can be applied to the special case of CF that we are interested in. The noise is considered to be an exogenous input of the generalized plant and is assumed to be bounded in $\mathcal{L}_2$. His approach involves the transformation of the finite-length discrete recordings of the input, output, and noise signals into the frequency domain using a Fast Fourier Transform algorithm. Then he studies the consistency problem in the frequency domain, as we do in this thesis.

Apart from the fact that we use frequency-response data, the main differences between Smith's work and ours lie in the noise models and the consistency equations at each measurement frequency. As mentioned above, Smith considers norm-bounded noises in $\mathcal{L}_2$ whereas our noise model consists of norm-bounded signals in $\mathcal{L}_\infty$. A more significant difference is that in the MIMO cases we are led to matrix consistency equations, whereas Smith obtains vector consistency equations. Our approach with matrix consistency equations guarantees that there exists at least *one* admissible constant perturbation accounting for the matrix datum at one frequency. In contrast, it is not clear how one can show that there exists *one* admissible constant perturbation accounting for the data with the technique of [48], [47] when the m inputs of the systems are sequentially excited by sinusoids of the same frequency, leading to m vector consistency equations.

Finally, we carefully show that there exists a perturbation $\mathbf{\Delta} \in \mathcal{BRH}_\infty$ interpolating all the constant perturbations provided that they are all of norm less than one. This was not done in [48], [47].

Poolla and co-workers [39] also recently addressed the model/data consistency problem for discrete-time input-output data and gave results in the form of tests involving the solutions to quadratic and linear programs. These solutions can be computed in polynomial time using, e.g., the recent interior point methods given by Nesterov and Nemirovskii [38]. The approach of [39] avoids the transformation to frequency domain needed in [48], but cannot deal with structured uncertainty.

1.4 Contribution of Thesis

1.4.1 An LCF Model of LFSS Dynamics

Chapter 2 presents a very simple method to obtain a left-coprime factorization of LFSS dynamics in modal coordinates that preserves the decoupled structure of the equations. The plant uncertainty is described as stable perturbations of the coprime factors. The structure of the LCF allows one to transform easily bounded modal parameter uncertainty into an unstructured description of the uncertainty as stable norm-bounded perturbations in the factors, as discussed in Section 2.3. The resulting set of perturbed LCFs is guaranteed to include all perturbed plant models produced by variations in the modal parameters within their bounds. Moreover, the bound on the factor uncertainty is relatively tight on the imaginary axis in the sense that it is close to the norm of the worst-case factor perturbation induced by perturbations of the modal parameters. This allows a good, nonconservative description of the uncertainty set and hence should lead to better closed-loop performance and guaranteed robustness for LFSS.

1.4.2 The Model/Data Consistency Problem

The general model/data consistency problem is formulated in Chapter 3 and then specialized to coprime factorizations in $\mathcal{RH}_\infty$ and frequency-response data. The problem can be posed as follows: Given some experimental data obtained by running open-loop or closed-loop experiments on the system, show that these (possibly noisy) data are consistent with a family of perturbed coprime factor models. In other words, do there exist a perturbation and a noise belonging to the uncertainty and noise sets such that the input-output data can be reproduced

by the perturbed model? A mathematical formulation of this problem is given in Section 3.2.

Chapter 3 and Chapter 4 address the problem of checking consistency of, respectively, open-loop and closed-loop experimental frequency-response data with perturbed coprime factor plant descriptions. It is assumed that we are given N frequency-response data points obtained at N distinct frequencies to test the model. The open-loop noise-free and noisy single-input, single-output (SISO) and multi-input, multi-output (MIMO) cases are studied in Chapter 3, and complete solutions to the open-loop noise-free MIMO and noisy SISO consistency problems are given. The closed-loop noise-free MIMO and noisy SISO cases are also considered in Chapter 4. If frequency-response experiments are performed on an experimental setup with flexibilities or on an actual LFSS, then the results presented are of interest to obtain better uncertainty models by shaping the bound $\boldsymbol{r}$ on the factor uncertainty.

Consistency of Open-Loop Frequency-Response Data with CF Models

The open-loop noise-free model/data consistency problem for CF boils down to the existence of an interpolating function in $\mathcal{RH}_\infty$ that evaluates to N complex matrices of compatible dimensions at N distinct points on the imaginary axis. Our central result is a theorem on boundary interpolation in $\mathcal{RH}_\infty$ that is based on Nevanlinna-Pick interpolation theory. This necessary and sufficient condition allows us to devise a simple test consisting of computing minimum-norm solutions to N underdetermined linear complex matrix equations to check if the perturbed coprime factorization is consistent with the data. Left-coprime factorizations are studied, but the results can be trivially extended to right-coprime factorizations (RCF). We also treat the case of the special factorization for LFSS introduced in Chapter 2. This case turns out to be quite a bit more difficult than the standard coprime factorization case, but a complete solution is nonetheless provided for square p-input, p-output LFSS plant models. This necessary and sufficient condition uses the Schmidt-Mirsky Theorem [50, Theorem 4.18] and involves computing the p^{th} singular value of a complex matrix for each measurement frequency.

Then the open-loop noisy model/data consistency problem considered is for time-domain $\mathcal{L}_\infty$ noise norm-bounded by M corrupting the measured output signals in frequency-response measurements. It is shown that a good approximation of the effect of such noises in the frequency-domain is disk-like uncertainty in the complex plane around each entry of the complex frequency-response matrices for each of N distinct frequencies. So the problem is again decomposed into N consistency problems for constant complex matrices, and then the boundary

interpolation theorem is invoked to show whether or not there exists a norm-bounded $\mathcal{RH}_\infty$ perturbation of the coprime factors that could have produced the noisy frequency-response measurements.

For the noisy SISO case, N μ tests on linear fractional transformations (LFT) provide a necessary and sufficient condition for consistency. The noisy MIMO case is more difficult, but for square plants we derive a sufficient condition consisting of N singular value tests on linear fractional transformations. We show that if some of the singular value tests are inconclusive, then the norm bound on the coprime factor uncertainty model may be increased at the corresponding frequencies until all N tests eventually lead to a positive conclusion of consistency of the model with the data. On the other hand, it is also possible to reduce the norm bound at those frequencies where the tests show that there is too much uncertainty in the model. This provides a way to refine the model by reducing conservativeness at some frequencies while ensuring consistency for all measurements.

Consistency of Closed-Loop Frequency-Response Data With CF Models

The closed-loop noise-free MIMO consistency problem for coprime factorizations is more difficult, but potentially very useful for unstable or lightly-damped systems. Frequency responses are very difficult or even impossible to obtain on such systems unless a feedback controller is implemented to add sufficient damping for the experiments to be carried out. A necessary condition is given, which is a simple test consisting of computing minimum-norm solutions to underdetermined linear complex matrix equations, as in the open-loop case. For the case of the special factorization for square $p \times p$ LFSS, a necessary condition based on the Schmidt-Mirsky Theorem is derived. It requires the computation of the p^{th} singular values of N LFTs. The theorem on boundary interpolation in $\mathcal{RH}_\infty$ is used in those two cases. An observation is made that sufficient conditions for this consistency problem involve strongly stabilizing perturbations, which is the main difficulty over the open-loop case.

Then the closed-loop noisy model/data consistency problem considered is for SISO plants only. The noise model is the same as described in Chapter 3, and a necessary condition for consistency is given. This necessary condition involves μ computations on N LFTs.

A general sufficient condition for consistency based on a theorem of robust performance involving the structured singular value μ and applicable to all cases treated is given. A numerical example using a 23-input, 23-output, 46^{th}-order model of Daisy is worked out to show that this

test is applicable to LFSS and not too conservative.

1.4.3 Robust Control Design for LFSS

In Chapter 5, a controller design technique based on $\mathcal{H}_\infty$-optimal control theory and providing robust stability and nominal performance for LFSS is proposed. It uses the perturbed LCF model of LFSS dynamics introduced in Chapter 2 with the uncertainty bound $\boldsymbol{r}$. Note that this bound may be improved by using frequency-response data as suggested in Chapters 3 and 4 prior to the design process. The performance specifications are chosen to be desired shapes of some closed-loop sensitivity matrices in the frequency domain. Two multivariable $\mathcal{H}_\infty$ designs based on LCFs of 46^{th}-order collocated and noncollocated models of an LFSS experimental testbed (Daisy) are presented together with some simulation and experimental results. Controller implementation issues are discussed.

Chapter 6 presents a control design method providing robust performance for LFSS. It is based on μ-synthesis and uses the perturbed LCF introduced in Chapter 2 with a factor uncertainty bound $\boldsymbol{r}$. The initial bound $\boldsymbol{r}$ given in Chapter 2 can be modified and improved by using experimental data as previously mentioned. The performance specifications are again chosen to be desired shapes of some closed-loop sensitivity matrices in the frequency domain. Two μ-synthesis designs achieving robust performance for Daisy are described and their implementation is discussed. Simulations and experimental results are given for both controllers.

1.5 Notation

Let H be an $n \times m$ complex matrix with singular values $\sigma_1 \geq \cdots \geq \sigma_q,\ q := \min\{m, n\}$. The (i, j) entry of H is denoted as $[H]_{ij}$. The maximum and minimum singular values of H are written as $\overline{\sigma}(H) = \sigma_1$ and $\underline{\sigma}(H) = \sigma_q$ respectively. H^* denotes the conjugate transpose of H and H^T its transpose. H is *Hermitian* if $H^* = H$. The norm associated with $\mathbb{C}^m$ is the usual Euclidean norm $\|x\| := (x^*x)^{\frac{1}{2}}$. For $x \in \mathbb{R}^r$ with components $x_i,\ i = 1, \ldots, r$, $\|x\|_\infty = \max_{i=1,\ldots,r} |x_i|$. The norm of H is taken to be its maximum singular value: $\|H\| = \overline{\sigma}(H)$, which is the matrix norm induced by the Euclidean norm on $\mathbb{C}^m$. The left-nullspace of H is denoted as $\mathcal{N}_L\{H\}$ and its range as $\mathrm{Ra}\{H\}$. The identity matrix I of dimensions $r \times r$ is often written as I_r.

We denote the open and closed right half-planes of complex numbers as $\mathbb{C}_+$ and $\overline{\mathbb{C}}_+$ respec-

tively. The extension of $\overline{\mathbb{C}}_+$ to infinity is written as $\overline{\mathbb{C}}_+ \cup \{\infty\}$. The open unit disk in $\mathbb{C}$ is denoted as $\mathbb{D}$ and the unit circle as $\partial\mathbb{D}$. The closed unit disk is written as $\overline{\mathbb{D}}$. The space $\mathcal{H}_\infty$ is the class of functions analytic in $\mathbb{C}_+$ and bounded on the imaginary axis, with norm defined as $\|\boldsymbol{Q}\|_\infty = \sup_{\omega\in\mathbb{R}} \|\boldsymbol{Q}(j\omega)\|$. The space $\mathcal{H}_\infty(\mathbb{D})$ is the class of functions analytic and bounded in $\mathbb{D}$ with norm defined as $\|\boldsymbol{G}\|_\infty := \sup_{\theta\in[0,2\pi)} \|\boldsymbol{G}(e^{j\theta})\|$. The prefix $\mathcal{R}$ on $\mathcal{RH}_\infty$ denotes real-rational; so $\mathcal{RH}_\infty$ is the class of scalar or matrix-valued proper stable real-rational transfer functions. Similarly, $\mathcal{CH}_\infty$ is the space of complex-rational functions in $\mathcal{H}_\infty$. According to the context, it should be clear whether we are considering scalar or matrix-valued functions, but sometimes we will write, say, $\mathcal{H}_\infty^{m\times n}$. For a normed space $\mathcal{X}$, $\mathcal{BX}$ denotes its open unit ball.

A function in $\mathcal{H}_\infty$ ($\mathcal{RH}_\infty$) is called a unit if its inverse also belongs to $\mathcal{H}_\infty$ ($\mathcal{RH}_\infty$). For example, the units in $\mathcal{RH}_\infty^{n\times n}$ are those $n \times n$ real-rational stable, proper functions whose determinants are biproper (i.e., proper but not strictly proper) and with no zeros in $\overline{\mathbb{C}}_+$. For a transfer matrix $\boldsymbol{Q}$ and frequencies ω and ω_i, we will often define $Q := \boldsymbol{Q}(j\omega)$ and $Q_i := \boldsymbol{Q}(j\omega_i)$ in order to ease the notation. A tilde ($\tilde{}$) over a constant matrix $\tilde{H}$ or a transfer matrix $\tilde{\boldsymbol{Q}}$ means that the norms of H and $\boldsymbol{Q}$ have been normalized to be less than one, except for the nominal factors $\tilde{\boldsymbol{M}}$ and $\tilde{\boldsymbol{N}}$ for which it means *left-coprime* in an effort to be consistent with the literature on coprime factorizations.

Signals are represented with lower-case letters and their Laplace transforms are just the same letters with hats. For finite-dimensional linear time-invariant operators, scalar constants and functions are represented respectively by regular and boldface lower-case letters, while matrix constants and matrix-valued functions are assigned respectively regular and boldface upper-case letters.

Upper and lower linear fractional transformations (LFTs) are now defined. Suppose the matrix P is partitioned as $P := \begin{bmatrix} P_{11} & P_{12} \\ P_{21} & P_{22} \end{bmatrix}$, K is such that its transpose K^T has the same dimensions as P_{22}, and Δ is such that its transpose Δ^T has the same dimensions as P_{11}. Then the lower LFT of P by K is $\mathcal{F}_L(P,K) := P_{11} + P_{12}K(I - P_{22}K)^{-1}P_{21}$ whenever the inverse exists. The upper LFT of P by Δ is $\mathcal{F}_U(P,\Delta) := P_{22} + P_{21}\Delta(I - P_{11}\Delta)^{-1}P_{12}$ whenever the inverse exists. These definitions, which also hold for system matrices, are best illustrated by the two block diagrams in Figure 1.1 where $\mathcal{F}_L(P,K) = u_1 \mapsto v_1$ and $\mathcal{F}_U(P,\Delta) = u_2 \mapsto v_2$.

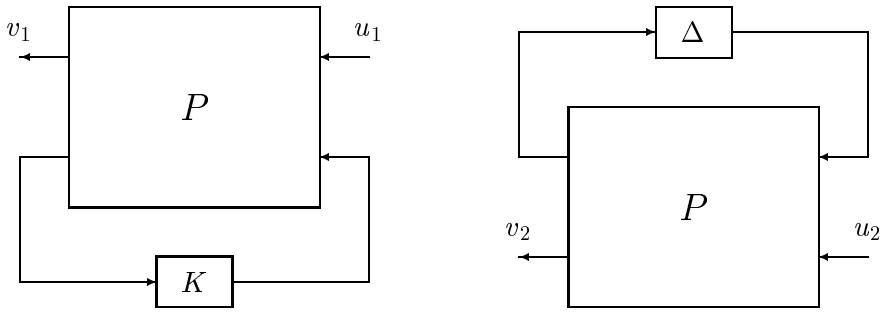

Figure 1.1: Lower LFT $\mathcal{F}_L(P, K)$ and upper LFT $\mathcal{F}_U(P, \Delta)$

Chapter 2

Left-Coprime Factor Models for LFSS

2.1 Introduction

Mathematical linear dynamic models of LFSS are usually obtained using FE methods. These models are known to be reasonably accurate only for a few of the most significant modes of the structure. Modes with limited input-output influence are often highly uncertain, even if they lie in the main cluster. Furthermore, unmodeled modes may be present in the plant, or the model may contain modes which do not exist in the LFSS.

Chapter 1 provided some motivation for the use of a perturbed coprime factorization of LFSS dynamics over other models in order to cover this uncertainty. It was argued that the uncertainty in the coprime factors can account for both modal parameter uncertainty and unmodeled dynamics with one full perturbation in $\mathcal{RH}_\infty$. With this uncertainty model, standard $\mathcal{H}_\infty$ and μ-synthesis controller design techniques can be used to design for robust stability or robust performance with guaranteed stability or performance margins with respect to variations in the modal parameters. These issues will be discussed in Chapters 5 and 6.

In this chapter, a nominal left-coprime factorization of LFSS dynamics is introduced, and a norm bound $\boldsymbol{r}$ on the factor perturbations is derived. This bound has the property that the corresponding family of perturbed plants contains all plants induced by variations in the modal parameters within some a priori known bounds. It works best for plants with clustered flexible modes at low frequencies such as LFSS. It is also not too conservative in the sense that it tightly

covers the worst-case factor perturbation induced by variations in the modal parameters.

2.2 A Left-Coprime Factorization of LFSS Dynamics

An FE method gives a high-order model of the flexible part of the structure consisting of perhaps thousands of ordinary differential equations. Rigid-body modes may be included to account for the attitude and position of rigid parts of the structure. In order to have a fixed model for our discussion, we consider three rigid-body modes accounting for the attitude of the main rigid part. (Daisy has these dynamics, although two of the rigid-body modes are pendulous so they can be viewed as flexible modes.) The model is undamped, and essentially consists of a constant positive definite mass matrix M and a constant positive semidefinite stiffness matrix K which are used to express the dynamics as

$$M\ddot{q} + Kq = B_0 u, \tag{2.1}$$

$$y = C_0 q, \tag{2.2}$$

where $q(t) \in \mathbb{R}^{n_{FE}}$ is a vector of attitude coordinates for the rigid part and physical coordinates (displacements and rotations) of the flexible parts of the LFSS, the input $u(t) \in \mathbb{R}^m$ is a vector of actuator forces and torques applied to the structure, and $y(t) \in \mathbb{R}^p$ is the vector of measured outputs.

Remark 2.1 Note that velocity sensors could have been chosen as well, but this was not done to simplify the development of the LCF model. Combinations of position and velocity sensors can be accommodated by including sensor dynamics in C_1 in Figure 2.3 after the LCF has been computed. Accelerometers were not considered in this research, partly because they are not well adapted to the inherently small accelerations produced by slow oscillations in LFSS. Another reason is that the use of accelerometers cause the modal uncertainty to become coupled into the output equation, which makes the robust control problem more difficult.

Definition 2.1 A real matrix E whose columns are eigenvectors of the matrix $M^{-1}K$ and such that it diagonalizes both M and K, i.e., $E^T M E = I$ and $E^T K E = \Lambda$, where Λ is diagonal with the squared mode frequencies in its main diagonal, always exists [23, Theorem 4.5.15]. It defines a coordinate transformation from the modal coordinate vector η to the physical coordinate vector q, i.e., $q = E\eta$. Such a matrix is called a *mode shape matrix*

and its columns are *mode shapes* of the structure.

Remark 2.2 Note that given M and K, one can compute a mode shape matrix and the mode frequencies of the model as follows. The mode frequencies are just the square roots of the eigenvalues of $M^{-1}K$. Let $\hat{E}$ be a diagonalizing matrix of eigenvectors of $M^{-1}K$, that is, $\hat{E}^{-1}M^{-1}K\hat{E} = \Lambda$ Then [23, Theorem 4.5.15 II(b)] says that $\hat{E}$ also diagonalizes M as follows: $\hat{E}^T M\hat{E} = F$, where F is a nonsingular diagonal matrix. Let $F^{\frac{1}{2}}$ be the square root of F and let $E := \hat{E}F^{-\frac{1}{2}}$. Then E is a mode shape matrix of the LFSS model.

We start with LFSS dynamics in modal coordinates, reduced to a reasonable order by discarding the less significant flexible modes according to some measure of their input-output influence [45], [21]. The first three are the rigid-body modes. The modal frequencies of the $n-3$ retained flexible modes, $\{\omega_i\}_{i=4}^n$, are given by the FE model; uncertainties will be introduced later. Note that the flexible modes are observable and controllable as a consequence of the above reduction procedure. Damping is added to the nominal model as it is known that damping ratios of flexible modes are nonzero since flexibilities in any LFSS are dissipative in nature. So if $\{\overline{\zeta}_i\}_{i=4}^n$ is a set of positive upper bounds and $\{\underline{\zeta}_i\}_{i=4}^n$ is a set of nonnegative lower bounds on the otherwise unknown damping ratios, we may take $\{\zeta_i := (\underline{\zeta}_i + \overline{\zeta}_i)/2\}_{i=4}^n$ as the nominal ones. Transforming (2.1) using the mode shape matrix E, truncating and adding a diagonal damping matrix D, we get the nominal dynamic equations in modal coordinates,

$$\ddot{\eta} + D\dot{\eta} + \Lambda\eta = B_1 u, \tag{2.3}$$

$$y = C_1\eta, \tag{2.4}$$

where $D = \mathrm{diag}\{0,0,0,2\zeta_4\omega_4,\ldots,2\zeta_n\omega_n\}$, $\Lambda = \mathrm{diag}\{0,0,0,\omega_4^2,\ldots,\omega_n^2\}$, $B_1 = E_r^T B_0 \in \mathbb{R}^{n\times m}$, $C_1 = C_0E_r \in \mathbb{R}^{p\times n}$, and $E_r \in \mathbb{R}^{n_{FE}\times n}$ is composed of the columns of E corresponding to the rigid-body modes and the elastic modes kept in the model. Then, taking the Laplace transform on both sides of (2.3) and (2.4) with zero initial conditions yields

$$\hat{\eta}(s) = \left[s^2 I + sD + \Lambda\right]^{-1} B_1\,\hat{u}(s), \tag{2.5}$$

$$\hat{y}(s) = C_1\left[s^2 I + sD + \Lambda\right]^{-1} B_1\,\hat{u}(s). \tag{2.6}$$

The assumptions here are as follows:

(A2.1) The sensors have no dynamics.

(A2.2) No pole-zero cancellation occurs at $s = 0$ when the product $C_1 [s^2 I + sD + \Lambda]^{-1} B_1$ is formed.

(A2.3) The uncertainty in the output matrix C_1 can be lumped in the input uncertainty.

The motivation behind Assumptions (A2.1) and (A2.3) is that space sensors are usually accurate and fast while space actuators, which include torque wheels and gas jet thrusters, may add quite a bit of uncertainty in the torque and force inputs. Assumption (A2.2) is standard and just says that the unstable rigid-body modes must be controllable and observable with the set of actuators and sensors used. Assumption (A2.3) is also motivated by the fact that C_1 comes from the postmultiplication of C_0 by E_r, which bears some uncertainty since it contains mode shapes of the structure. If the perturbed C_0 is written as $\overline{C}_0(I + \Delta_{C_0})$ and the norm of the $n \times n$ matrix Δ_{C_0} is small, then $(I + \Delta_{C_0})$ approximately commutes with $[s^2 I + sD + \Lambda]^{-1}$ in (2.6).

Consider the matrix $[s^2 I + sD + \Lambda]$ in (2.5). It is diagonal, so its inverse is simply

$$[s^2 I + sD + \Lambda]^{-1} = \text{diag}\left\{\frac{1}{s^2}, \frac{1}{s^2}, \frac{1}{s^2}, \frac{1}{s^2 + 2\zeta_4\omega_4 s + \omega_4^2}, \ldots, \frac{1}{s^2 + 2\zeta_n\omega_n s + \omega_n^2}\right\}. \tag{2.7}$$

The matrix B_1 in (2.5) is an $n \times m$ real matrix. Let the polynomial $s^2 + as + b$ be Hurwitz with real zeros. Form the matrices $\tilde{\boldsymbol{M}}(s)$ and $\tilde{\boldsymbol{N}}(s)$ as follows:

$$\tilde{\boldsymbol{M}}(s) := \frac{1}{s^2 + as + b}\text{diag}\left\{s^2, s^2, s^2, s^2 + 2\zeta_4\omega_4 s + \omega_4^2, \ldots, s^2 + 2\zeta_n\omega_n s + \omega_n^2\right\}, \tag{2.8}$$

$$\tilde{\boldsymbol{N}}(s) := \frac{1}{s^2 + as + b}B_1. \tag{2.9}$$

The complex argument s is dropped hereafter to ease the notation. Note that $\tilde{\boldsymbol{M}}$ and $\tilde{\boldsymbol{N}}$ are stable and proper, hence they belong to $\mathcal{RH}_\infty$. Let the transfer function matrix from $\hat{u}$ to $\hat{\eta}$ be denoted as $\boldsymbol{G}$. Then $\boldsymbol{G}$ can be written as $\tilde{\boldsymbol{M}}^{-1}\tilde{\boldsymbol{N}}$, i.e., $\tilde{\boldsymbol{M}}$ and $\tilde{\boldsymbol{N}}$ form a left factorization of $\boldsymbol{G}$ in $\mathcal{RH}_\infty$.

Proposition 1 *$\tilde{\boldsymbol{M}}$ and $\tilde{\boldsymbol{N}}$ are left-coprime.*

Proof An equivalent condition for $\tilde{\boldsymbol{M}}$ and $\tilde{\boldsymbol{N}}$ to be coprime is that $\begin{bmatrix} \tilde{\boldsymbol{M}} & \tilde{\boldsymbol{N}} \end{bmatrix}$ have full rank for all $s \in \overline{\mathbb{C}}_+ \cup \{\infty\}$ (see Appendix A). But Assumption (A2.2) implies that the first three rows of B_1 are linearly independent and hence $\begin{bmatrix} \tilde{\boldsymbol{M}} & \tilde{\boldsymbol{N}} \end{bmatrix}$ has full rank for all $s \in \overline{\mathbb{C}}_+ \cup \{\infty\}$. Therefore $\tilde{\boldsymbol{M}}$ and $\tilde{\boldsymbol{N}}$ constitute an LCF of the transfer function matrix $\boldsymbol{G}$. ■

2.3 Uncertainty Modeling for LFSS

Uncertainty in FE models is usually characterized by uncertainty in the modal parameters $\{\zeta_i\}_{i=4}^n$ and $\{\omega_i\}_{i=4}^n$, in the mode gains and in the mode shape matrix E. Unmodeled modes can also be considered as perturbations changing the order of the model. Uncertainty in the modal parameters appears easier to characterize based on heuristics and experience, at least for the most significant modes, than uncertainty in E. The uncertainty modeling process proposed here uses the a priori knowledge of the bounds for $\{\zeta_i\}_{i=4}^n$ and $\{\omega_i\}_{i=4}^n$. For example, the structure designer could say with good certainty that the second mode has natural frequency between say, 0.01 and 0.013 rad/s, and that its damping ratio ζ is almost surely less than 0.05. This information is used to derive a bound on the norm of the coprime factor perturbations at each frequency which will be needed in the design process for robustness issues. Of course, some uncertainty is also present in the mode shape matrix E of the structure and will be accounted for as uncertainty in the entries of B_1. We will see that it is easy to go from parametric uncertainty to unstructured uncertainty in the coprime factors.

This section can be outlined as follows. First we start with the parametric uncertainty of (2.11); this induces stable perturbations in $\tilde{\boldsymbol{M}}$ and $\tilde{\boldsymbol{N}}$. These induced perturbations and their corresponding perturbed factors are given the subscript "*rp*" for *real parameter*. On the other hand, some of the results stated apply to more general perturbations in $\mathcal{RH}_\infty$, but then the subscript is dropped. Two scalings are performed on $\tilde{\boldsymbol{M}}_{rp}$ and $\tilde{\boldsymbol{N}}_{rp}$ so that the perturbations are better balanced. Finally, a third scaling normalizes the combined factor perturbations.

It is desired to lump the uncertainty in the mode frequencies, damping ratios and mode gains into unstructured uncertainty in the coprime factors such that the perturbed LCF of $\boldsymbol{G}$ can be written as

$$\boldsymbol{G}_p = (\tilde{\boldsymbol{M}} + \Delta\boldsymbol{M})^{-1}(\tilde{\boldsymbol{N}} + \Delta\boldsymbol{N}), \tag{2.10}$$

with $\Delta\boldsymbol{M}$, $\Delta\boldsymbol{N} \in \mathcal{RH}_\infty$. Perturbations in the modal parameters and the entries of B_1 are assumed bounded by nonnegative numbers as follows

$$|\delta\omega_i| \le l_\omega^i \ , \quad |\delta\zeta_i| \le l_\zeta^i \ , \quad |\delta b_{1ij}| \le l_b^{ij} \ , \quad i = 1, \ldots, n, \ j = 1, \ldots, m \ . \tag{2.11}$$

The following matrices will be useful later on:

$$\Delta B_1 := \begin{bmatrix} \delta b_{111} & \cdots & \delta b_{11m} \\ \vdots & \ddots & \vdots \\ \delta b_{1n1} & \cdots & \delta b_{1nm} \end{bmatrix}, \tag{2.12}$$

$$L_B := \begin{bmatrix} l_b^{11} & \cdots & l_b^{1m} \\ \vdots & \ddots & \vdots \\ l_b^{n1} & \cdots & l_b^{nm} \end{bmatrix}. \tag{2.13}$$

The uncertainty in the entries of B_1, which are also the numerators of the fractional entries of $\tilde{\boldsymbol{N}}$, comes from different sources. First, uncertainty in a particular mode gain can be represented as an uncertain factor multiplying the corresponding row of B_1. Second, uncertainty in the mode shape matrix E affects B_1 because in the change from physical to modal coordinates in (2.1), the original input matrix B_0 gets premultiplied by E_r^T to form B_1. Third, the matrix B_0 itself is uncertain because the actuator gains are not known perfectly. Finally, by (A2.3), output uncertainty is transformed into input uncertainty.

Unmodeled modes, usually (but not necessarily) occurring at high frequencies, can be handled by adjusting the norm bound on the factor uncertainty (though not necessarily at high frequencies only). This can be done iteratively according to the following heuristics: Design a controller using the techniques discussed in this thesis and test it on a set of perturbed full-order evaluation models. If all closed loops are stable (while achieving some desired performance level in the robust performance case), stop — the controller is satisfactory with respect to the evaluation models. If not, increase the norm bound on factor uncertainty and redesign the controller.

Perturbations of the coprime factors resulting from perturbations of the real parameters only are easily computed. The perturbed factor $\tilde{\boldsymbol{M}}_{rp}$ is defined as

$$\tilde{\boldsymbol{M}}_{rp} := \tilde{\boldsymbol{M}} + \Delta \boldsymbol{M}_{rp}, \tag{2.14}$$

where

$$\Delta \boldsymbol{M}_{rp} := \operatorname{diag}\left\{0, 0, 0, \frac{[2\zeta_4\delta\omega_4 + 2\delta\zeta_4(\omega_4 + \delta\omega_4)]s + 2\omega_4\delta\omega_4 + \delta\omega_4^2}{s^2 + as + b}, \ldots, \frac{[2\zeta_n\delta\omega_n + 2\delta\zeta_n(\omega_n + \delta\omega_n)]s + 2\omega_n\delta\omega_n + \delta\omega_n^2}{s^2 + as + b}\right\}, \tag{2.15}$$

and the perturbed factor $\tilde{\boldsymbol{N}}_{rp}$ is defined as

$$\tilde{\boldsymbol{N}}_{rp} := \tilde{\boldsymbol{N}} + \Delta \boldsymbol{N}_{rp}, \tag{2.16}$$

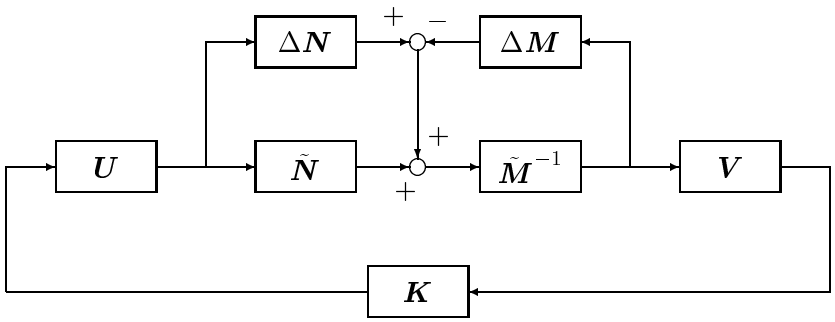

Figure 2.1: Feedback control of a perturbed LCF model.

where

$$\Delta \boldsymbol{N}_{rp} := \frac{\Delta B_1}{s^2 + as + b}. \tag{2.17}$$

Now let us consider the closed-loop stability of the system in Figure 2.1, where a controller $\boldsymbol{K}$ is connected as a feedback around a perturbed LCF. The operators $\boldsymbol{U}$ and $\boldsymbol{V}$ in the diagram are arbitrary transfer matrices such that no pole-zero cancellation occurs in $\overline{\mathbb{C}}_+$ when the product $\boldsymbol{V}(\tilde{\boldsymbol{M}} + \Delta \boldsymbol{M})^{-1}(\tilde{\boldsymbol{N}} + \Delta \boldsymbol{N})\boldsymbol{U}$ is formed. The purpose of this stability analysis is to introduce the weighting function $\boldsymbol{r}$ bounding the uncertainty in the factors. We will see that the magnitude of $\boldsymbol{r}$ on the imaginary axis limits our ability to design robust controllers. Define the uncertainty matrix

$$\boldsymbol{\Delta} := [\Delta \boldsymbol{N} \ -\Delta \boldsymbol{M}]. \tag{2.18}$$

Clearly, if $\Delta \boldsymbol{M}_{rp}$ and $\Delta \boldsymbol{N}_{rp}$ are substituted in (2.18), the resulting $\boldsymbol{\Delta}_{rp}$ belongs to $\mathcal{RH}_\infty$. This matrix is defined because the result on stability of the feedback system in Figure 2.1 is expressed in terms of a norm bound on $\boldsymbol{\Delta}(j\omega)$ ([34], [51]). Introduce an uncertainty set

$$\mathcal{D}_r := \{\boldsymbol{\Delta} \in \mathcal{RH}_\infty \ : \ \|\boldsymbol{r}^{-1}\boldsymbol{\Delta}\|_\infty < 1\}, \tag{2.19}$$

where $\boldsymbol{r}$ is a unit in $\mathcal{H}_\infty$. The small-gain theorem of Zames [55] and Sandberg [42] yields the following slightly modified result of [51] (see also [34]).

Theorem 1 *The closed-loop system of Figure 2.1 with controller $\boldsymbol{K}$ is internally stable for every $\boldsymbol{\Delta} \in \mathcal{D}_r$ iff*

(a) $\boldsymbol{K}$ internally stabilizes $\boldsymbol{VGU}$, and

(b) $$\left\| \boldsymbol{r} \begin{bmatrix} \boldsymbol{UKV}(I - \boldsymbol{GUKV})^{-1}\tilde{\boldsymbol{M}}^{-1} \\ (I - \boldsymbol{GUKV})^{-1}\tilde{\boldsymbol{M}}^{-1} \end{bmatrix} \right\|_\infty \leq 1.$$

Sketch of Proof Define a new input signal by stacking up the inputs of $\Delta\boldsymbol{N}$ and $\Delta\boldsymbol{M}$. This new signal is the input to the perturbation $\boldsymbol{\Delta}$ defined in (2.18). Then the block diagram can be redrawn as a feedback interconnection of $\boldsymbol{\Delta}$ and the transfer matrix appearing in part (b) of the theorem statement. The small-gain theorem can then be applied to this equivalent feedback system, see [34] for details of a proof along those lines. ■

Condition (b) in Theorem 1 says that the larger the magnitude of $\boldsymbol{r}$ on the imaginary axis, the more difficult it is to design a stabilizing controller that would be robust to all factor perturbations $\boldsymbol{\Delta} \in \mathcal{D}_r$. Thus, given the parametric uncertainty in (2.11), it is desirable to find a bound $|\boldsymbol{r}(j\omega)|$ which would tightly cover $\|\boldsymbol{\Delta}_{rp}(j\omega)\|$. But before this weighting function is constructed, different scalings must be performed on the factors and their perturbations to avoid any undue conservativeness and to balance the perturbations, i.e., to minimize the difference between the ∞-norms of $\Delta\boldsymbol{N}_{rp}$ and $\Delta\boldsymbol{M}_{rp}$.

2.3.1 Scaling the factors and their perturbations

The first scaling aims at making the components of the rows and columns of B_1 have the same order of magnitude. First write B_1 as a set of column vectors as follows,

$$B_1 = [v_1 \; v_2 \; \cdots \; v_m]\,. \tag{2.20}$$

Let $\beta_j := \|v_j\|_\infty$ and form $J_2 := \mathrm{diag}\{\beta_1, \ldots, \beta_m\}$. Now express the product $B_1 J_2^{-1}$ as a set of row vectors: $B_1 J_2^{-1} = \begin{bmatrix} u_1 \\ u_2 \\ \vdots \\ u_n \end{bmatrix}$. Define $\alpha_i := \|u_i\|_\infty$ and form $J_1 := \mathrm{diag}\{\alpha_1, \ldots, \alpha_n\}$. Let $\gamma := \|J_1^{-1} L_B J_2^{-1}\|$ and define the scaled matrices $B_{sc} := \gamma^{-1} J_1^{-1} B_1 J_2^{-1}$ and $\Delta B_{sc} := \gamma^{-1} J_1^{-1} \Delta B_1 J_2^{-1}$. For all ΔB_1 satisfying the inequalities in (2.11), $\|\Delta B_{sc}\| \leq 1$.

Proof: $|[\Delta B_1]_{ij}| \leq [L_B]_{ij}$, and since $J_1, J_2 \geq 0$ are diagonal, we have $|[J_1^{-1}\Delta B_1 J_2^{-1}]_{ij}| \leq [J_1^{-1} L_B J_2^{-1}]_{ij}$. Then [23, §8.1], $\|J_1^{-1}\Delta B_1 J_2^{-1}\| \leq \|J_1^{-1} L_B J_2^{-1}\| = \gamma$.

Finally, we can define the scaled factor

$$\tilde{\boldsymbol{N}}_0 := b\gamma^{-1}J_1^{-1}\tilde{\boldsymbol{N}}J_2^{-1} = \frac{bB_{sc}}{s^2+as+b}, \tag{2.21}$$

and the scaled factor perturbation produced by perturbations of the entries of B_1

$$\Delta\boldsymbol{N}_{rp0} := b\gamma^{-1}J_1^{-1}\Delta\boldsymbol{N}_{rp}J_2^{-1} = \frac{b\Delta B_{sc}}{s^2+as+b}, \tag{2.22}$$

The second scaling is performed on $\tilde{\boldsymbol{M}}$ to make sure that the norm of any perturbation of it induced by variations in the modal parameters is less than or equal to one, but close to one at low frequencies. Let $c_i := 2\zeta_i l_\omega^i + 2l_\zeta^i(\omega_i + l_\omega^i)$ and $d_i := 2\omega_i l_\omega^i + l_\omega^{i2}$ for $i = 4, \ldots, n$. These constants are the coefficients of the numerator of the (i,i) entry of $\Delta\boldsymbol{M}_{rp}$ in (2.15) when all modal perturbations are replaced by their upper bounds. Compute $c_{max} := \max_{i=4,\ldots,n} c_i$ and $d_{max} := \max_{i=4,\ldots,n} d_i$. We can now define the second scaled factor,

$$\tilde{\boldsymbol{M}}_0 := \frac{b}{d_{max}}\tilde{\boldsymbol{M}}, \tag{2.23}$$

and the corresponding scaled factor perturbation produced by modal perturbations,

$$\Delta\boldsymbol{M}_{rp0} := \frac{b}{d_{max}}\Delta\boldsymbol{M}_{rp}. \tag{2.24}$$

Remark 2.3 If d_{max} is large compared to the other d_i's, then some of the singular values of $\tilde{\boldsymbol{M}}_0(j\omega)$ may be smaller than the largest singular value of $\Delta\boldsymbol{M}_{rp0}(j\omega)$ at low frequencies. This occurs when some of the modes are at higher frequencies than the main cluster, and makes the robust controller design problem more difficult. Hence, if it is found that those high-frequency modes do not have much influence in the plant model's input-output characteristics, e.g., by plotting the singular values of the plant model versus frequency, their corresponding factors d_i and c_i should not be used in the definitions of d_{max} and c_{max}.

These two scalings are best illustrated by a sequence of block diagrams, Figure 2.2, showing the transformations performed on the coprime factors and their perturbations. We have included a block for the diagonal transfer matrix $\boldsymbol{T}_a$ which models actuator dynamics. Note that the properties of linearity and commutativity of diagonal matrices are used in order to move blocks around and get the desired final block diagram.

It is easy to check that $\tilde{\boldsymbol{N}}_0$ and $\tilde{\boldsymbol{M}}_0$ are still coprime and that they form an LCF of $\boldsymbol{G}_0 := d_{max}\gamma^{-1}J_1^{-1}\boldsymbol{G}J_2^{-1}$. It is our experience that these types of scalings help a lot in reducing

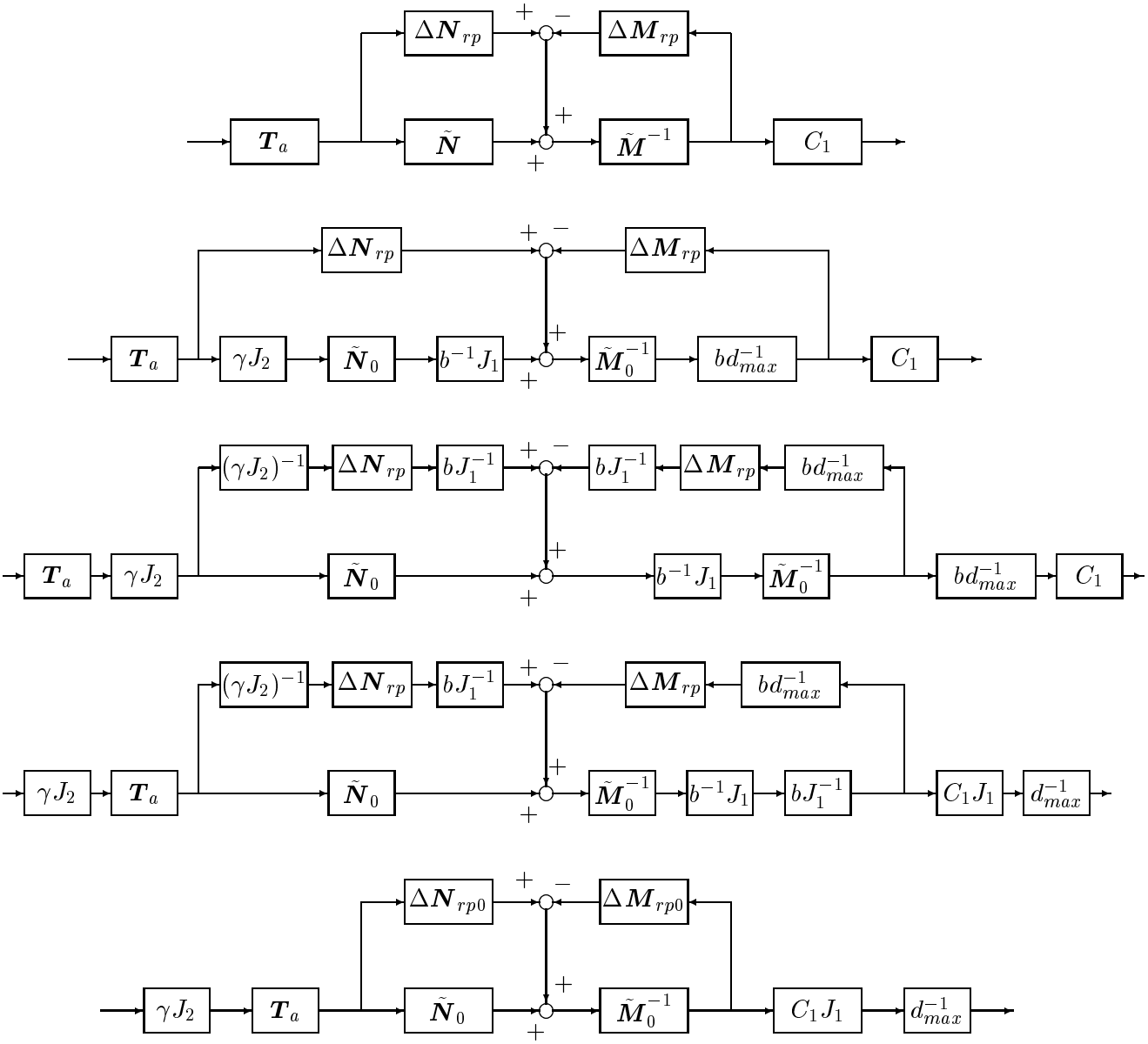

γJ_2 and d_{max}^{-1} may be absorbed by the controller.

Figure 2.2: Sequence of transformations applied on the perturbed factors.

the $\mathcal{H}_\infty$ norm of the generalized plant's weighted transfer matrix in an actual controller design. The last scaling performed on the perturbation $\boldsymbol{\Delta}_{rp0} := [\Delta \boldsymbol{N}_{rp0} \;\; -\Delta \boldsymbol{M}_{rp0}]$ normalizes it with the weighting function $\boldsymbol{r}(s)$ to get $\|\tilde{\boldsymbol{\Delta}}_{rp0}\| < 1$. This is illustrated in Figure 2.3. We will call the perturbation $\tilde{\boldsymbol{\Delta}}_{rp0}$ the *worst-case factor perturbation* induced by variations in the modal parameters when all perturbations of the modal parameters are replaced by their upper bounds in (2.11). It is a worst-case perturbation in the sense that of all factor perturbations induced by variations in the modal parameters, it has the highest norm on the imaginary axis.

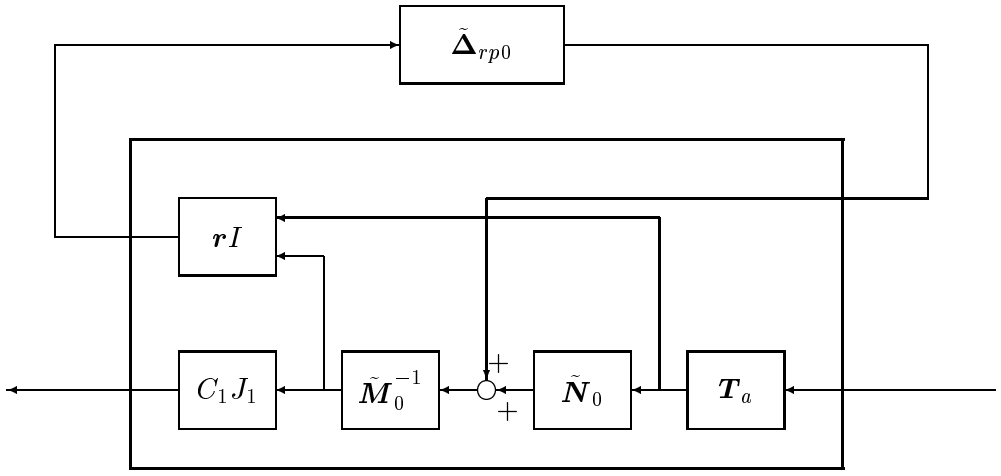

Figure 2.3: Perturbed factorization after all three scalings.

We are now ready to design a weighting function $\boldsymbol{r}$ for the scaled perturbation $\boldsymbol{\Delta}_{rp0}$. In doing so, the freedom provided by coefficients of the common denominator $s^2 + as + b$ will be used to our advantage to keep the order of $\boldsymbol{r}$ as low as possible without paying the price of added conservativeness. Here is the result.

Proposition 2 *For $k > 0$, define a and b via $s^2 + as + b := \left(s + \frac{d_{max}}{c_{max}}\right)(s + k)$ and let the unit weighting function $\boldsymbol{r}$ be given by $\boldsymbol{r}(s) = \frac{\epsilon_1 s + \sqrt{2} + \epsilon_0}{(s/k+1)}$, where ϵ_0 and ϵ_1 are small positive numbers. Then $\|\boldsymbol{r}^{-1}\boldsymbol{\Delta}_{rp0}\|_\infty < 1$.*

Proof An upper bound on $\|\boldsymbol{\Delta}_{rp0}(j\omega)\|$ at each $\omega \in [0, \infty]$ is given by

$$\|\boldsymbol{\Delta}_{rp0}(j\omega)\| \leq \sqrt{2}\max\{\|\Delta \boldsymbol{N}_{rp0}(j\omega)\|, \|\Delta \boldsymbol{M}_{rp0}(j\omega)\|\}.$$

But

$$\begin{aligned}\|\Delta \boldsymbol{N}_{rp0}(j\omega)\| &= \left\| \frac{\frac{kd_{max}}{c_{max}}\Delta B_{sc}}{\left(j\omega + \frac{d_{max}}{c_{max}}\right)(j\omega + k)} \right\| \\ &\leq \left| \frac{\frac{kd_{max}}{c_{max}}}{\left(j\omega + \frac{d_{max}}{c_{max}}\right)(j\omega + k)} \right|,\end{aligned}$$

and similarly,

$$\begin{aligned}\|\Delta \boldsymbol{M}_{rp0}(j\omega)\| &\leq \left\| \frac{\frac{kd_{max}}{c_{max}}}{\left(j\omega + \frac{d_{max}}{c_{max}}\right)(j\omega + k)} \operatorname{diag}\left\{0, 0, 0, \frac{c_4 j\omega + d_4}{d_{max}}, \ldots, \frac{c_n j\omega + d_n}{d_{max}}\right\} \right\| \\ &\leq \left| \frac{\frac{kd_{max}}{c_{max}}}{\left(j\omega + \frac{d_{max}}{c_{max}}\right)(j\omega + k)} \right| \cdot \max_{i=4,\ldots,n} \frac{|c_i j\omega + d_i|}{d_{max}} \\ &\leq \left| \frac{\frac{kd_{max}}{c_{max}}}{\left(j\omega + \frac{d_{max}}{c_{max}}\right)(j\omega + k)} \right| \cdot \left| \frac{c_{max}}{d_{max}} j\omega + 1 \right|.\end{aligned}$$

Hence,

$$\begin{aligned}\|\boldsymbol{\Delta}_{rp0}(j\omega)\| &\leq \frac{\frac{\sqrt{2}kd_{max}}{c_{max}}}{\left|j\omega + \frac{d_{max}}{c_{max}}\right| \cdot |j\omega + k|} \max\left\{1, \left|\frac{c_{max}}{d_{max}} j\omega + 1\right|\right\} \\ &= \frac{\frac{\sqrt{2}kd_{max}}{c_{max}}}{\left|j\omega + \frac{d_{max}}{c_{max}}\right| \cdot |j\omega + k|} \left|\frac{c_{max}}{d_{max}} j\omega + 1\right| \\ &= \frac{\sqrt{2}}{\left|\frac{j\omega}{k} + 1\right|} < |\boldsymbol{r}(j\omega)|.\end{aligned}$$

Since $\boldsymbol{r}$ is a unit, it follows that $\|\boldsymbol{r}^{-1}\boldsymbol{\Delta}_{rp0}\|_\infty < 1$. ■

Remark 2.4 This weighting function is of first order, which is a benefit considering that it will be duplicated $m + n$ times in the generalized plant of Figure 5.1. By construction, for small ϵ_0, ϵ_1, $|\boldsymbol{r}(j\omega)|$ is a relatively tight bound on $\|\boldsymbol{\Delta}_{rp0}(j\omega)\|$, especially at low and high frequencies.

With the unit $\boldsymbol{r}$ given by Proposition 2, the factor perturbation $\boldsymbol{\Delta}_{rp0}$ belongs to the uncertainty set $\mathcal{D}_r$ and the normalized $\tilde{\boldsymbol{\Delta}}_{rp0}$ belongs to $\mathcal{BRH}_\infty^{n\times(m+n)}$. Now introduce a normalized scaled perturbation $\tilde{\boldsymbol{\Delta}}_0 \in \mathcal{BRH}_\infty^{n\times(m+n)}$. Then letting $\boldsymbol{\Delta}_0 := \boldsymbol{r}\tilde{\boldsymbol{\Delta}}_0$, one obtains that $\boldsymbol{\Delta}_0$ is a free perturbation in $\mathcal{RH}_\infty^{n\times(m+n)}$ with $\|\boldsymbol{\Delta}_0(j\omega)\| < |\boldsymbol{r}(j\omega)|$, $\forall\omega \in \mathbb{R}$, i.e., $\boldsymbol{\Delta}_0$ is an arbitrary element in $\mathcal{D}_r$. This way, the weighting function $\boldsymbol{r}$ can be included in the generalized plants

of Figures 2.3 and 5.1. Figure 5.1 shows the scaled closed-loop system with all the weights for designing a controller $\boldsymbol{K}$ providing robust stability and nominal performance. Notice that the control input is u_{sc}, a scaled version of u. This block diagram and the associated control design problem will be discussed in Chapters 5 and 6. According to Theorem 1, our robust stability objective will be to minimize the ∞-norm of the map $w \mapsto z_1$ to a value no more than 1 over all stabilizing controllers.

2.4 Summary

In this chapter, we have introduced a left-coprime factorization in $\mathcal{H}_\infty$ of LFSS dynamics, together with a factor uncertainty bound $\boldsymbol{r}$. This bound has the property that the corresponding family of perturbed plants contains all LFSS plant models induced by variations in the modal parameters within some a priori known bounds. It is also not too conservative in the sense that it tightly covers the worst-case factor perturbations induced by variations in the modal parameters. The factor uncertainty model can account for unmodeled dynamics as well, such as unmodeled modes or modeled modes not present in the plant. It can also account for uncertain actuator dynamics.

Given a family of perturbed left-coprime factor models of LFSS dynamics, one can design robust controllers providing stability or some desired performance level for all plant models in the family. Design techniques achieving such goals will be discussed in Chapters 5 and 6. Chapters 3 and 4 discuss the possibility of improving the bound $\boldsymbol{r}$ given respectively open-loop and closed-loop frequency-response data obtained on the plant.

Chapter 3

Consistency of Experimental Open-Loop Frequency-Response Data with Coprime Factor Models

This chapter addresses the problem of checking consistency of open-loop experimental frequency-response data with perturbed coprime factor plant descriptions. The results are applicable to LCF models of LFSS introduced in Chapter 2, but also more generally to any coprime factorization of a plant model, normalized or not.

3.1 Introduction

The general model/data consistency problem is this: Given some experimental data obtained by running open-loop or closed-loop experiments on the system, show that these (possibly noisy) data are consistent with a family of perturbed plant models. In other words, do there exist a perturbation and a noise belonging to the uncertainty and noise sets such that the input-output data can be reproduced by the perturbed model? A mathematical formulation of this problem is given in the next section.

We treat the case where we have N frequency-response data points to test the model. The open-loop noise-free and noisy SISO and MIMO cases are studied, and complete solutions to the open-loop noise-free MIMO and noisy SISO consistency problems are given. The closed-loop noise-free MIMO and noisy SISO cases will be studied in the next chapter.

If frequency-response experiments are performed on an experimental testbed with flexibilities or an actual LFSS, then the results presented in this chapter and in Chapter 4 are of interest to obtain better uncertainty models. That is, the bound $|\boldsymbol{r}(j\omega)|$ introduced in Proposition 2 can be shaped using the consistency theorems so that it covers the uncertainty in the actual plant in a more realistic manner.

3.2 Problem Formulation

This section introduces a general model/data consistency problem and then specializes it to coprime factorizations. The formulation includes as special cases all the problems considered in this chapter. Define an experiment as follows: Apply an input to the system, and record the input and the resulting output.

The general model/data consistency problem is comprised of (i) a set $\mathcal{M}$ of N experiments, (ii) a set $\mathcal{W}$ of noise signals, (iii) a nominal model $\boldsymbol{T}$, and (iv) an uncertainty set $\mathcal{D}$. The noise affects the measurements in a specified way, and uncertainty in the plant model has a specified structure (e.g., additive, multiplicative, etc.) Note that the experiments can be open-loop or closed-loop, and hence $\boldsymbol{T}$ may be an open-loop or a closed-loop model. The general problem is formulated as follows:

Problem 1 *Given the sets $\mathcal{M}$, $\mathcal{W}$, $\mathcal{D}$ and a nominal model $\boldsymbol{T}$, do there exist a fixed perturbation $\boldsymbol{\Delta} \in \mathcal{D}$ of $\boldsymbol{T}$ and a subset $\mathcal{V} \subset \mathcal{W}$ of N noise signals, one for each experiment, such that the experiments $\mathcal{M}$ can be reproduced with $\boldsymbol{T}$ perturbed by $\boldsymbol{\Delta}$ together with the noises $\mathcal{V}$?*

Note that this problem is weaker than the model validation problem where one seeks to validate the model triple ($\boldsymbol{T}$, $\mathcal{D}$, $\mathcal{W}$) using the measurements $\mathcal{M}$. As a matter of fact, this latter problem was abandoned when the English philosopher Karl Popper [40] showed that a model can never be validated using a finite set of data. The best one can do is to show that the model triple ($\boldsymbol{T}$, $\mathcal{D}$, $\mathcal{W}$) is not invalidated by the experimental data $\mathcal{M}$, and this is what the model/data consistency problem is all about [39], [47]. A negative answer to Problem 1 forces us to modify $\boldsymbol{T}$ and $\mathcal{D}$ until we get consistency. In that sense, our knowledge of the system increases. Note that the noise set $\mathcal{W}$ is usually a hard constraint that we have to live with; more on this in Section 3.3.

Let us now specialize Problem 1 to finite-dimensional linear time-invariant $\boldsymbol{T}$, which would be the plant model $\boldsymbol{G}$ of which we have a coprime factorization in $\mathcal{RH}_\infty$ in the open-loop case. $\boldsymbol{T}$ would be some closed-loop transfer matrix incorporating $\boldsymbol{G}$ in the closed-loop case. In this case, only the plant model $\boldsymbol{G}$ is assumed to be uncertain in the closed-loop transfer matrix.

The data set $\mathcal{M}$ is a set of N complex matrices (or complex scalars for SISO systems) obtained by running open or closed-loop frequency-response experiments at N distinct frequencies. Each entry (i,j) of one of these matrices is a complex number whose magnitude and phase represent respectively the gain and phase of the plant from the j^{th} input to the i^{th} output at the corresponding frequency. The noise set $\mathcal{W}$ is composed of complex matrices with magnitude-bounded entries, of the same dimensions as the plant model in the open-loop case, or the closed-loop transfer matrix in the closed-loop case. Each entry (i,j) of a matrix in $\mathcal{W}$ represents a complex additive perturbation of the corresponding entry of the nominal frequency response matrix $\boldsymbol{T}(j\omega)$ at frequency ω. Finally, the uncertainty set $\mathcal{D}$ is composed of norm-bounded factor perturbations in $\mathcal{RH}_\infty$.

Let the nominal plant model $\boldsymbol{G}$ be a proper real-rational transfer matrix. Let $\tilde{\boldsymbol{M}}$ and $\tilde{\boldsymbol{N}}$ in $\mathcal{RH}_\infty$ be left-coprime, C be a real output matrix and $\boldsymbol{J}$ be a diagonal input transfer matrix in $\mathcal{RH}_\infty$ such that the nominal plant model can be factorized as $\boldsymbol{G} = C\tilde{\boldsymbol{M}}^{-1}\tilde{\boldsymbol{N}}\boldsymbol{J}$. The matrices C and $\boldsymbol{J}$ are included for compatibility with the special factorization for large flexible space structures introduced in Chapter 2. When set to identity matrices, a standard left-coprime factorization of $\boldsymbol{G}$ is obtained. Let the perturbed plant model $\boldsymbol{G}_p$ be expressed as a perturbed factorization with $\tilde{\boldsymbol{M}}_p$, $\tilde{\boldsymbol{N}}_p \in \mathcal{RH}_\infty$

$$\boldsymbol{G}_p = C\tilde{\boldsymbol{M}}_p^{-1}\tilde{\boldsymbol{N}}_p\boldsymbol{J}, \tag{3.1}$$

where

$$\tilde{\boldsymbol{M}}_p = \tilde{\boldsymbol{M}} + \Delta\boldsymbol{M}, \quad \tilde{\boldsymbol{N}}_p = \tilde{\boldsymbol{N}} + \Delta\boldsymbol{N}, \quad \Delta\boldsymbol{M}, \Delta\boldsymbol{N} \in \mathcal{RH}_\infty \ .$$

Recall that the uncertainty matrix $\boldsymbol{\Delta} = [\Delta\boldsymbol{N} \ \ -\Delta\boldsymbol{M}]$ was defined in (2.18). Clearly $\boldsymbol{\Delta} \in \mathcal{RH}_\infty$. This matrix was introduced because the result on robust closed-loop internal stability of the system (see, e.g., [20] for a definition and treatment of internal stability) in Figure 2.1 for a perturbed coprime factor plant description is expressed in terms of a norm bound on $\boldsymbol{\Delta}(j\omega)$ [34], [51].

Consider the uncertainty set $\mathcal{D}_r$ as defined in (2.19), and define the family of plants

$$\mathcal{P} := \{\boldsymbol{G}_p \ : \ \boldsymbol{\Delta} \in \mathcal{D}_r\} \ , \tag{3.2}$$

where $\boldsymbol{r}$ is a unit in $\mathcal{RH}_\infty$. In the open-loop case, $\boldsymbol{r}$ is assumed small enough so that $\tilde{\boldsymbol{M}}_p$ is also a unit in $\mathcal{RH}_\infty$, that is, every $\boldsymbol{G}_p \in \mathcal{P}$ is stable. For this to hold, we will require in this chapter that

$$\text{(A3.1)}\quad \underline{\sigma}\left[\tilde{\boldsymbol{M}}(j\omega)\right] > |\boldsymbol{r}(j\omega)|,\ \forall \omega \in \mathbb{R} \cup \{\infty\}.$$

The unit $\boldsymbol{r}$ characterizes the size of the uncertainty in the coprime factors at each frequency ω because $\|\boldsymbol{r}^{-1}\boldsymbol{\Delta}\|_\infty < 1$ implies $\|\boldsymbol{\Delta}(j\omega)\| < |\boldsymbol{r}(j\omega)|$.

Theorem 1 on robust stability of a closed-loop system with a perturbed coprime factorization as in Figure 2.1 gives the main motivation to make $\boldsymbol{r}$ as small as possible. Indeed, condition (b) in the theorem is difficult to satisfy if $\boldsymbol{r}$ is large on the imaginary axis. On the other hand, a small $\boldsymbol{r}$ would make condition (b) easier to satisfy and provide some freedom to achieve some desired performance specifications. Note that here $\boldsymbol{U} = \boldsymbol{J}$ and $\boldsymbol{V} = C$.

In order to be able to use the result of Theorem 1 in the design of a robust controller for a real plant, one has to construct and modify the bound $|\boldsymbol{r}(j\omega)|$ until it properly captures the uncertainty in the physical system. One way to do this is to start with a nominal model and a first approximation for $\boldsymbol{r}$, and then use open-loop or closed-loop experimental data to check if $|\boldsymbol{r}(j\omega)|$ is large enough to account for the full data set. It can be made larger if necessary, but not too large to avoid making the model too conservative. It can also be made smaller to reduce the uncertainty at some frequencies. The consistency tests proposed in this chapter are suitable for that purpose when frequency-response data are available.

Note that it is assumed throughout that the plant is linear. We will consider the case of time-domain $\mathcal{L}_\infty$-bounded output noises corrupting the frequency-response measurements, and show that their effects can be modeled as complex noises in the frequency domain, i.e., the noise set $\mathcal{W}$. Mild nonlinearities or time-variances which would have an effect comparable to $\mathcal{L}_\infty$ noise in the time domain (such as a bias) cannot be detected, so checking consistency of the data with a linear model would be feasible in this case. But the interpretation and implications of the results are not studied here. However, an exception to this is the case of a nonlinearity at the output of an *open-loop* plant, which would have the same effect as additive $\mathcal{L}_\infty$-bounded output noise. For example, a quantizer at the output can be modeled as an additive output noise bounded in $\mathcal{L}_\infty$ and corrupting the output signal of a linear plant. In this case, the theory developed in this chapter is valid.

3.3 The Noise Model

The goal of this section is to show that time-domain $\mathcal{L}_\infty$-bounded additive output noise corrupting a frequency-response measurement at frequency ω can be modeled as a complex additive perturbation of $\boldsymbol{T}(j\omega)$.

A frequency-response experiment consists of exciting the system with a sine wave of a given frequency ω and recording the time-response of the output after the transients have died down. The input sinusoid is assumed to have unit amplitude. The noise affects the phase and zero-crossing readings on the recorded output signal as shown in Figure 3.1. This figure illustrates a purely hypothetical situation used to derive bounds on the additive amplitude uncertainty δA and the additive phase uncertainty $\delta\theta$. It is not meant to show a procedure to obtain bounds from experimental data. For instance, the sinusoidal envelope of the signal is impossible to obtain in practice.

We assume that this noise is any signal in $\mathcal{L}_\infty$ bounded in magnitude; thus the noise set $\mathcal{N}$ considered here is all scalar time-domain noises in $\mathcal{L}_\infty$ with norm bounded by M, i.e.,

$$\mathcal{N} := \{n \in \mathcal{L}_\infty \,:\, \|n\|_\infty < M\} \ . \tag{3.3}$$

Let A_m be the measured magnitude of the output signal and τ_m be any measured time-delay between the output signal and the input sinusoid at zero crossings. We have $A_m = A + \delta A$ and $\tau_m = \tau + \delta\tau$. The uncertainty in amplitude is then bounded by M,

$$|\delta A| \leq M \ , \tag{3.4}$$

and the uncertainty in phase $\delta\theta$ is derived by first characterizing the uncertainty $\delta\tau$ in the time-delay τ. A first-order approximation of the sine function around a zero crossing yields the bound:

$$|\delta\tau| \leq L_\tau, \qquad L_\tau = \frac{M}{A\omega}, \tag{3.5}$$

which leads to the following bound on the phase uncertainty:

$$|\delta\theta| \leq \omega L_\tau = \frac{M}{A} \leq \frac{M}{A_m - M} =: L_\theta.$$

This uncertainty in the magnitude and phase of a complex number is then approximated by a disk $\mathcal{W}_0$ in the complex plane. The measured frequency response of the system ϕ at frequency ω lies in $\mathcal{U}$, as shown in Figure 3.2.

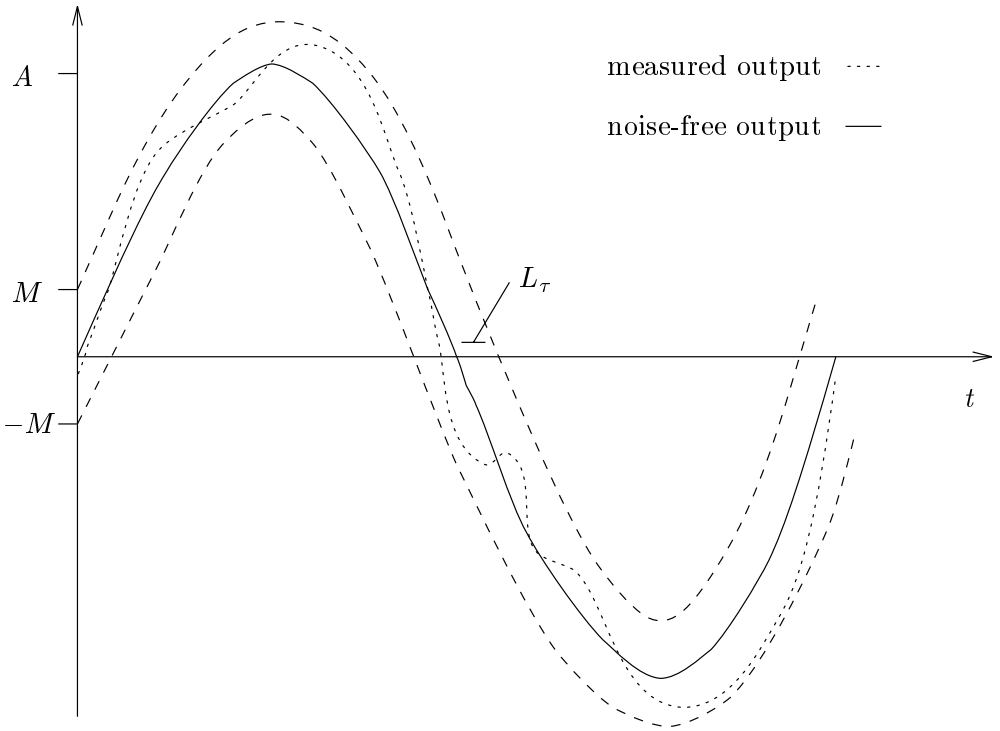

Figure 3.1: Recorded noisy output signal.

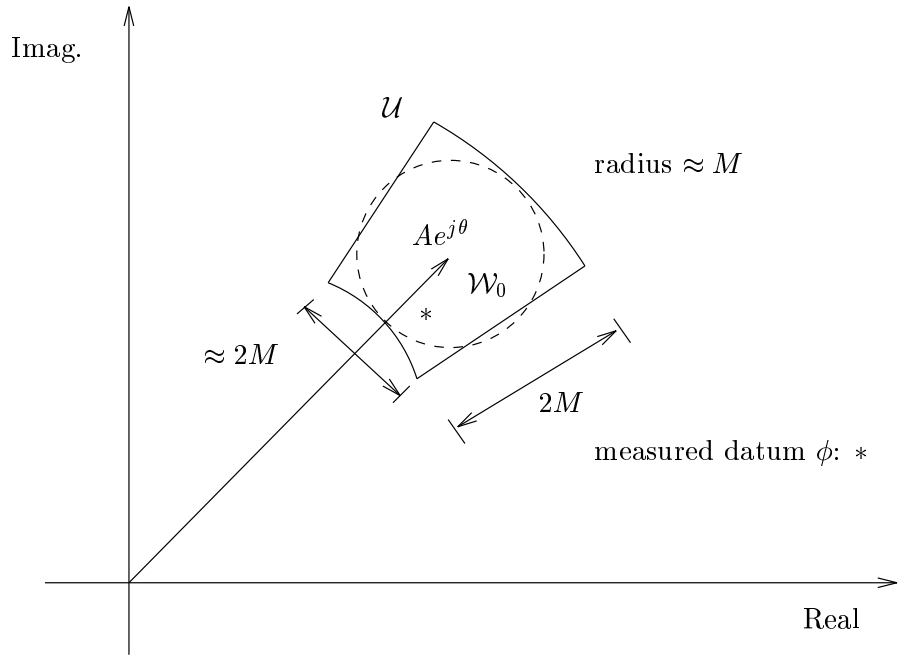

Figure 3.2: Uncertainty in the frequency response for one particular frequency.

Thus, for SISO plants, the corresponding frequency-domain noise set $\mathcal{W}$ that appears in the specialized version of Problem 1 above is the set of additive norm-bounded complex perturbations

$$\mathcal{W} := \{\delta_a \in \mathbb{C} \ : \ |\delta_a| < L_a\}, \tag{3.6}$$

where $L_a = M$ under the approximation that the uncertainty region containing the disk is square. This approximation makes sense if the $\mathcal{L}_\infty$ signal-to-noise ratio is sufficiently large, i.e., M is small compared to A_m (Figure 3.2). Note that $\mathcal{W}$ is just the disk $\mathcal{W}_0$ translated to the origin.

For MIMO plants, we assume that a noise $n_{ij} \in \mathcal{N}$ affects each output channel for each sinusoidal test input in the frequency-response experiment. This assumption is good if the noise has basically the same source for all the plant sensors. For example, noises caused by external vibrations in a mechanical system, or electrical noises affecting the sensors may be bounded by a unique constant for all outputs. Quantization noise may also be bounded in this way in the open-loop case, and in the closed-loop case where the quantizer would be external to the linear loop, e.g., part of a measuring device. The corresponding noise set $\mathcal{W}$ in the frequency domain is the set of additive complex perturbations whose entries are magnitude-bounded:

$$\mathcal{W} := \left\{\Delta_a \in \mathbb{C}^{p\times m} \ : \ |[\Delta_a]_{ij}| < L_a,\ i = 1, \ldots, p,\ j = 1, \ldots, m\right\}. \tag{3.7}$$

Here $L_a = M$ as in the SISO case. Note that L_a does not depend on the frequency ω or the amplitude of the output sinusoid, which is a nice property.

The introduction of the disk $\mathcal{W}_0$ is a bit conservative in the sense that it limits the effect of the noise in the complex plane to a subset of what it really is. Let us explain how this conservativeness is introduced. Suppose that for the SISO case, $\boldsymbol{r} \equiv 0$ and the measured complex number ϕ lies outside of the disk $\mathcal{W}_0$, but inside the uncertainty set $\mathcal{U}$. Then this datum is not consistent with our plant and noise models, but $|\boldsymbol{r}(j\omega)|$ can be increased, at the price of added conservativeness, until an admissible factor perturbation together with a noise in $\mathcal{W}$ will account for it. On the other hand, had we chosen to approximate $\mathcal{U}$ by a disk covering it, then a measured datum lying inside the disk but outside of $\mathcal{U}$ could be concluded to be consistent with the plant and noise models, even though it is not. The noise set $\mathcal{U}$ is a hard constraint that cannot be enlarged without risking an erroneous conclusion of consistency. This might lead to instability of a closed-loop system with a controller designed using the model. We can, however, consider a subset of $\mathcal{U}$ that will make the problem more tractable, as we did

by choosing $\mathcal{W}_0$.

3.4 Consistency with Open-Loop Frequency-Response Measurements

3.4.1 Noise-Free Case

3.4.1.1 Standard Factorization

Suppose we are given a family of m-input, p-output stable plants $\mathcal{P}$ as in (3.2) with $C = I_p$ and $\boldsymbol{J} = I_m$, and a set of noise-free, open-loop frequency-response data. In this section, we derive a necessary and sufficient condition for consistency of these data with the family of plants $\mathcal{P}$. The exact statement of the open-loop noise-free model/data consistency problem considered here is the following.

Problem 2 *Given noise-free, open-loop frequency-response data* $\{\Phi_i\}_{i=1}^N \subset \mathbb{C}^{p\times m}$ *of an* m*-input,* p*-output plant obtained at the distinct frequencies* $\omega_1, \ldots, \omega_N$*, could the data have been produced by at least one model in* $\mathcal{P}$*? Or, in other words, does there exist a fixed* $\boldsymbol{\Delta} \in \mathcal{D}_r$ *such that the corresponding perturbed model* $\boldsymbol{G}_p$ *interpolates the complex matrices* $\{\Phi_i\}_{i=1}^N$ *at* $j\omega_1, \ldots, j\omega_N$*?*

Premultiplying (3.1) by $\tilde{\boldsymbol{M}} + \Delta\boldsymbol{M}$ and taking $\Delta\boldsymbol{M}$ and $\Delta\boldsymbol{N}$ onto the left-hand side, we get

$$\Delta\boldsymbol{M}\boldsymbol{G} - \Delta\boldsymbol{N} = \tilde{\boldsymbol{N}} - \tilde{\boldsymbol{M}}\boldsymbol{G} \,. \tag{3.8}$$

Let $U := (\tilde{\boldsymbol{N}} - \tilde{\boldsymbol{M}}\boldsymbol{G})(j\omega)$, $W := \begin{bmatrix} -I_m \\ -\boldsymbol{G} \end{bmatrix}(j\omega)$ and $\Delta := \boldsymbol{\Delta}(j\omega)$. Then (3.8) at frequency ω can be written as

$$\Delta W = U \,, \tag{3.9}$$

where $W \in \mathbb{C}^{(m+p)\times m}$, $U \in \mathbb{C}^{p\times m}$, and $\Delta \in \mathbb{C}^{p\times(m+p)}$. Equation (3.9) is just an underdetermined system of linear equations over the field $\mathbb{C}$.

Let $\Delta_i = \boldsymbol{\Delta}(j\omega_i)$ for $i = 1, \ldots, N$, with similar definitions for W_i and U_i. We seek a test that would show whether or not there exists a rational matrix $\boldsymbol{\Delta}$ that belongs to the uncertainty set $\mathcal{D}_r$ and satisfies the interpolation constraints given by (3.9) at the distinct frequencies

$\{\omega_1, \ldots, \omega_N\}$. This is done in two steps: First, with $\boldsymbol{G}(j\omega_i) = \Phi_i$ solve the matrix equation (3.9) for Δ_i, $i = 1, \ldots, N$, such that Δ_i has minimum norm. Note that $U_i^* \subset \mathrm{Ra}\{W_i^*\}$, so there exist an infinity of solutions to (3.9) and a minimum-norm solution can always be computed. For instance, the matrix W_i has full column rank, so a minimum-norm solution Δ_i to (3.9) is given by the premultiplication of the Moore-Penrose left-inverse of W_i by U_i:

$$\Delta_i = U_i(W_i^* W_i)^{-1} W_i^* \ . \tag{3.10}$$

If the norm of Δ_i is greater than or equal to $|\boldsymbol{r}(j\omega_i)|$ for some $i \in \{1, \ldots, N\}$, then the test fails: The family of coprime factorizations cannot account for the frequency-response data. If $\|\Delta_i\| < |\boldsymbol{r}(j\omega_i)|$, $\forall i \in \{1, \ldots, N\}$, then we must show that there exists a matrix-valued function $\boldsymbol{\Delta} \in \mathcal{RH}_\infty$ taking on the complex matrix values $\{\Delta_i\}_{i=1}^N$ at the frequencies $\{\omega_i\}_{i=1}^N$ and such that $\|\boldsymbol{\Delta}(j\omega)\| < |\boldsymbol{r}(j\omega)|$, $\forall \omega \in \mathbb{R}$. Those are the two steps in the proof of the main result of this section, which goes as follows.

Theorem 2 *The noise-free open-loop MIMO CF model/data consistency problem (Problem 2) has a positive answer iff* $\|\Delta_i\| < |\boldsymbol{r}(j\omega_i)|$ *for all* $i = 1, \ldots, N$.

A few results must be introduced before the proof of Theorem 2 can be presented.

The interpolation problem at hand can be scaled as follows: Find a function $\boldsymbol{\Psi} \in \mathcal{RH}_\infty$ interpolating the product $\boldsymbol{r}^{-1}(j\omega_i)\Delta_i$ at $s = j\omega_i$, $i = 1, \ldots, N$ and such that $\|\boldsymbol{\Psi}\|_\infty < 1$. The interpolation problem in $\mathcal{RH}_\infty$ of the right half-plane is then transformed to an interpolation problem in $\mathcal{RH}_\infty(\mathbb{D})$ by using the one-to-one scalar bilinear transformation $s \mapsto z$ defined by $z = (1-s)/(1+s)$ which maps the closed right half-plane onto the closed unit disk $\overline{\mathbb{D}}$. Thus the boundary interpolation problem can be stated as

Problem 3 *Given a set of distinct points* $\{e^{j\theta_i}\}_{i=1}^r$ *on the unit circle* $\partial\mathbb{D}$ *and a set* $\{\tilde{\Psi}_i\}_{i=1}^r$ *in* $\mathbb{C}^{m\times n}$ *satisfying* $\|\tilde{\Psi}_i\| < 1$ *for* $i = 1, \ldots, N$, $\tilde{\Psi}_l = (\tilde{\Psi}_j^*)^T$ *for* $\theta_l = -\theta_j$, *and* $\tilde{\Psi}_k \in \mathbb{R}^{m\times n}$ *for* $\theta_k = 0, \pi$, *does there exist a function* $\tilde{\boldsymbol{\Psi}} \in \mathcal{RH}_\infty(\mathbb{D})$, $\|\tilde{\boldsymbol{\Psi}}\|_\infty < 1$ *such that* $\tilde{\boldsymbol{\Psi}}(e^{j\theta_i}) = \tilde{\Psi}_i$ $i = 1, \ldots, r$ *?*

To solve Problem 3, a classical result on interpolation in $\mathbb{D}$ from Fedčina [17] (see also [12]) is needed. A modified version of it in [51, Theorem 71] leads to a corollary that gives a necessary and sufficient condition for the following matrix Nevanlinna-Pick problem to have a solution:

Problem 4 *Given a set of distinct points* $\{z_i\}_{i=1}^r$ *in* $\mathbb{D}$ *and a set* $\{\Theta_i\}_{i=1}^r$ *in* $\mathbb{C}^{p\times p}$ *satisfying* $\|\Theta_i\| < 1$, $i = 1,\ldots,r$, $\Theta_l = (\Theta_j^*)^T$ *for* $z_l = z_j^*$, *and* $\Theta_k \in \mathbb{R}^{p\times p}$ *for* $z_k \in (-1,1)$, *does there exist a matrix* $\mathbf{\Theta} \in \mathcal{BRH}_\infty(\mathbb{D})^{p\times p}$ *such that* $\mathbf{\Theta}(z_i) = \Theta_i$, $i = 1,\ldots,r$ *?*

The result derived from [51, Theorem 71] goes as follows:

Theorem 3 *Problem 4 has a solution iff the block-Pick matrix* P *is positive definite, where*

$$P := \begin{bmatrix} \frac{I-\Theta_1^*\Theta_1}{1-z_1^*z_1} & \cdots & \frac{I-\Theta_1^*\Theta_r}{1-z_1^*z_r} \\ \vdots & \ddots & \vdots \\ \frac{I-\Theta_r^*\Theta_1}{1-z_r^*z_1} & \cdots & \frac{I-\Theta_r^*\Theta_r}{1-z_r^*z_r} \end{bmatrix} . \tag{3.11}$$

Proof Theorem 71 in [51] says that there exists a function $\mathbf{\Theta} \in \mathcal{BCH}_\infty(\mathbb{D})^{p\times p}$ interpolating the matrices Θ_i as given in Problem 4 iff P is positive definite. This result is equivalent to the theorem statement for Problem 4 modified so that $\mathbf{\Theta}$ is allowed to be in $\mathcal{BCH}_\infty(\mathbb{D})^{p\times p}$, the space of $p\times p$ complex-rational matrices in $\mathcal{H}_\infty(\mathbb{D})$. Based on this, we are ready to prove the two implications in the theorem statement.

Sufficiency If P is positive definite, then there exists $\mathbf{\Phi}$ in $\mathcal{BCH}_\infty(\mathbb{D})^{p\times p}$ such that $\mathbf{\Phi}(z_i) = \Theta_i$, $i = 1,\ldots,N$. Let $\underline{\mathbf{\Phi}}(z)$ denote the complex-rational matrix-valued function $\mathbf{\Phi}(z)$ with its coefficients replaced by their complex conjugates. Define the function

$$\mathbf{\Theta}(z) := \frac{1}{2}\left[\mathbf{\Phi}(z) + \underline{\mathbf{\Phi}}(z)\right].$$

Note that $\mathbf{\Theta}(z) \in \mathcal{BRH}_\infty(\mathbb{D})^{p\times p}$ and it interpolates the matrices Θ_i as we now show:

$$\begin{aligned} \mathbf{\Theta}(z_i) &:= \frac{1}{2}\left[\mathbf{\Phi}(z_i) + \underline{\mathbf{\Phi}}(z_i)\right] \\ &= \frac{1}{2}\left\{\Theta_i + [\mathbf{\Phi}(z_i^*)^*]^T\right\} \\ &= \frac{1}{2}\left(\Theta_i + \left\{[(\Theta_i^*)^T]^*\right\}^T\right) \\ &= \Theta_i. \end{aligned}$$

Necessity Suppose P is not positive definite. Then by Theorem 71 in [51], there exists no function in $\mathcal{BCH}_\infty(\mathbb{D})^{p\times p}$ interpolating the Θ_i's. It follows that there exists no function in $\mathcal{BRH}_\infty(\mathbb{D})^{p\times p}$ interpolating these same matrices as $\mathcal{BRH}_\infty(\mathbb{D})^{p\times p} \subset \mathcal{BCH}_\infty(\mathbb{D})^{p\times p}$. ■

For interpolation points on the unit circle $\partial\mathbb{D}$, it is not possible to use Theorem 3 directly. Consider the mapping $g_\epsilon : \mathbb{C} \to \mathbb{C}$ defined by $g_\epsilon(z) := z/(1+\epsilon)$, $z \in \mathbb{C}$, $\epsilon > 0$. Now define the open disk of radius $1+\epsilon$

$$\mathbb{D}_{1+\epsilon} := \{z \ : \ |z| < 1+\epsilon\}, \tag{3.12}$$

and consider the class $\mathcal{BRH}_\infty(\mathbb{D}_{1+\epsilon})^{p\times p}$ of square matrix-valued, real-rational functions analytic and with norm less than one on $\mathbb{D}_{1+\epsilon}$.

Lemma 1 *For ϵ small enough, there exists a function in $\mathcal{BRH}_\infty(\mathbb{D}_{1+\epsilon})^{p\times p}$ solving Problem 4 modified such that the interpolation points $\{z_i\}_{i=1}^r$ are on the unit circle.*

The proof requires the following proposition from [23, p. 367, ex. 2].

Proposition 3 *Let $A \in \mathbb{C}^{q\times q}$, $E \in \mathbb{C}^{q\times q}$ be both Hermitian. Let $\lambda_1 \le \cdots \le \lambda_q$ be the ordered eigenvalues of A and $\hat\lambda_1 \le \cdots \le \hat\lambda_q$ be the ordered eigenvalues of $A+E$. Then $|\lambda_k - \hat\lambda_k| \le \rho(E)$, $k = 1, \ldots, q$.*

Proof of Lemma 1 Apply g_ϵ to $z_i \in \partial\mathbb{D}$ to get $\{\tilde z_i(\epsilon) := z_i/(1+\epsilon)\}_{i=1}^r$. Construct the block-Pick matrix for Problem 4 but for the $\tilde z_i(\epsilon)$'s in $\mathbb{D}$ instead of the z_i's on the unit circle:

$$P = \begin{bmatrix} \frac{(I-\Theta_1^*\Theta_1)(1+\epsilon)^2}{\epsilon(2+\epsilon)} & \frac{(I-\Theta_1^*\Theta_2)(1+\epsilon)^2}{(1+\epsilon)^2 - z_2 z_1^*} & \cdots & \frac{(I-\Theta_1^*\Theta_r)(1+\epsilon)^2}{(1+\epsilon)^2 - z_r z_1^*} \\ \frac{(I-\Theta_2^*\Theta_1)(1+\epsilon)^2}{(1+\epsilon)^2 - z_1 z_2^*} & \ddots & & \vdots \\ \vdots & & & \\ \frac{(I-\Theta_r^*\Theta_1)(1+\epsilon)^2}{(1+\epsilon)^2 - z_1 z_r^*} & \cdots & & \frac{(I-\Theta_r^*\Theta_r)(1+\epsilon)^2}{\epsilon(2+\epsilon)} \end{bmatrix}. \tag{3.13}$$

Note that P is positive definite iff ϵP is positive definite. Write ϵP as

$$\epsilon P = P_a + P_e \ , \tag{3.14}$$

where

$$P_a := \text{blockdiag}\left\{ \frac{(I-\Theta_1^*\Theta_1)(1+\epsilon)^2}{2+\epsilon}, \ldots, \frac{(I-\Theta_r^*\Theta_r)(1+\epsilon)^2}{2+\epsilon} \right\}$$

and $P_e := \epsilon P - P_a$. Note that each nonzero (off-diagonal) block in P_e has ϵ as a factor. Clearly P_a is positive definite, thus $\lambda_i(P_a) > 0$, $i = 1, \ldots, rp$. Also, note that P_a and P_e are

both Hermitian. Identifying A with P_a and E with P_e in Proposition 3, we get the following inequality:

$$|\lambda_k - \hat{\lambda}_k| \leq \rho(P_e),\ k = 1, \ldots, rp. \tag{3.15}$$

This says that since we can make the spectral radius $\rho(P_e)$ as small as we want by proper choice of ϵ, we can make it smaller than λ_1 for some ϵ_1, thereby causing $\epsilon_1 P$ to be positive definite. Hence there exists $\mathbf{\Theta} \in \mathcal{BRH}_\infty(\mathbb{D})^{p\times p}$ solving Problem 4 for the set of interpolation points $\{\tilde{z}_i(\epsilon_1)\}_{i=1}^r \subset \mathbb{D}$. Now let $\mathbf{\Psi} := \mathbf{\Theta} \circ g_{\epsilon_1}$, i.e., $\mathbf{\Psi}(z) = \mathbf{\Theta}(g_{\epsilon_1}(z)) = \mathbf{\Theta}(z/(1+\epsilon_1))$. Then $\mathbf{\Psi} : \mathbb{D}_{1+\epsilon_1} \to \mathbb{C}^{p\times p}$ is analytic, belongs to $\mathcal{BRH}_\infty(\mathbb{D}_{1+\epsilon})^{p\times p}$, and takes on the value Θ_k at z_k for $k = 1, \ldots, r$. ■

The idea of extending $\mathbb{D}$ to $\mathbb{D}_{1+\epsilon}$ and using the function g_ϵ comes from [27]. We now have all the tools to establish the following result on boundary interpolation which gives an answer to Problem 3.

Theorem 4 *Given a set of distinct points $\{e^{j\theta_i}\}_{i=1}^r$ on $\partial\mathbb{D}$ and a set $\{\tilde{\Psi}_i\}_{i=1}^r$ in $\mathbb{C}^{m\times n}$ satisfying $\tilde{\Psi}_l = \left(\tilde{\Psi}_j^*\right)^T$ for $\theta_l = -\theta_j$ and $\tilde{\Psi}_k \in \mathbb{R}^{m\times n}$ for $\theta_k = 0, \pi$, there exists a function $\tilde{\mathbf{\Psi}} \in \mathcal{BRH}_\infty(\mathbb{D})^{m\times n}$ satisfying $\tilde{\mathbf{\Psi}}(e^{j\theta_i}) = \tilde{\Psi}_i$, $i = 1, \ldots, r$ iff $\|\tilde{\Psi}_i\| < 1$ for $i = 1, \ldots, r$.*

Proof *Necessity* Follows immediately from the bound on the norm of $\tilde{\mathbf{\Psi}}$.
Sufficiency Let $q = \max\{m, n\}$. Append zeros to the complex matrices $\{\tilde{\Psi}_k\}_{k=1}^r$ to make them square:

$$\Gamma_k := \begin{bmatrix} \tilde{\Psi}_k \\ 0 \end{bmatrix} \text{ if } n = q\ ,\ k = 1, \ldots, r\ , \tag{3.16}$$

$$\Gamma_k := \begin{bmatrix} \tilde{\Psi}_k & 0 \end{bmatrix} \text{ if } m = q\ ,\ k = 1, \ldots, r\ . \tag{3.17}$$

Note that $\|\Gamma_k\| = \|\tilde{\Psi}_k\| < 1$, $k = 1, \ldots, r$. By Lemma 1, there exists $\mathbf{\Gamma} \in \mathcal{BRH}_\infty(\mathbb{D})^{q\times q}$ taking on the value Γ_k at the boundary point $z_k = e^{j\theta_k}$, $k = 1, \ldots, r$. Extract the $m \times n$ matrix $\tilde{\mathbf{\Psi}}(z)$ from the $q \times q$ matrix $\mathbf{\Gamma}(z)$ (the first m rows and n columns). Then, $\|\tilde{\mathbf{\Psi}}\|_\infty \leq \|\mathbf{\Gamma}\|_\infty < 1$, and $\tilde{\mathbf{\Psi}}$ takes on the value $\tilde{\Psi}_k$ at the boundary point z_k, for $k = 1, \ldots, r$. ■

With Theorem 4 in hand, proving our main result (Theorem 2) on consistency of the perturbed CF model with the noise-free experimental frequency-response data becomes a simple matter. Given a nominal coprime factor model $\boldsymbol{G} = \tilde{\boldsymbol{M}}^{-1}\tilde{\boldsymbol{N}}$, an uncertainty set $\mathcal{D}_r$ and a set of

frequency-response measurements $\{\Phi_i\}_{i=1}^N$, it suffices to compute the minimum-norm complex matrices Δ_i for $i = 1, \ldots, N$ and to check that $\|\Delta_i\| < |\boldsymbol{r}(j\omega_i)|$, $\forall i = 1, \ldots, N$. If this inequality does not hold for some $j \in \{1, \ldots, N\}$, then no perturbation of the coprime factors in $\mathcal{D}_r$ could have produced the data. This is summarized in the following proof of Theorem 2.

Proof of Theorem 2 Scale the minimum-norm Δ_i with $\boldsymbol{r}$ to get $\tilde{\Delta}_i := |\boldsymbol{r}(j\omega_i)|^{-1}\Delta_i$ and compute $z_i = \frac{1-j\omega_i}{1+j\omega_i}$ for $i = 1, \ldots, N$. Then apply Theorem 4 to show that there exists a function in $\mathcal{BRH}_\infty(\mathbb{D})$ that interpolates the $\tilde{\Delta}_i$'s at the z_i's iff $\|\tilde{\Delta}_i\| < 1$ for all $i = 1, \ldots, N$. Use the bilinear transformation on this function and unscale to get the factor perturbation $\boldsymbol{\Delta} \in \mathcal{D}_r$. Finally, notice that the corresponding $\boldsymbol{G}_p$ is stable from Assumption (A3.1). ■

The bound $|\boldsymbol{r}(j\omega)|$ can be shaped such that the inequality in the theorem statement is satisfied for all i. One can see how $\boldsymbol{r}$ can be constructed and improved as new experimental data become available.

3.4.1.2 Numerical Example

Suppose we are given a nominal coprime factorization $\boldsymbol{G} = \tilde{\boldsymbol{M}}^{-1}\tilde{\boldsymbol{N}}$, with

$$\tilde{\boldsymbol{M}} = \begin{bmatrix} \frac{s+2}{s+1} & \frac{s+3}{s+2} \\ 0 & \frac{s+1}{s+2} \end{bmatrix}, \qquad \tilde{\boldsymbol{N}} = \begin{bmatrix} \frac{1}{s+1} & \frac{2}{s+1} & 0 \\ 0 & \frac{1}{s+3} & \frac{2}{s+2} \end{bmatrix},$$

and a bound on the factor perturbations $\boldsymbol{r}(s) = \frac{10^{-8}s+0.3}{s+1}$. With these, Assumption (A3.1) holds. Consider the following coprime factorization of the "true" plant (unknown to us) $\boldsymbol{G}_p = \tilde{\boldsymbol{M}}_p^{-1}\tilde{\boldsymbol{N}}_p$, where

$$\tilde{\boldsymbol{M}}_p = \begin{bmatrix} \frac{s+1.9}{s+1} & \frac{s+2.9}{s+2} \\ 0.1 & \frac{1.1s+1}{s+2} \end{bmatrix}, \qquad \tilde{\boldsymbol{N}}_p = \begin{bmatrix} \frac{1.1}{s+1} & \frac{2.2}{s+1} & 0 \\ 0 & \frac{0.9}{s+3} & \frac{1.8}{s+2} \end{bmatrix}.$$

The factor perturbations are

$$\Delta\boldsymbol{M} = \begin{bmatrix} \frac{-0.1}{s+1} & \frac{-0.1}{s+2} \\ 0.1 & \frac{0.1s}{s+2} \end{bmatrix}, \qquad \Delta\boldsymbol{N} = \begin{bmatrix} \frac{0.1}{s+1} & \frac{0.2}{s+1} & 0 \\ 0 & \frac{-0.1}{s+3} & \frac{-0.2}{s+2} \end{bmatrix}.$$

Now suppose we take five frequency-response measurements on the plant at the frequencies $\omega_1 = 0.01$, $\omega_2 = 0.1$, $\omega_3 = 1$, $\omega_4 = 10$, $\omega_5 = 100$ radians/s. These measurements are

$$G_1 := \boldsymbol{G}_p(j\omega_1) = \begin{bmatrix} 0.6832 - 0.0039j & 0.8261 - 0.0043j & -1.6210 + 0.0135j \\ -0.1366 + 0.0016j & 0.4347 - 0.0038j & 2.1239 - 0.0244j \end{bmatrix},$$

$$G_2 := \boldsymbol{G}_p(j\omega_2) = \begin{bmatrix} 0.6809 - 0.0393j & 0.8241 - 0.0428j & -1.6099 + 0.1339j \\ -0.1348 + 0.0159j & 0.4310 - 0.0371j & 2.0968 - 0.2413j \end{bmatrix},$$

$$G_3 := \boldsymbol{G}_p(j\omega_3) = \begin{bmatrix} 0.5140 - 0.2913j & 0.6483 - 0.3483j & -0.9691 + 0.8077j \\ -0.0563 + 0.0688j & 0.2578 - 0.1888j & 0.9066 - 1.0618j \end{bmatrix},$$

$$G_4 := \boldsymbol{G}_p(j\omega_4) = \begin{bmatrix} 0.0210 - 0.1172j & 0.0264 - 0.1474j & -0.0151 + 0.1804j \\ -0.0008 + 0.0110j & 0.0136 - 0.0644j & 0.0144 - 0.1790j \end{bmatrix},$$

$$G_5 := \boldsymbol{G}_p(j\omega_5) = \begin{bmatrix} 0.0002 - 0.0121j & 0.0003 - 0.0152j & -0.0001 + 0.0180j \\ 0.0000 + 0.0011j & 0.0001 - 0.0068j & 0.0001 - 0.0180j \end{bmatrix}.$$

Equation (3.10) is used repeatedly to compute the following five 2×5 minimum-norm perturbations solving the consistency equation (3.8) at the five measurement frequencies.

$$\Delta_1 = \begin{bmatrix} 0.0710 - 0.0008j & 0.1463 - 0.0017j & 0.0128 - 0.0001j & 0.1486 - 0.0010j & 0.0811 - 0.0002j \\ -0.0273 + 0.0001j & -0.0546 + 0.0001j & 0.0002 - 0.0002j & -0.0640 + 0.0001j & -0.0197 - 0.0005j \end{bmatrix},$$

$$\Delta_2 = \begin{bmatrix} 0.0703 - 0.0082j & 0.1448 - 0.0168j & 0.0129 - 0.0013j & 0.1474 - 0.0101j & 0.0807 - 0.0016j \\ -0.0273 + 0.0009j & -0.0547 + 0.0011j & -0.0002 - 0.0019j & -0.0638 + 0.0012j & -0.0198 - 0.0053j \end{bmatrix},$$

$$\Delta_3 = \begin{bmatrix} 0.0325 - 0.0436j & 0.0700 - 0.0915j & 0.0121 - 0.0138j & 0.0838 - 0.0443j & 0.0561 - 0.0099j \\ -0.0285 + 0.0106j & -0.0641 + 0.0178j & -0.0211 - 0.0064j & -0.0503 + 0.0096j & -0.0298 - 0.0344j \end{bmatrix},$$

$$\Delta_4 = \begin{bmatrix} -0.0000 - 0.0097j & -0.0000 - 0.0198j & 0.0000 - 0.0006j & 0.0039 - 0.0007j & 0.0013 - 0.0003j \\ -0.0018 + 0.0104j & -0.0078 + 0.0292j & -0.0068 + 0.0177j & -0.0025 + 0.0006j & -0.0051 - 0.0011j \end{bmatrix},$$

$$\Delta_5 = \begin{bmatrix} -0.0000 - 0.0010j & -0.0000 - 0.0020j & 0.0000 - 0.0000j & 0.0000 - 0.0000j & 0.0000 - 0.0000j \\ -0.0000 + 0.0011j & -0.0001 + 0.0032j & -0.0001 + 0.0020j & -0.0000 + 0.0000j & -0.0001 - 0.0000j \end{bmatrix},$$

Figure 3.3 shows a plot of the magnitude of $\boldsymbol{r}(j\omega)$, the norm of $\boldsymbol{\Delta}(j\omega)$, and the norms of the Δ_i's. The model is inconsistent with the data at the two frequencies ω_4 and ω_5, but it can be made consistent by simply shifting $|\boldsymbol{r}(j\omega)|$ towards higher frequencies. For instance, $\boldsymbol{r}_1(s) = \frac{10^{-8}s+0.3}{0.5s+1}$ makes the model consistent with all the data.

Interestingly, the actual factor perturbations used to generate $\boldsymbol{G}_p$ are not accounted for by either $\boldsymbol{r}$ or $\boldsymbol{r}_1$ ($\|\boldsymbol{\Delta}(j\omega)\| > |\boldsymbol{r}_1(j\omega)|$ at high frequencies). So a legitimate question arises: Would a controller designed to be robust to all factor perturbations of norm less than $|\boldsymbol{r}_1(j\omega)|$ necessarily destabilize $\boldsymbol{G}_p$? The answer is no for two reasons. First, Theorem 1 does not say that the closed-loop system is unstable for all plant models not belonging to $\mathcal{P}$. Second, the

perturbed factors $\tilde{\boldsymbol{M}}_p$ and $\tilde{\boldsymbol{N}}_p$ used to form $\boldsymbol{G}_p$ are one possible factorization of $\boldsymbol{G}_p$. What Figure 3.3 suggests, in light of Theorem 2, is that there *may* exist at least one factorization of $\boldsymbol{G}_p$ that leads to a perturbation $\boldsymbol{\Delta}$ of norm less than the magnitude of $\boldsymbol{r}_1$ on the $j\omega$-axis. This is not as strong as saying that there *does* exist such a factorization. What Theorem 2 says is that there exists at least one $\boldsymbol{\Delta} \in \mathcal{D}_{r_1}$ that can reproduce the frequency-response data.

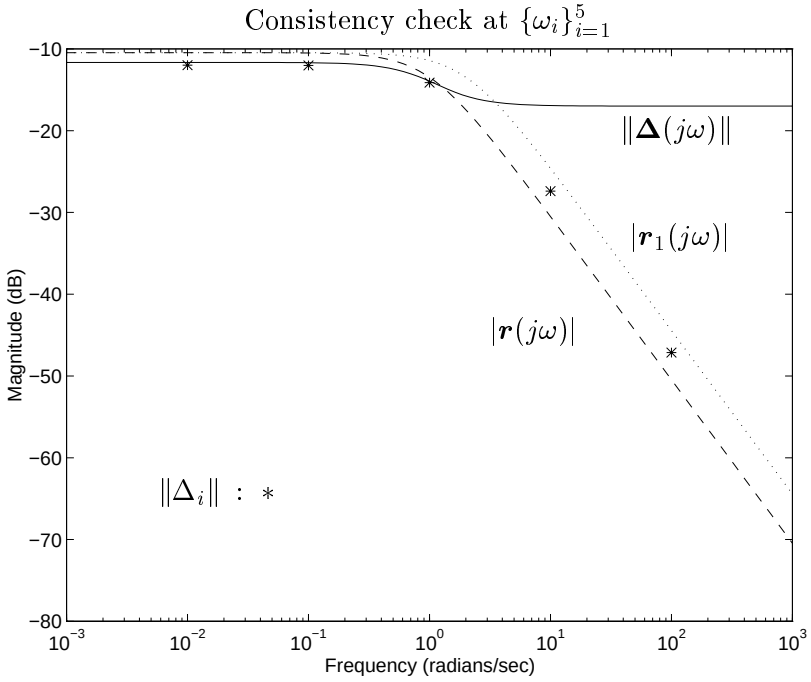

Figure 3.3: Consistency check for noise-free MIMO example.

3.4.1.3 Special Factorization for Square LFSS Models

Let us now consider a nominal factorization of a square open-loop plant model $\boldsymbol{G}$ of the form $\boldsymbol{G} = C\tilde{\boldsymbol{M}}^{-1}\tilde{\boldsymbol{N}}\boldsymbol{J}$, where $C \in \mathbb{C}^{p\times n}$, $\boldsymbol{J} \in \mathcal{RH}_\infty^{p\times p}$ is diagonal and nonsingular on the $j\omega$-axis, $\tilde{\boldsymbol{M}} \in \mathcal{RH}_\infty^{n\times n}$, $\tilde{\boldsymbol{N}} \in \mathcal{RH}_\infty^{n\times p}$. This is the type of factorization proposed for LFSS in Chapter 2. In this case, n is the number of modes and the factor perturbations are mainly induced by variations in the modal parameters of the system. The input and output matrices are $\boldsymbol{J} = \gamma J_2 \boldsymbol{T}_a$ and $C = d_{max}^{-1} C_1 J_1$, where $\boldsymbol{T}_a$ is a diagonal transfer matrix in $\mathcal{RH}_\infty^{p\times p}$ modeling actuator dynamics.

As before, it is assumed that $\underline{\sigma}\left[\tilde{\boldsymbol{M}}(j\omega)\right] > |\boldsymbol{r}(j\omega)|$, $\forall\omega \in \mathbb{R}\cup\{\infty\}$ (Assumption (A3.1)) so that the perturbed plant is stable for all $\boldsymbol{\Delta} \in \mathcal{D}_r$. Fix a measurement frequency ω and let

$J := \boldsymbol{J}(j\omega)$, $\tilde{M} := \tilde{\boldsymbol{M}}(j\omega)$, $\tilde{N} := \tilde{\boldsymbol{N}}(j\omega)$, $\Delta M := \Delta\boldsymbol{M}(j\omega)$, $\Delta N := \Delta\boldsymbol{N}(j\omega)$, $\Delta := \boldsymbol{\Delta}(j\omega)$, $r := \boldsymbol{r}(j\omega)$ and $\tilde{\Delta} := r^{-1}\Delta$. The following assumption is made:

(A3.2) The datum $\Phi \in \mathbb{C}^{p\times p}$ is invertible.

This property should be generic in practice.

The consistency equation at frequency ω is

$$C(\tilde{M} + \Delta M)^{-1}(\tilde{N} + \Delta N)J - \Phi = 0. \tag{3.18}$$

The model/data consistency problem that we want to solve is the following.

Problem 5 *Given noise-free, invertible, open-loop frequency-response data $\{\Phi_i\}_{i=1}^N \subset \mathbb{C}^{p\times p}$ at the distinct frequencies $\omega_1, \ldots, \omega_N$, could they have been produced by at least one model in $\mathcal{P}$? Or, in other words, does there exist $\boldsymbol{\Delta} \in \mathcal{D}_r$ such that $\boldsymbol{G}_p(j\omega_i) = \Phi_i$, $i = 1, \ldots, N$?*

Note that this problem is not as easily solved as the previous one because in general C is not square. We make three other assumptions:

(A3.3) $n \geq p$,

(A3.4) C has full row rank,

(A3.5) $\hat{\Phi} - P_{22}$ is nonsingular, where $\hat{\Phi} := \Phi J^{-1}$ and P_{22} is defined below.

Assumption (A3.3) says that there are more modes in the model than there are outputs (and inputs). Assumptions (A3.3) and (A3.4) hold for most LFSS or experimental testbeds and are not really restrictive. Some motivation for these assumptions is provided by the following observation. Referring to Figure 3.4, we can see that a necessary condition for consistency is that the columns of the $p \times p$ matrix $(\hat{\Phi} - P_{22})$ lie in $\mathrm{Ra}\{P_{21}\}$, where $\hat{\Phi} := \Phi J^{-1}$ is the scaled datum and P_{21} is $p \times n$. But we have to assume that $\hat{\Phi} - P_{22}$ is nonsingular (Assumption (A3.5)) for Lemma 3 to hold true, so it follows that P_{21} must have full row rank p. This is turn implies that we must have $n \geq p$.

For convenience, let us postmultiply both sides of (3.18) by J^{-1} and rewrite it using LFT notation;

$$\hat{\Phi} - \mathcal{F}_U(P, \tilde{\Delta}) = 0, \tag{3.19}$$

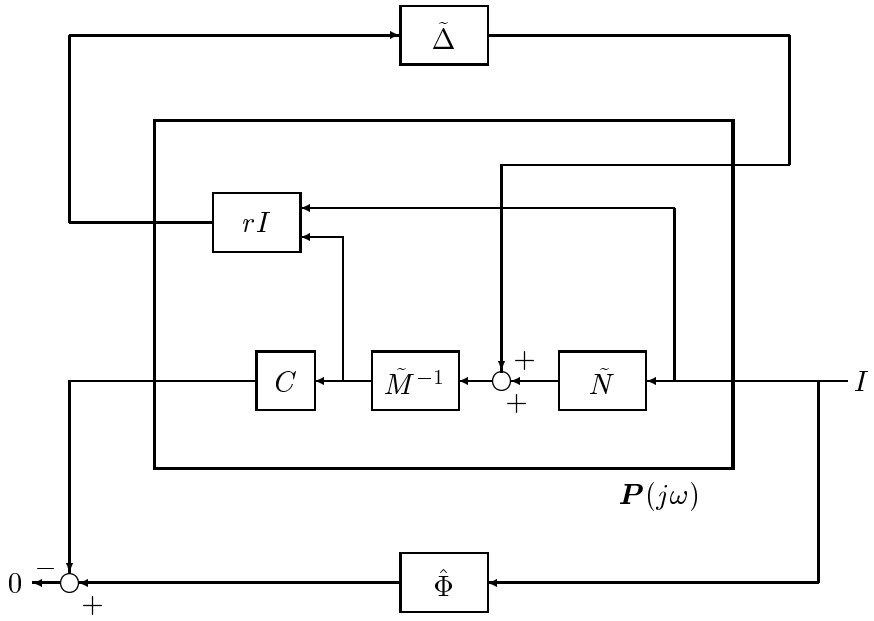

Figure 3.4: Block diagram of consistency equation for noise-free MIMO flexible system.

where

$$P := \begin{bmatrix} P_{11} & P_{12} \\ P_{21} & P_{22} \end{bmatrix} ,$$

$$P_{11} := \begin{bmatrix} 0 \\ r\tilde{M}^{-1} \end{bmatrix}, \qquad P_{12} := \begin{bmatrix} rI \\ r\tilde{M}^{-1}\tilde{N} \end{bmatrix},$$

$$P_{21} := C\tilde{M}^{-1}, \qquad P_{22} := C\tilde{M}^{-1}\tilde{N} \ .$$

This consistency equation is illustrated in Figure 3.4. Let $P_i := \boldsymbol{P}(j\omega_i)$, $J_i := \boldsymbol{J}(j\omega_i)$ and $\hat{\Phi}_i := \Phi_i J_i^{-1}$. Then the main result for the square MIMO model/data consistency problem with noise-free invertible measurements and special factorization for flexible systems is the following.

Theorem 5 *Problem 5 has a positive answer iff* $\sigma_p[\mathcal{F}_L(P_i, \hat{\Phi}_i^{-1})]^{-1} < 1$ *for* $i = 1, \ldots, N$.

In order to establish this result, we need to study consistency at one frequency. The consistency problem at frequency ω is stated as follows.

Problem 6 *Given a noise-free invertible frequency-response datum* $\Phi \in \mathbb{C}^{p\times p}$ *at frequency* ω, *does there exist* $\tilde{\Delta} \in \mathcal{B}\mathbb{C}^{n\times(n+p)}$ *such that* $C(\tilde{M}+\Delta M)^{-1}(\tilde{N}+\Delta N)J = \Phi$, *i.e.,* $\hat{\Phi} - \mathcal{F}_U(P,\tilde{\Delta}) = 0$*?*

Let $P_{12}^{\dagger}$ be the Moore-Penrose left-inverse of the full column-rank matrix P_{12} given by $P_{12}^{\dagger} := (P_{12}^{*}P_{12})^{-1}P_{12}^{*}$. It is easy to show that $\mathcal{N}_L\{P_{12}\} = \text{row span}\{[\tilde{N} \; -\tilde{M}]\}$, an n-dimensional subspace of $\mathbb{C}^{p+n}$. Notice that $\begin{bmatrix} P_{12}^{\dagger} \\ \begin{bmatrix} \tilde{N} & -\tilde{M} \end{bmatrix} \end{bmatrix}$ is invertible and recall that subspaces are said to be independent if their intersection is $\{0\}$. The first lemma is of a rather technical nature and is used in the proof of Lemma 3 which gives equivalent conditions for consistency at frequency ω.

Lemma 2 *Let* $\mathcal{Y} := \left\{\text{row span}\left(UP_{12}^{\dagger} + Q[\tilde{N} \; -\tilde{M}]\right) \; : \; U \in \mathbb{C}^{p\times p}\text{invertible}, \; Q \in \mathbb{C}^{p\times n}\right\}$. *Then* $\mathcal{Y} = \{p\text{-dimensional subspaces of } \mathbb{C}^{p+n} \text{ that are independent of } \mathcal{N}_L\{P_{12}\}\}$.

Proof ($\subset$) First, note that the rows of $P_{12}^{\dagger}$ are orthogonal to the rows of $[\tilde{N} \; -\tilde{M}]$. The matrix $P_{12}^{\dagger}$ has full row rank, hence any element of $\mathcal{Y}$ is a p-dimensional subspace of $\mathbb{C}^{p+n}$. But for each subspace $\mathcal{U} = \text{row span}\left(UP_{12}^{\dagger} + Q[\tilde{N} \; -\tilde{M}]\right)$ in $\mathcal{Y}$, $\mathcal{U} \cap \mathcal{N}_L\{P_{12}\} = \{0\}$ because the matrix U is invertible, and hence any vector in $\mathcal{U}$ has a nonzero component orthogonal to $\mathcal{N}_L\{P_{12}\}$. Hence, $\mathcal{U}$ is a p-dimensional subspace of $\mathbb{C}^{p+n}$ independent of $\mathcal{N}_L\{P_{12}\}$.
($\supset$) Let $\mathcal{U}$ be a p-dimensional subspace in $\mathbb{C}^{p+n}$ independent of $\mathcal{N}_L\{P_{12}\}$. Then $\exists U \in \mathbb{C}^{p\times p}$, $Q \in \mathbb{C}^{p\times n}$ such that

$$\mathcal{U} = \text{row span}\left\{UP_{12}^{\dagger} + Q[\tilde{N} \; -\tilde{M}]\right\}.$$

For a contradiction, suppose U is rank deficient. Then $\exists T \in \mathbb{C}^{p\times p}$ invertible such that $TU = \begin{bmatrix} U_1 \\ 0 \end{bmatrix}$. Then

$$\begin{aligned} \mathcal{U} &= \text{row span}\left\{TUP_{12}^{\dagger} + TQ[\tilde{N} \; -\tilde{M}]\right\} \\ &= \text{row span}\left\{\begin{bmatrix} U_1P_{12}^{\dagger} \\ 0 \end{bmatrix} + TQ[\tilde{N} \; -\tilde{M}]\right\}, \end{aligned}$$

i.e., $\mathcal{U}$ is not independent of $\mathcal{N}_L\{P_{12}\}$, a contradiction. Hence U must have full rank, and $\mathcal{U} \in \mathcal{Y}$. ■

The following lemma gives equivalent conditions for consistency at frequency ω.

Lemma 3 *For $\omega \in \mathbb{R}_+$, we are given the noise-free, invertible frequency-response measurement $\Phi \in \mathbb{C}^{p\times p}$. Assume $\hat{\Phi} - P_{22}$ is invertible. Then for $\tilde{\Delta} \in \mathcal{B}\mathbb{C}^{n\times(p+n)}$, the following consistency conditions are equivalent.*

(a) $\hat{\Phi} - \mathcal{F}_U(P, \tilde{\Delta}) = 0$

(b) $\left(P_{12}^\dagger - Q \begin{bmatrix} \tilde{N} & -\tilde{M} \end{bmatrix}\right)\left[I - \mathcal{F}_L(P, \hat{\Phi}^{-1})\tilde{\Delta}\right] = 0$ *for some* $Q \in \mathbb{C}^{p\times n}$

(c) $\operatorname{rank}\left[I - \mathcal{F}_L(P, \hat{\Phi}^{-1})\tilde{\Delta}\right] \le n$

Proof First note that $\tilde{\Delta} \in \mathcal{B}\mathbb{C}^{n\times(p+n)}$ implies that $I - P_{11}\tilde{\Delta}$ is nonsingular by Assumption (A3.1).

(a) $\Leftrightarrow$ (b) The consistency condition (a) holds iff

$$
\begin{aligned}
& \hat{\Phi} - P_{22} - P_{21}\tilde{\Delta}(I - P_{11}\tilde{\Delta})^{-1}P_{12} = 0 \\
\Leftrightarrow \quad & \left[(\hat{\Phi} - P_{22})P_{12}^\dagger - P_{21}\tilde{\Delta}(I - P_{11}\tilde{\Delta})^{-1}\right]P_{12} = 0 \\
\Leftrightarrow \quad & (\hat{\Phi} - P_{22})P_{12}^\dagger - P_{21}\tilde{\Delta}(I - P_{11}\tilde{\Delta})^{-1} = Q[\tilde{N} \ -\tilde{M}] && \text{for some } Q \in \mathbb{C}^{p\times n} \\
\Leftrightarrow \quad & P_{12}^\dagger(I - P_{11}\tilde{\Delta}) - (\hat{\Phi} - P_{22})^{-1}P_{21}\tilde{\Delta} = Q[\tilde{N} \ -\tilde{M}](I - P_{11}\tilde{\Delta}) && \text{for some } Q \in \mathbb{C}^{p\times n} \\
\Leftrightarrow \quad & P_{12}^\dagger - Q[\tilde{N} \ -\tilde{M}] - \left[\left(P_{12}^\dagger - Q[\tilde{N} \ -\tilde{M}]\right)P_{11} + (\hat{\Phi} - P_{22})^{-1}P_{21}\right]\tilde{\Delta} = 0 && \text{for some } Q \in \mathbb{C}^{p\times n} \\
\Leftrightarrow \quad & \left(P_{12}^\dagger - Q[\tilde{N} \ -\tilde{M}]\right)\{I - \underbrace{\left[P_{11} + P_{12}\left(I - \hat{\Phi}^{-1}P_{22}\right)^{-1}\hat{\Phi}^{-1}P_{21}\right]}_{\mathcal{F}_L(P,\hat{\Phi}^{-1})}\tilde{\Delta}\} = 0 && \text{for some } Q \in \mathbb{C}^{p\times n}
\end{aligned}
$$

(c) $\Rightarrow$ (b) Suppose that (c) holds. Then $\dim\left(\mathcal{N}_L\left\{I - \mathcal{F}_L(P, \hat{\Phi}^{-1})\tilde{\Delta}\right\}\right) \ge p$. We now show that $\mathcal{N}_L\{P_{12}\}$ and $\mathcal{N}_L\left\{I - \mathcal{F}_L(P, \hat{\Phi}^{-1})\tilde{\Delta}\right\}$ are independent, that is, for any nonzero $q \in \mathbb{C}^n$, $q^*\begin{bmatrix} \tilde{N} & -\tilde{M} \end{bmatrix}\left[I - \mathcal{F}_L(P, \hat{\Phi}^{-1})\tilde{\Delta}\right] \ne 0$. We have

$$
\begin{aligned}
q^*\begin{bmatrix} \tilde{N} & -\tilde{M} \end{bmatrix}\left[I - \mathcal{F}_L(P, \hat{\Phi}^{-1})\tilde{\Delta}\right] &= q^*\begin{bmatrix} \tilde{N} & -\tilde{M} \end{bmatrix}\left(I - P_{11}\tilde{\Delta}\right) \\
&= q^*\begin{bmatrix} \tilde{N} & -\tilde{M} \end{bmatrix}\left(I - \begin{bmatrix} 0 \\ r\tilde{M}^{-1} \end{bmatrix}\begin{bmatrix} r^{-1}\Delta N & -r^{-1}\Delta M \end{bmatrix}\right) \\
&= q^*\begin{bmatrix} \tilde{N} & -\tilde{M} \end{bmatrix}\begin{bmatrix} I & 0 \\ -\tilde{M}^{-1}\Delta N & I + \tilde{M}^{-1}\Delta M \end{bmatrix} \\
&= q^*\begin{bmatrix} \tilde{N} + \Delta N & -(\tilde{M} + \Delta M) \end{bmatrix} \ne 0.
\end{aligned}
$$

The last inequality follows from the fact that the matrix $\tilde{M} + \Delta M$ has full rank from our assumption that $\|\tilde{\Delta}\| < 1$ and (A3.1). This shows that $\mathcal{N}_L\{I - \mathcal{F}_L(P, \hat{\Phi}^{-1})\tilde{\Delta}\}$ and $\mathcal{N}_L\{P_{12}\}$ are independent, but also that $\dim\left(\mathcal{N}_L\{I - \mathcal{F}_L(P, \hat{\Phi}^{-1})\tilde{\Delta}\}\right) = p$. The latter implication follows from the inequality $\dim\left(\mathcal{N}_L\{I - \mathcal{F}_L(P, \hat{\Phi}^{-1})\tilde{\Delta}\}\right) \leq n + p - \dim\left(\mathcal{N}_L\{P_{12}\}\right) = p$ and the inequality obtained above: $\dim\left(\mathcal{N}_L\left\{I - \mathcal{F}_L(P, \hat{\Phi}^{-1})\tilde{\Delta}\right\}\right) \geq p$. But by Lemma 2, this implies that $\mathcal{N}_L\{I - \mathcal{F}_L(P, \hat{\Phi}^{-1})\tilde{\Delta}\} \in \mathcal{Y}$. Hence, $\exists U$ invertible, Q such that

$$\mathcal{N}_L\{I - \mathcal{F}_L(P, \hat{\Phi}^{-1})\tilde{\Delta}\} = \text{row span}\left(UP_{12}^{\dagger} + Q[\tilde{N} \ -\tilde{M}]\right),$$

and therefore

$$\begin{aligned}\left(UP_{12}^{\dagger} + Q[\tilde{N} \ -\tilde{M}]\right)\left[I - \mathcal{F}_L(P, \hat{\Phi}^{-1})\tilde{\Delta}\right] &= 0,\\ \left(P_{12}^{\dagger} - Q_0[\tilde{N} \ -\tilde{M}]\right)\left[I - \mathcal{F}_L(P, \hat{\Phi}^{-1})\tilde{\Delta}\right] &= 0,\end{aligned}$$

where $Q_0 = -U^{-1}Q$.

(b) $\Rightarrow$ (c) Suppose that $\exists Q$ such that

$$\left(P_{12}^{\dagger} - Q\begin{bmatrix} \tilde{N} & -\tilde{M} \end{bmatrix}\right)\left[I - \mathcal{F}_L(P, \hat{\Phi}^{-1})\tilde{\Delta}\right] = 0\ .$$

But $P_{12}^{\dagger} - Q\begin{bmatrix} \tilde{N} & -\tilde{M} \end{bmatrix}$ has full row rank p, hence $\text{rank}\left\{I - \mathcal{F}_L(P, \hat{\Phi}^{-1})\tilde{\Delta}\right\} \leq n$. ■

With this lemma in hand, it is now possible to set up an optimization problem to find a $\tilde{\Delta}$ of norm less than one such that $\text{rank}\left\{I - \mathcal{F}_L(P, \hat{\Phi}^{-1})\tilde{\Delta}\right\} \leq n$.

Problem 7 *Compute* $\beta := \inf\left\{\|\tilde{\Delta}\| : \text{rank}\left\{I - \mathcal{F}_L(P, \hat{\Phi}^{-1})\tilde{\Delta}\right\} \leq n,\ \tilde{\Delta} \in \mathbb{C}^{n\times(p+n)}\right\}$.

If the infimum β is less than 1, then the coprime factor model is consistent with the datum, otherwise it is not. Problem 7 is readily solved by a version of the Schmidt-Mirsky Theorem [50].

Theorem 6 (Schmidt-Mirsky) *Let* $E \in \mathbb{C}^{q\times r}$, $F \in \mathbb{C}^{r\times q}$. *Then for* $i = 1, \ldots, \min\{q, r\}$,

$$\inf\{\|E\| \ :\ \text{rank}(I - FE) \leq r - i\} = \sigma_i(F)^{-1}.$$

Furthermore, the infimum is achieved by a matrix $\hat{E}$ *for which* $\text{rank}(I - F\hat{E}) = r - i$.

Remark 3.1 A matrix $\hat{E}$ can be computed as follows. Let F have the singular value decomposition $F = U\Sigma_F V^*$, where $U \in \mathbb{C}^{r\times r}$ and $V \in \mathbb{C}^{q\times q}$ are unitary and $\Sigma_F \in \mathbb{C}^{r\times q}$ has the singular values of F in decreasing order as its (j,j) entries and zeros elsewhere. Then $\hat{E} = V\Sigma_E U^*$, where $\Sigma_E \in \mathbb{C}^{q\times r}$ and $[\Sigma_E]_{jj}$ is the inverse of the j^{th} singular value of F for $1 \le j \le i$. All other entries of Σ_E are zeros.

The result of Theorem 6 tailored to our problem is just

$$\beta = \sigma_p[\mathcal{F}_L(P, \hat{\Phi}^{-1})]^{-1} \ .$$

Hence the main lemma leading to our main consistency result, Theorem 5, goes as follows.

Lemma 4 *For a frequency ω and an invertible measurement datum $\Phi \in \mathbb{C}^{p\times p}$ with $\hat{\Phi} - P_{22}$ also invertible, Problem 6 has a positive answer iff $\sigma_p[\mathcal{F}_L(P, \hat{\Phi}^{-1})]^{-1} < 1$.*

Proof *Sufficiency* Suppose $\sigma_p[\mathcal{F}_L(P, \hat{\Phi}^{-1})]^{-1} < 1$. Then by Theorem 6, $\exists \tilde{\Delta} \in \mathcal{B}\mathbb{C}^{n\times(p+n)}$ such that $\operatorname{rank}\left\{I - \mathcal{F}_L(P, \hat{\Phi}^{-1})\tilde{\Delta}\right\} = n$. Moreover, $I - P_{11}\tilde{\Delta}$ is nonsingular since

$$\|P_{11}\tilde{\Delta}\| \le \|P_{11}\|\|\tilde{\Delta}\| \le |r|\underline{\sigma}(\tilde{M})^{-1} < 1,$$

where the last inequality follows from (A3.1). Hence by Lemma 3, $\hat{\Phi} - \mathcal{F}_U(P, \tilde{\Delta}) = 0$.
Necessity Suppose that for $\tilde{\Delta} \in \mathcal{B}\mathbb{C}^{n\times(p+n)}$, $\hat{\Phi} - \mathcal{F}_U(P, \tilde{\Delta}) = 0$. Obviously, $I - P_{11}\tilde{\Delta}$ is nonsingular since $\|\tilde{\Delta}\| < 1$. Thus by Lemma 3, this is equivalent to $\operatorname{rank}\left\{I - \mathcal{F}_L(P, \hat{\Phi}^{-1})\tilde{\Delta}\right\} \le n$, which implies that $\beta < 1$, i.e., $\sigma_p[\mathcal{F}_L(P, \hat{\Phi}^{-1})]^{-1} < 1$. ■

Finally, Lemma 4 and the boundary interpolation theorem (Theorem 4) can be used to prove the consistency result of Theorem 5.

Proof of Theorem 5 *Sufficiency* Suppose that $\forall i = 1, \ldots, N$, $\sigma_p[\mathcal{F}_L(P_i, \hat{\Phi}_i^{-1})]^{-1} < 1$. Then for each i, Lemma 4 says that $\exists \tilde{\Delta}_i \in \mathcal{B}\mathbb{C}^{n\times(p+n)}$ making the perturbed CF model and the datum Φ_i consistent at frequency ω_i. The unscaled Δ_i is such that $\|\Delta_i\| < |r_i|$, and the boundary interpolation theorem (Theorem 4) used as in the proof of Theorem 2 says that there is a stable perturbation $\mathbf{\Delta} \in \mathcal{D}_r$ that interpolates the matrices $\{\Delta_i\}_{i=1}^N$ at $\{j\omega_i\}_{i=1}^N$.
Necessity Suppose that for some k, $1 \le k \le N$, $\sigma_p[\mathcal{F}_L(P_k, \hat{\Phi}_k^{-1})]^{-1} \ge 1$. Then Lemma 4 says that Φ_k is inconsistent with the model at frequency ω_k, i.e., the answer to Problem 5 is negative. ■

3.4.2 Noisy SISO Case

The model/data consistency problem will be studied for standard and special left-coprime factorizations of SISO plants with noisy open-loop experimental data. Suppose we are given N nonzero noisy scalar frequency-response measurements $\{\phi_i\}_{i=1}^N \subset \mathbb{C}$ corresponding to the distinct frequencies $\omega_1, \ldots, \omega_N$. For more generality, we consider a stable nominal left-coprime factorization of the plant where the factor $\tilde{\boldsymbol{M}}$ has dimensions $n \times n$ and the factor $\tilde{\boldsymbol{N}}$ has dimensions $n \times 1$, together with an output transfer matrix $\boldsymbol{C}$ of dimension $1 \times n$. Any input scaling factor or actuator dynamics is lumped into $\boldsymbol{C}$, so referring back to Chapter 2, for an n-mode SISO LFSS we have $\boldsymbol{C} = d_{max}^{-1}\gamma J_2 \boldsymbol{T}_a C_1 J_1$, where $\boldsymbol{T}_a$ and J_2 are obviously scalar. Thus the nominal plant transfer function $\boldsymbol{g}$ is written as

$$\boldsymbol{g} = \boldsymbol{C}\tilde{\boldsymbol{M}}^{-1}\tilde{\boldsymbol{N}}. \tag{3.20}$$

A unit $\boldsymbol{r}(s)$ in $\mathcal{RH}_\infty$ bounding the factor uncertainty is also part of the model as before.

Define the normalized perturbations $\widetilde{\Delta \boldsymbol{N}} := \boldsymbol{r}^{-1}\Delta \boldsymbol{N}$, $\widetilde{\Delta \boldsymbol{M}} := \boldsymbol{r}^{-1}\Delta \boldsymbol{M}$ and the normalized uncertainty matrix

$$\tilde{\boldsymbol{\Delta}} := \begin{bmatrix} \widetilde{\Delta \boldsymbol{N}} & -\widetilde{\Delta \boldsymbol{M}} \end{bmatrix} = \boldsymbol{r}^{-1}\boldsymbol{\Delta}. \tag{3.21}$$

The factor uncertainty set $\mathcal{D}_r$ and the family of perturbed plants $\mathcal{P}$ are as defined in (2.19) and (3.2) respectively. The scalar noise set $\mathcal{W}$ was defined in (3.6). The noisy open-loop SISO consistency problem can be stated as follows:

Problem 8 *Given nonzero noisy open-loop frequency-response data $\{\phi_i\}_{i=1}^N \subset \mathbb{C}$ at $\omega_1, \ldots, \omega_N$, could they have been produced by at least one model in $\mathcal{P}$ and N noises in $\mathcal{W}$? Or, in other words, do there exist $\boldsymbol{\Delta} \in \mathcal{D}_r$ and complex noises $\{\delta_{ai}\}_{i=1}^N$ in $\mathcal{W}$ such that $\boldsymbol{g}_p(j\omega_i) + \delta_{ai} = \phi_i$, $i = 1, \ldots, N$?*

Fix a measurement frequency ω and let ϕ be the complex measurement at that frequency. For the nominal left-coprime factorization, let $C := \boldsymbol{C}(j\omega)$, $\widetilde{\Delta M} := \widetilde{\Delta \boldsymbol{M}}(j\omega)$ and $\widetilde{\Delta N} := \widetilde{\Delta \boldsymbol{N}}(j\omega)$. The normalized additive complex perturbation (the noise) at frequency ω is $\tilde{\delta}_a := L_a^{-1}\delta_a$ where $\delta_a \in \mathcal{W}$.

The block diagram of Figure 3.5 represents a general model/data consistency equation at frequency ω that can be specialized to the two different consistency problems considered. Referring to the block diagram, these configurations are: (1) Scalar factorization ($n = 1$), i.e., $\tilde{\boldsymbol{M}} \in$

$\mathcal{RH}_\infty^{1\times 1}$, $\tilde{\boldsymbol{N}} \in \mathcal{RH}_\infty^{1\times 1}$, $\boldsymbol{C} = 1$; (2) Special factorization for LFSS, i.e., $\tilde{\boldsymbol{M}} \in \mathcal{RH}_\infty^{n\times n}$, $\tilde{\boldsymbol{N}} \in \mathcal{RH}_\infty^{n\times 1}$, $\boldsymbol{C} \in \mathcal{RH}_\infty^{1\times n}$.

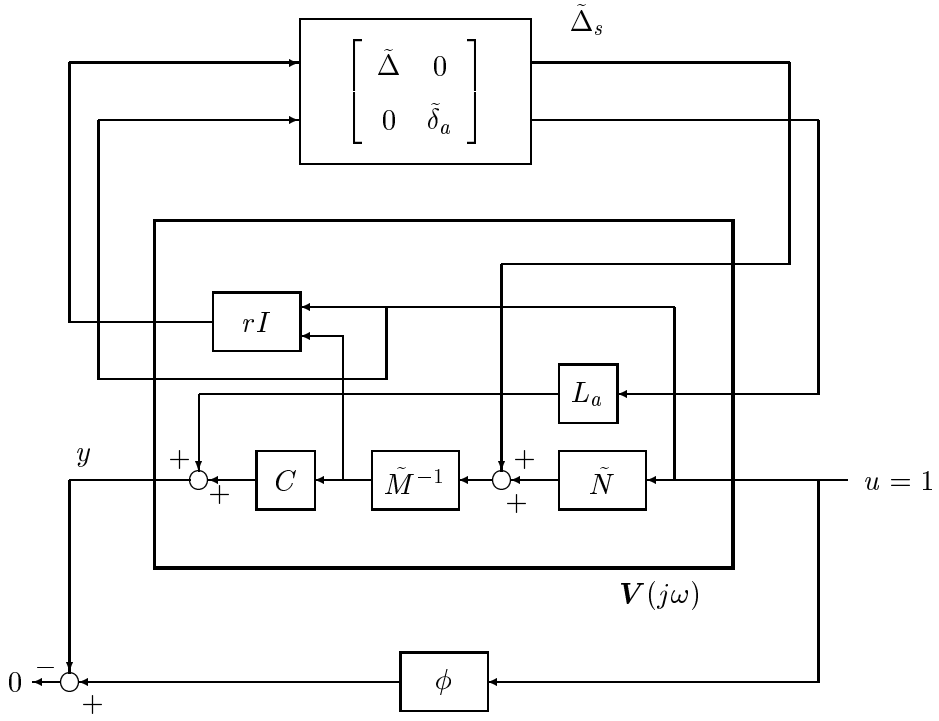

Figure 3.5: Block diagram of consistency equation for noisy open-loop SISO flexible system at frequency ω.

The following assumptions are made:

(A3.6) $\phi \neq 0$ (nonzero complex measurement),

(A3.7) $(\phi - V_{22}) \neq 0$, where V_{22} is the map $u \mapsto y$ in Figure 3.5 for $\tilde{\Delta}_s = 0$.

These assumptions are required for invertibility of the complex numbers ϕ and $(\phi - V_{22})$ in the proofs, and should hold generically in practice. Note that $\boldsymbol{V}_{22}$ is just the nominal open-loop plant model. It is convenient to define $q := (\phi - V_{22})^{-1}$. The generalized consistency equation at frequency ω is

$$\phi - C(\tilde{M} + r\widetilde{\Delta M})^{-1}(\tilde{N} + r\widetilde{\Delta N}) - L_a\tilde{\delta}_a = 0. \tag{3.22}$$

Using LFT notation, (3.22) becomes

$$\phi - \mathcal{F}_U\left[\boldsymbol{V}(j\omega), \tilde{\Delta}_s\right] = 0, \tag{3.23}$$

where

$$\tilde{\Delta}_s := \begin{bmatrix} \tilde{\Delta} & 0 \\ 0 & \tilde{\delta}_a \end{bmatrix},$$

and

$$\boldsymbol{V} := \begin{bmatrix} \boldsymbol{V}_{11} & \boldsymbol{V}_{12} \\ \boldsymbol{V}_{21} & \boldsymbol{V}_{22} \end{bmatrix},$$

$$\boldsymbol{V}_{11} := \begin{bmatrix} 0 & 0 \\ \boldsymbol{r}\tilde{\boldsymbol{M}}^{-1} & 0 \\ 0 & 0 \end{bmatrix}, \qquad \boldsymbol{V}_{12} := \begin{bmatrix} \boldsymbol{r} \\ \boldsymbol{r}\tilde{\boldsymbol{M}}^{-1}\tilde{\boldsymbol{N}} \\ 1 \end{bmatrix}$$

$$\boldsymbol{V}_{21} := \begin{bmatrix} \boldsymbol{C}\tilde{\boldsymbol{M}}^{-1} & L_a \end{bmatrix}, \qquad \boldsymbol{V}_{22} := \boldsymbol{C}\tilde{\boldsymbol{M}}^{-1}\tilde{\boldsymbol{N}} .$$

Note that V, V_{ij} are defined in the usual way at frequency ω. Thus the general consistency problem at frequency ω can be stated as follows.

Problem 9 *Given a nonzero noisy frequency-response datum ϕ at frequency ω, do there exist $\tilde{\Delta} \in \mathcal{B}\mathbb{C}^{n\times(n+1)}$ and a complex noise $\delta_a \in \mathcal{W}$ such that $\phi - \mathcal{F}_U(V, \tilde{\Delta}_s) = 0$?*

The key idea for solving this problem is to write a consistency equation equivalent to (3.23), but that has a feedback interpretation as in Figure 3.6:

$$1 - \phi^{-1}\mathcal{F}_U(V, \tilde{\Delta}_s) = 0, \tag{3.24}$$

Then consistency becomes analogous to noninvertibility (or instability) of a feedback system at frequency ω, and tools developed for stability analysis of linear systems, such as the structured singular value μ, can be used to derive consistency results. Based on this idea, the following lemma forms a basis for the solution of the consistency problem.

Lemma 5 *For a frequency $\omega \in \mathbb{R}_+$, we are given a nonzero complex measurement ϕ. Then for $\Delta \in \mathbb{C}^{(n+1)\times(n+2)}$ with $I - V_{11}\Delta$ nonsingular, $\phi - \mathcal{F}_U(V, \Delta) = 0$ iff $I - \mathcal{F}_L(V, \phi^{-1})\Delta$ is singular.*

Proof *Sufficiency* Suppose that $\det[I - \mathcal{F}_L(V, \phi^{-1})\Delta] = 0$. Then $\exists 0 \neq x \in \mathbb{C}^{n+2}$ such that

$$\begin{aligned} x &= \left[V_{11}\Delta + V_{12}(1 - \phi^{-1}V_{22})^{-1}\phi^{-1}V_{21}\Delta\right] x. \\ &= V_{11}\Delta x + V_{12}(\phi - V_{22})^{-1}V_{21}\Delta x. \end{aligned} \tag{3.25}$$

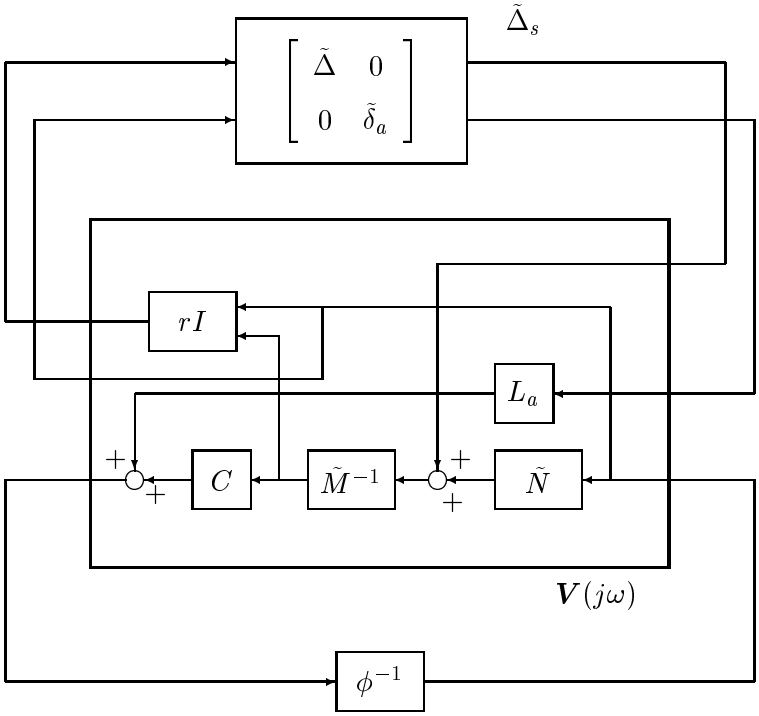

Figure 3.6: Block diagram of equivalent feedback problem.

Now $(I - V_{11}\Delta)$ is invertible by assumption, so we can write

$$\begin{aligned}(I - V_{11}\Delta)x &= qV_{12}V_{21}\Delta x,\\ q^{-1}x &= (I - V_{11}\Delta)^{-1}V_{12}V_{21}\Delta x\end{aligned}$$

Let $y \in \mathbb{C}^{n+1}$ be defined as $y := \Delta x$. Note that $y \neq 0$. Premultiply the last equation by Δ to get

$$\begin{aligned}q^{-1}y &= \Delta(I - V_{11}\Delta)^{-1}V_{12}V_{21}y,\\ &= (I - \Delta V_{11})^{-1}\Delta V_{12}V_{21}y,\end{aligned}$$

where the last equation follows from the identity $\Delta(I - V_{11}\Delta)^{-1} = (I - \Delta V_{11})^{-1}\Delta$. Let $z \in \mathbb{C}$ be defined as $z := V_{21}y \neq 0$, and premultiply both sides of the last equation by V_{21} to get

$$(\phi - V_{22})z = V_{21}(I - \Delta V_{11})^{-1}\Delta V_{12}z,$$

or

$$\left[\phi - V_{22} - V_{21}(I - \Delta V_{11})^{-1}\Delta V_{12}\right] z = 0.$$

This last equation implies $\phi - \mathcal{F}_U(V, \Delta) = 0$.

Necessity Suppose that $\phi - \mathcal{F}_U(V, \Delta) = 0$, that is,

$$\phi - V_{22} - V_{21}\Delta(I - V_{11}\Delta)^{-1}V_{12} = 0.$$

Let $V_{12}^{\dagger}$ be the Moore-Penrose left-inverse of V_{12}. Then the last equation is equivalent to

$$\left[q^{-1}V_{12}^{\dagger} - V_{21}\Delta(I - V_{11}\Delta)^{-1}\right] V_{12} = 0,$$

or, equivalently,

$$\begin{aligned}
& q^{-1}V_{12}^{\dagger} - V_{21}\Delta(I - V_{11}\Delta)^{-1} = z^* && \text{for some nonzero } z^* \in \mathcal{N}_L\{V_{12}\} \\
\Leftrightarrow \quad & q^{-1}V_{12}^{\dagger}(I - V_{11}\Delta) - V_{21}\Delta = z^*(I - V_{11}\Delta) && \text{for some nonzero } z^* \in \mathcal{N}_L\{V_{12}\} \\
\Leftrightarrow \quad & V_{12}^{\dagger}(I - V_{11}\Delta) - qV_{21}\Delta = z^*(I - V_{11}\Delta) && \text{for some nonzero } z^* \in \mathcal{N}_L\{V_{12}\} \\
\Leftrightarrow \quad & V_{12}^{\dagger} - V_{12}^{\dagger}\left[V_{11} + V_{12}qV_{21}\right]\Delta = z^*(I - V_{11}\Delta) && \text{for some nonzero } z^* \in \mathcal{N}_L\{V_{12}\} \\
\Leftrightarrow \quad & V_{12}^{\dagger} - z^* - \left[(V_{12}^{\dagger} - z^*)V_{11} + qV_{21}\right]\Delta = 0 && \text{for some nonzero } z^* \in \mathcal{N}_L\{V_{12}\} \\
\Leftrightarrow \quad & (V_{12}^{\dagger} - z^*)\{I - \underbrace{\left[V_{11} + V_{12}(1 - \phi^{-1}V_{22})^{-1}\phi^{-1}V_{21}\right]}_{\mathcal{F}_L(V,\phi^{-1})}\Delta\} = 0 && \text{for some nonzero } z^* \in \mathcal{N}_L\{V_{12}\}.
\end{aligned}$$

By orthogonality of $V_{12}^{\dagger}$ and z^*, this implies that $I - \mathcal{F}_L(V, \phi^{-1})\Delta$ is singular. ■

Define the structured perturbation set

$$\Gamma := \left\{ \Delta_s = \begin{bmatrix} \Delta & 0 \\ 0 & \delta_a \end{bmatrix} \; : \; \Delta \in \mathbb{C}^{n\times(n+1)},\, \delta_a \in \mathbb{C} \right\}. \tag{3.26}$$

This set will be useful in deriving the consistency results for the general factorization.

Recall that we are given N nonzero noisy scalar frequency-response measurements $\{\phi_i\}_{i=1}^N$ in $\mathbb{C}$ corresponding to the distinct frequencies $\omega_1, \ldots, \omega_N$. We seek a solution to Problem 8, and the main result, Theorem 7, provides a complete one.

Introduce the normalized perturbations $\tilde{\Delta}_i := \tilde{\mathbf{\Delta}}(j\omega_i)$, and $\tilde{\delta}_{ai} := L_a^{-1}\delta_{ai}$. For each ω_i, the consistency equation to be satisfied by admissible normalized perturbation and noise of norm less than one is just (3.22) at $\omega = \omega_i$. This equation can be rewritten in the form of (3.24), i.e., in LFT form with ϕ_i^{-1} as a feedback:

$$1 - \phi_i^{-1}\mathcal{F}_U\left[\boldsymbol{V}(j\omega_i), \tilde{\Delta}_{si}\right] = 0 \tag{3.27}$$

Recall that the structured singular value $\mu_\Gamma : \mathbb{C}^{(n+2)\times(n+1)} \to \mathbb{R}_+$ corresponding to the structured perturbations in Γ is defined as follows [13]:

$$\mu_\Gamma(M) := [\min\{\|\Delta_s\| \ : \ \Delta_s \in \Gamma, \ \det(I - M\Delta_s) = 0\}]^{-1} \ , \tag{3.28}$$

unless no $\Delta_s \in \Gamma$ makes $I - M\Delta_s$ singular, in which case $\mu_\Gamma(M) := 0$.

Definition 3.1 Let $U := \begin{bmatrix} U_{11} & U_{12} \\ U_{21} & U_{22} \end{bmatrix}$ be complex and let $\Delta_s \in \Gamma$ have the same dimensions as U_{11}^T. Then the LFT $\mathcal{F}_U(U, \Delta_s)$ is *well-posed* if $I - U_{11}\Delta_s$ is invertible.

Lemma 6 *The LFT $\mathcal{F}_U(U, \Delta_s)$ is well-posed $\forall \Delta_s \in \mathcal{B}\Gamma$ iff $\mu_\Gamma(U_{11}) < 1$.*

Proof This is merely a restatement of the definition of μ_Γ. ■

Lemma 7 *The LFT $\mathcal{F}_U(V, \tilde{\Delta}_s)$ is well-posed for all $\tilde{\Delta}_s \in \mathcal{B}\Gamma$.*

Proof Note that for a complex matrix $M \in \mathbb{C}^{(n+2)\times(n+1)}$,

$$\|M\| = \left[\min\left\{\|\Delta\| \ : \ \Delta \in \mathbb{C}^{(n+1)\times(n+2)}, \ \det(I - M\Delta) = 0\right\}\right]^{-1}.$$

Since $\Gamma \subset \mathbb{C}^{(n+1)\times(n+2)}$, we have $\mu_\Gamma(V_{11}) \leq \|V_{11}\| = |r|\underline{\sigma}(M)^{-1} < 1$, where the last inequality follows from (A3.1). ■

Thus for each frequency ω_i, a problem equivalent to the consistency problem can be formulated:

Problem 10 *Does there exist a perturbation $\tilde{\Delta}_{si}$ of norm less than one that satisfies (3.27)?*

This problem can be readily solved by computing $\mu_\Gamma\left\{\mathcal{F}_L[\boldsymbol{V}(j\omega_i), \phi_i^{-1}]\right\}$ and checking that its value is larger than one (the Matlab^{TM} μ-Tools toolbox contains algorithms to compute μ [2]). That is, for each ω_i, the consistency problem can be interpreted as a μ test for non-robustness of the feedback interconnection in Figure 3.7. This result is summarized in the following lemma.

Lemma 8 *We are given a frequency $\omega \in \mathbb{R}_+$, and a nonzero complex measurement ϕ. Then $\exists \tilde{\Delta}_s \in \mathcal{B}\Gamma$ such that $\phi - \mathcal{F}_U(V, \tilde{\Delta}_s) = 0$ iff $\mu_\Gamma\left[\mathcal{F}_L(V, \phi^{-1})\right] > 1$.*

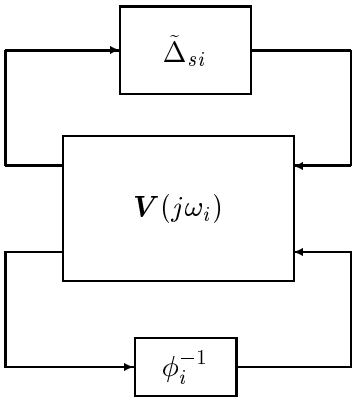

Figure 3.7: Equivalent problem of instability of a perturbed feedback interconnection.

Proof We have $\mu_\Gamma\left[\mathcal{F}_L(V,\phi^{-1})\right] > 1$ iff there exists $\tilde{\Delta}_s \in \mathcal{B}\Gamma$ such that $I - \mathcal{F}_L(V,\phi^{-1})\tilde{\Delta}_s$ is singular. By Lemma 7 on well-posedness of $\mathcal{F}_U(V,\tilde{\Delta}_s)$, $I - V_{11}\tilde{\Delta}_s$ is nonsingular, so Lemma 5 applies and we have: $I - \mathcal{F}_L(V,\phi^{-1})\tilde{\Delta}_s$ is singular iff $\phi - \mathcal{F}_U(V,\tilde{\Delta}_s) = 0$. ■

The main result of this section can now be stated. It gives a necessary and sufficient condition for a positive answer to Problem 8, the consistency problem for noisy open-loop measurements on SISO plants.

Theorem 7 *Problem 8 has a positive answer, i.e., there exist* $\boldsymbol{g}_p \in \mathcal{P}$ *and noises* $\delta_{ai} \in \mathcal{W}$, $i = 1,\ldots,N$, *that could have produced the* ϕ_i*'s, iff* $\mu_\Gamma\left\{\mathcal{F}_L\left[\boldsymbol{V}(j\omega_i),\phi_i^{-1}\right]\right\} > 1$ *for* $i = 1,\ldots,N$.

Proof *Necessity* Suppose that Problem 8 has a positive answer, i.e., there exist $\boldsymbol{\Delta} \in \mathcal{D}_r$ and complex noises $\{\delta_{ai}\}_{i=1}^N$ in $\mathcal{W}$ such that $\mathcal{F}_U(V_i,\tilde{\Delta}_{si}) = \phi_i$, $i = 1,\ldots,N$. Then $\|\tilde{\Delta}_{si}\| < 1$, and by Lemma 8, $\mu_\Gamma\left\{\mathcal{F}_L\left[\boldsymbol{V}(j\omega_i),\phi_i^{-1}\right]\right\} > 1$, for $i = 1,\ldots,N$.
Sufficiency Suppose that $\mu_\Gamma\left\{\mathcal{F}_L\left[\boldsymbol{V}(j\omega_i),\phi_i^{-1}\right]\right\} > 1$, for $i = 1,\ldots,N$. Then by Lemma 8, there exist $\{\tilde{\Delta}_i\}_{i=1}^N$, $\{\tilde{\delta}_{ai}\}_{i=1}^N$ of norm all less than one, such that the consistency equation (3.27) holds for each i. If we let $\Delta_i := \boldsymbol{r}(j\omega_i)\tilde{\Delta}_i$ and $\delta_{ai} = L_a\tilde{\delta}_{ai}$ (the unscaled perturbations and noises), it follows that for each i, $\|\Delta_i\| < |\boldsymbol{r}(j\omega_i)|$ and $\delta_{ai} \in \mathcal{W}$. Finally, the boundary interpolation theorem (Theorem 4) is used to show that there exists a $\boldsymbol{\Delta} \in \mathcal{D}_r$ that interpolates the matrices $\{\Delta_i\}_{i=1}^N$ at $\{j\omega_i\}_{i=1}^N$. Hence, the corresponding perturbed plant $\boldsymbol{g}_p$ belongs to $\mathcal{P}$, and Problem 8 has a positive answer. ■

This result provides a sufficient condition for the *original* consistency problem in the complex plane, i.e., Problem 8 with the uncertainty disk $\mathcal{W}_0$ replaced by $\mathcal{U}$ in Figure 3.2, under the assumption that $\mathcal{U}$ is square.

Suppose that for a given set of frequency-response measurements, the μ test reveals that the LCF and noise models are inconsistent because at one measurement frequency ω_j, $\mu_\Gamma\left\{\mathcal{F}_L\left[\boldsymbol{V}(j\omega_j), \phi_j^{-1}\right]\right\}$ is less than, but close to one. Then it may be possible to increase $|r_j|$ slightly to get consistency as the following proposition suggests.

Proposition 4 *$\mu_\Gamma\left\{\mathcal{F}_L[\boldsymbol{V}(j\omega_j), \phi_j^{-1}]\right\}$ is a nondecreasing function of $|r_j|$ on $\left[0, \underline{\sigma}(\tilde{M}_j)\right)$.*

Proof Follows from the fact that if $|r_j'| > |r_j|$, then

$$\{\Delta \ : \ \|\Delta\| < |r_j|\} \subset \{\Delta \ : \ \|\Delta\| < |r_j'|\}. \qquad \blacksquare$$

3.4.2.1 Numerical Example

Experimental frequency-response data obtained on a planar two-link flexible robot [36] are used for a numerical example illustrating the result. The plant has two motor voltage inputs at the joints and two outputs, namely the tip position of the first link, and the angle of the second joint. The measurements were taken in the zero-angle configuration. Here we want to test a coprime factor model of the SISO plant from the motor voltage of the first joint to the tip position of the first link.

This factorization was derived from the nominal model of the flexible robot given in [36], and a bound $\boldsymbol{r}$ on the factor uncertainty was obtained using the method proposed in Chapter 2 for factorizations of large flexible space structures. This bound would guarantee robustness to roughly 0.1% uncertainty in the modal frequencies, 1% uncertainty in the entries of the input matrix, and 1% uncertainty in the damping ratios if a robust controller were designed using the technique of Chapter 2. These margins are quite small, but this is because the method of Chapter 2 works better for systems with clustered flexible modes, such as LFSS, than for systems with flexible modes far apart, such as flexible beams or flexible robots. We had to reduce further the size of $\boldsymbol{r}$ by a half such that Assumption (A3.1) holds. The noise level in the data was estimated to be roughly $L_a = 0.06$. The measurements were taken at 211 distinct frequencies ranging from 1 rad/s to 64 rad/s. Here is the nominal 10^{th}-order model

$\boldsymbol{g} = C\tilde{\boldsymbol{M}}^{-1}\tilde{\boldsymbol{N}}$ composed of 5 flexible modes:

$$\boldsymbol{g}(s) = C\tilde{\boldsymbol{M}}^{-1}\tilde{\boldsymbol{N}}, \tag{3.29}$$

where

$$\begin{aligned}\tilde{\boldsymbol{M}}(s) &= \frac{1}{s^2+41.2s+40.2}\mathrm{diag}\left\{4.0s^2+4.1s+105.0,\ 4.0s^2+36.1s+8228.6,\right.\\ &\left. 4.0s^2+16.1s+1634.0,\ 4.0s^2+90.8s+20116,\ 4.0s^2+22.8s+1310.3\right\}, \end{aligned}\tag{3.30}$$

$$\tilde{\boldsymbol{N}}(s) = \frac{1}{s^2+41.2s+40.2}\begin{bmatrix} 1800 \\ -1800 \\ -1800 \\ 1800 \\ 1800 \end{bmatrix}, \tag{3.31}$$

$$C = \begin{bmatrix} -0.00330 & 0.00340 & -0.00339 & -0.00000 & -0.00001 \end{bmatrix}. \tag{3.32}$$

Notice that rigid-body modes were not included in order to keep the nominal model stable, although the data in Figure 3.8 shows that there seem to be two poles at $s = 0$, as one would expect. Nonetheless, we will check if the data are consistent with this model and the noise level L_a. The weighting function bounding the factor uncertainty is $\boldsymbol{r}(s) = \frac{5\times 10^{-4}s+.75}{s+1}$. Figure 3.9 shows a plot of the singular values of $\tilde{\boldsymbol{M}}(j\omega)$ and of the magnitude of the weighting function $\boldsymbol{r}$.

Finally, the structured singular value $\mu_\Gamma\left\{\mathcal{F}_L\left[\boldsymbol{V}(j\omega_i), \phi_i^{-1}\right]\right\}$ is plotted in Figure 3.10. Because the structured perturbation $\tilde{\Delta}_s$ has only one scalar block and one full block, μ_Γ can be computed to any desired accuracy [2]. It is seen to be smaller than one at many measurement frequencies. Hence, it can be concluded that the family of plants $\mathcal{P}$ and the noise set $\mathcal{W}$ are not consistent with the data with this $\boldsymbol{r}$. One would have to reshape the bound $\boldsymbol{r}$, and perhaps even adopt a new nominal coprime factorization to get consistency. Note that once the LFTs were computed, the μ-test only took a few seconds on a Sun^{TM} SPARCstation^{TM} 10.

3.4.3 Noisy MIMO Case

The general model/data consistency problem for a coprime factorization of a noisy open-loop MIMO system is quite difficult and as yet unsolved. This section introduces a sufficient condition for consistency of a standard left-coprime factorization of a square $p \times p$ MIMO stable plant with noisy experimental frequency-response measurements performed on the plant. Suppose we are given N invertible noisy frequency-response measurements $\{\Phi_i\}_{i=1}^N$ in $\mathbb{C}^{p\times p}$ corresponding

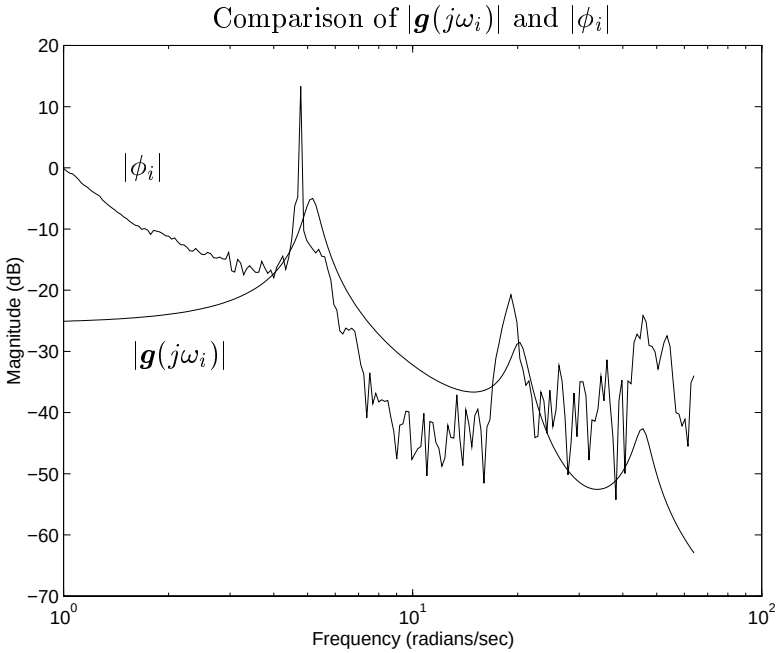

Figure 3.8: Fit between the magnitudes of the measured frequency response and the nominal model.

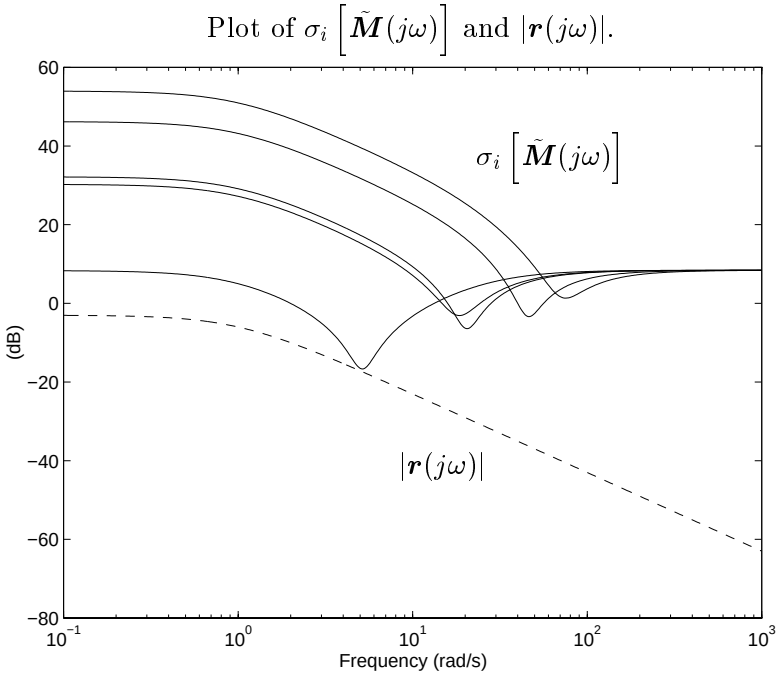

Figure 3.9: Singular values of the nominal factors and worst-case factor perturbations.

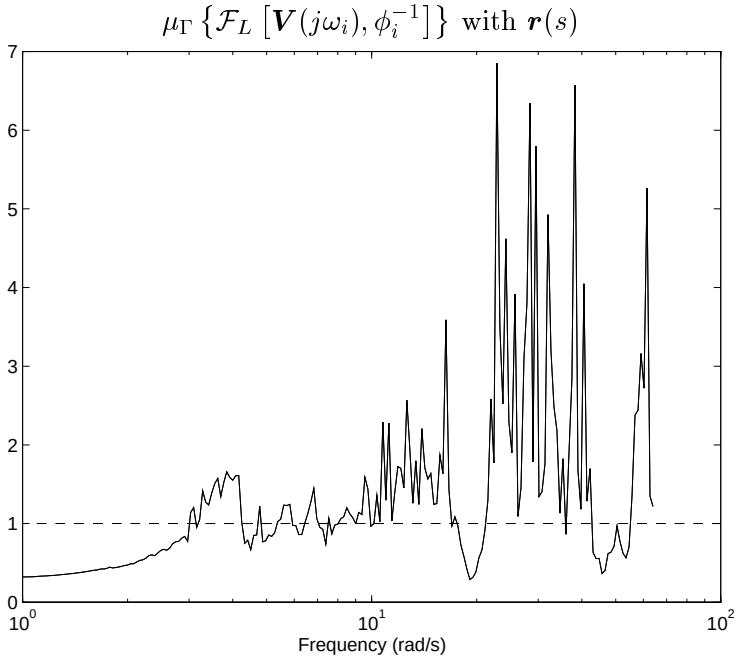

Figure 3.10: Structured singular value test for consistency with $\boldsymbol{r}$.

to the distinct frequencies $\omega_1, \ldots, \omega_N$, a stable nominal left-coprime factorization of the plant, $\boldsymbol{G} = \tilde{\boldsymbol{M}}^{-1}\tilde{\boldsymbol{N}}$, and a unit $\boldsymbol{r}(s)$ in $\mathcal{RH}_\infty$ bounding the factor uncertainty as before. We will use the factor uncertainty set $\mathcal{D}_r$ and the family of plants $\mathcal{P}$ as defined in (2.19) and (3.2). The noise set is defined in (3.7) and consists of $p \times p$ additive complex perturbations. The consistency problem can be stated as follows:

Problem 11 *Given noisy invertible frequency-response data* $\{\Phi_i\}_{i=1}^N \subset \mathbb{C}^{p\times p}$ *at* $\omega_1, \ldots, \omega_N$, *could they have been produced by at least one model in* $\mathcal{P}$ *and* N *noises in* $\mathcal{W}$*? Or, in other words, do there exist* $\boldsymbol{\Delta} \in \mathcal{D}_r$ *and complex noise matrices* $\{\Delta_{ai}\}_{i=1}^N$ *in* $\mathcal{W}$ *such that* $\boldsymbol{G}_p(j\omega_i) + \Delta_{ai} = \Phi_i$, $i = 1, \ldots, N$*?*

This problem turns out to be quite difficult because of the way the perturbations are bounded —the factor perturbation is norm-bounded, whereas the noise perturbation is bounded elementwise. To avoid this difficulty, but at the price of added conservativeness, we will consider norm-bounded noise perturbations instead. This will lead to our sufficient condition for consistency. But before we proceed, it is interesting to derive a problem equivalent to Problem 11 at a discrete set of measurement frequencies.

Introduce the normalized additive perturbation $\tilde{\Delta}_{ai} := L_a^{-1}\Delta_{ai}$. For each ω_i, the consistency equation to be satisfied by admissible normalized perturbation and noise is

$$\Phi_i - \mathcal{F}_U\left[\boldsymbol{P}(j\omega_i), \tilde{\Delta}_{si}\right] = 0, \tag{3.33}$$

where

$$\tilde{\Delta}_{si} := \begin{bmatrix} \tilde{\Delta}_i & 0 \\ 0 & \tilde{\Delta}_{ai} \end{bmatrix},$$

and

$$\boldsymbol{P} := \begin{bmatrix} \boldsymbol{P}_{11} & \boldsymbol{P}_{12} \\ \boldsymbol{P}_{21} & \boldsymbol{P}_{22} \end{bmatrix},$$

$$\boldsymbol{P}_{11} := \begin{bmatrix} 0 & 0 \\ \boldsymbol{r}\tilde{\boldsymbol{M}}^{-1} & 0 \\ 0 & 0 \end{bmatrix}, \qquad \boldsymbol{P}_{12} := \begin{bmatrix} \boldsymbol{r}I \\ \boldsymbol{r}\tilde{\boldsymbol{M}}^{-1}\tilde{\boldsymbol{N}} \\ I \end{bmatrix},$$
$$\boldsymbol{P}_{21} := \begin{bmatrix} \tilde{\boldsymbol{M}}^{-1} & L_a I \end{bmatrix}, \qquad \boldsymbol{P}_{22} := \tilde{\boldsymbol{M}}^{-1}\tilde{\boldsymbol{N}}\ .$$

Much like the SISO problem, this consistency equation is best illustrated by the block diagram of Figure 3.11. Now define the structured set of admissible perturbations

$$\Omega := \left\{ \Delta_s = \begin{bmatrix} \Delta & 0 \\ 0 & \Delta_a \end{bmatrix} \ :\ \Delta \in \mathcal{BC}^{p\times 2p},\ \Delta_a \in \mathbb{C}^{p\times p},\ |[\Delta_a]_{ij}| < 1,\ i,j = 1,\ldots,p \right\}. \tag{3.34}$$

For each frequency ω_i, a problem equivalent to the consistency problem (Problem 11) can be formulated:

Problem 12 *Does there exist a perturbation $\tilde{\Delta}_{si} \in \Omega$ that satisfies (3.33)?*

We do not have a solution to this problem yet. We could rearrange the noise perturbation by putting each of its entries on a diagonal to get something closer to the μ problem, but the function μ itself is not what is needed here as we will see later on. To render the problem more tractable, we restrict the class of additive noise matrices to the set

$$\mathcal{V} := \{\Delta_a \in \mathbb{C}^{p\times p} \ :\ \|\Delta_a\| < L_a\}\ . \tag{3.35}$$

It is easy to show that $\mathcal{V} \subset \mathcal{W}$, so we are making the perturbed coprime factor model more conservative. That is, we are reducing the effect of the noise in our model, so the uncertainty in the factors may have to be increased to account for the data.

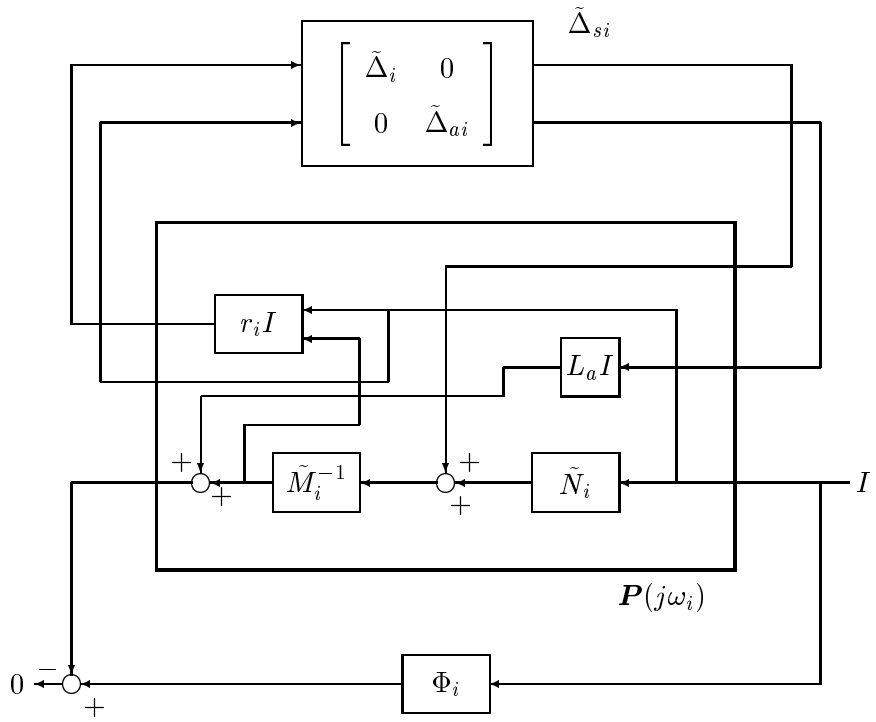

Figure 3.11: Illustration of the consistency equation in the noisy open-loop MIMO case.

The idea is then to set up a compromise consistency problem at a single frequency with only one full uncertainty block $\hat{\Delta}$ such that any solution for it is also a solution to the original problem at that frequency (Problem 12). A solution to the compromise problem is given by the Schmidt-Mirsky Theorem.

Consider the block diagram in Figure 3.12 corresponding to the equation (at frequency ω_i)

$$\Phi_i - (I + \Delta_{yi})(\tilde{M}_i + \Delta M_i)^{-1}(\tilde{N}_i + \Delta N_i) - \Delta_{xi} = 0 \ . \tag{3.36}$$

Letting $G_{pi} := (\tilde{M}_i + \Delta M_i)^{-1}(\tilde{N}_i + \Delta N_i)$ and $\Delta_{ai} := \Delta_{yi} G_{pi} + \Delta_{xi}$, and rearranging the terms, we get

$$\Phi_i - G_{pi} - \Delta_{ai} = 0 \ . \tag{3.37}$$

This equation will be our new consistency equation needed to derive the test sufficient for model/data consistency. According to Figure 3.12, the (new) consistency equation can be

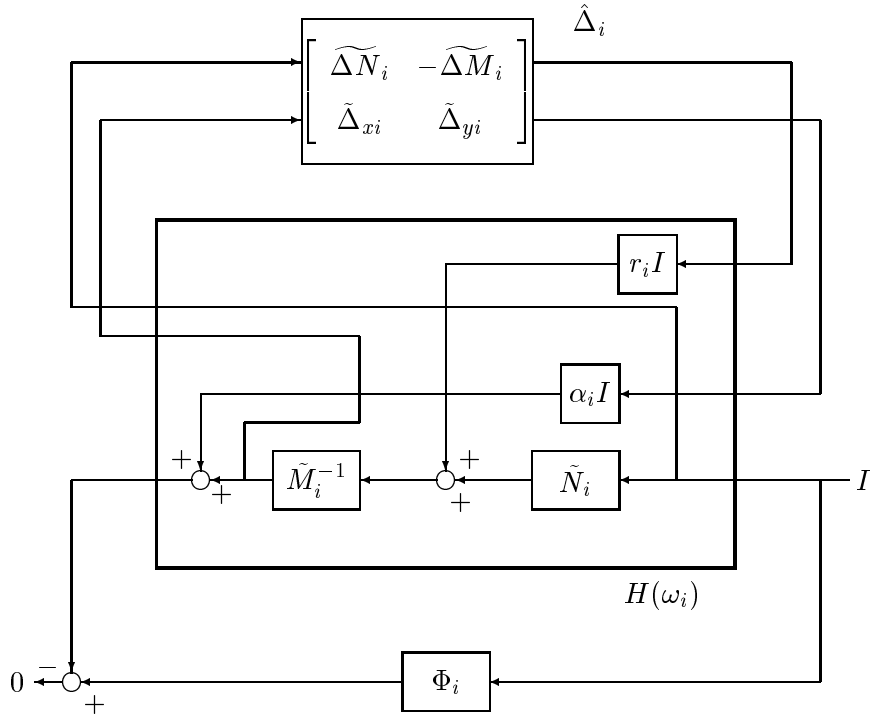

Figure 3.12: Illustration of the consistency equation for the compromise problem.

written as follows:

$$\Phi_i - \mathcal{F}_U \left[H(\omega_i), \hat{\Delta}_i \right] = 0 \ . \tag{3.38}$$

where

$$\hat{\Delta}_i := \begin{bmatrix} \widetilde{\Delta N}_i & -\widetilde{\Delta M}_i \\ \tilde{\Delta}_{xi} & \tilde{\Delta}_{yi} \end{bmatrix},$$

and

$$H(\omega) := \begin{bmatrix} H_{11} & H_{12} \\ H_{21} & H_{22} \end{bmatrix}(\omega) \tag{3.39}$$

where

$$H_{11}(\omega) := \begin{bmatrix} 0 & 0 \\ \boldsymbol{r}(j\omega)\tilde{\boldsymbol{M}}(j\omega)^{-1} & 0 \end{bmatrix}, \quad H_{12}(\omega) := \begin{bmatrix} I \\ \tilde{\boldsymbol{M}}(j\omega)^{-1}\tilde{\boldsymbol{N}}(j\omega) \end{bmatrix},$$
$$H_{21}(\omega) := \begin{bmatrix} \boldsymbol{r}(j\omega)\tilde{\boldsymbol{M}}(j\omega)^{-1} & \alpha(\omega)I \end{bmatrix}, \quad H_{22}(\omega) := \tilde{\boldsymbol{M}}(j\omega)^{-1}\tilde{\boldsymbol{N}}(j\omega)\ .$$

The weight $\alpha_i = \alpha(\omega_i)$ scaling the norm of $[\Delta_{xi}\ \Delta_{yi}]$ must be determined so that

$$\|[\Delta_{xi}\ \Delta_{yi}]\| < \alpha_i \quad \Rightarrow \quad \|\Delta_{ai}\| < L_a\ .$$

Here is a choice of α_i that works:

Proposition 5 *Let* $\alpha_i := \frac{L_a}{\sqrt{2}\max\{1,\ \|\Phi_i\|+pL_a\}}$. *Then* $\|[\Delta_{xi}\ \Delta_{yi}]\| < \alpha_i \ \Rightarrow\ \|\Delta_{ai}\| < L_a$.

Proof First recall that the "true" noise set is $\mathcal{W}$, so it is possible to bound the norm of G_{pi}:

$$\|G_{pi}\| = \|\Phi_i - \Delta_{ai}\| \le \|\Phi_i\| + \|\Delta_{ai}\| < \|\Phi_i\| + pL_a\ ,$$

where the last inequality follows from the fact that a $p \times p$ matrix with all entries equal to L_a has norm equal to pL_a. This is the matrix in the closure of $\mathcal{W}$ with highest norm. Let $\alpha_i := \frac{L_a}{\sqrt{2}\max\{1,\ \|\Phi_i\|+pL_a\}}$, and suppose $\|[\Delta_{xi}\ \Delta_{yi}]\| < \alpha_i$. Then,

$$\|\Delta_{ai}\| = \left\| [\Delta_{xi}\ \Delta_{yi}] \begin{bmatrix} I \\ G_{pi} \end{bmatrix} \right\| \le \|[\Delta_{xi}\ \Delta_{yi}]\| \left\| \begin{bmatrix} I \\ G_{pi} \end{bmatrix} \right\| < \sqrt{2}\alpha_i \max\{1,\ \|G_{pi}\|\}$$
$$\le \sqrt{2}\alpha_i \max\{1,\ \|\Phi_i\| + pL_a\} = L_a. \qquad \blacksquare$$

With this proposition, $\alpha(\omega)$ is defined only at those frequencies where measurements were taken, but it suffices for our purpose.

We are now ready to formulate a compromise problem at a single frequency that will lead to a sufficient condition for consistency.

Problem 13 *Does there exist a perturbation $\hat{\Delta}_i \in \mathcal{B}\mathbb{C}^{2p\times 2p}$ that satisfies (3.38)?*

A positive answer to this problem implies that Problem 12 also has a positive answer. A few results are needed before we can state the main lemma (Lemma 10) which gives a solution to Problem 13. With Lemma 10, the main consistency result of this section (Theorem 8) is then easy to obtain.

The first lemma gives equivalent conditions for consistency at frequency ω. This result is identical to Lemma 3, but the proofs differ slightly. For a measurement frequency ω, let $H := H(\omega)$, and $H_{ij} := H_{ij}(\omega)$, $i,j = 1,2$. Let $H_{12}^{\dagger} := (H_{12}^* H_{12})^{-1} H_{12}^*$, the Moore-Penrose left-inverse of H_{12}. The left-nullspace of H_{12}, $\mathcal{N}_L\{H_{12}\}$, is spanned by the rows of $[\tilde{N} \ -\tilde{M}]$. Note that Lemma 2 still holds with $P_{12}^{\dagger}$ replaced with $H_{12}^{\dagger}$ and $n = p$. This result is used to prove the following lemma.

Lemma 9 *For $\omega \in \mathbb{R}_+$, we are given the invertible, noisy frequency-response datum $\Phi \in \mathbb{C}^{p\times p}$. Assume $\Phi - H_{22}$ is invertible. Then for $\hat{\Delta} \in \mathcal{B}\mathbb{C}^{2p\times 2p}$, the following consistency conditions are equivalent.*

(a) $\Phi - \mathcal{F}_U(H,\hat{\Delta}) = 0$

(b) $\left(H_{12}^{\dagger} - Q\begin{bmatrix} \tilde{N} & -\tilde{M} \end{bmatrix}\right)\left[I - \mathcal{F}_L(H,\Phi^{-1})\hat{\Delta}\right] = 0$ *for some* $Q \in \mathbb{C}^{p\times p}$

(c) $\operatorname{rank}\left[I - \mathcal{F}_L(H,\Phi^{-1})\hat{\Delta}\right] \le p$

Proof First note that $\hat{\Delta} \in \mathcal{B}\mathbb{C}^{2p\times 2p}$ implies that $I - H_{11}\hat{\Delta}$ is nonsingular.

(a) $\Leftrightarrow$ (b) Suppose that for $\hat{\Delta} \in \mathcal{B}\mathbb{C}^{2p\times 2p}$, the consistency condition (a) holds. Then

$$
\begin{aligned}
& \Phi - H_{22} - H_{21}\hat{\Delta}(I - H_{11}\hat{\Delta})^{-1}H_{12} = 0 \\
\Leftrightarrow \quad & \left[(\Phi - H_{22})H_{12}^{\dagger} - H_{21}\hat{\Delta}(I - H_{11}\hat{\Delta})^{-1}\right] H_{12} = 0 \\
\Leftrightarrow \quad & (\Phi - H_{22})H_{12}^{\dagger} - H_{21}\hat{\Delta}(I - H_{11}\hat{\Delta})^{-1} = Q[\tilde{N} \ -\tilde{M}] && \text{for some } Q \in \mathbb{C}^{p\times p} \\
\Leftrightarrow \quad & H_{12}^{\dagger}(I - H_{11}\hat{\Delta}) - (\Phi - H_{22})^{-1}H_{21}\hat{\Delta} = Q[\tilde{N} \ -\tilde{M}](I - H_{11}\hat{\Delta}) && \text{for some } Q \in \mathbb{C}^{p\times p} \\
\Leftrightarrow \quad & H_{12}^{\dagger} - Q[\tilde{N} \ -\tilde{M}] - \left[\left(H_{12}^{\dagger} - Q[\tilde{N} \ -\tilde{M}]\right)H_{11} + (\Phi - H_{22})^{-1}H_{21}\right]\hat{\Delta} = 0 && \text{for some } Q \in \mathbb{C}^{p\times p} \\
\Leftrightarrow \quad & \left(H_{12}^{\dagger} - Q[\tilde{N} \ -\tilde{M}]\right)\{I - \underbrace{\left[H_{11} + H_{12}\left(I - \Phi^{-1}H_{11}\right)^{-1}\Phi^{-1}H_{21}\right]}_{\mathcal{F}_L(H,\Phi^{-1})}\hat{\Delta}\} = 0 && \text{for some } Q \in \mathbb{C}^{p\times p}
\end{aligned}
$$

(c) $\Rightarrow$ (b) Suppose that for $\|\hat{\Delta}\| < 1$, (c) holds. Then the left-nullspace of $I - \mathcal{F}_L(H,\Phi^{-1})\hat{\Delta}$ has dimension $\ge p$. We now show that the subspaces $\mathcal{N}_L\{H_{12}\}$ and $\mathcal{N}_L\{I - \mathcal{F}_L(H,\Phi^{-1})\hat{\Delta}\}$ are

independent. That is, for any nonzero $q \in \mathbb{C}^p$, $q^* \begin{bmatrix} \tilde{N} & -\tilde{M} \end{bmatrix} \left[I - \mathcal{F}_L(H, \Phi^{-1})\hat{\Delta} \right] \neq 0$. Let $\alpha := \alpha(\omega)$.

$$\begin{aligned} q^* \begin{bmatrix} \tilde{N} & -\tilde{M} \end{bmatrix} \left[I - \mathcal{F}_L(H, \Phi^{-1})\hat{\Delta} \right] &= q^* \begin{bmatrix} \tilde{N} & -\tilde{M} \end{bmatrix} - q^* \begin{bmatrix} \tilde{N} & -\tilde{M} \end{bmatrix} H_{11}\hat{\Delta} \\ &= q^*[\tilde{N} \ -\tilde{M}] \left(I - \begin{bmatrix} 0 & 0 \\ r\tilde{M}^{-1} & 0 \end{bmatrix} \begin{bmatrix} r^{-1}\Delta N & -r^{-1}\Delta M \\ \alpha^{-1}\Delta_x & \alpha^{-1}\Delta_y \end{bmatrix} \right) \\ &= q^*[\tilde{N} \ -\tilde{M}] \begin{bmatrix} I & 0 \\ -\tilde{M}^{-1}\Delta N & I + \tilde{M}^{-1}\Delta M \end{bmatrix} \\ &= q^* \begin{bmatrix} \tilde{N} + \Delta N & -(\tilde{M} + \Delta M) \end{bmatrix} \neq 0 \end{aligned}$$

The last inequality follows from the fact that the matrix of perturbed factors has full row rank by (A3.1). This shows the independence of $\mathcal{N}_L\{I - \mathcal{F}_L(H, \Phi^{-1})\hat{\Delta}\}$ and $\mathcal{N}_L\{H_{12}\}$, but also $\dim\left(\mathcal{N}_L\{I - \mathcal{F}_L(H, \Phi^{-1})\hat{\Delta}\}\right) = p$. The latter implication follows from the inequality $\dim\left(\mathcal{N}_L\{I - \mathcal{F}_L(H, \hat{\Phi}^{-1})\tilde{\Delta}\}\right) \leq 2p - \dim\left(\mathcal{N}_L\{H_{12}\}\right) = p$ and the inequality obtained above: $\dim\left(\mathcal{N}_L\left\{I - \mathcal{F}_L(H, \hat{\Phi}^{-1})\tilde{\Delta}\right\}\right) \geq p$. But by Lemma 2, this implies that $\mathcal{N}_L\{I - \mathcal{F}_L(H, \Phi^{-1})\hat{\Delta}\} \in \mathcal{Y}$. Hence, $\exists U$ invertible, Q such that

$$\mathcal{N}_L\{I - \mathcal{F}_L(H, \Phi^{-1})\hat{\Delta}\} = \text{row span}\left(UH_{12}^{\dagger} + Q[\tilde{N} \ -\tilde{M}]\right),$$

and therefore

$$\begin{aligned} \left(UH_{12}^{\dagger} + Q[\tilde{N} \ -\tilde{M}]\right) \left[I - \mathcal{F}_L(H, \Phi^{-1})\hat{\Delta} \right] = 0, \\ \left(H_{12}^{\dagger} + Q_0[\tilde{N} \ -\tilde{M}]\right) \left[I - \mathcal{F}_L(H, \Phi^{-1})\hat{\Delta} \right] = 0, \end{aligned}$$

where $Q_0 = U^{-1}Q$.

(b) $\Rightarrow$ (c) Suppose that for $\|\hat{\Delta}\| < 1$, $\exists Q$ such that

$$\left(H_{12}^{\dagger} - Q \begin{bmatrix} \tilde{N} & \tilde{M} \end{bmatrix}\right) \left[I - \mathcal{F}_L(H, \Phi^{-1})\hat{\Delta} \right] = 0.$$

But $H_{12}^{\dagger} - Q \begin{bmatrix} \tilde{N} & \tilde{M} \end{bmatrix}$ has full row rank p, hence $\text{rank}\left[I - \mathcal{F}_L(H, \Phi^{-1})\hat{\Delta} \right] \leq p$. ■

With this lemma in hand, it is now possible to set up an optimization problem to find a $\hat{\Delta}$ of norm less than one.

Problem 14 *Compute* $\beta := \inf\left\{ \|\hat{\Delta}\| : \text{rank}\left\{ I - \mathcal{F}_L(H, \Phi^{-1})\hat{\Delta} \right\} \leq p, \ \hat{\Delta} \in \mathbb{C}^{2p \times 2p} \right\}$.

If the infimum β is less than 1, then the noise and coprime factor models are consistent with the datum. If $\beta \geq 1$, then we cannot conclude anything. Problem 14 is readily solved by a version of the Schmidt-Mirsky Theorem, Theorem 6. This result tailored to our problem is just

$$\beta = \inf \left\{ \|\hat{\Delta}\| : \text{rank} \left[I - \mathcal{F}_L(H, \Phi^{-1})\hat{\Delta} \right] \leq p,\ \hat{\Delta} \in \mathbb{C}^{2p \times 2p} \right\} = \sigma_p[\mathcal{F}_L(H, \Phi^{-1})]^{-1} \ .$$

Thus, under the following assumptions:

(A3.8) Φ is invertible,

(A3.9) $\Phi - H_{22}$ is invertible,

the test for consistency at one particular frequency ω is as follows.

Lemma 10 *If $\sigma_p[\mathcal{F}_L(H, \Phi^{-1})]^{-1} < 1$, then the family of square plant models $\mathcal{P}$ and the noise model $\mathcal{W}$ are consistent with the datum Φ at the frequency ω.*

Proof From the Schmidt-Mirsky Theorem, there exists a perturbation $\hat{\Delta}$ with norm $\sigma_p[\mathcal{F}_L(H, \Phi^{-1})]^{-1} = \|\hat{\Delta}\| < 1$ that satisfies the consistency conditions in Lemma 9. It follows that

$$\left\| \begin{bmatrix} \widetilde{\Delta N} & -\widetilde{\Delta M} \end{bmatrix} \right\| = \left\| \begin{bmatrix} r^{-1}\Delta N & -r^{-1}\Delta M \end{bmatrix} \right\| < 1 \ \Rightarrow \ \left\| \begin{bmatrix} \Delta N & -\Delta M \end{bmatrix} \right\| < r$$

and

$$\left\| \begin{bmatrix} \tilde{\Delta}_x & \tilde{\Delta}_y \end{bmatrix} \right\| = \left\| \begin{bmatrix} \alpha^{-1}\Delta_x & \alpha^{-1}\Delta_y \end{bmatrix} \right\| < 1 \ \Rightarrow \ \left\| \begin{bmatrix} \Delta_x & \Delta_y \end{bmatrix} \right\| < \alpha \ .$$

By Proposition 5, this last inequality says that $\|\Delta_a\| < L_a$, i.e., $\Delta_a \in \mathcal{V} \subset \mathcal{W}$. ■

With this lemma in hand, it is now easy to prove the main result of this section. It is a sufficient condition for the original noisy square MIMO model/data consistency problem (Problem 11).

Theorem 8 *There exist $\boldsymbol{G}_p \in \mathcal{P}$ and noises $\Delta_{ai} \in \mathcal{W}$ that could have produced the noisy frequency-response data if $\sigma_p \left\{ \mathcal{F}_L \left[H(\omega_i), \Phi_i^{-1} \right] \right\}^{-1} < 1$ for $i = 1, \ldots, N$.*

Proof Follows readily from Lemma 10 and Theorem 4. ■

3.4.3.1 How conservative is this test?

To see how conservative the singular value test based on the sufficient condition of Theorem 8 is, we first have to identify the sources of conservativeness. Consider a datum obtained at a single frequency ω. The first source of conservativeness is the minimization of an upper bound on $\max_{ij} |[\Delta_a]_{ij}|$ instead of minimizing it directly, namely the norm of Δ_a. Obviously, these two functions are the same in the SISO case, but for square MIMO plants, the conservativeness grows with the number of inputs. To see this for a p-input, p-output plant, assume the norm of Δ_a was minimized such that $\max_{ij} |[\Delta_a]_{ij}| \leq \|\Delta_a\| < L_a$. There exists a Δ_{a0} for which $\max_{ij} |[\Delta_{a0}]_{ij}| = L_a$, but $\|\Delta_{a0}\| = pL_a$. Therefore, in the worst-case, we minimize too much by a factor p. The second source of conservativeness is the minimization of $\left\| \begin{bmatrix} \Delta_x & \Delta_y \end{bmatrix} \right\|$ instead of $\|\Delta_a\|$. The problem here is the weight α, as given in Proposition 5, which can be quite small. This constrains the search only to small $\left\| \begin{bmatrix} \Delta_x & \Delta_y \end{bmatrix} \right\|$, and the natural solution $\Delta_x = \Delta_a$ and $\Delta_y = 0$ (see (3.36)) may not be allowed because the "true" $\|\Delta_a\|$ is larger than α. The third source of conservativeness is the minimization of $\left\| \begin{bmatrix} \Delta N & -\Delta M \\ \Delta_x & \Delta_y \end{bmatrix} \right\|$ instead of concurrently minimizing $\left\| \begin{bmatrix} \Delta N & -\Delta M \end{bmatrix} \right\|$ and $\left\| \begin{bmatrix} \Delta_x & \Delta_y \end{bmatrix} \right\|$. In the worst case, we are minimizing too much by a factor $\sqrt{2}$. Several numerical examples in which the "true" noise and factor perturbation matrices were randomly generated showed that for plants with few inputs (say fewer than 5), the weight α seemed to introduce the most conservativeness in the test, whereas for plants with many inputs, the first source of conservativeness identified above was dominant, rendering the test much less useful for such systems. In any case, it may be possible to increase the norm bound on the factor perturbation until an inconclusive test becomes conclusive as we will show next. In other words, increasing the uncertainty in the factorization without increasing the noise bound may eventually lead to a model accounting for the datum. But it should be remembered that $|\boldsymbol{r}(j\omega)|$ is bounded above by $\underline{\sigma}\left[\tilde{\boldsymbol{M}}(j\omega)\right]$ to guarantee that $\tilde{\boldsymbol{M}}_p$ is a unit. Finally, the following proposition suggests that if $|r|$ is increased, we might eventually get consistency.

Proposition 6 *$\sigma_p \left[\mathcal{F}_L(H, \Phi^{-1})\right]^{-1}$ is a nonincreasing function of $|r|$ on $[0, \underline{\sigma}[\tilde{M}])$.*

Proof Let $F := (\Phi - H_{22})^{-1}$ and expand $\mathcal{F}_L(H, \Phi^{-1})$ to get

$$\mathcal{F}_L(H, \Phi^{-1}) = \begin{bmatrix} rF\tilde{M}^{-1} & \alpha F \\ r\tilde{M}^{-1}(I + \tilde{N}F\tilde{M}^{-1}) & \alpha\tilde{M}^{-1}\tilde{N}F \end{bmatrix} =: \begin{bmatrix} rA & B \end{bmatrix} .$$

The singular values of $\mathcal{F}_L(H, \Phi^{-1})$ are just the square roots of the eigenvalues of $|r|^2AA^* + BB^*$. Let $\hat{r}$ be a complex number of magnitude larger than $|r|$, and define ϵ by $|\hat{r}|^2 = |r|^2 + \epsilon$. Then

$$\text{spectrum}\left\{|\hat{r}|^2AA^* + BB^*\right\} = \text{spectrum}\left\{|r|^2AA^* + BB^* + \epsilon AA^*\right\} .$$

But ϵAA^* is positive semidefinite, hence

$$\lambda_p\left(|r|^2AA^* + BB^* + \epsilon AA^*\right) \geq \lambda_p\left(|r|^2AA^* + BB^*\right) ,$$

where $\lambda_i(Q)$ is the i^{th} nonnegative eigenvalue of the $n \times n$ positive semidefinite matrix Q with eigenvalues ordered as $\lambda_1 \geq \lambda_2 \geq \cdots \geq \lambda_n$. Therefore $\sigma_p\left[\mathcal{F}_L(H, \Phi^{-1})\right]^{-1} = \lambda_p\left(|r|^2AA^* + BB^*\right)^{-\frac{1}{2}}$ is nonincreasing. ■

This result tells us that the infimum β may be made smaller than one by increasing $|r|$. If $|r|$ has to be increased significantly to ensure consistency, then a lot of uncertainty is introduced in the coprime factorization. This is obviously undesirable if the model is to be used for robust control design because it limits the achievable closed-loop performance.

3.4.3.2 Numerical Example

The full experimental data set obtained on the two-link flexible robot will be used this time. The noise level is again $L_a = 0.06$. We consider a normalized left-coprime factorization of the 2-input, 2-output nominal plant model given by $\boldsymbol{G} = \tilde{\boldsymbol{M}}^{-1}\tilde{\boldsymbol{N}}$, where

$$\begin{bmatrix} \tilde{\boldsymbol{M}} & \tilde{\boldsymbol{N}} \end{bmatrix} = C_n(sI - A_n)^{-1}B_n + D_n,$$

with the minimal realization (A_n, B_n, C_n, D_n) given by

$$A_n = 10^3 \begin{bmatrix} -.0009 & 0 & 0 & 0 & 0 & -.0275 & .0026 & -.0019 & -.0248 & -.0124 \\ 0 & -.0046 & 0 & 0 & 0 & .0065 & -2.1000 & .0137 & .1805 & .0903 \\ 0 & 0 & -.0020 & 0 & 0 & -.0087 & .0249 & -.4316 & -.2407 & -.1205 \\ 0 & 0 & 0 & -.0115 & 0 & -.0003 & .0008 & -.0006 & -5.0959 & -.0039 \\ 0 & 0 & 0 & 0 & -.0029 & -.0011 & .0032 & -.0024 & -.0314 & -.3471 \\ .0010 & 0 & 0 & 0 & 0 & -.0030 & .0085 & -.0062 & -.0819 & -.0410 \\ 0 & .0010 & 0 & 0 & 0 & .0004 & -.0013 & .0009 & .0124 & .0062 \\ 0 & 0 & .0010 & 0 & 0 & -.0009 & .0025 & -.0018 & -.0244 & -.0122 \\ 0 & 0 & 0 & .0010 & 0 & -.0001 & .0002 & -.0001 & -.0017 & -.0008 \\ 0 & 0 & 0 & 0 & .0010 & -.0002 & .0007 & -.0005 & -.0066 & -.0033 \end{bmatrix},$$

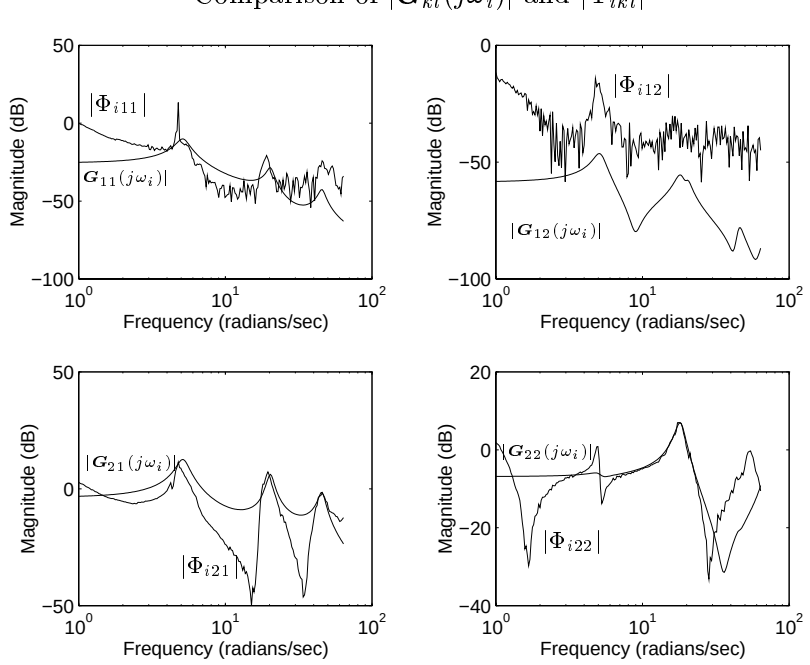

Figure 3.13: Fit between the magnitudes of the measured data and the nominal model.

$$
B_n = \begin{bmatrix}
0.0718 & -0.2565 & 5.8651 & 0.0887 \\
-0.0385 & 1.8685 & -17.5637 & -0.2486 \\
0.0980 & -2.4921 & -11.7164 & 0.1978 \\
0.0046 & -0.0806 & 0.0652 & 4.7609 \\
0.0117 & -0.3247 & 0.1354 & 2.3841 \\
0.0719 & -0.8484 & 0 & 0 \\
-0.0009 & 0.1288 & 0 & 0 \\
0.0058 & -0.2522 & 0 & 0 \\
-0.0000 & -0.0173 & 0 & 0 \\
-0.0007 & -0.0687 & 0 & 0
\end{bmatrix},
$$

$$
C_n = \begin{bmatrix}
0 & 0 & 0 & 0 & 0 & -0.2561 & 0.0883 & -0.1318 & -0.0180 & -0.0340 \\
0 & 0 & 0 & 0 & 0 & 3.4651 & -10.0042 & 7.3288 & 96.5954 & 48.3456
\end{bmatrix},
$$

$$
D_n = \begin{bmatrix}
1 & 0 & 0 & 0 \\
0 & 1 & 0 & 0
\end{bmatrix}.
$$

The fit between the magnitudes of the entries of $\boldsymbol{G}(j\omega_i)$ and the entries of Φ_i is shown in Figure 3.13. It can be observed that the fit is not very good, yet we will see that the factorization and noise models are consistent with the data. Figure 3.14 shows that Assumption (A3.1) holds. The inverse of the second singular value of $\mathcal{F}_L\left[H(\omega_i), \Phi_i^{-1}\right]$ is plotted in Figure 3.15; it is smaller

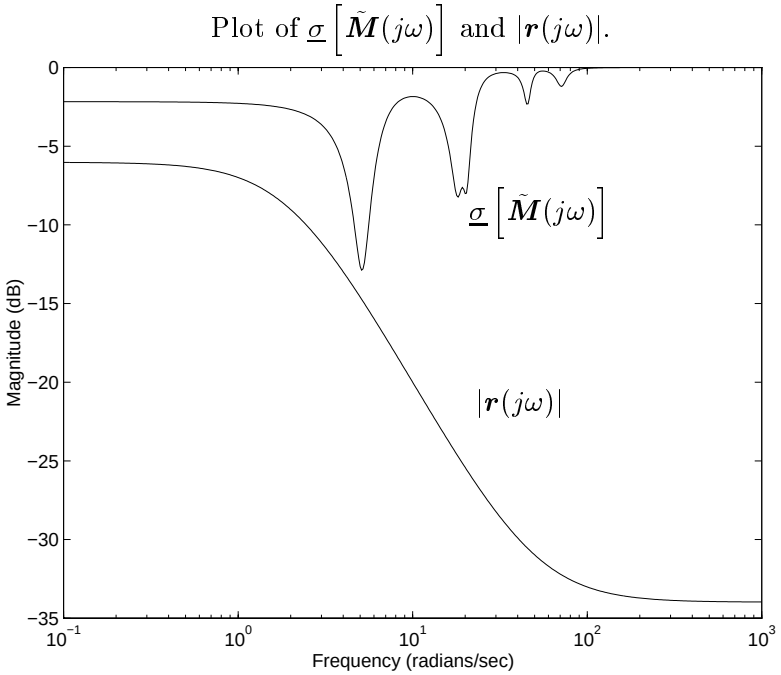

Figure 3.14: Smallest singular value of $\tilde{\boldsymbol{M}}(j\omega)$ and bound $|\boldsymbol{r}(j\omega)|$.

than one for all ω_i and therefore it can be concluded that the family of perturbed coprime factorizations and the noise set are consistent with the data. This may seem a bit surprising, considering the poor fit between the nominal model and the data shown in Figure 3.13. But given that coprime factor models are well-suited to modeling lightly-damped systems, and the relatively high noise bound, this result is not so surprising after all. This example shows that the sufficient condition of Theorem 8 can be useful for practical problems.

3.5 Summary and Discussion

In this chapter, a general model/data consistency problem was formulated and then specialized to perturbed coprime factor models and frequency-response data. The results are applicable to LCF models of LFSS introduced in Chapter 2, but also more generally to any coprime factorization of a plant model, normalized or not.

In frequency-response experiments, output noise usually introduces uncertainty in the time-delay and amplitude readings at the recorded output signal. This uncertainty then translates into uncertainty in the magnitude and phase of the noise-free frequency response. We considered the class of time-domain output noises in $\mathcal{L}_\infty$ with norm bounded by M, and showed that their

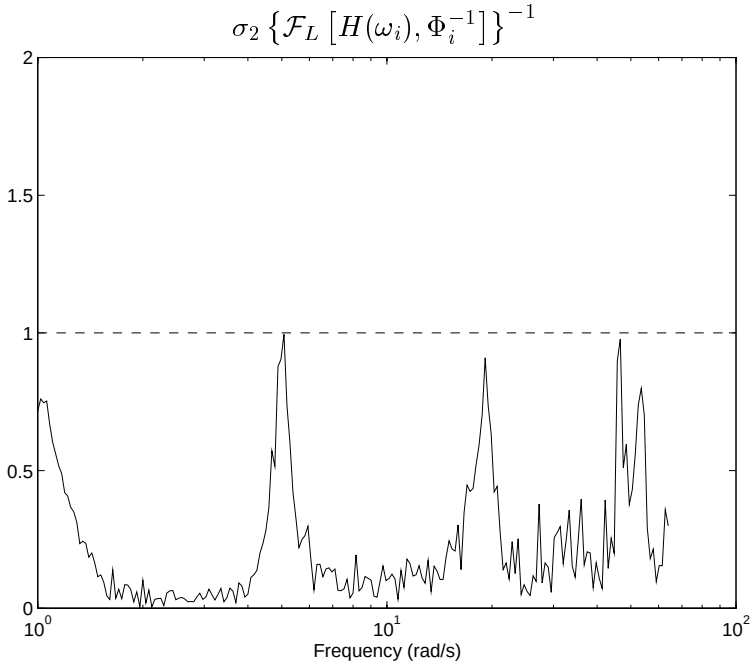

Figure 3.15: Test of sufficient condition for consistency with $\sigma_2\left\{\mathcal{F}_L\left[H(\omega_i),\Phi_i^{-1}\right]\right\}^{-1}$.

effect is approximately equivalent to an additive perturbation $\delta_a \in \mathbb{C}$ of the noise-free frequency response with magnitude bounded by M.

The cases treated for open-loop measurements were: (i) noise-free MIMO with standard coprime factorization, (ii) noise-free MIMO with special factorization for square LFSS model, (iii) general noisy SISO, and (iv) noisy MIMO with standard coprime factorization of square plant. Necessary and sufficient conditions for model/data consistency were given for all these cases, except (iv) which is quite difficult. A practical sufficient condition was nonetheless provided for this case.

A building block for the solutions of all consistency problems is a boundary interpolation theorem in $\mathcal{RH}_\infty(\mathbb{D})$ (Theorem 4) that allowed us to focus on consistency problems at one single measurement frequency at a time. This simplified the problems because then the consistency equations involved constant complex matrices only. Thus the underlying minimization problems required to show the existence of a perturbation of norm less than one were finite-dimensional and tractable.

The tests for checking consistency boil down to showing that there exist constant factor perturbations and additive complex noises of norm less than one such that the complex consistency equations hold at each measurement frequency. These tests involve singular value or structured

singular value computations on LFTs constructed with the complex frequency-response data and the a priori information consisting of the nominal coprime factorization, the bound $\boldsymbol{r}$ on the factor uncertainty, and noise bounds.

One can see how $\boldsymbol{r}$ can be constructed and improved as new experimental data become available. This allows the control system designer to reduce the uncertainty about the size of the plant's uncertainty. Since the former type of uncertainty is unmodeled, it is highly desirable to reduce it to a minimum.

The next chapter presents a set of consistency results for the closed-loop case. It will be seen that consistency at each measurement frequency is only necessary for full model/data consistency because a potential admissible perturbation $\boldsymbol{\Delta} \in \mathcal{D}_r$ must not only interpolate the complex minimum-norm perturbations, but it also must stabilize the nominal plant. A general sufficient condition for consistency based on this remark will be given.

Chapter 4

Consistency of Experimental Closed-Loop Frequency-Response Data with Coprime Factor Models

This chapter addresses the model/data consistency problem for coprime factorizations and closed-loop frequency-response measurements. Standard factorizations and LCF models of LFSS are considered.

4.1 Introduction

The closed-loop consistency problem for coprime factorizations is more difficult than the open-loop one, but potentially very useful. Many systems are very lightly damped or unstable, and perturbed coprime factorizations are often a good choice to model them [51]. It may be difficult or even impossible to run open-loop frequency-response experiments on these systems, so the open-loop results for consistency given in Chapter 3 may be of limited use. In this chapter, it is assumed that a stabilizing controller providing sufficient damping was designed for such a system, allowing measurement of the closed-loop frequency response at distinct frequencies. We will see that these measurements can be used to refine the norm bound $|\boldsymbol{r}(j\omega)|$. This improved characterization of the uncertainty in the model allows the design of a better controller achieving desired performance goals.

It should be noted that finding a necessary and sufficient condition for consistency of the

model with the data is much more difficult than in the open-loop case. The reason is that we must not only show the existence of a stable perturbation of norm less than one interpolating a set of complex matrices, but we must also show that there exists such a perturbation that stabilizes the nominal closed-loop system. Thus we will give only separate necessary conditions and sufficient conditions for the problems formulated.

A necessary condition for the noise-free problem is given which is a simple test consisting of computing minimum-norm solutions to underdetermined linear complex matrix equations, just as in the open-loop case. For the case of the special factorization for square $p \times p$ LFSS, a necessary condition based on the Schmidt-Mirsky Theorem is derived. It requires the computation of the p^{th} singular values of N LFTs. The theorem on boundary interpolation in $\mathcal{RH}_\infty$ is used in those two cases. A numerical example using a coprime factor description of Daisy's 46^{th}-order, 23-input, 23-output plant model is worked out to illustrate the result.

Then the closed-loop noisy model/data consistency problem considered is for SISO plants only. The noise model is as described in Section 3.3, and necessary conditions for consistency are given. The necessary conditions involve μ computations on LFTs.

A general sufficient condition for consistency is given for all cases considered. It is based on an observation that strongly stabilizing perturbations are required, together with a robust performance theorem involving the structured singular value μ.

4.2 Noise-Free Case

Consider the feedback system in Figure 4.1. Two controllers were included in order to treat the two different configurations of input tracking ($\boldsymbol{K}_1 = I_p$) and input disturbance rejection ($\boldsymbol{K}_2 = I_m$) in a unified way. The tracking configuration is generally used to ensure that the output of the plant $y \in \mathbb{R}^p$ tracks the reference input $v \in \mathbb{R}^p$ over a given frequency band. On the other hand, the input disturbance rejection configuration is used to attenuate the effect of an input disturbance $v \in \mathbb{R}^m$ on the output of the plant $y \in \mathbb{R}^p$. This configuration may facilitate frequency-response experiments on a mechanical system with a force/torque input v that can be applied by control actuators or external ones.

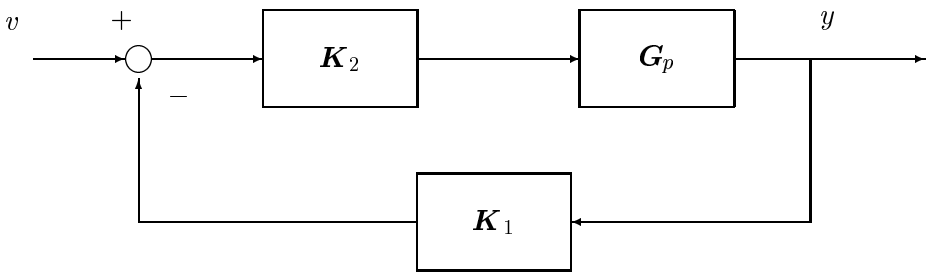

Figure 4.1: Feedback configuration for input tracking or disturbance rejection.

4.2.1 Standard Factorization

Here we treat the case of a standard LCF of $\boldsymbol{G}$, i.e., $C = I_p$. Note that one has to be careful with the dimensions of the transfer matrices in the equations that follow: They have different dimensions depending on which configuration one is interested in.

Let the transfer matrix from v to y in Figure 4.1 be denoted as $\boldsymbol{T}$. Then the closed-loop equation is

$$\begin{aligned} \boldsymbol{T} &= (I + \boldsymbol{G}_p\boldsymbol{K}_2\boldsymbol{K}_1)^{-1}\boldsymbol{G}_p\boldsymbol{K}_2 \\ &= \left[I + (\tilde{\boldsymbol{M}} + \Delta\boldsymbol{M})^{-1}(\tilde{\boldsymbol{N}} + \Delta\boldsymbol{N})\boldsymbol{K}_2\boldsymbol{K}_1\right]^{-1}(\tilde{\boldsymbol{M}} + \Delta\boldsymbol{M})^{-1}(\tilde{\boldsymbol{N}} + \Delta\boldsymbol{N})\boldsymbol{K}_2 \\ &= (\tilde{\boldsymbol{M}} + \Delta\boldsymbol{M} + \tilde{\boldsymbol{N}}\boldsymbol{K}_2\boldsymbol{K}_1 + \Delta\boldsymbol{N}\boldsymbol{K}_2\boldsymbol{K}_1)^{-1}(\tilde{\boldsymbol{N}} + \Delta\boldsymbol{N})\boldsymbol{K}_2 \ . \end{aligned} \tag{4.1}$$

After rearranging this equation in the form of (3.8), we get

$$\Delta\boldsymbol{N}\boldsymbol{K}_2(I - \boldsymbol{K}_1\boldsymbol{T}) - \Delta\boldsymbol{M}\boldsymbol{T} = \tilde{\boldsymbol{M}}\boldsymbol{T} + \tilde{\boldsymbol{N}}\boldsymbol{K}_2(\boldsymbol{K}_1\boldsymbol{T} - I) \ . \tag{4.2}$$

We now state the model/data consistency problem for closed-loop frequency-response data for a feedback control system as in Figure 4.1.

Problem 15 *We are given noise-free closed-loop frequency-response data* $\{\Phi_i\}_{i=1}^N$ *obtained on the closed-loop system of Figure 4.1 at the distinct frequencies* $\omega_1, \ldots, \omega_N$. *Could the data have been produced by at least one plant model in* $\mathcal{P}$? *Or, in other words, does there exist a fixed* $\boldsymbol{\Delta} \in \mathcal{D}_r$ *such that the closed-loop transfer matrix* $\boldsymbol{T}$ *in (4.1) with the corresponding perturbed model* $\boldsymbol{G}_p$ *is stable and interpolates the complex matrices* Φ_i *at* $\omega_1, \ldots, \omega_N$?

A necessary condition for this question to have a positive answer can be obtained using exactly the same procedure as in the open-loop case. For a measurement frequency ω, let

$U := [\tilde{\boldsymbol{M}}\boldsymbol{T}+\tilde{\boldsymbol{N}}\boldsymbol{K}_2(\boldsymbol{K}_1\boldsymbol{T}-I)](j\omega)$ and $W := \begin{bmatrix} \boldsymbol{K}_2(I-\boldsymbol{K}_1\boldsymbol{T}) \\ \boldsymbol{T} \end{bmatrix}(j\omega)$. Then (4.2) at frequency ω can be written as

$$\Delta W = U \ , \tag{4.3}$$

where $W \in \mathbb{C}^{(m+p)\times p}$, $U \in \mathbb{C}^{p\times p}$ and $\Delta \in \mathbb{C}^{p\times(m+p)}$ for the tracking configuration, and $W \in \mathbb{C}^{(m+p)\times m}$, $U \in \mathbb{C}^{p\times m}$ and $\Delta \in \mathbb{C}^{p\times(m+p)}$ for the input disturbance rejection configuration. Equation (4.3) is an underdetermined system of linear equations over the field $\mathbb{C}$. Let $\Delta_i := \boldsymbol{\Delta}(j\omega_i)$ for $i = 1, \ldots, N$, with similar definitions for W_i and U_i. Note that $U_i^* \subset \mathrm{Ra}\{W_i^*\}$, so there exist an infinity of solutions to (4.3). If W_i does not have full column rank, then the redundant equations can be deleted from (4.3). After these equations are removed, the new W_i has full column rank. Then the matrix equation (4.3) can be solved with $\boldsymbol{T} = \Phi_i$ for a minimum-norm Δ_i, $i = 1, \ldots, N$, for example with

$$\Delta_i = U_i(W_i^*W_i)^{-1}W_i^* \ . \tag{4.4}$$

Note that this is one possible way of computing a minimum-norm solution to (4.3). Software packages such as Matlab^{TM} offer quicker ways of computing such a solution. The following theorem gives a necessary condition for consistency of the perturbed coprime factor model of the plant with the closed-loop frequency-response data.

Theorem 9 *The noise-free closed-loop MIMO CF model/data consistency problem of Problem 15 has a positive answer only if* $\|\Delta_i\| < |\boldsymbol{r}(j\omega_i)|$ *for all* $i = 1, \ldots, N$.

Proof Problem 15 has a positive answer only if there exists a perturbation $\boldsymbol{\Delta} \in \mathcal{D}_r$ interpolating Δ_i at ω_i, $i = 1, \ldots, N$. As in the proof of Theorem 2, such a function exists iff $\|\Delta_i\| < |\boldsymbol{r}(j\omega_i)|$ for $i = 1, \ldots, N$. ■

Just as in the open-loop case, the bound $|\boldsymbol{r}(j\omega)|$ can be adjusted such that the inequality in the theorem statement is satisfied for all i. This is necessary for the new model to be consistent with all the data. A sufficient condition for Problem 15 to have a positive answer is deferred to Section 4.4 where a general feedback configuration including as special cases standard coprime factorizations and special factorizations for flexible systems is treated.

4.2.2 Special Factorization for Square LFSS Models

We now derive a necessary condition for consistency of a factorization of a square, p-input, p-output LFSS introduced in Chapter 2 with closed-loop frequency-response data. More specifically, the factorization described in Section 3.2 and given by (3.1) for the open-loop consistency problem will be used. We consider the setup of Figure 4.1 for tracking or input disturbance rejection closed-loop configurations.

Two standing assumptions in this section are the following:

(A4.1) $\left[\tilde{\boldsymbol{N}}_p \ -\tilde{\boldsymbol{M}}_p\right](j\omega)$ has full row rank for all $\boldsymbol{\Delta} \in \mathcal{D}_r$ and for all $\omega \in \mathbb{R}$.

(A4.2) For all $\boldsymbol{\Delta} \in \mathcal{D}_r$, no pole-zero cancellation occurs in $\overline{\mathbb{C}}_+$ when the product $C\tilde{\boldsymbol{M}}_p^{-1}$ is formed.

Assumption (A4.1) holds for the two models of Daisy used in Chapters 5 and 6. Motivation for this assumption is now discussed. It was found empirically that the minimum distance between $\underline{\sigma}\left\{\left[\tilde{\boldsymbol{N}} \ -\tilde{\boldsymbol{M}}\right](j\omega)\right\}$ and $|\boldsymbol{r}(j\omega)|$ across frequency for an LCF of Daisy is a good a priori indication of the achievable robustness and performance levels with a controller to be designed. The closer this minimum distance was to zero, the harder it was to achieve the performance specification while maintaining robustness to the uncertainty in the modal parameters. If this distance is greater than zero, then the full row rank assumption above is satisfied.

Another way to state Assumption (A4.2) is that the pair $(C, \ \tilde{\boldsymbol{M}}_p)$ is right-coprime for every $\boldsymbol{\Delta} \in \mathcal{D}_r$ (see Appendix A). This assumption is quite mild; without it, robust internal stability for all $\boldsymbol{\Delta} \in \mathcal{D}_r$ could not be achieved.

The main result of this section is Theorem 10 which gives a necessary condition for a positive answer to the noise-free closed-loop consistency problem for flexible systems, Problem 17.

Consider the following consistency equation at frequency ω illustrated in Figure 4.2, where the input transfer matrix $\boldsymbol{J}$ has been absorbed into $\boldsymbol{K}_2$:

$$\Phi - \left[I + C(\tilde{M} + r\tilde{\Delta}M)^{-1}(\tilde{N} + r\tilde{\Delta}N)K_2K_1\right]^{-1} C(\tilde{M} + r\tilde{\Delta}M)^{-1}(\tilde{N} + r\tilde{\Delta}N)K_2 = 0. \quad (4.5)$$

It is assumed that:

(A4.3) $\boldsymbol{K}_2(j\omega)$ is nonsingular for all $\omega \in \mathbb{R}$,

(A4.4) the combination of $\boldsymbol{K}_1$ and $\boldsymbol{K}_2$ internally stabilizes the plant and its nominal model,

(A4.5) $n \geq p$, i.e., there are more modes in the model than there are inputs (and outputs),

(A4.6) C has full row rank.

Assumptions (A4.5) and (A4.6) hold for most LFSS or experimental testbeds and are not really restrictive. Some motivation for these two assumptions is provided by the following observation. Referring to Figure 4.2, we can see that a necessary condition for consistency is that the columns of the $p \times p$ matrix $(\Phi - H_{22})$ lie in $\mathrm{Ra}\{H_{21}\}$ where H_{21} is $p \times n$. But we have to assume that $\Phi - H_{22}$ is nonsingular for Lemma 11 to hold true, so it follows that H_{21} must have full row rank p. This is turn implies that we must have $n \geq p$.

In LFT notation, Equation (4.5) takes the simpler form:

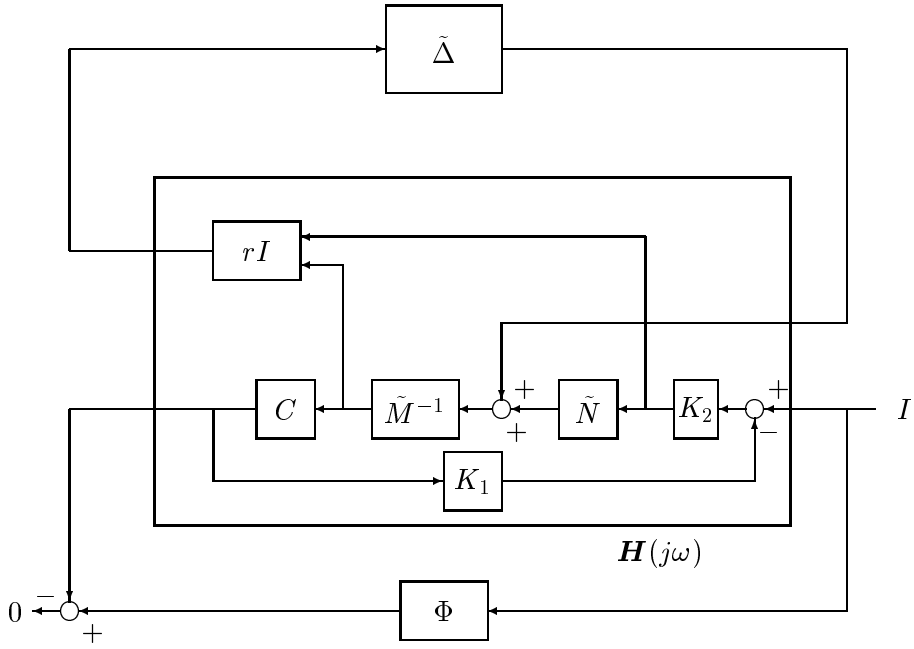

Figure 4.2: Block diagram of consistency equation for a noise-free feedback-controlled MIMO flexible system.

$$\Phi - \mathcal{F}_U(H, \tilde{\Delta}) = 0, \tag{4.6}$$

where

$$H := \boldsymbol{H}(j\omega) = \begin{bmatrix} H_{11} & H_{12} \\ H_{21} & H_{22} \end{bmatrix},$$

$$H_{11} := \begin{bmatrix} -r(I + K_2K_1C\tilde{M}^{-1}\tilde{N})^{-1}K_2K_1C\tilde{M}^{-1} \\ r(I + \tilde{M}^{-1}\tilde{N}K_2K_1C)^{-1}\tilde{M}^{-1} \end{bmatrix}, \quad H_{12} := \begin{bmatrix} r(I + K_2K_1C\tilde{M}^{-1}\tilde{N})^{-1}K_2 \\ r(I + \tilde{M}^{-1}\tilde{N}K_2K_1C)^{-1}\tilde{M}^{-1}\tilde{N}K_2 \end{bmatrix},$$
$$H_{21} := (I + C\tilde{M}^{-1}\tilde{N}K_2K_1)^{-1}C\tilde{M}^{-1}, \qquad H_{22} := (I + C\tilde{M}^{-1}\tilde{N}K_2K_1)^{-1}C\tilde{M}^{-1}\tilde{N}K_2 .$$

This general feedback configuration includes as special cases the reference tracking configuration ($\boldsymbol{K}_1 = I_p$), and the input disturbance rejection configuration ($\boldsymbol{K}_2 = \boldsymbol{J}$). The consistency problem at frequency ω can be stated as follows.

Problem 16 *Given an invertible, noise-free, closed-loop frequency-response datum $\Phi \in \mathbb{C}^{p\times p}$ at ω, does there exist a $\tilde{\Delta} \in \mathcal{B}\mathbb{C}^{n\times(n+p)}$ such that $I - H_{11}\tilde{\Delta}$ is nonsingular and $\Phi - \mathcal{F}_U(H, \tilde{\Delta}) = 0$?*

But the more general model/data consistency problem that we want to solve here is the following.

Problem 17 *Given invertible, noise-free, closed-loop frequency-response data $\{\Phi_i\}_{i=1}^N \subset \mathbb{C}^{p\times p}$ at the distinct frequencies $\omega_1, \ldots, \omega_N$, could they have been produced by at least one model in $\mathcal{P}$? Or, in other words, does there exist a $\boldsymbol{\Delta} \in \mathcal{D}_r$ that stabilizes $\boldsymbol{H}$ and such that $\mathcal{F}_U\left[\boldsymbol{H}(j\omega_i), \tilde{\boldsymbol{\Delta}}(j\omega_i)\right] = \Phi_i$, for $i = 1, \ldots, N$?*

We first look for a solution to Problem 16. Recall that K_2 is assumed to have full rank in (A4.3), and hence H_{12} has full column rank. Let $H_{12}^\dagger \in \mathbb{C}^{p\times(p+n)}$ be the Moore-Penrose left-inverse of H_{12}. It is easy to show that $\mathcal{N}_L\{H_{12}\} = \text{row span}\left([\tilde{N} \; -\tilde{M}]\right)$. Note that Lemma 2 still holds if we replace P_{12} by H_{12}. This result allows us to establish the following lemma which is very similar to Lemma 3, although the proofs differ slightly.

Lemma 11 *For $\omega \in \mathbb{R}_+$, we are given the invertible frequency-response datum $\Phi \in \mathbb{C}^{p\times p}$. Assume $\Phi - H_{22}$ is invertible and $I - H_{11}\tilde{\Delta}$ is nonsingular. Then for $\tilde{\Delta} \in \mathcal{B}\mathbb{C}^{n\times(p+n)}$, the following consistency conditions are equivalent.*

(a) $\Phi - \mathcal{F}_U(H, \tilde{\Delta}) = 0$

(b) $\left(H_{12}^\dagger - Q\begin{bmatrix} \tilde{N} & -\tilde{M} \end{bmatrix}\right)\left[I - \mathcal{F}_L(H, \Phi^{-1})\tilde{\Delta}\right] = 0$ *for some* $Q \in \mathbb{C}^{p\times n}$

(c) $\text{rank}\left[I - \mathcal{F}_L(H, \Phi^{-1})\tilde{\Delta}\right] \le n$

Proof

(a) $\Leftrightarrow$ (b) Same as in proof of Lemma 3.

(b) $\Rightarrow$ (c) This is obvious.

(c) $\Rightarrow$ (b) Suppose $\text{rank}\left[I - \mathcal{F}_L(H, \Phi^{-1})\tilde{\Delta}\right] \leq n$. Then $\dim\left(\mathcal{N}_L\{I - \mathcal{F}_L(H, \Phi^{-1})\tilde{\Delta}\}\right) \geq p$. We show that the nullspaces $\mathcal{N}\{H_{12}\}$ and $\mathcal{N}_L\{I - \mathcal{F}_L(H, \Phi^{-1})\tilde{\Delta}\}$ are independent, i.e., for any nonzero $q \in \mathbb{C}^n$,

$$q^* \begin{bmatrix} \tilde{N} & -\tilde{M} \end{bmatrix} \left[I - \mathcal{F}_L(H, \Phi^{-1})\tilde{\Delta}\right] \neq 0.$$

We have

$$\begin{aligned}
q^* \begin{bmatrix} \tilde{N} & -\tilde{M} \end{bmatrix} \left[I - \mathcal{F}_L(H, \Phi^{-1})\tilde{\Delta}\right] &= q^* \begin{bmatrix} \tilde{N} & -\tilde{M} \end{bmatrix} \left(I - H_{11}\tilde{\Delta}\right) \\
&= q^* \begin{bmatrix} \tilde{N} & -\tilde{M} \end{bmatrix} \begin{bmatrix} I + (I + K_2K_1C\tilde{M}^{-1}\tilde{N})^{-1}K_2K_1C\tilde{M}^{-1}\Delta N & -(I + K_2K_1C\tilde{M}^{-1}\tilde{N})^{-1}K_2K_1C\tilde{M}^{-1}\Delta M \\ -(I + \tilde{M}^{-1}\tilde{N}K_2K_1C)^{-1}\tilde{M}^{-1}\Delta N & I + (I + \tilde{M}^{-1}\tilde{N}K_2K_1C)^{-1}\tilde{M}^{-1}\Delta M \end{bmatrix} \\
&= q^* \Big[\tilde{N} + \tilde{N}(I + K_2K_1C\tilde{M}^{-1}\tilde{N})^{-1}K_2K_1C\tilde{M}^{-1}\Delta N + \tilde{M}(I + \tilde{M}^{-1}\tilde{N}K_2K_1C)^{-1}\tilde{M}^{-1}\Delta N \\
&\qquad -\tilde{N}(I + K_2K_1C\tilde{M}^{-1}\tilde{N})^{-1}K_2K_1C\tilde{M}^{-1}\Delta M - \tilde{M} - \tilde{M}(I + \tilde{M}^{-1}\tilde{N}K_2K_1C)^{-1}\tilde{M}^{-1}\Delta M\Big] \\
&= q^* \Big[\tilde{N} + \tilde{N}K_2K_1C\tilde{M}^{-1}(I + \tilde{N}K_2K_1C\tilde{M}^{-1})^{-1}\Delta N + (I + \tilde{N}K_2K_1C\tilde{M}^{-1})^{-1}\Delta N \\
&\qquad -\tilde{N}K_2K_1C\tilde{M}^{-1}(I + \tilde{N}K_2K_1C\tilde{M}^{-1})^{-1}\Delta M - \tilde{M} - (I + \tilde{N}K_2K_1C\tilde{M}^{-1})^{-1}\Delta M\Big] \\
&= q^* \begin{bmatrix} \tilde{N} + \Delta N & -(\tilde{M} + \Delta M) \end{bmatrix} \neq 0,
\end{aligned}$$

where the last inequality follows from (A4.1). This shows the independence of $\mathcal{N}_L\{I - \mathcal{F}_L(H, \Phi^{-1})\tilde{\Delta}\}$ and $\mathcal{N}_L\{H_{12}\}$, and also that $\dim\left(\mathcal{N}_L\{I - \mathcal{F}_L(H, \Phi^{-1})\tilde{\Delta}\}\right) = p$. The latter follows from the inequality $\dim\left(\mathcal{N}_L\{I - \mathcal{F}_L(H, \hat{\Phi}^{-1})\tilde{\Delta}\}\right) \leq 2p - \dim\left(\mathcal{N}_L\{H_{12}\}\right) = p$ and the inequality obtained above: $\dim\left(\mathcal{N}_L\left\{I - \mathcal{F}_L(H, \hat{\Phi}^{-1})\tilde{\Delta}\right\}\right) \geq p$. But by Lemma 2, this implies that $\mathcal{N}_L\{I - \mathcal{F}_L(H, \Phi^{-1})\tilde{\Delta}\} \in \mathcal{Y}$. Hence, $\exists U$ invertible, Q such that

$$\mathcal{N}_L\{I - \mathcal{F}_L(H, \Phi^{-1})\tilde{\Delta}\} = \text{row span}\left(UH_{12}^{\dagger} + Q[\tilde{N} \ -\tilde{M}]\right),$$

and therefore

$$\begin{aligned}
\left(UH_{12}^{\dagger} + Q[\tilde{N} \ -\tilde{M}]\right)\left[I - \mathcal{F}_L(H, \Phi^{-1})\tilde{\Delta}\right] &= 0, \\
\left(H_{12}^{\dagger} - Q_0[\tilde{N} \ -\tilde{M}]\right)\left[I - \mathcal{F}_L(H, \Phi^{-1})\tilde{\Delta}\right] &= 0,
\end{aligned}$$

where $Q_0 = -U^{-1}Q$. ■

This result leads us to the following minimization problem that we have already encountered in Problem 7.

Problem 18 *Compute* $\beta := \inf\left\{\|\tilde{\Delta}\| : \text{rank}\left\{I - \mathcal{F}_L(H, \Phi^{-1})\tilde{\Delta}\right\} \leq n,\ \tilde{\Delta} \in \mathbb{C}^{p\times(p+n)}\right\}$.

A solution to this problem is readily given by Theorem 6: $\beta = \sigma_p[\mathcal{F}_L(H, \Phi^{-1})]^{-1}$.

The only difference with the open-loop case of §3.4.1.3 is that the nonsingularity of $I - P_{11}\tilde{\Delta}$ for all $\tilde{\Delta} \in \mathcal{B}\mathbb{C}^{n\times(n+p)}$ was guaranteed by the assumption that $\underline{\sigma}\left[\tilde{\boldsymbol{M}}(j\omega)\right] > |\boldsymbol{r}(j\omega)|,\ \forall\omega$ (Assumption (A3.1)). Here, nonsingularity of $I - H_{11}\tilde{\Delta}$ for all $\tilde{\Delta} \in \mathcal{B}\mathbb{C}^{n\times(n+p)}$ is equivalent to robust stability of the closed-loop system of Figure 4.2 with the constant matrices replaced by their corresponding transfer matrices. This is certainly too strong an assumption to use in a proof of a lemma similar to Lemma 4. Indeed, if the combination $\boldsymbol{K}_2\boldsymbol{K}_1$ is already a controller providing robust stability, why bother refining the model to design a new robust controller? Instead, we will show in the following lemma (Lemma 12) that if the factor perturbation $\tilde{\Delta}$ renders the matrix $I - \boldsymbol{H}_{11}(j\omega)\tilde{\Delta}$ singular, then $\exists\tilde{\Delta}_0$ as close to $\tilde{\Delta}$ as desired and with the same properties, but that makes $I - \boldsymbol{H}_{11}(j\omega)\tilde{\Delta}_0$ nonsingular. This is the last technical result needed before we can give a solution to Problem 16. The proof is rather long and not very illuminating, so it was put in Appendix B.

Lemma 12 *Suppose that for* $\tilde{\Delta} \in \mathcal{B}\mathbb{C}^{n\times(n+p)}$, $\text{rank}\left\{I - \mathcal{F}_L(H, \Phi^{-1})\tilde{\Delta}\right\} = n$ *and* $I - H_{11}\tilde{\Delta}$ *is singular. Then for* $\epsilon > 0$, *there exists a* $\tilde{\Delta}_0$ *with* $\|\tilde{\Delta}_0 - \tilde{\Delta}\| < \epsilon$ *such that* $\text{rank}\left\{I - \mathcal{F}_L(H, \Phi^{-1})\tilde{\Delta}_0\right\} \leq n$ *and* $I - H_{11}\tilde{\Delta}_0$ *is nonsingular.*

Proof Given in Appendix B.

We are now in a position to establish the following result which provides an answer to Problem 16, the noise-free closed-loop MIMO consistency problem for square flexible systems at one frequency. The proof makes use of the solution to Problem 18 given above.

Lemma 13 *For an invertible noise-free frequency-response datum* $\Phi \in \mathbb{C}^{p\times p}$ *obtained at frequency* ω, *Problem 16 has a positive answer iff* $\sigma_p\left[\mathcal{F}_L(H, \Phi^{-1})\right]^{-1} < 1$.

Proof *Sufficiency* Suppose $\sigma_p\left[\mathcal{F}_L(H, \Phi^{-1})\right]^{-1} < 1$. By Theorem 6, $\exists\tilde{\Delta} \in \mathcal{B}\mathbb{C}^{n\times(n+p)}$ such that $\text{rank}\left\{I - \mathcal{F}_L(H, \Phi^{-1})\tilde{\Delta}\right\} = n$. Moreover, Lemma 12 says that $\exists\tilde{\Delta}_0$ as close to $\tilde{\Delta}$ as wanted such that $I - H_{11}\tilde{\Delta}_0$ is nonsingular and $\text{rank}\left\{I - \mathcal{F}_L(H, \Phi^{-1})\tilde{\Delta}_0\right\} \leq n$. In particular,

we can select it such that $\|\tilde{\Delta}_0 - \tilde{\Delta}\| < 1 - \|\tilde{\Delta}\|$, in which case $\|\tilde{\Delta}_0\| < 1$. Then Lemma 11 says that this perturbation is consistent with the datum, i.e., $\Phi - \mathcal{F}_U(H, \tilde{\Delta}_0) = 0$.

Necessity Suppose $\sigma_p \left[\mathcal{F}_L(H, \Phi^{-1})\right]^{-1} \geq 1$. Then by Lemma 11, there exists no $\tilde{\Delta} \in \mathcal{BC}^{n\times(n+p)}$ such that $\Phi - \mathcal{F}_U(H, \tilde{\Delta}) = 0$ and $I - H_{11}\tilde{\Delta}$ is nonsingular. ■

Finally, a necessary condition is given for the noise-free closed-loop MIMO consistency problem for square flexible systems, Problem 17.

Theorem 10 *The closed-loop special CF model/data consistency problem of Problem 17 has a positive answer only if* $\sigma_p \left\{\mathcal{F}_L \left[\boldsymbol{H}(j\omega_i), \Phi_i^{-1}\right]\right\}^{-1} < 1$ *for all* $i = 1, \ldots, N$.

Proof A necessary condition for Problem 17 to have a positive answer is that there exist a normalized perturbation $\tilde{\boldsymbol{\Delta}} \in \mathcal{BRH}_\infty$ interpolating the minimum-norm $\tilde{\Delta}_i$ satisfying (4.6) with the datum Φ_i and such that $I - \boldsymbol{H}_{11}(j\omega_i)\tilde{\Delta}_i$ is nonsingular, for $i = 1, \ldots, N$. By Theorem 4 and Lemma 13, such a function exists iff $\sigma_p \left\{\mathcal{F}_L \left[\boldsymbol{H}(j\omega_i), \Phi_i^{-1}\right]\right\}^{-1} < 1$ for $i = 1, \ldots, N$. ■

The condition in Theorem 10 is obviously not sufficient as $\boldsymbol{\Delta}$ must also be stabilizing. Again, the bound $|\boldsymbol{r}(j\omega)|$ can be modified such that the inequality in the theorem statement is satisfied for all i. This is necessary to make the new model consistent with all the data. A sufficient condition for Problem 15 to have a positive answer is deferred to Section 4.4.

4.2.2.1 Numerical Example

The plant model considered here is for Daisy. It has 23 inputs and 23 outputs, and its 46^{th}-order model has three rigid-body modes and 20 flexible modes. This model is described in details in Section 5.1.1. The perturbed coprime factor model developed in Chapter 5 for the collocated $\mathcal{H}_\infty$ controller design will be used. The nominal factorization has the usual form $\boldsymbol{G} = C\tilde{\boldsymbol{M}}^{-1}\tilde{\boldsymbol{N}}\boldsymbol{J}$ where $\tilde{\boldsymbol{M}}$, $\tilde{\boldsymbol{N}} \in \mathcal{RH}_\infty^{23\times 23}$, $\boldsymbol{J} \in \mathcal{RH}_\infty^{23\times 23}$ is diagonal, $C \in \mathbb{R}^{23\times 23}$. In terms of the input and output matrices of Chapter 2, $\boldsymbol{J} = \gamma J_2 \boldsymbol{T}_a$ and $C = d_{max}^{-1} C_1 J_1$, where $\boldsymbol{T}_a$ is a diagonal transfer matrix modeling actuator dynamics given in §5.1.1.1.

The unit $\boldsymbol{r}$ bounding the factor uncertainty is $\boldsymbol{r}(s) = \frac{0.001s+1.414}{2.32s+1}$. This $\boldsymbol{r}$ makes $\mathcal{P}$ include all perturbations of $\boldsymbol{G}$ induced by variations in the modal parameters to within 10% uncertainty in the modal frequencies, 50% uncertainty in the modal damping ratios, and 8% uncertainty in the entries of the input matrix B_1. An actual frequency-response experiment was not performed on

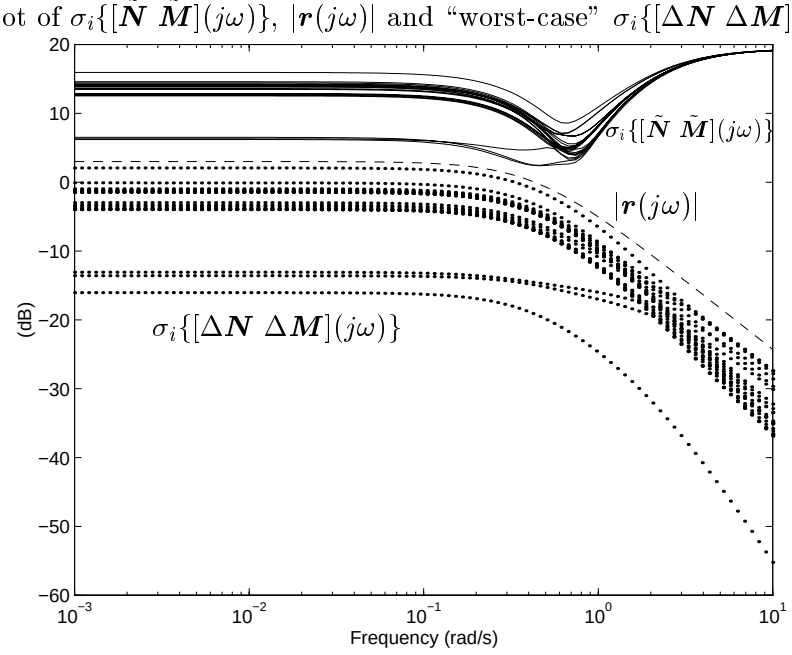

Figure 4.3: Singular values of the nominal factors and worst-case factor perturbations.

Daisy in fear of burning out the power amplifiers of the DC motors driving the torque wheels. These amplifiers tend to overheat after a few minutes of use. Thus one of the plant models perturbed by variations in the modal parameters within the limits given above was randomly picked to be the actual plant $\boldsymbol{G}_a$, and a simple decentralized 23^{rd}-order controller $\boldsymbol{K}_1$ was designed to stabilize it, as well as the nominal plant model. This controller is composed of 23 first-order lead compensators implementing local feedback loops.

The noise-free frequency-response data $\{\Phi_i\}_{i=1}^{50} \subset \mathbb{C}^{23\times 23}$ computed at 50 distinct frequencies between 0.001 rad/s and 10 rad/s were generated for the input disturbance rejection closed-loop configuration with $\boldsymbol{G}_a$ and $\boldsymbol{K}_1$. Figure 4.3 shows plots of the singular values of $[\tilde{\boldsymbol{N}}\ \tilde{\boldsymbol{M}}](j\omega)$, the bound $|\boldsymbol{r}(j\omega)|$, and the singular values of the worst-case perturbation induced by variations in the modal parameters $[\Delta\boldsymbol{N}\ \ -\Delta\boldsymbol{M}](j\omega)$. It can be observed that $\underline{\sigma}\{[\tilde{\boldsymbol{N}}\ \tilde{\boldsymbol{M}}](j\omega)\} > |\boldsymbol{r}(j\omega)|,\ \forall\omega$, implying that $\left[\tilde{\boldsymbol{N}}+\Delta\boldsymbol{N}\ \ -(\tilde{\boldsymbol{M}}+\Delta\boldsymbol{M})\right](j\omega)$ has full rank $\forall\boldsymbol{\Delta}\in\mathcal{D}_r$, which was assumed at the outset in (A4.1). The necessary condition of Theorem 10 is tested by computing $\sigma_{23}\left\{\mathcal{F}_L\left[\boldsymbol{H}(j\omega_i),\Phi_i^{-1}\right]\right\}^{-1}$ for $i=1,\ldots,50$ and checking that all these numbers are less than 1. The results plotted in Figure 4.4 show that the necessary condition has been satisfied. This had to be expected since the data were generated by an admissible plant in $\mathcal{P}$.

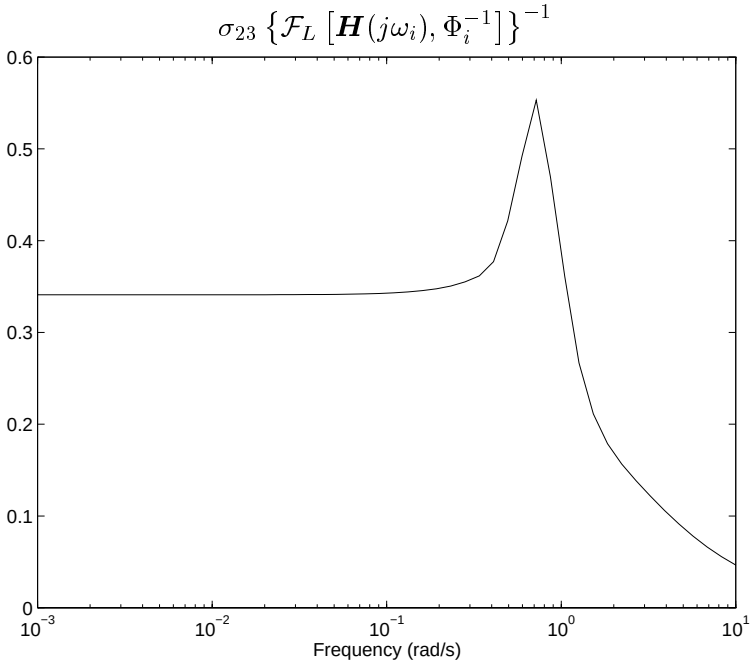

Figure 4.4: Test of necessary condition for consistency with $\sigma_{23}\left\{\mathcal{F}_L\left[\boldsymbol{H}(j\omega_i), \Phi_i^{-1}\right]\right\}^{-1}$.

4.3 Noisy SISO Case

The model/data consistency problem will be studied for four different combinations of left-coprime factorizations and noisy closed-loop experimental data. Suppose we are given N nonzero noisy scalar frequency-response measurements $\{\phi_i\}_{i=1}^N$ in $\mathbb{C}$ corresponding to the distinct frequencies $\omega_1, \ldots, \omega_N$. For more generality, we consider a stable nominal left-coprime factorization of the plant where the factor $\tilde{\boldsymbol{M}}$ has dimensions $n \times n$ and the factor $\tilde{\boldsymbol{N}}$ has dimensions $n \times 1$, together with an output transfer matrix $\boldsymbol{C}$ of dimension $1 \times n$. Thus the plant transfer function $\boldsymbol{g}$ is written as

$$\boldsymbol{g} = \boldsymbol{C}\tilde{\boldsymbol{M}}^{-1}\tilde{\boldsymbol{N}} \ . \tag{4.7}$$

This model allows us to treat scalar factorizations with $n = 1$ and $\boldsymbol{C} = 1$, but also our special LCF of LFSS. Then $\boldsymbol{C}$ may contain nominal actuator dynamics and input and output scaling factors. A unit $\boldsymbol{r}(s)$ in $\mathcal{RH}_\infty$ bounding the factor uncertainty is also part of the model as before.

Consider the feedback system in Figure 4.5. The sensor noise $\hat{n}(t)$ affects not only the measurements of the output signal, but also the signal fed back to the controller. Define

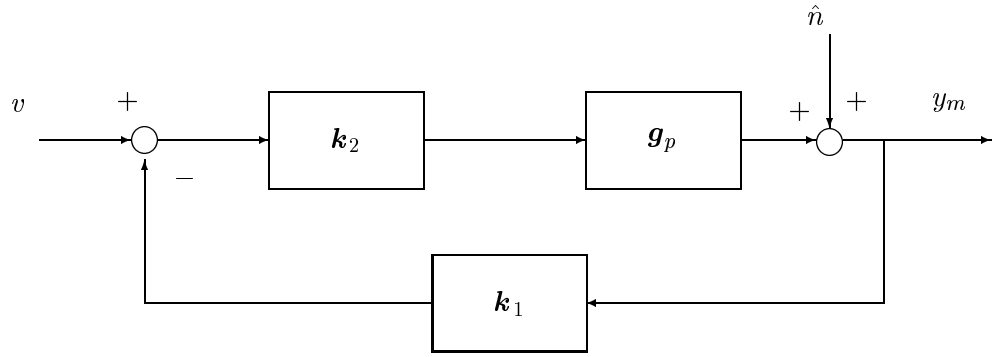

Figure 4.5: Noisy SISO feedback system.

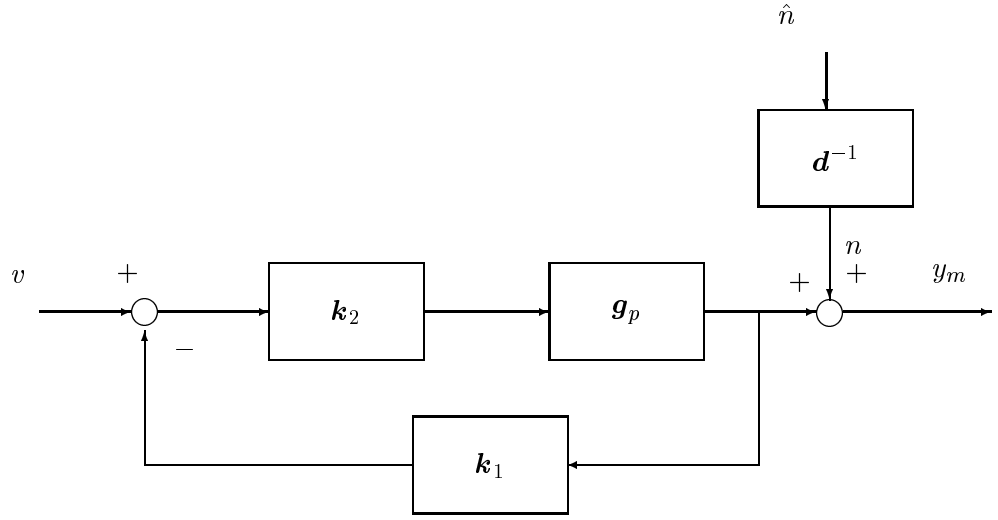

Figure 4.6: Equivalent noisy SISO feedback system.

$\boldsymbol{d} := 1 + \boldsymbol{k}_1\boldsymbol{k}_2\boldsymbol{C}\tilde{\boldsymbol{M}}^{-1}\tilde{\boldsymbol{N}}$, the inverse of the sensitivity function. By linearity, the block diagram of Figure 4.5 can be modified to the equivalent system of Figure 4.6 in which the filtered noise does not enter the feedback path.

We assume that the filtered noise n is in $\mathcal{L}_\infty$ with bound $\|n\|_\infty < M$. This is not a bad assumption because the effect of $n(t)$ is the distortion directly visible on the distorted sinusoidal output $y_m(t)$. Hence the bound M should not be too difficult to obtain after recording the frequency response at different frequencies, including DC. Here we consider sensor noise, but other noises in the system could be lumped into a single filtered output noise n. This assumption allows us to model the effect of the noise n on the measurements as additive uncertainty in the complex plane (see Figure 3.2) as in the open-loop case. Hence the noise set $\mathcal{W}$ considered here

is as defined in (3.6).

Define the transfer function from v to y_m in Figure 4.6 as $\boldsymbol{t} := \frac{\boldsymbol{k}_2\boldsymbol{g}_p}{1+\boldsymbol{k}_1\boldsymbol{k}_2\boldsymbol{g}_p}$. The model/data consistency problem for noisy closed-loop frequency-response data for a control system as in Figure 4.6 can now be stated.

Problem 19 *Given nonzero closed-loop noisy frequency-response data* $\{\phi_i\}_{i=1}^N$ *at* $\omega_1, \ldots, \omega_N$, *could they have been produced by the closed-loop system of Figure 4.6 with at least one* $\boldsymbol{g}_p$ *in* $\mathcal{P}$ *and* N *noises in* $\mathcal{W}$*? Or, in other words, do there exist* $\boldsymbol{\Delta} \in \mathcal{D}_r$ *and complex noises* $\{\delta_{ai}\}_{i=1}^N$ *in* $\mathcal{W}$ *such that the closed-loop system of Figure 4.6 is internally stable and* $\boldsymbol{t}(j\omega_i) + \delta_{ai} = \phi_i$, $i = 1, \ldots, N$*?*

Fix a measurement frequency ω and let ϕ be the complex measurement. We define two controllers $\boldsymbol{k}_1(s)$ and $\boldsymbol{k}_2(s)$ as in Figure 4.5 to encompass tracking and disturbance rejection feedback configurations, and we define $k_1 := \boldsymbol{k}_1(j\omega)$, $k_2 := \boldsymbol{k}_2(j\omega)$. It is also convenient to define $\mathcal{K}$, the set of scalar transfer functions. The block diagram of Figure 4.7 represents a general model/data consistency equation at frequency ω that can be specialized to four different consistency problems. Referring to the block diagram, these configurations are:

(1) Tracking configuration, scalar factorization ($n = 1$):
$\tilde{\boldsymbol{M}} \in \mathcal{RH}_\infty^{1\times 1}$, $\tilde{\boldsymbol{N}} \in \mathcal{RH}_\infty^{1\times 1}$, $\boldsymbol{C} = 1$, $\boldsymbol{k}_1 = 1$, $\boldsymbol{k}_2 \in \mathcal{K}$

(2) Disturbance rejection configuration, scalar factorization ($n = 1$):
$\tilde{\boldsymbol{M}} \in \mathcal{RH}_\infty^{1\times 1}$, $\tilde{\boldsymbol{N}} \in \mathcal{RH}_\infty^{1\times 1}$, $\boldsymbol{C} = 1$, $\boldsymbol{k}_1 \in \mathcal{K}$, $\boldsymbol{k}_2 = 1$

(3) Tracking configuration, special factorization for LFSS:
$\tilde{\boldsymbol{M}} \in \mathcal{RH}_\infty^{n\times n}$, $\tilde{\boldsymbol{N}} \in \mathcal{RH}_\infty^{n\times 1}$, $\boldsymbol{C} \in \mathcal{RH}_\infty^{1\times n}$, $\boldsymbol{k}_1 = 1$, $\boldsymbol{k}_2 \in \mathcal{K}$

(4) Disturbance rejection configuration, special factorization for LFSS:
$\tilde{\boldsymbol{M}} \in \mathcal{RH}_\infty^{n\times n}$, $\tilde{\boldsymbol{N}} \in \mathcal{RH}_\infty^{n\times 1}$, $\boldsymbol{C} \in \mathcal{RH}_\infty^{1\times n}$, $\boldsymbol{k}_1 \in \mathcal{K}$, $\boldsymbol{k}_2 = 1$

Assumptions

(A4.7) $\phi \neq 0$ (nonzero complex measurement).

(A4.8) $d := \boldsymbol{d}(j\omega) \neq 0$, $\forall \omega \in \mathbb{R}$.

(A4.9) $(\phi - V_{22}) \neq 0$, where V_{22} is the map $u \mapsto y$ in Figure 4.7 for $\tilde{\Delta}_s = 0$.

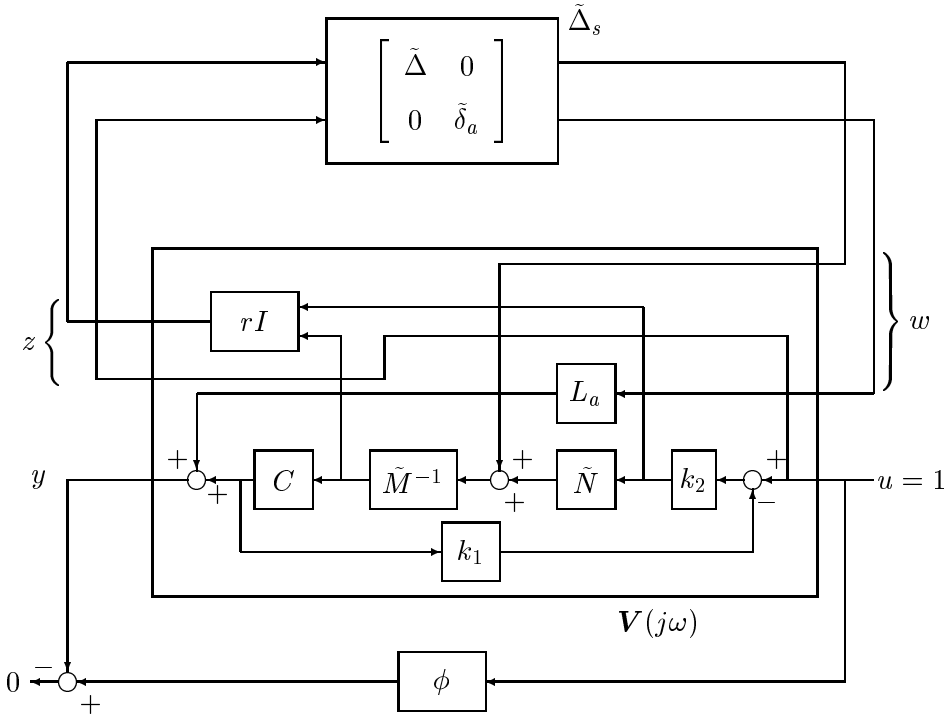

Figure 4.7: Block diagram of consistency equation for generalized SISO system.

(A4.10) $k_1 \neq 0$ and $k_2 \neq 0$.

(A4.11) $\forall \boldsymbol{\Delta} \in \mathcal{D}_r$, the pair $(C,\ \tilde{\boldsymbol{M}}_p)$ is right-coprime.

Assumptions (A4.7) and (A4.9) are required for invertibility of the complex numbers ϕ and $(\phi - V_{22})$ in the proofs, and should hold generically in practice. With (A4.9), it is convenient to define $q := (\phi - V_{22})^{-1}$. Some motivation is provided for (A4.8) in that the stabilizing controllers $\boldsymbol{k}_1$ or $\boldsymbol{k}_2$ would normally be designed using the nominal coprime factorization of the plant. These controllers are meant to stabilize the plant and provide sufficient damping to allow frequency-response measurements. Typically, these controllers would not contain zeros in $\overline{\mathbb{C}}_+$, which gives some motivation for (A4.10). Assumption (A4.11) is required because otherwise robust internal stability could not be achieved.

All configurations (1)-(4) are treated in a unified way. The generalized consistency equation at frequency ω illustrated in Figure 4.7 is

$$\phi - \left[1 + C(\tilde{M} + r\widetilde{\Delta M})^{-1}(\tilde{N} + r\widetilde{\Delta N})k_1 k_2\right]^{-1} C(\tilde{M} + r\widetilde{\Delta M})^{-1}(\tilde{N} + r\widetilde{\Delta N})k_2 - L_a\tilde{\delta}_a = 0. \quad (4.8)$$

Using LFT notation, (4.8) becomes

$$\phi - \mathcal{F}_U\left[\boldsymbol{V}(j\omega), \tilde{\Delta}_s\right] = 0, \tag{4.9}$$

where

$$\tilde{\Delta}_s := \begin{bmatrix} \tilde{\Delta} & 0 \\ 0 & \tilde{\delta}_a \end{bmatrix},$$

and

$$\boldsymbol{V} := \begin{bmatrix} \boldsymbol{V}_{11} & \boldsymbol{V}_{12} \\ \boldsymbol{V}_{21} & \boldsymbol{V}_{22} \end{bmatrix},$$

$$\boldsymbol{V}_{11} := \begin{bmatrix} -\boldsymbol{d}^{-1}\boldsymbol{r}\boldsymbol{k}_1\boldsymbol{k}_2\boldsymbol{C}\tilde{\boldsymbol{M}}^{-1} & 0 \\ \boldsymbol{r}(I + \tilde{\boldsymbol{M}}^{-1}\tilde{\boldsymbol{N}}\boldsymbol{k}_1\boldsymbol{k}_2\boldsymbol{C})^{-1}\tilde{\boldsymbol{M}}^{-1} & 0 \\ 0 & 0 \end{bmatrix}, \qquad \boldsymbol{V}_{12} := \begin{bmatrix} \boldsymbol{r}\boldsymbol{d}^{-1}\boldsymbol{k}_2 \\ \boldsymbol{r}\boldsymbol{d}^{-1}\boldsymbol{k}_2\tilde{\boldsymbol{M}}^{-1}\tilde{\boldsymbol{N}} \\ 1 \end{bmatrix},$$

$$\boldsymbol{V}_{21} := \begin{bmatrix} \boldsymbol{d}^{-1}\boldsymbol{C}\tilde{\boldsymbol{M}}^{-1} & L_a \end{bmatrix}, \qquad \boldsymbol{V}_{22} := \boldsymbol{d}^{-1}\boldsymbol{k}_2\boldsymbol{C}\tilde{\boldsymbol{M}}^{-1}\tilde{\boldsymbol{N}}.$$

As usual, let $V := \boldsymbol{V}(j\omega)$, $V_{ij} := \boldsymbol{V}_{ij}(j\omega)$, and likewise for the other transfer functions and matrices in the definition of $\boldsymbol{V}$ above. Thus the general consistency problem at frequency ω can be stated as follows.

Problem 20 *Given a nonzero noisy frequency-response datum ϕ at frequency ω, do there exist $\tilde{\Delta} \in \mathcal{B}\mathbb{C}^{n\times(n+1)}$ and a noise $\delta_a \in \mathcal{W}$ such that $I - V_{11}\tilde{\Delta}$ is nonsingular and $\phi - \mathcal{F}_U(V, \tilde{\Delta}_s) = 0$?*

The key idea for solving this problem is again to write a consistency equation equivalent to (4.9), but that has a feedback interpretation as in Figure 4.8.

$$1 - \phi^{-1}\mathcal{F}_U(V, \tilde{\Delta}_s) = 0, \tag{4.10}$$

Then consistency becomes analogous to noninvertibility (or instability) of a feedback system, and as mentioned in Section 3.4.2, the structured singular value μ can be used to derive consistency results. Based on this idea, Lemma 5 in Section 3.4.2 forms a basis for the solutions of all four noisy closed-loop SISO consistency problems. The structured uncertainty set Γ used here is as defined in (3.26). For a frequency ω, a problem equivalent to the closed-loop consistency problem can be formulated:

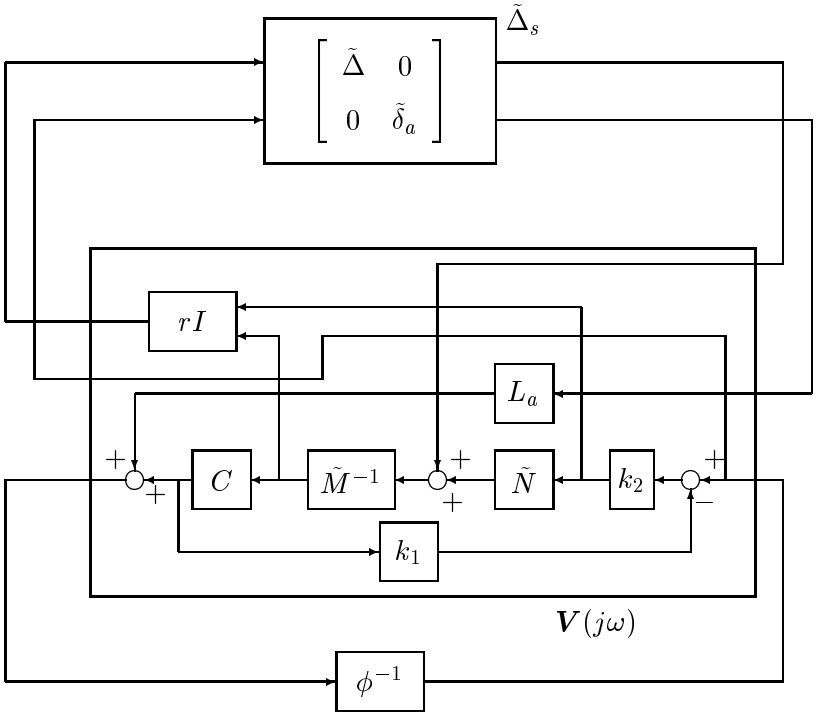

Figure 4.8: Feedback diagram for equivalent consistency condition for generalized SISO system.

Problem 21 *Does there exist a perturbation* $\tilde{\Delta}_s \in \mathcal{B}\Gamma$ *satisfying (4.10)?*

This problem can be solved by computing $\mu_\Gamma\left\{\mathcal{F}_L\left[\boldsymbol{V}(j\omega), \phi^{-1}\right]\right\}$ and checking that its value is larger than one, just as in the open-loop case. That is, for each ω_i, the closed-loop consistency problem can be interpreted as a μ test for non-robustness of the feedback interconnection in Figure 4.8.

The only difference with the open-loop case is the well-posedness property of $\mathcal{F}_U\left[\boldsymbol{V}(j\omega), \tilde{\Delta}_s\right]$ for all $\tilde{\Delta}_s \in \mathcal{B}\Gamma$, that can be shown to be equivalent to the nonsingularity of $\tilde{\boldsymbol{M}}(j\omega) + \Delta M$ for all $\|\tilde{\Delta}\| < 1$. Here, well-posedness of $\mathcal{F}_U\left[\boldsymbol{V}(j\omega), \tilde{\Delta}_s\right]$ for all $\tilde{\Delta}_s \in \mathcal{B}\Gamma$ is equivalent to robust stability of the closed-loop system of Figure 4.5. This is certainly too strong an assumption to use in a proof of a lemma similar to Lemma 8. Indeed, if the combination $\boldsymbol{k}_2\boldsymbol{k}_1$ already forms a controller providing robust stability, why bother refining the model to design a new robust controller?

Instead, we will show in Lemma 14 that if the structured perturbation $\tilde{\Delta}_s$ renders the matrix $I - \boldsymbol{V}_{11}(j\omega)\tilde{\Delta}_s$ singular, then $\exists\tilde{\Delta}_{s0}$ as close to $\tilde{\Delta}_s$ as desired and with the same properties, but that makes $I - \boldsymbol{V}_{11}(j\omega)\tilde{\Delta}_{s0}$ nonsingular. Then, the result provided by Lemma 5, which still

holds true here, can be used to prove the main consistency result, Theorem 11. Here is the lemma needed to circumvent the singularity problem. The proof has been put in Appendix C as it is quite long.

Lemma 14 *For $\tilde{\Delta}_s \in \mathcal{B}\Gamma$ with $I - V_{11}\tilde{\Delta}_s$ and $I - \mathcal{F}_L(V, \phi^{-1})\tilde{\Delta}_s$ singular, and for $\epsilon > 0$, $\exists\, \tilde{\Delta}_{s0} \in \Gamma$, $\|\tilde{\Delta}_{s0} - \tilde{\Delta}_s\| < \epsilon$ such that $I - \mathcal{F}_L(V, \phi^{-1})\tilde{\Delta}_{s0}$ is singular and $I - V_{11}\tilde{\Delta}_{s0}$ is nonsingular.*

Proof Given in Appendix C.

The idea behind the proof is to select a vector z in the nullspace of $I - \mathcal{F}_L(V, \phi^{-1})\tilde{\Delta}_s$ and to perturb $\tilde{\Delta}$ (the upper block in $\tilde{\Delta}_s$) along directions orthogonal to the first $n+1$ components of z. The resulting perturbation $\tilde{\Delta}_{s0}$ leaves $I - \mathcal{F}_L(V, \phi^{-1})\tilde{\Delta}_{s0}$ singular, but it turns out that $I - V_{11}\tilde{\Delta}_{s0}$ becomes nonsingular. Before we can prove the main result of this section, we need the following lemma which is analogous to Lemma 8.

Lemma 15 *We are given a nonzero complex measurement ϕ at frequency ω. Then $\exists \tilde{\Delta}_s \in \mathcal{B}\Gamma$ such that $\phi - \mathcal{F}_U(V, \tilde{\Delta}_s) = 0$ and $I - V_{11}\tilde{\Delta}_s$ is nonsingular iff $\mu_\Gamma\left[\mathcal{F}_L(V, \phi^{-1})\right] > 1$.*

Proof We have $\mu_\Gamma\left[\mathcal{F}_L(V, \phi^{-1})\right] > 1$ iff there exists $\tilde{\Delta}_s \in \mathcal{B}\Gamma$ such that $I - \mathcal{F}_L(V, \phi^{-1})\tilde{\Delta}_s$ is singular.

Sufficiency Assume $\mu_\Gamma\left[\mathcal{F}_L(V, \phi^{-1})\right] > 1$. By the equivalent condition above and Lemma 14, there exists a Δ_{s0} in $\mathcal{B}\Gamma$ such that $I - \mathcal{F}_L(V, \phi^{-1})\tilde{\Delta}_{s0}$ is singular, but not $I - V_{11}\tilde{\Delta}_{s0}$. Then Lemma 5 applies and we have $\phi - \mathcal{F}_U(V, \tilde{\Delta}_{s0}) = 0$.

Necessity Suppose $\exists \tilde{\Delta}_s \in \mathcal{B}\Gamma$ such that $\phi - \mathcal{F}_U(V, \tilde{\Delta}_s) = 0$ and $I - V_{11}\tilde{\Delta}_s$ is nonsingular. Then by Lemma 5, $I - \mathcal{F}_L(V, \phi^{-1})\tilde{\Delta}_s$ is singular, and hence $\mu_\Gamma\left[\mathcal{F}_L(V, \phi^{-1})\right] > 1$. ■

The main result of this section can now be stated. It gives a necessary condition for a positive answer to Problem 19.

Theorem 11 *The noisy closed-loop SISO model/data consistency problem (Problem 19) has a positive answer, i.e., there exist $\boldsymbol{g}_p \in \mathcal{P}$ and N noises $\delta_{ai} \in \mathcal{W}$ that could have produced*

the noisy closed-loop frequency-response data $\{\phi_i\}_{i=1}^N$, *only if* $\mu_\Gamma\left\{\mathcal{F}_L\left[\boldsymbol{V}(j\omega_i), \phi_i^{-1}\right]\right\} > 1$ *for* $i = 1, \ldots, N$.

Proof A necessary condition for Problem 19 to have a positive answer is that there exist $\boldsymbol{\Delta} \in \mathcal{D}_r$ interpolating the minimum-norm $r_i\tilde{\Delta}_i$ satisfying (4.9) together with $\delta_{ai} \in \mathcal{W}$, and such that $I - \boldsymbol{V}_{11}(j\omega_i)\tilde{\Delta}_{si}$ is nonsingular, for $i = 1, \ldots, N$. By Theorem 4 and Lemma 15, such a function $\boldsymbol{\Delta}$ and noises $\{\delta_{ai}\}_{i=1}^N \subset \mathcal{W}$ exist iff $\mu_\Gamma\left\{\mathcal{F}_L\left[\boldsymbol{V}(j\omega_i), \phi_i^{-1}\right]\right\} > 1$ for $i = 1, \ldots, N$. ■

The condition in Theorem 11 is not sufficient, but the only additional constraint to make it sufficient would be that $\boldsymbol{\Delta}$ be stabilizing.

Suppose that for a given set of frequency-response measurements, the μ test reveals that the LCF and noise models are inconsistent because at one measurement frequency ω_k, $\mu_\Gamma\left\{\mathcal{F}_L\left[\boldsymbol{V}(j\omega_k), \phi_k^{-1}\right]\right\}$ is less than, but close to one. Then again it may be possible to increase $|r_k|$ slightly to get $\mu_\Gamma\left\{\mathcal{F}_L\left[\boldsymbol{V}(j\omega_k), \phi_k^{-1}\right]\right\} > 1$ as Proposition 4 suggests, with $\boldsymbol{P}$ replaced by $\boldsymbol{V}$.

4.4 Sufficient Condition for Consistency

Looking back at Problems 17 and 19, we see that we still have to look for *stabilizing* stable perturbations. For all cases treated so far, stability can be studied in a unified way by rearranging the perturbation and the generalized plant as shown in the block diagram of Figure 4.9. Note that since the class of perturbations considered is a subset of $\mathcal{RH}_\infty$, what we are really looking at is a strong stabilization problem (i.e., stabilization with a stable controller, or with a stable perturbation in our case) with interpolation constraints. A classic paper by Youla, Bongiorno and Lu [53] gives a nice, complete characterization of multivariable plants that are strongly stabilizable (see also [52]). But the norm-constrained strong stabilization problem is still partly open. Suppose we are given a plant $\boldsymbol{P}$ and a norm bound γ on the controller. To the author's knowledge, general necessary and sufficient conditions that would guarantee the existence of a stable controller of norm less than γ that would stabilize $\boldsymbol{P}$ have not been found yet — let alone with additional interpolation constraints! Thus we will settle for sufficient conditions for the strong stabilization problem with interpolation constraints that stems from our closed-loop model/data consistency problems.

Let us characterize all stabilizing perturbations (stable or not) for $\boldsymbol{H}$ (or $\boldsymbol{V}$ in the noisy

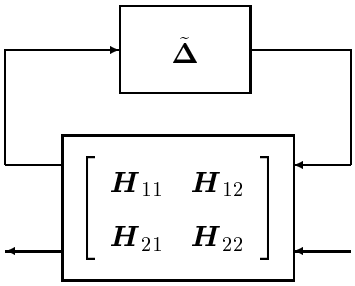

Figure 4.9: Block diagram for strong stabilization of $\boldsymbol{H}$ with $\tilde{\boldsymbol{\Delta}}$.

SISO case). Note that the standard LCF setup of an MIMO plant considered in Section 4.2.1 is a special case of the block diagram of $\boldsymbol{H}$ in Figure 4.2, so $\boldsymbol{H}$ can be computed for this case as well. Actually, only $\boldsymbol{H}_{11}$ is needed as we now show. With nominal internal stability of $\boldsymbol{H}$, a well-known result [18] states that $\mathcal{F}_U(\boldsymbol{H}, \tilde{\boldsymbol{\Delta}})$ is internally stable iff the interconnection of $\boldsymbol{H}_{11}$ and $\tilde{\boldsymbol{\Delta}}$ is internally stable. Thus we will focus without loss of generality on stabilization of $\boldsymbol{H}_{11}$. Let $(\tilde{\boldsymbol{M}}_H, \tilde{\boldsymbol{N}}_H)$ and $(\boldsymbol{N}_H, \boldsymbol{M}_H)$ be respectively *normalized* LCF and RCF [34] of $\boldsymbol{H}_{11}$. There exist matrices $\boldsymbol{X}$, $\boldsymbol{Y}$, $\tilde{\boldsymbol{X}}$, $\tilde{\boldsymbol{Y}} \in \mathcal{RH}_\infty$ such that

$$\begin{bmatrix} \boldsymbol{Y} & -\boldsymbol{X} \\ \tilde{\boldsymbol{N}}_H & \tilde{\boldsymbol{M}}_H \end{bmatrix} \begin{bmatrix} \boldsymbol{M}_H & \tilde{\boldsymbol{X}} \\ -\boldsymbol{N}_H & \tilde{\boldsymbol{Y}} \end{bmatrix} = \begin{bmatrix} I & 0 \\ 0 & I \end{bmatrix}. \tag{4.11}$$

These matrices can always be found [18]. All stabilizing real-rational perturbations can then be parametrized as follows (Youla parametrization):

$$\tilde{\boldsymbol{\Delta}} = (\tilde{\boldsymbol{X}} + \boldsymbol{M}_H\boldsymbol{Q})(\tilde{\boldsymbol{Y}} - \boldsymbol{N}_H\boldsymbol{Q})^{-1}, \ \ \boldsymbol{Q} \in \mathcal{RH}_\infty, \ \ \det(\tilde{\boldsymbol{Y}} - \boldsymbol{N}_H\boldsymbol{Q}) \neq 0, \text{ or} \tag{4.12}$$

$$\tilde{\boldsymbol{\Delta}} = (\boldsymbol{Y} - \boldsymbol{R}\tilde{\boldsymbol{N}}_H)^{-1}(\boldsymbol{X} + \boldsymbol{R}\tilde{\boldsymbol{M}}_H), \ \ \boldsymbol{R} \in \mathcal{RH}_\infty, \ \ \det(\boldsymbol{Y} - \boldsymbol{R}\tilde{\boldsymbol{N}}_H) \neq 0. \tag{4.13}$$

Suppose that the necessary condition for the problem at hand holds. Then let $\tilde{\Delta}_i$ be a minimum-norm solution of the consistency equation at frequency ω_i for $i = 1, \ldots, N$. The constraints that an admissible stabilizing $\tilde{\boldsymbol{\Delta}}$ must satisfy are

(C1) $\tilde{\boldsymbol{\Delta}} \in \mathcal{RH}_\infty$,

(C2) $\|\tilde{\boldsymbol{\Delta}}\|_\infty < 1$,

(C3) $\tilde{\boldsymbol{\Delta}}(j\omega_i) = \tilde{\Delta}_i, \ \ i = 1, \ldots, N$.

Thus, the problem of strong stabilization with interpolation constraints can be reduced to the following problem.

Problem 22 *Does there exist a matrix $\boldsymbol{Q} \in \mathcal{RH}_\infty$ such that $\tilde{\boldsymbol{\Delta}}$ given by (4.12) satisfies (C1)-(C3), or a matrix $\boldsymbol{R} \in \mathcal{RH}_\infty$ such that $\tilde{\boldsymbol{\Delta}}$ given by (4.13) satisfies (C1)-(C3)?*

Our approach to this problem is the following. First note that since $\boldsymbol{H}_{11}$ is stable, it is strongly stabilizable. Solve the N equations in (C3) for Q_i, check that they all have norm less than one, and give a sufficient condition for existence of a $\boldsymbol{Q} \in \mathcal{BRH}_\infty$ interpolating the Q_i's and satisfying (C1), (C2). This sufficient condition (Theorem 13) is a robust performance type of result based on the Main-Loop Theorem [2]. Of course the same procedure can be repeated for $\boldsymbol{R}$ in (4.13). We begin by rewriting the parametrizations of (4.12) and (4.13) using LFT notation.

$$\tilde{\boldsymbol{\Delta}} = \mathcal{F}_L(\boldsymbol{U}, \boldsymbol{Q}), \quad \boldsymbol{Q} \in \mathcal{RH}_\infty, \tag{4.14}$$

$$\tilde{\boldsymbol{\Delta}} = \mathcal{F}_L(\boldsymbol{W}, \boldsymbol{R}), \quad \boldsymbol{R} \in \mathcal{RH}_\infty, \tag{4.15}$$

where

$$\boldsymbol{U} := \begin{bmatrix} \boldsymbol{U}_{11} & \boldsymbol{U}_{12} \\ \boldsymbol{U}_{21} & \boldsymbol{U}_{22} \end{bmatrix},$$

$$\begin{aligned} \boldsymbol{U}_{11} &:= \tilde{\boldsymbol{X}}\tilde{\boldsymbol{Y}}^{-1}, & \boldsymbol{U}_{12} &:= \boldsymbol{M}_H + \tilde{\boldsymbol{X}}\tilde{\boldsymbol{Y}}^{-1}\boldsymbol{N}_H, \\ \boldsymbol{U}_{21} &:= \tilde{\boldsymbol{Y}}^{-1}, & \boldsymbol{U}_{22} &:= \tilde{\boldsymbol{Y}}^{-1}\boldsymbol{N}_H \ , \end{aligned}$$

and

$$\boldsymbol{W} := \begin{bmatrix} \boldsymbol{W}_{11} & \boldsymbol{W}_{12} \\ \boldsymbol{W}_{21} & \boldsymbol{W}_{22} \end{bmatrix},$$

$$\begin{aligned} W_{11} &:= \boldsymbol{Y}^{-1}\boldsymbol{X}, & W_{12} &:= \boldsymbol{Y}^{-1}, \\ W_{21} &:= \tilde{\boldsymbol{M}}_H + \tilde{\boldsymbol{N}}_H\boldsymbol{Y}^{-1}\boldsymbol{X}, & W_{22} &:= \tilde{\boldsymbol{N}}_H\boldsymbol{Y}^{-1} \ . \end{aligned}$$

If $\boldsymbol{Y}$ and $\tilde{\boldsymbol{Y}}$ are chosen to be units, e.g., $\boldsymbol{Y} = \boldsymbol{M}_H^{-1}$ and $\tilde{\boldsymbol{Y}} = \tilde{\boldsymbol{M}}_H^{-1}$, it follows that $\boldsymbol{U}$ and $\boldsymbol{W}$ are stable. Then stability of $\mathcal{F}_L(\boldsymbol{U}, \boldsymbol{Q})$ is equivalent to stability of the feedback interconnection of $\boldsymbol{U}_{22}$ and $\boldsymbol{Q}$ [18], and similarly for $\mathcal{F}_L(\boldsymbol{W}, \boldsymbol{R})$. Thus from now on, fix $\boldsymbol{Y} := \boldsymbol{M}_H^{-1}$ and $\tilde{\boldsymbol{Y}} := \tilde{\boldsymbol{M}}_H^{-1}$. It follows that we must have $\boldsymbol{X} := 0$ and $\tilde{\boldsymbol{X}} := 0$ and the parametrizations (4.12) and (4.13)

basically reduce to the model reference transformation of Zames [56] for stable systems. With these choices, $\boldsymbol{U}$ and $\boldsymbol{W}$ become

$$\boldsymbol{U} = \begin{bmatrix} 0 & \boldsymbol{M}_H \\ \tilde{\boldsymbol{M}}_H & \tilde{\boldsymbol{M}}_H \boldsymbol{N}_H \end{bmatrix}, \qquad \boldsymbol{W} = \begin{bmatrix} 0 & \boldsymbol{M}_H \\ \tilde{\boldsymbol{M}}_H & \tilde{\boldsymbol{N}}_H \boldsymbol{M}_H \end{bmatrix}.$$

At this point, we need a theorem on robust performance which can be easily proved using Doyle's Main Loop Theorem [2], the latter being a substantial generalization of a result obtained by Redheffer [41, Theorem X]. Define the structured set

$$\Lambda := \left\{ Q_s = \begin{bmatrix} Q_a & 0 \\ 0 & Q_b \end{bmatrix} \; : \; Q_a \in \mathbb{C}^{q \times r}, \; Q_b \in \mathbb{C}^{p \times l} \right\}. \tag{4.16}$$

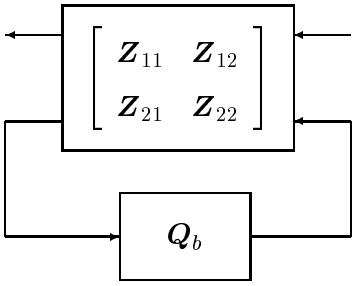

Figure 4.10: Block diagram of parametrization of $\tilde{\boldsymbol{\Delta}}$.

Theorem 12 *For a matrix function* $\boldsymbol{Z} := \begin{bmatrix} \boldsymbol{Z}_{11} & \boldsymbol{Z}_{12} \\ \boldsymbol{Z}_{21} & \boldsymbol{Z}_{22} \end{bmatrix}$ *in* $\mathcal{RH}_\infty^{(r+l)\times(q+p)}$, *the loop shown in Figure 4.10 is well-posed, internally stable, and* $\|\mathcal{F}_L(\boldsymbol{Z}, \boldsymbol{Q}_b)\|_\infty < 1$, $\forall \boldsymbol{Q}_b \in \mathcal{BRH}_\infty^{p\times l}$ *if* $\sup_{\omega\in\mathbb{R}} \mu_\Lambda [\boldsymbol{Z}(j\omega)] < 1$.

Proof Suppose that $\sup_{\omega\in\mathbb{R}} \mu_\Lambda [\boldsymbol{Z}(j\omega)] < 1$. Then by the Main-Loop Theorem [2], this implies that for all $\omega \in \mathbb{R} \cup \{\infty\}$, (i) $\|\boldsymbol{Z}_{22}(j\omega)\| < 1$ and (ii) $\|\mathcal{F}_L(\boldsymbol{Z}, \boldsymbol{Q}_b)(j\omega)\| < 1$, $\forall \boldsymbol{Q}_b \in \mathcal{BRH}_\infty^{p\times l}$. It follows from (i) that $\|\boldsymbol{Z}_{22}\|_\infty < 1$, and by the small-gain theorem, the closed-loop system in Figure 4.10 is well-posed and internally stable. The inequality $\|\mathcal{F}_L(\boldsymbol{Z}, \boldsymbol{Q}_b)\|_\infty < 1$, $\forall \boldsymbol{Q}_b \in \mathcal{BRH}_\infty^{p\times l}$ is implied by (ii). ■

We are almost in a position to state our general sufficient condition for consistency of closed-loop frequency-response data with a coprime factor model. If this condition is fulfilled, then the answer to Problem 22 is positive, which in turn implies consistency. But before, provided the minimum-norm $\tilde{\Delta}_i$ are available, we must compute the Q_i's and R_i's which turn out to be unique. Using (4.12) at frequency ω_i, we get the following linear matrix equation that can be solved for Q_i:

$$\tilde{\Delta}_i \tilde{Y}_i - \tilde{X}_i = (\tilde{\Delta}_i N_{Hi} + M_{Hi}) Q_i. \tag{4.17}$$

The matrix premultiplying Q_i on the right-hand side is invertible, so the unique solution to this equation is given by

$$Q_i = (\tilde{\Delta}_i N_{Hi} + M_{Hi})^{-1} (\tilde{\Delta}_i \tilde{Y}_i - \tilde{X}_i). \tag{4.18}$$

Now if we use (4.13) at frequency ω_i, we get the following linear matrix equation that can be solved for R_i.

$$Y_i \tilde{\Delta}_i - X_i = R_i (\tilde{N}_{Hi} \tilde{\Delta}_i + \tilde{M}_{Hi}). \tag{4.19}$$

The matrix postmultiplying R_i on the right-hand side is invertible, so the unique solution to this equation is given by

$$R_i = (Y_i \tilde{\Delta}_i - X_i)(\tilde{N}_{Hi} \tilde{\Delta}_i + \tilde{M}_{Hi})^{-1}. \tag{4.20}$$

Now select weighting functions $\boldsymbol{q}$ and $\boldsymbol{p}$ in $\mathcal{BRH}_\infty$ such that $|\boldsymbol{q}(j\omega_i)| > \|Q_i\|$ and $|\boldsymbol{p}(j\omega_i)| > \|R_i\|$. Ideally, $\boldsymbol{q}$ and $\boldsymbol{p}$ would tightly cover $\|Q_i\|$ and $\|R_i\|$ respectively on the imaginary axis. Define the scaled matrices $\boldsymbol{U}_0$ and $\boldsymbol{W}_0$ as follows.

$$\boldsymbol{U}_0 := \begin{bmatrix} \boldsymbol{U}_{11} & \boldsymbol{q}\boldsymbol{U}_{12} \\ \boldsymbol{U}_{21} & \boldsymbol{q}\boldsymbol{U}_{22} \end{bmatrix},$$

$$\boldsymbol{W}_0 := \begin{bmatrix} \boldsymbol{W}_{11} & \boldsymbol{p}\boldsymbol{W}_{12} \\ \boldsymbol{W}_{21} & \boldsymbol{p}\boldsymbol{W}_{22} \end{bmatrix}.$$

We will now focus on one particular closed-loop consistency problem in order to simplify the statement of the general theorem. Consider Problem 19 for the noisy SISO case. Suppose that the necessary condition for consistency of Theorem 11 holds and that a minimum-norm factor perturbation $\tilde{\Delta}_i$ is available to compute Q_i and R_i, $i = 1, \ldots, N$.

Theorem 13 *If* $\|Q_i\| < 1$, $i = 1, \ldots, N$ *and* $\sup_{\omega \in \mathbb{R}} \mu_\Gamma [\boldsymbol{U}_0(j\omega)] < 1$, *or if* $\|R_i\| < 1$, $i = 1, \ldots, N$ *and* $\sup_{\omega \in \mathbb{R}} \mu_\Gamma [\boldsymbol{W}_0(j\omega)] < 1$, *then the answer to Problem 19 is positive.*

Proof We prove the first part of the theorem only as the second part is entirely similar. Suppose that $\|Q_i\| < 1$ and define $\hat{Q}_i := \boldsymbol{q}(j\omega_i)^{-1}Q_i,\ i = 1, \ldots, N$. Then by Theorem 4, there exists $\hat{\boldsymbol{Q}} \in \mathcal{BRH}_\infty$ interpolating $\hat{Q}_i$ at ω_i. Scale $\hat{\boldsymbol{Q}}$ to get $\boldsymbol{Q} := \boldsymbol{q}\hat{\boldsymbol{Q}} \in \mathcal{BRH}_\infty$ and notice that $\mathcal{F}_L(\boldsymbol{U}_0, \hat{\boldsymbol{Q}}) = \mathcal{F}_L(\boldsymbol{U}, \boldsymbol{Q})$. Now assuming that $\sup_{\omega\in\mathbb{R}} \mu_\Gamma[\boldsymbol{U}_0(j\omega)] < 1$, Theorem 12 says that the loop in Figure 4.10 with $\boldsymbol{Q}_b = \hat{\boldsymbol{Q}}$ and $\boldsymbol{Z} = \boldsymbol{U}_0$ is internally stable and $\|\tilde{\boldsymbol{\Delta}}\|_\infty = \|\mathcal{F}_L(\boldsymbol{U}_0, \hat{\boldsymbol{Q}})\|_\infty < 1$. Now since $\boldsymbol{Q}(j\omega_i) = Q_i$, it follows that $\tilde{\boldsymbol{\Delta}}(j\omega_i) = \tilde{\Delta}_i$. Hence Problem 22 has a positive answer, and this implies that the consistency problem considered also has a positive answer. ■

This theorem gives a sufficient condition for all noise-free or noisy closed-loop consistency problems in this chapter provided that the minimum-norm factor perturbations $\tilde{\Delta}_i$'s can be computed. For the noise-free case with standard coprime factorization, $\tilde{\Delta}_i = r_i^{-1}\Delta_i$ can be computed using (4.4) or Matlab^{TM}. For the special factorization, $\tilde{\Delta}_i$ can be computed using a singular value decomposition of $\mathcal{F}_L\left[\boldsymbol{H}(j\omega_i), \Phi_i^{-1}\right]$ as explained in Remark 3.1 following the Schmidt-Mirsky Theorem.

If it occurs that $\tilde{\Delta}_i$ makes $I - \boldsymbol{H}_{11}(j\omega_i)\tilde{\Delta}_i$ singular, then Lemma 12 says that there is another perturbation $\tilde{\Delta}_{0i}$ as close to $\tilde{\Delta}_i$ as desired such that $I - \boldsymbol{H}_{11}(j\omega_i)\tilde{\Delta}_{0i}$ is nonsingular. However, since $\tilde{\Delta}_i N_{Hi} + M_{Hi}$ and $\tilde{N}_{Hi}\tilde{\Delta}_i + \tilde{M}_{Hi}$ are singular, and using a continuity argument, Q_i or R_i computed with $\tilde{\Delta}_{0i}$ (if available) would have very large norms, hence making the sufficient condition of Theorem 13 impractical. The same is true for the standard factorization case of Section 4.2.1.

For the noisy SISO case, the size of the minimum-norm $\tilde{\Delta}_i$ is given by $\mu_\Gamma\left\{\mathcal{F}_L\left[\boldsymbol{V}(j\omega_i), \phi_i^{-1}\right]\right\}^{-1}$, but it may prove difficult to compute $\tilde{\Delta}_i$. Fortunately, an algorithm for computing a lower bound on $\mu_\Gamma\left\{\mathcal{F}_L\left[\boldsymbol{V}(j\omega_i), \phi_i^{-1}\right]\right\}$ (implemented in Matlab^{TM}'s μ-Tools toolbox) also provides a destabilizing perturbation Δ_i' whose norm is an upper bound on $\|\tilde{\Delta}_i\|$, and is quite frequently equal to it [2]. Thus Δ_i' can be used to compute Q_i and R_i in Theorem 13. The remark pertaining to the singularity of $I - \boldsymbol{H}_{11}(j\omega_i)\tilde{\Delta}_i$ made above applies here as well for $I - \boldsymbol{V}_{11}(j\omega_i)\Delta_i'$.

4.4.1 Numerical Example

We will use Daisy's model again and the controller $\boldsymbol{K}_1$ as described in §4.2.2.1. The purpose of this example is twofold: We want to show that the sufficient condition for consistency with

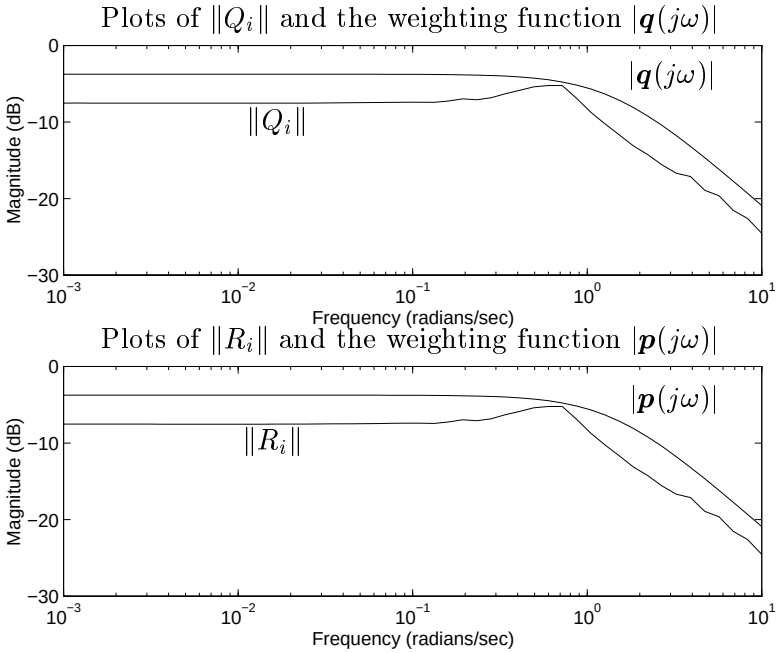

Figure 4.11: Covering $\|Q_i\|$ and $\|R_i\|$ with the scalar functions $\boldsymbol{q}$ and $\boldsymbol{p}$ in $\mathcal{BRH}_\infty$.

closed-loop data is not overly conservative, and we also want to demonstrate that it is applicable to MIMO systems of high order and with a large number of inputs and outputs. From the fifty closed-loop measurements $\{\Phi_i\} \subset \mathbb{C}^{23\times 23}$ generated in §4.2.2.1, the LFTs $\mathcal{F}_L\left[\boldsymbol{H}(j\omega_i), \Phi_i^{-1}\right]$ were computed and minimum-norm perturbations $\tilde{\Delta}_i$ were obtained using the formula given in Remark 3.1 following the Schmidt-Mirsky Theorem. Then the Q_i's and the R_i's were computed using (4.18) and (4.20), and weighting functions $\boldsymbol{q}$ and $\boldsymbol{p}$ were designed to cover $\|Q_i\|$ and $\|R_i\|$ respectively on the imaginary axis. These functions are identical, i.e., $\boldsymbol{q}(s) = \boldsymbol{p}(s) = \frac{0.65}{0.714s+1}$, and their magnitudes are plotted in Figure 4.11, together with the norms $\|Q_i\|$ and $\|R_i\|$ which are all less than 1. Then, the structured singular values of $\boldsymbol{U}_0(j\omega)$ and $\boldsymbol{W}_0(j\omega)$ were computed and found to be less than one and almost equal, see Figure 4.12. Hence, the sufficient condition of Theorem 13 holds and it can be concluded that the family of perturbed factorizations $\mathcal{P}$ described in the example of §4.2.2.1 is consistent with the data.

4.5 Summary and Discussion

The closed-loop consistency problem for coprime factorizations was shown to be difficult, but potentially very useful for unstable or lightly-damped systems. The noise-free closed-loop MIMO

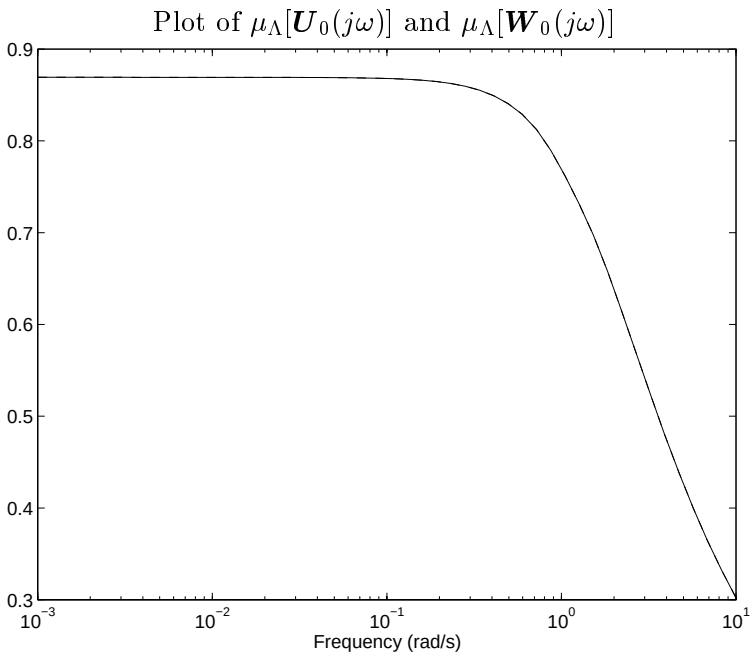

Figure 4.12: Structured singular values of $\boldsymbol{U}_0$ and $\boldsymbol{W}_0$.

consistency problem was first studied. For a standard LCF, a necessary condition was given, which is a simple test consisting of computing minimum-norm solutions to underdetermined linear complex matrix equations, as in the open-loop case. For an LCF model of an LFSS, we gave a necessary condition based on the Schmidt-Mirsky Theorem and Lemma 11 on equivalence of consistency to a rank condition on a certain return difference matrix. It was shown that sufficient conditions for this consistency problem involve strongly stabilizing perturbations, which is the main difficulty over the open-loop case.

Then the closed-loop noisy model/data consistency problem considered was for SISO plants only. Tracking and disturbance rejection closed-loop configurations were treated. The noise model is the same as described in Chapter 3, and a necessary condition for consistency is given. This necessary condition involves μ computations on LFTs. A practical result for noisy closed-loop MIMO plants has not been found yet.

A general sufficient condition for consistency based on a theorem of robust performance involving the structured singular value μ and applicable to all closed-loop cases treated was given. As an illustration, a numerical example using a 23-input, 23-output 46^{th}-order model of Daisy was worked out to show that this test is applicable to LFSS and not too conservative.

Chapter 5

Robust $\mathcal{H}_\infty$ Control of LFSS Using an LCF Model

In this chapter, an $\mathcal{H}_\infty$ control design technique providing robust stability and nominal performance for LFSS is presented. This technique is based on a nominal left-coprime factorization of LFSS dynamics as derived in Chapter 2, and requires a bound $\boldsymbol{r}$ on the factor uncertainty, and a weighting function $\boldsymbol{w}$ for performance. The general performance requirements for LFSS considered here are: attitude regulation, vibration attenuation, and tracking for accurate slewing maneuvers.

Then Daisy, an LFSS experimental testbed at UTIAS, is described, and two controller designs are carried out for it. The implementation of these collocated and noncollocated controllers on Daisy is discussed, and experimental results are given and commented upon.

5.1 Robust $\mathcal{H}_\infty$ Design

Consider first the problems of attitude regulation and vibration attenuation. For these problems, it makes sense to ask for good torque/force disturbance rejection at low frequencies as a first requirement for nominal performance. For example, this may be required on a flexible space station on which there may be large robots or humans producing significant torque disturbances. As a second requirement for nominal performance, we will ask for good tracking of reference angle trajectories to allow accurate slewing maneuvers of the rigid part of the structure. These requirements can be translated into desired shapes for the norms of the sensitivity functions $\boldsymbol{S}_{rhh} := r_h \mapsto e_h$ and $\boldsymbol{S}_{dh} := d \mapsto y_h$, where r is the vector of input references, r_h is the

vector of hub reference angles (r_h is the first part of r), e_h is the vector of attitude angle errors for the rigid part of the structure (the h subscript stands for *hub*, the rigid part of Daisy), d is the vector of external torque/force disturbances, and $y_h = [\theta_{hx}\, \theta_{hy} \theta_{hz}]^T$ is the vector of attitude angles of the rigid part. Let $\boldsymbol{S}_{rh} := r \mapsto e_h$ and notice that $\|\boldsymbol{S}_{rhh}(j\omega)\| \leq \|\boldsymbol{S}_{rh}(j\omega)\|,\ \forall\omega$.

Note that if we define $\boldsymbol{S}_r := r \mapsto e$, where e is the vector of all position/angle errors, and $\boldsymbol{S}_d := d \mapsto y$, then $\boldsymbol{S}_{rh} = \left[I_{3\times 3}\ 0_{3\times(p-3)}\right] \boldsymbol{S}_r$ and $\boldsymbol{S}_{dh} = \left[I_{3\times 3}\ 0_{3\times(p-3)}\right] \boldsymbol{S}_d$. Frequency-domain specifications are well-suited for the $\mathcal{H}_\infty$ design method (see, e.g., [14]) or a μ-synthesis [2]. Here we discuss the $\mathcal{H}_\infty$ problem.

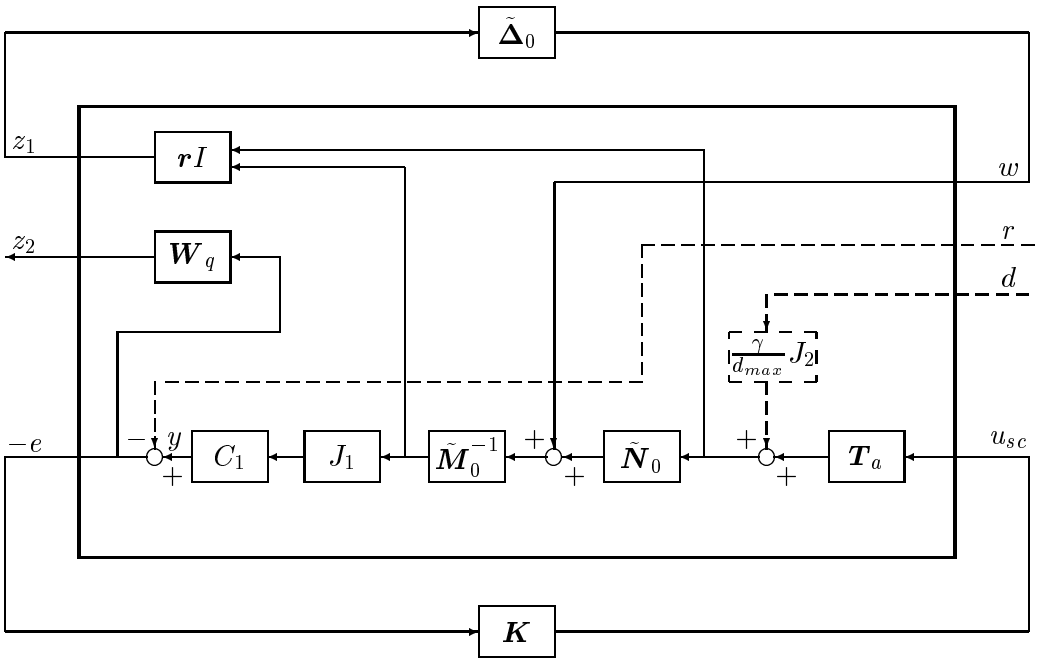

Figure 5.1: Generalized plant with scaled perturbation and controller for $\mathcal{H}_\infty$ design.

The block diagram of Figure 5.1 shows the interconnections between the scaled factors and their perturbations, actuator dynamics, scaling and output matrices, controller, and weighting functions that form the controlled perturbed generalized plant used in the $\mathcal{H}_\infty$ design. The weighting function $\boldsymbol{W}_q$ will allow us to shape the sensitivity functions as desired. Note that the signals w, z_1 and z_2 do not have physical interpretations, but r, d and e do, as previously defined. The input signal u_{sc} is just a scaled version of the physical signal u: $u_{sc} := \frac{\gamma}{d_{max}} J_2 u$. A few algebraic computations done on the system of Figure 5.1 show that

$\boldsymbol{S}_r := \left(I - C_1 J_1 \tilde{\boldsymbol{M}}_0^{-1} \tilde{\boldsymbol{N}}_0 \boldsymbol{T}_a \boldsymbol{K}\right)^{-1}$ and $\boldsymbol{S}_d := \frac{\gamma}{d_{max}} \boldsymbol{S}_r C_1 J_1 \tilde{\boldsymbol{M}}_0^{-1} \tilde{\boldsymbol{N}}_0 J_2$. For $q > 0$, let $\boldsymbol{W}_q := q\boldsymbol{w}\left[I_{3\times 3}\ 0_{3\times(p-3)}\right]$, and let $\boldsymbol{W}_1 := \boldsymbol{W}_q|_{q=1}$. Referring to Figure 5.1, the full robust performance problem is this:

Problem RP *Design a finite-dimensional, proper, linear time-invariant controller* $\boldsymbol{K}$ *such that with* $q = 1$*, the closed-loop system has the following properties:*

(i) *robust stability (i.e.,* $\|w \mapsto z_1\|_\infty \leq 1$ *for* $\tilde{\boldsymbol{\Delta}}_0 \equiv 0$*),*

(ii) $\|r_h \mapsto z_2\|_\infty \leq 1,\ \forall \tilde{\boldsymbol{\Delta}}_0 \in \mathcal{BRH}_\infty^{n\times(m+n)}$,

(iii) $\|d \mapsto z_2\|_\infty \leq 1,\ \forall \tilde{\boldsymbol{\Delta}}_0 \in \mathcal{BRH}_\infty^{n\times(m+n)}$.

This problem can be solved using μ-synthesis as discussed in Chapter 6. Here we consider the following easier problem of robust stability and nominal performance. It is desired to reduce the ∞-norm of the transfer matrix $\boldsymbol{W}_1 \boldsymbol{S}_d = \boldsymbol{w}\boldsymbol{S}_{dh}$ to a value less than or equal to one in order to achieve $\|\boldsymbol{S}_{dh}(j\omega)\| \leq |\boldsymbol{w}^{-1}(j\omega)|,\ \forall\omega$ for good force/torque disturbance rejection at low frequencies. As a second requirement, we would like to keep the norm of $\boldsymbol{S}_{rhh}(j\omega)$ small at low frequencies, say smaller than $|\boldsymbol{w}^{-1}(j\omega)|$, to achieve good input tracking. These specifications lead to the following robust stability and nominal performance problem:

Problem RSNP *Design a finite-dimensional, proper, linear time-invariant controller* $\boldsymbol{K}$ *such that with* $q = 1$ *and* $\tilde{\boldsymbol{\Delta}}_0 \equiv 0$*, the closed-loop system has the following properties:*

(i) *robust stability (i.e.,* $\|w \mapsto z_1\|_\infty \leq 1$*),*

(ii) $\|r_h \mapsto z_2\|_\infty \leq 1$,

(iii) $\|d \mapsto z_2\|_\infty \leq 1$.

Note that the reference and torque/force disturbance input channels labeled respectively r and d and represented by dashed lines in Figure 5.1 are not included in the design process. This is to avoid introducing too many cross terms in the closed-loop transfer matrix whose ∞-norm is to be minimized. Thus, a compromise standard $\mathcal{H}_\infty$ problem is set up to solve Problem RSNP. The basic goal of the proposed $\mathcal{H}_\infty$ design is to achieve $\left\| w \mapsto \begin{bmatrix} z_1 \\ z_2 \end{bmatrix} \right\|_\infty \leq 1$ for $\boldsymbol{\Delta}_0 \equiv 0$.

The $\mathcal{H}_\infty$ design method minimizes the ∞-norm of the closed-loop map $w \mapsto z$ over all stabilizing controllers in Figure 5.2, where $z := \begin{bmatrix} z_1 \\ z_2 \end{bmatrix}$. The design block diagram of Figure 5.2

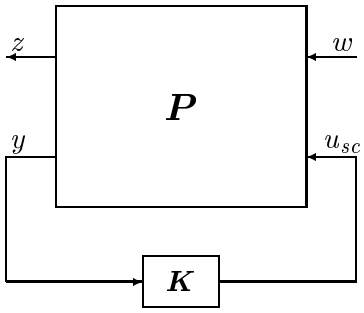

Figure 5.2: Generalized plant for $\mathcal{H}_\infty$ design.

represents the same system as the one in Figure 5.1 but without the perturbation $\tilde{\boldsymbol{\Delta}}_0$ and the exogenous signals r and d. The generalized design plant $\boldsymbol{P}$ is given by

$$\boldsymbol{P} := \begin{bmatrix} \boldsymbol{P}_{11} & \boldsymbol{P}_{12} \\ \boldsymbol{P}_{21} & \boldsymbol{P}_{22} \end{bmatrix} \tag{5.1}$$

where

$$\boldsymbol{P}_{11} := \begin{bmatrix} 0 \\ \boldsymbol{r}\tilde{\boldsymbol{M}}_0^{-1} \\ \boldsymbol{W}_q C_1 J_1 \tilde{\boldsymbol{M}}_0^{-1} \end{bmatrix}, \qquad \boldsymbol{P}_{12} := \begin{bmatrix} \boldsymbol{r}\boldsymbol{T}_a \\ \boldsymbol{r}\tilde{\boldsymbol{M}}_0^{-1}\tilde{\boldsymbol{N}}_0\boldsymbol{T}_a \\ \boldsymbol{W}_q C_1 J_1 \tilde{\boldsymbol{M}}_0^{-1}\tilde{\boldsymbol{N}}_0\boldsymbol{T}_a \end{bmatrix},$$

$$\boldsymbol{P}_{21} := C_1 J_1 \tilde{\boldsymbol{M}}_0^{-1}, \qquad \boldsymbol{P}_{22} := C_1 J_1 \tilde{\boldsymbol{M}}_0^{-1}\tilde{\boldsymbol{N}}_0\boldsymbol{T}_a.$$

The compromise $\mathcal{H}_\infty$ problem is stated as follows.

Problem COMP *Design a finite-dimensional, proper, linear time-invariant controller* $\boldsymbol{K}$ *such that for* $\tilde{\boldsymbol{\Delta}}_0 \equiv 0$*, the nominal closed loop of Figure 5.2 achieves* $\|w \mapsto z\|_\infty \leq 1$.

Justification that a solution to Problem COMP also solves Problem RSNP is given by Proposition 7 that, more specifically, states that we can shape the norms of $\boldsymbol{S}_{dh}$ and $\boldsymbol{S}_{rh}$ (and hence $\boldsymbol{S}_{rhh}$) indirectly by minimizing $\|w \mapsto z_2\|_\infty$. Referring to Figure 5.1 again, let $\boldsymbol{S}_1 := \left(I - \tilde{\boldsymbol{M}}_0^{-1}\tilde{\boldsymbol{N}}_0\boldsymbol{T}_a\boldsymbol{K}C_1J_1\right)^{-1}$. In the sequel, fix $k = c_{max}/d_{max}$ in the second-order common denominator of the scaled factors.

Proposition 7 *Assume C_1 is right invertible and let $C_1^\ddagger$ be a right inverse of C_1. Let $q = \max\left\{\|\tilde{\boldsymbol{M}}_0 J_1^{-1} C_1^\ddagger\|_\infty,\, d_{max}^{-1}\|J_1^{-1}B_1\|\right\}$. If the controller $\boldsymbol{K}$ is internally stabilizing and achieves*

$$\left\| w \mapsto \begin{bmatrix} z_1 \\ z_2 \end{bmatrix} \right\|_\infty = \left\| \begin{bmatrix} \boldsymbol{r}\boldsymbol{T}_a \boldsymbol{K} C_1 J_1 \boldsymbol{S}_1 \tilde{\boldsymbol{M}}_0^{-1} \\ \boldsymbol{r}\boldsymbol{S}_1 \tilde{\boldsymbol{M}}_0^{-1} \\ \boldsymbol{W}_q \boldsymbol{S}_r C_1 J_1 \tilde{\boldsymbol{M}}_0^{-1} \end{bmatrix} \right\|_\infty \leq 1 \ , \tag{5.2}$$

then the closed-loop system of Figure 5.1 is robustly stable to all perturbations $\tilde{\boldsymbol{\Delta}}_0 \in \mathcal{BRH}_\infty^{n\times(m+n)}$, and for every $\omega \in \mathbb{R}$ we have

$$\|\boldsymbol{S}_{dh}(j\omega)\| \leq |\boldsymbol{w}^{-1}(j\omega)| \ , \tag{5.3}$$

$$\|\boldsymbol{S}_{rh}(j\omega)\| \leq |\boldsymbol{w}^{-1}(j\omega)| \ . \tag{5.4}$$

Proof The proof uses the submultiplicativity property of the norm $\|\cdot\|$. Assume $\boldsymbol{K}$ is stabilizing and achieves (5.2), which implies that $\|w \mapsto z_1\|_\infty \leq 1$. This inequality says that the closed-loop system is robustly stable to all perturbations $\tilde{\boldsymbol{\Delta}}_0 \in \mathcal{BRH}_\infty^{n\times(m+n)}$. Furthermore, (5.2) implies that $\|\boldsymbol{W}_q \boldsymbol{S}_r C_1 J_1 \tilde{\boldsymbol{M}}_0^{-1}\|_\infty \leq 1$. Then $\forall \omega \in \mathbb{R}$,

$$\begin{aligned} & q|\boldsymbol{w}(j\omega)|\|(\boldsymbol{S}_{rh} C_1 J_1 \tilde{\boldsymbol{M}}_0^{-1})(j\omega)\| \leq 1 \\ \Longrightarrow \quad & \|\boldsymbol{S}_{rh}(j\omega)\| \leq q^{-1}|\boldsymbol{w}^{-1}(j\omega)|\|\tilde{\boldsymbol{M}}_0(j\omega) J_1^{-1} C_1^\ddagger\| \\ \Longrightarrow \quad & \|\boldsymbol{S}_{rh}(j\omega)\| \leq q^{-1}|\boldsymbol{w}^{-1}(j\omega)|\|\tilde{\boldsymbol{M}}_0 J_1^{-1} C_1^\ddagger\|_\infty \ . \end{aligned}$$

But $q \geq \|\tilde{\boldsymbol{M}}_0 J_1^{-1} C_1^\ddagger\|_\infty$, hence $\|\boldsymbol{S}_{rh}(j\omega)\| \leq |\boldsymbol{w}^{-1}(j\omega)|$.

Now $\boldsymbol{S}_{dh} = \frac{\gamma}{d_{max}} \boldsymbol{S}_{rh} C_1 J_1 \tilde{\boldsymbol{M}}_0^{-1} \tilde{\boldsymbol{N}}_0 J_2$, so our assumption implies that $\forall \omega$,

$$\begin{aligned} & \|\boldsymbol{S}_{dh}(j\omega)\| = \tfrac{\gamma}{d_{max}} \|(\boldsymbol{S}_{rh} C_1 J_1 \tilde{\boldsymbol{M}}_0^{-1} \tilde{\boldsymbol{N}}_0 J_2)(j\omega)\| \\ \leq \tfrac{\gamma}{d_{max}} & \|(\boldsymbol{S}_{rh} C_1 J_1 \tilde{\boldsymbol{M}}_0^{-1})(j\omega)\| \|\tilde{\boldsymbol{N}}_0(j\omega) J_2\| \leq \tfrac{\gamma}{d_{max}} q^{-1} |\boldsymbol{w}^{-1}(j\omega)| \|\tilde{\boldsymbol{N}}_0(j\omega) J_2\| \\ & \leq q^{-1} d_{max}^{-1} |\boldsymbol{w}^{-1}(j\omega)| \|J_1^{-1} B_1\| \ . \end{aligned}$$

But $q \geq d_{max}^{-1}\|J_1^{-1}B_1\|$, therefore $\|\boldsymbol{S}_{dh}(j\omega)\| \leq |\boldsymbol{w}^{-1}(j\omega)|$. ■

Remark 5.1 The choice of q in Proposition 7 may be used for a first design to get insight into the tradeoff between robustness and performance, but smaller values of q may be tried to reach a satisfactory design achieving (5.3) and (5.4).

Remark 5.2 Other forms for $\boldsymbol{W}_1$ may be used to achieve other objectives such as weighting some or all of the outputs corresponding to the flexible part of the structure. Then it is easy to see that Proposition 7 remains basically the same, and particularly the expression for q is unchanged. In our experiments with Daisy, it was found that weighting all the outputs was asking too much given the uncertainty in the model and the actuator saturation levels. Hence only the hub angles were weighted with $\boldsymbol{W}_q$ as above. In any case, the modal coordinates are weighted by $\boldsymbol{r}$ (see Figure 5.1) which in our experiments on Daisy resulted in sufficient vibration attenuation.

To recap, if a stabilizing $\boldsymbol{K}$ satisfying (5.2) has been designed, it follows that (*i*) $\boldsymbol{K}$ provides robust stability to all perturbations of the modal parameters satisfying (2.11) and (*ii*) $\boldsymbol{K}$ provides nominal performance in the sense that inequalities (5.3) and (5.4) hold, the latter implying $\|\boldsymbol{S}_{rhh}(j\omega)\| \leq |\boldsymbol{w}^{-1}(j\omega)|$. Note that the controller $\boldsymbol{K}_p$ to be implemented on the real system is a scaled version of $\boldsymbol{K}$, i.e., $\boldsymbol{K}_p = \frac{d_{max}}{\gamma} J_2^{-1} \boldsymbol{K}$.

5.1.1 $\mathcal{H}_\infty$ Designs for Daisy

Daisy is an experimental testbed designed and built at UTIAS whose dynamics are meant to approximate those of real LFSS (Figure 5.3) [10]. It consists of a rigid hub (the "stem") mounted on a spherical joint and on top of which are ten ribs (the "petals") attached through passive two-degree-of-freedom rotary joints and low-stiffness springs. Each rib is coupled to its two neighbors via low-stiffness springs. The hub represents the rigid part of the LFSS, while the ribs model the flexibilities in the LFSS. Each rib is equipped with four unidirectional air jet thrusters which are essentially on-off devices, each capable of delivering a torque of 0.8 Nm at the rib joint. Pulse-width modulation (PWM) of the thrust is used to apply desired torques on the ribs. The four thrusters are aligned by pairs to implement two orthogonal bidirectional actuators (Figure 5.4). So from now on, when we use the word thruster alone, we will mean *bidirectional* thruster. Mounted at the tip of each rib are two linear accelerometers and an infra-red emitting diode.

Two hub-mounted infra-red CCD cameras measure the position of these diodes via ten lenses. The cameras are linked to a computer which from the kinematics of Daisy computes the 20 rib angles relative to the hub in real-time (at a 30 Hz sampling rate) from the sampled infra-red video frames. This vision system, called DEOPS (Digital Electro-Optic Position Sensor),

was developed at UTIAS [29]. Its resolution is approximately 0.1% of the cameras' fields of view, which roughly translates to an angle measurement accuracy of 3.5×10^{-4} radians (.02 degrees) in the ideal case.

The hub actuators consist of three torque wheels driven by DC motors whose axes are orthogonal. Each can deliver up to 58 Nm but is limited to 38.8 Nm. The hub orientation and angular velocity can be measured with position and velocity encoders. For this research, only DEOPS and the hub position encoders were used in the control experiments.

Daisy's control computer has an Intel^{TM} 80386 processor that operates at 25 MHz. Data acquisition through the DEOPS system is carried out by a separate 80386 processor that also operates at 25 MHz. This second processor communicates with one of the five Intel 80186 (12 MHz) input/output boards that operate in parallel with the central processor.

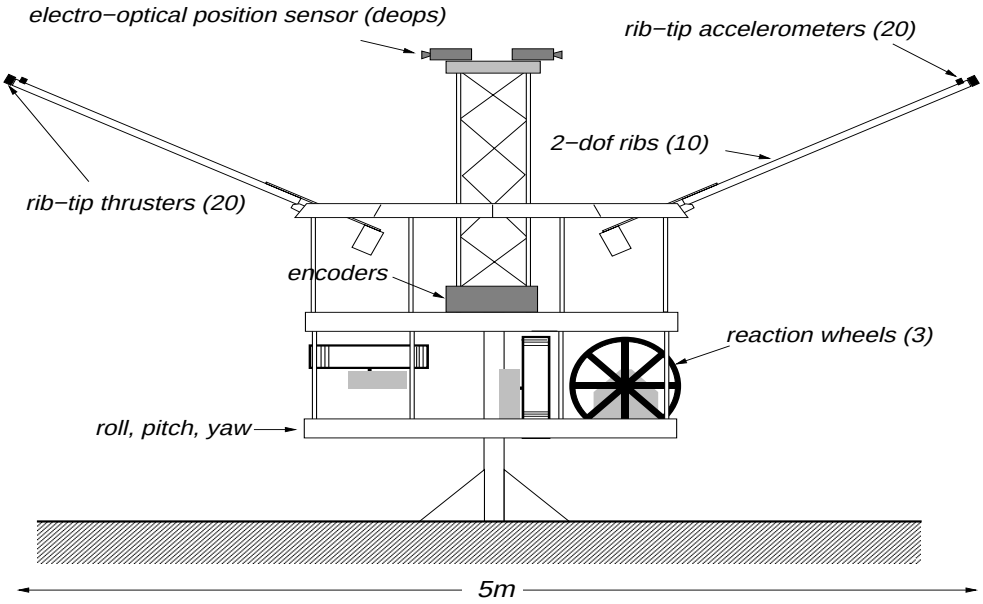

Figure 5.3: Daisy LFSS experimental testbed.

The linear dynamic model available for Daisy is of 46^{th} order. It was derived from a detailed analysis of the inertias of most components of Daisy and basic Newton-Euler dynamics [43]. The model includes 20 flexible modes with frequencies ranging from approximately 0.56 rad/s to 0.71 rad/s and damping ratios from 0.015 to 0.06. The modal parameters are listed in Table 5.1 with crude approximations of their uncertainties obtained simply from looking at time

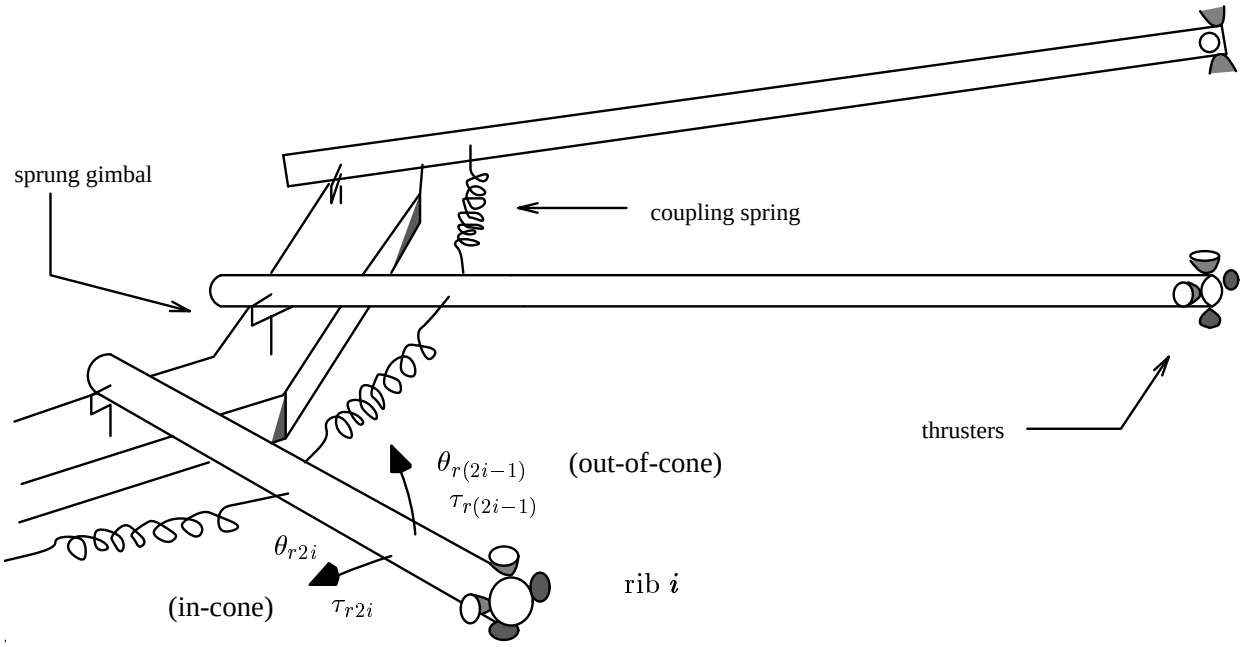

Figure 5.4: Details of Daisy's ribs.

responses. Some of the modes are multiple. Two of the rigid-body modes are pendulous, so they can be considered as flexible modes both with nominal frequency 0.29 rad/s and nominal damping ratios 0.11 and 0.09. The model has the form of (2.3).

The method described in Section 5.1 is illustrated by designing a robust controller for collocated and noncollocated configurations of Daisy using the $\mathcal{H}_\infty$ design method.

5.1.1.1 Collocated Case

Here, by collocation we mean that all rotations and displacements produced by the actuators at their locations are measured, and only these measurements are used for control. Thus 23 actuator/sensor pairs are used, namely the 20 bidirectional rib thrusters with the DEOPS system measuring the 20 rib angles, plus the three hub reaction wheels with the three corresponding angle encoders. In terms of system equations (2.3) and (2.4) and referring to Figure 5.4, the inputs are $u = [\tau_{hx}\ \tau_{hy}\ \tau_{hz}\ \tau_{r1}\ \tau_{r2} \cdots \tau_{r20}]^T$ where the first three are the hub torques around the x, y and z axes, and the last twenty inputs are the rib torques given by

$$\tau_{ri} = \begin{cases} \text{rib } (i+1)/2 \text{ out-of-cone torque}, & i \text{ odd}, \\ \text{rib } i/2 \text{ in-cone torque}, & i \text{ even}. \end{cases} \tag{5.5}$$

mode i	frequency ω_i (rad/s)	damping ratio ζ_i
1 (rigid)	0	0
2 (rigid)	$0.286 \pm 10\%$	$0.11 \pm 50\%$
3 (rigid)	$0.293 \pm 10\%$	$0.09 \pm 50\%$
4 (flex.)	$0.568 \pm 10\%$	$0.025 \pm 50\%$
5 (flex.)	$0.568 \pm 10\%$	$0.02 \pm 50\%$
6 (flex.)	$0.569 \pm 10\%$	$0.03 \pm 50\%$
7 (flex.)	$0.569 \pm 10\%$	$0.02 \pm 50\%$
8 (flex.)	$0.569 \pm 10\%$	$0.035 \pm 50\%$
9 (flex.)	$0.569 \pm 10\%$	$0.025 \pm 50\%$
10 (flex.)	$0.569 \pm 10\%$	$0.02 \pm 50\%$
11 (flex.)	$0.572 \pm 10\%$	$0.02 \pm 50\%$
12 (flex.)	$0.592 \pm 10\%$	$0.06 \pm 50\%$
13 (flex.)	$0.593 \pm 10\%$	$0.06 \pm 50\%$
14 (flex.)	$0.657 \pm 10\%$	$0.015 \pm 50\%$
15 (flex.)	$0.657 \pm 10\%$	$0.015 \pm 50\%$
16 (flex.)	$0.657 \pm 10\%$	$0.02 \pm 50\%$
17 (flex.)	$0.657 \pm 10\%$	$0.02 \pm 50\%$
18 (flex.)	$0.657 \pm 10\%$	$0.027 \pm 50\%$
19 (flex.)	$0.657 \pm 10\%$	$0.025 \pm 50\%$
20 (flex.)	$0.657 \pm 10\%$	$0.02 \pm 50\%$
21 (flex.)	$0.670 \pm 10\%$	$0.04 \pm 50\%$
22 (flex.)	$0.672 \pm 10\%$	$0.05 \pm 50\%$
23 (flex.)	$0.714 \pm 10\%$	$0.015 \pm 50\%$

Table 5.1: Modal parameters of Daisy's model.

All torque inputs are expressed in Nm. The input matrix $B_1 \in \mathbb{R}^{23\times 23}$ is assumed to have up to 8% uncertainty in its entries. Note that the torque wheels have some dynamics, i.e., for each wheel, the transfer function between the desired and produced torques is first-order and strictly proper. On the other hand, the PWM thrusters, which deliver average torques close to the desired ones, are modeled as pure gains. Overall, the transfer matrix $\boldsymbol{T}_a$ in Figure 5.1 is taken to be

$$\boldsymbol{T}_a = \text{diag}\left\{\frac{0.01s+1}{0.36s+1}, \frac{0.01s+1}{0.36s+1}, \frac{0.01s+1}{0.36s+1}, 1, 1, \ldots, 1\right\}\ , \tag{5.6}$$

where the terms $0.01s$ are added in the numerators to regularize the generalized plant for the $\mathcal{H}_\infty$ problem, and the 0.36 time constants were measured experimentally. Note that $\boldsymbol{T}_a$ commutes with J_2.

The outputs are the angles $y = [\theta_{hx}\, \theta_{hy}\, \theta_{hz}\, \theta_{r1}\, \theta_{r2} \cdots \theta_{r20}]^T$ which correspond to the input torques described above. The output matrix is just the mode shape matrix, $C_1 = E \in \mathbb{R}^{23\times 23}$, which is invertible. All angles are expressed in radians. Finally $\Lambda = \text{diag}\{\omega_1^2, \ldots, \omega_{23}^2\}$ and $D = \text{diag}\{2\zeta_1\omega_1, \ldots, 2\zeta_{23}\omega_{23}\}$, where the modal parameters are those given in Table 5.1.

A plot of the 23 singular values of $C_1\boldsymbol{G}(j\omega)$ is shown in Figure 5.5. It turns out that all the modes are almost equally significant and as a result it is very difficult to reduce the number of modes in the model. This was concluded from an analysis of the Hankel singular values of a normalized coprime factorization of the plant model $C_1\boldsymbol{G}$ [35]: They all lay between 0.2 and 0.9, which indicates that the model should not be reduced. Consequently, our design model includes all the modes in Table 5.1. It should be noted that this method of characterizing the input/output influence of the modes in the model seems appropriate for our control design method based on a coprime factorization. It avoids the singularity of measures such as modal costs [45] and Hankel singular values of the plant [21] when the damping ratios go to zero.

It is desired to control Daisy's model so that it remains stable for all bounded perturbations of the modal parameters in Table 5.1 and all perturbations of the entries of B_1 within 8% of their nominal values. We also want good torque/force disturbance rejection and good tracking in the sense of (5.3) and (5.4). The diagonal scaling matrices J_1 and J_2 are computed as explained in Section 2.3. The generalized plant for the robust $\mathcal{H}_\infty$ design is built according to Figure 5.2, and the different constants and weighting functions are

$$d_{max} = 0.107, \qquad c_{max} = 0.046, \qquad k = \frac{c_{max}}{d_{max}} = 0.43, \qquad \gamma = 0.79, \qquad q = 1000,$$

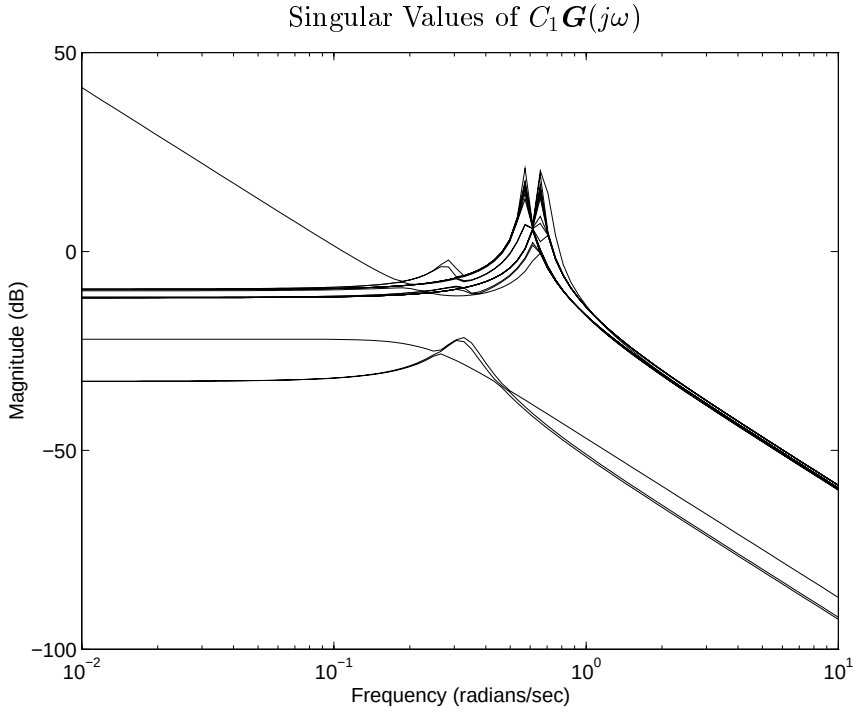

Figure 5.5: Singular values of $C_1\boldsymbol{G}(j\omega)$.

$$\boldsymbol{w}(s) = \frac{100}{s^2/(0.01)^2 + 2 \times 0.7s/0.01 + 1}, \tag{5.7}$$

$$\boldsymbol{r}(s) = \frac{0.001s + 1.415}{2.33s + 1}. \tag{5.8}$$

Note that $q = 1.42 \times 10^4$ when computed using the formula in Proposition 7, but this value turned out to be too large to get the ∞-norm of $w \mapsto z$ down to less than 1. However q reduced to 1000 led to a good tradeoff between robustness and performance. Also note that computational delay and zero-order hold models were not included in the generalized plant even though both were present in the digital implementation of the controller on Daisy. It was anticipated that the design would be robust to these unmodeled dynamics; this was borne out by experiments. No antialiasing analog filters were available to filter the measured hub angle signals, nor for DEOPS signals which are inherently digital. Even though this is rather undesirable, high-frequency noise levels seemed sufficiently small to avoid serious aliasing problems in the experiments.

The $\mathcal{H}_\infty$ design was carried out in Matlab^{TM} using the μ-Tools [2] command *hinfsyn* which minimizes the ∞-norm of the closed-loop map $w \mapsto z$ over all stabilizing controllers in Figure 5.2, and computes a suboptimal controller achieving an ∞-norm within some desired accuracy of the optimal. The generalized design plant $\boldsymbol{P}$ is given by (5.1). If a realization of it is obtained using

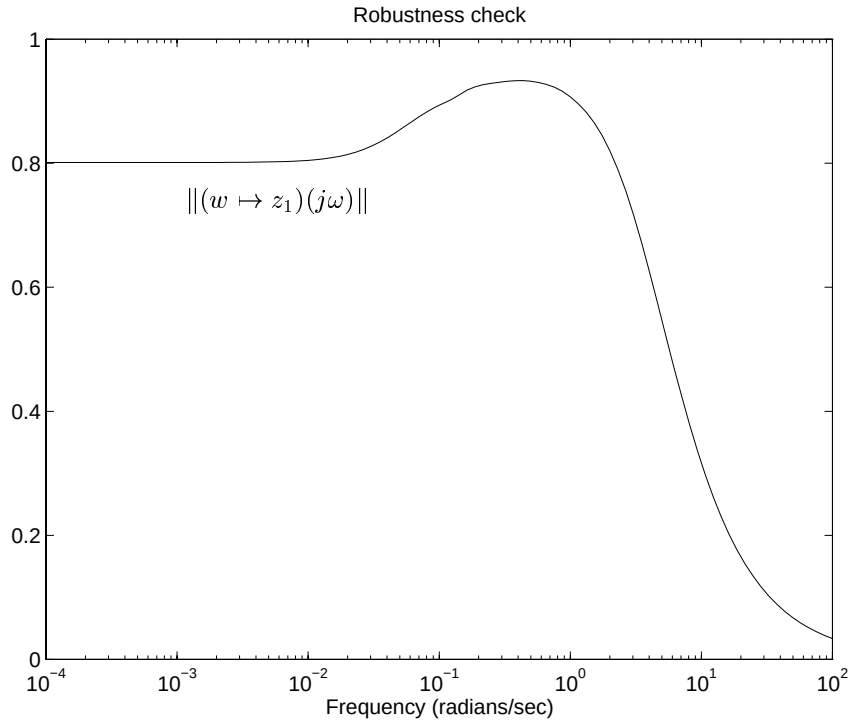

Figure 5.6: Stability robustness check: Norm of $w \mapsto z_1$ for $\boldsymbol{K}_1$.

a computer, this realization will be nonminimal in general because pole-zero cancellations might not be carried out. Also note that $\boldsymbol{P}$ is unstable, so one cannot use the balanced truncation method [37] to get rid of the unobservable and uncontrollable modes. Therefore we used the decentralized fixed-mode method [11] to obtain a minimal realization of $\boldsymbol{P}$, reducing it from 147 to 78 state variables, which equals its McMillan degree. This method has the advantage of being computationally simple and hence more reliable for such large systems.

A stable suboptimal controller achieving $\|w \mapsto z\|_\infty = 0.94$ was obtained. Its order was the same as the order of the minimal generalized plant, i.e. 78, but a balanced truncation reduced it to 55 state variables without noticeably affecting the closed-loop ∞-norm. With this reduced controller $\boldsymbol{K}_1$, Figure 5.6 shows that robust stability was achieved while Figure 5.7 shows that required performance has been attained, i.e., $\|\boldsymbol{S}_{rh}(j\omega)\|$ and $\|\boldsymbol{S}_{dh}(j\omega)\|$ are less than $|\boldsymbol{w}^{-1}(j\omega)|$ as desired. The least-damped closed-loop mode has a damping ratio of 0.38.

The 55^{th}-order controller $\boldsymbol{K}_1$ was rescaled to $\boldsymbol{K}_{p1} = \frac{d_{max}}{\gamma} J_2^{-1} \boldsymbol{K}_1$, a controller using the actual rib and hub angles to compute actual rib and hub control torques. Then, since the implementation of the controller must be digital, $\boldsymbol{K}_{p1}$ was discretized at a sampling rate of

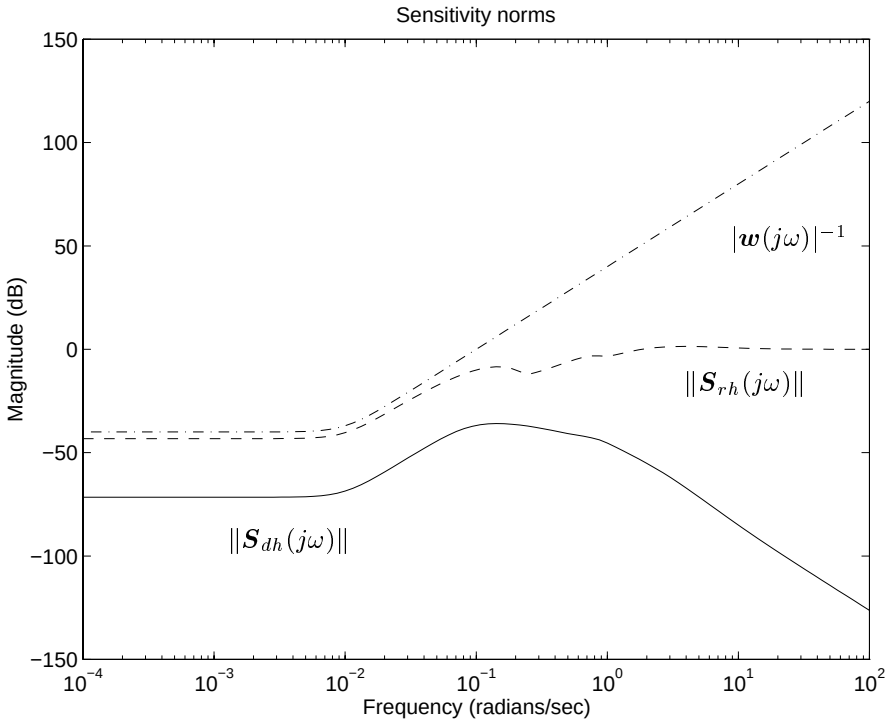

Figure 5.7: Norms of $\boldsymbol{S}_{dh}(j\omega)$ and $\boldsymbol{S}_{rh}(j\omega)$ for $\boldsymbol{K}_1$.

10 Hz using the bilinear transformation; call the resulting controller $\boldsymbol{K}_{p1d}$. Note that another discretized version of the controller was computed using the Matlab^{TM} function *c2d* —it destabilized Daisy both in simulations and experiments. The *c2d* function performs the discretization by placing a sampler at the output of the controller and a zero-order hold at the input. Figure 5.8 shows the frequency responses of two entries of $\boldsymbol{K}_{p1}$ and $\boldsymbol{K}_{p1d}$. The fit is good up to 10 rad/s whereas for the controller discretized with *c2d*, the frequency responses started to differ significantly from 1 rad/s.

The 10 Hz sampling rate was almost the highest achievable on the real-time control computer system with our control software. An earlier version of the program allowed a maximum control rate of 5 Hz only —when used to implement a discretized version of $\boldsymbol{K}_{p1}$, it destabilized the closed loop. This suggests that, for the current control computer, an $\mathcal{H}_\infty$-optimal sampled-data design would be warranted, but this is left for future work.

We used the standardized hub torque disturbance profile in Figure 5.9 for all our test experiments and simulations. It can be applied by any of the three torque wheels individually or in any combination. Notice that this disturbance is completely specified by three parameters:

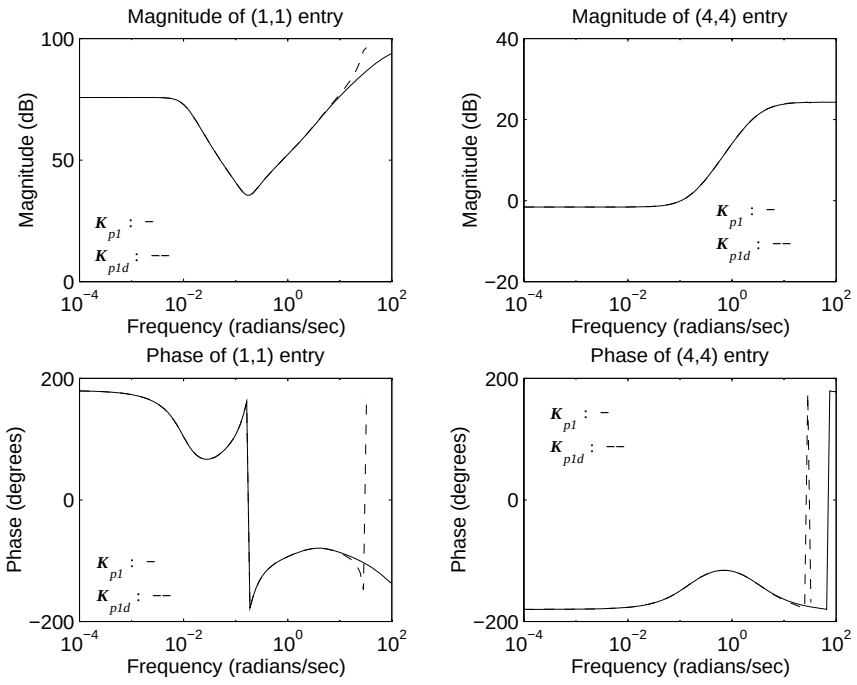

Figure 5.8: Frequency responses of the (1,1) and (4,4) entries of $\boldsymbol{K}_{p1}$ and $\boldsymbol{K}_{p1d}$.

The amplitude of the first torque pulse, A_d; the duration of the first and second pulses, T; and the combination of hub axes around which the disturbance is applied, $axes$. This latter parameter can take on values in the set $\{x, y, z, xy, xz, yz, xyz\}$. With these definitions, let us denote the disturbance as $D(A_d, T, axes)$. The main reason for using it is that it was already implemented as a subroutine in Daisy's control software and was used quite often by other researchers at UTIAS. Thus we could qualitatively compare our results to others' more easily.

In all the experiments and simulations, the controller is switched on after the hub angle experiencing the largest deviation changes sign. Thus the disturbance has roughly the effect of a torque impulse applied to the hub because the controller starts when the hub angles are small while the angular velocities are large. However, the rib angles may not be small at switch-on time. Although experimental controller performance would be best assessed by performing frequency-response experiments and comparing with $\boldsymbol{S}_{dh}(j\omega)$, these are not practical for Daisy because of the amplifier overheating problem mentioned in §4.2.2.1. But the torque impulse response matrix is just the inverse Laplace transform of the sensitivity $\boldsymbol{S}_d$. Hence this provides some motivation for judging and comparing controller performance using time responses of the rib and hub angles to the disturbance $D(A_d, T, axes)$.

For all the plots, $t = 0$ corresponds to the instant at which the controller is turned on. Most of the analyses of the experiments will be qualitative, based on the experimental plots. For instance, we will use the expression "settling time" in a loose way, without defining it rigorously.

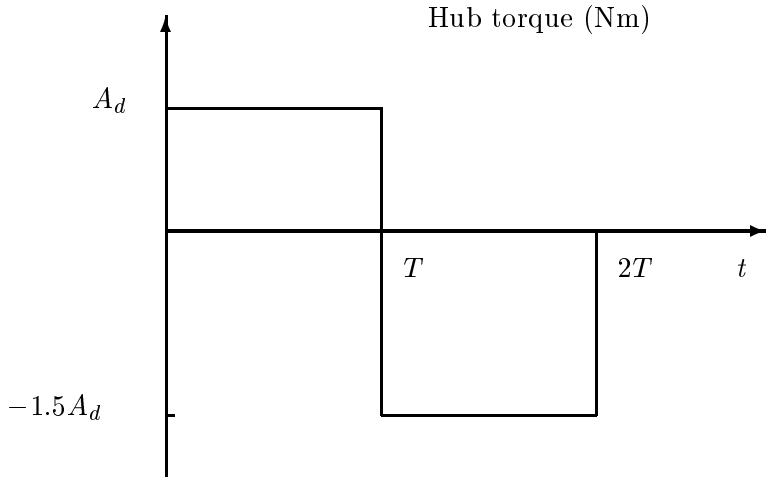

Figure 5.9: Standard hub torque disturbance $D(A_d, T, axes)$ used in simulations and experiments.

Before we proceed to present the closed-loop simulation and experimental results, an open-loop response of Daisy to $D(13.5\text{Nm}, 2s, x)$ is plotted in Figure 5.10 along with a simulated continuous-time response of the nominal model $C_1\boldsymbol{G}$. Discrepancies between some of the actual and nominal modal frequencies and damping ratios can be observed from these plots, illustrating the uncertainty in the model.

All simulations are linear and *discrete-time* with the plant model (including actuator dynamics) discretized at 10 Hz using *c2d*, which here is the natural choice since sampling and zero-order hold devices are present in Daisy's control system. The first closed-loop experiment with $\boldsymbol{K}_{p1d}$ is the response to an x-axis hub torque disturbance $D(13.5\text{Nm}, 2s, x)$. The simulated and actual hub angles are shown in Figure 5.11. When compared with the response in Figure 5.10, it is clear that the $\mathcal{H}_\infty$ controller vastly improves the dynamics of Daisy. Note that absolutely no experimental tuning was necessary to get all the responses in this chapter and in Chapter 6, unlike some PD, LQR and LQG controllers which were previously tested on Daisy.

The settling times of the experimental and simulated θ_{hx} are approximately the same but the transient response is much larger experimentally. This is due in part to hub torque saturation and actual torque slewing rate. This slewing rate was limited because of the way hub torques

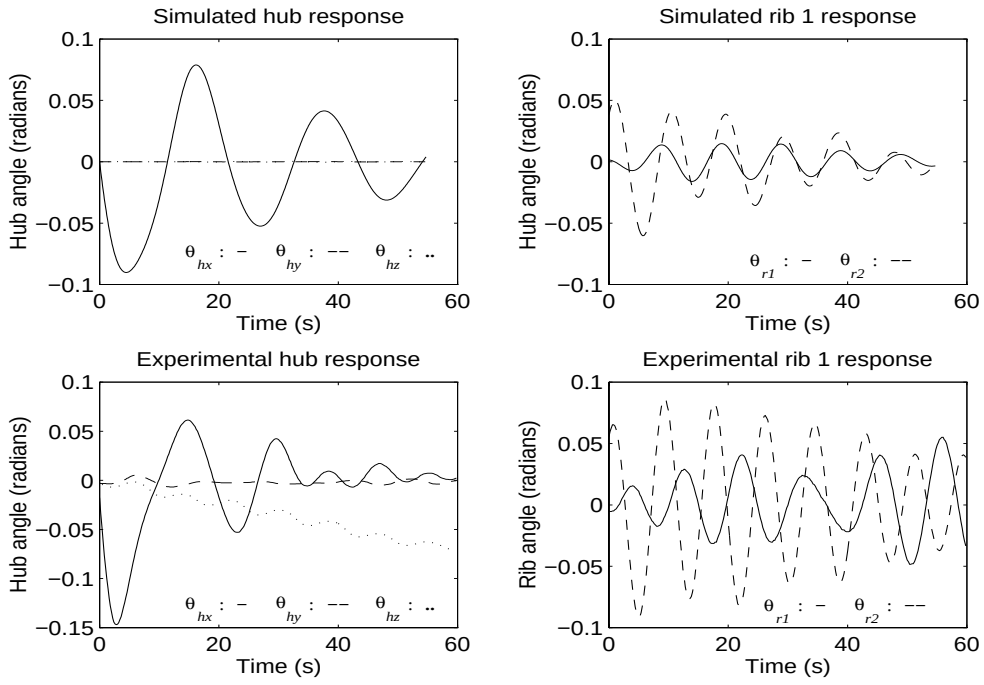

Figure 5.10: Sim. and exp. open-loop responses of Daisy to $D(13.5\text{Nm}, 2s, x)$.

were generated. A reaction wheel's momentum is the integral of the torque, so a routine implementing a discrete-time integrator processed and scaled the desired torque input in order to get the desired instantaneous wheel velocity, which was then transformed into an input voltage to the motor. The DC motor driving the reaction wheel then produced a desired velocity proportional to the applied voltage after a brief transient characterized by the dynamical part of $\boldsymbol{T}_a$. There was a bug in the digital integration routine that would limit the rate of change of the desired motor voltage, which in turn limited the rate of change of the reaction torque. This bug was not fixed during the course of the experimental tests.

The simulated and experimental *computed* control torques are plotted in Figure 5.13 for the hub. Notice how noisy the experimental desired torque is. This is not surprising since the controller has derivative action at high frequencies. However, this does not seem to have caused any problem as the integration routine described above takes care of smoothing this desired torque signal. Recall that the saturation levels are 38.8 Nm and 0.8 Nm for the hub and rib torques respectively, but the simulations do not have these limits. They are represented as dashed lines in the plots.

Figure 5.12 shows the simulated and actual rib angles, while the rib *computed* control torques

are shown in Figure 5.14. It can be observed from these figures that the experimental rib angles undergo larger deviations than the simulated ones, especially for the second "half-cycle" from 5 s to 10 s. This may have been caused by the rib torque saturation limits and uncertainty in the model. The experimental computed rib torques were for the first few seconds as large as three times the saturation levels. Also recall that this $\mathcal{H}_\infty$ design only guarantees *nominal* performance as opposed to the μ design of §6.1.1.1 which guarantees *robust* performance. Finally notice how the experimental rib responses do not converge to zero as rapidly as in the simulation. This is due to a significant deadband in the jet thrusters input-output characteristics. This deadband was not quantified but will be for future experiments. As we will now see, the results are much more consistent in the case of y-axis and z-axis torque disturbances.

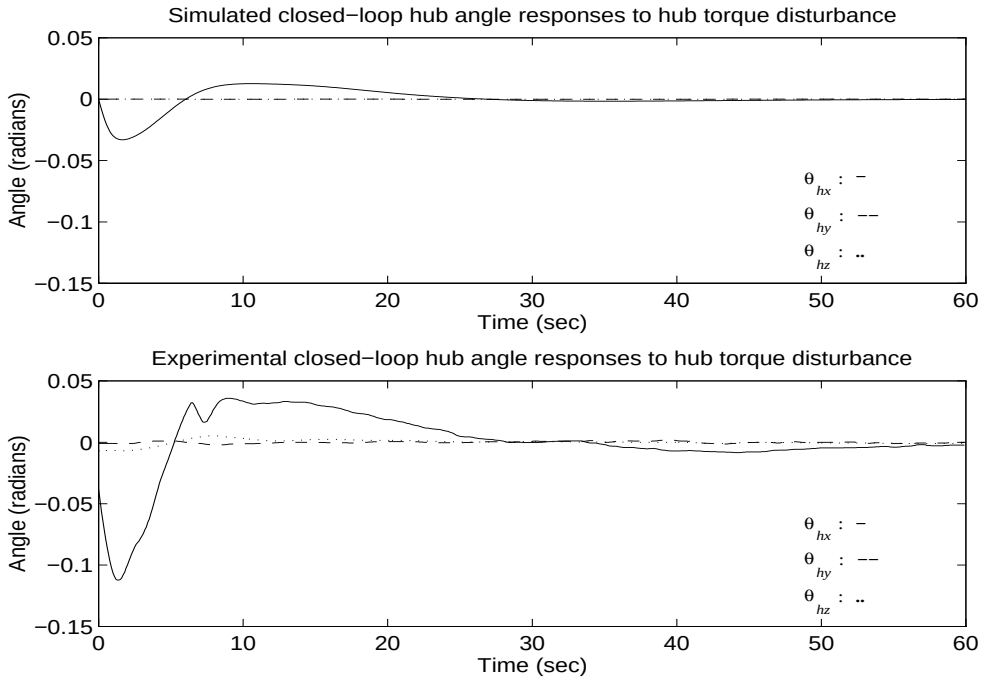

Figure 5.11: Sim. and exp. closed-loop hub angle responses with $\boldsymbol{K}_{p1d}$, $D(13.5\text{Nm}, 2s, x)$.

A series of graphs exhibit the results for two similar control experiments with $\boldsymbol{K}_{p1d}$ and torque disturbances $D(13.5\text{Nm}, 2s, y)$ and $D(13.5\text{Nm}, 2s, z)$. Figures 5.15 and 5.16 show respectively the hub and rib angle responses for the y-axis disturbance, while the hub control torques are plotted in Figure 5.17 and the rib control torques are in Figure 5.18. The experimental response of θ_{hy} has a slightly longer settling time than its simulated counterpart. Again, the experimental transient is significantly larger than shown by simulation, and the explanation

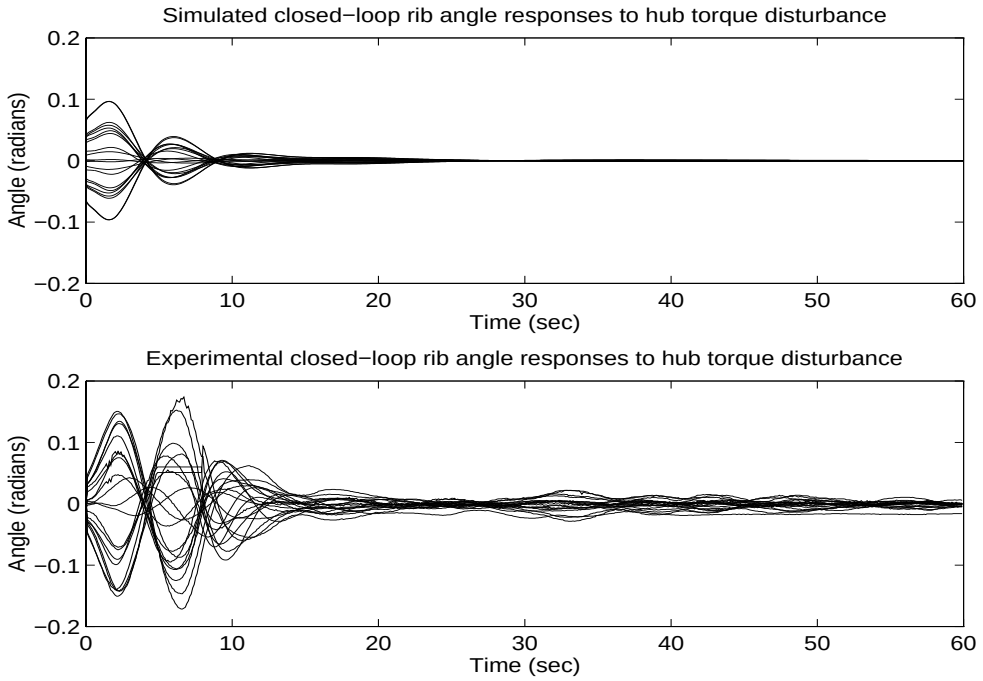

Figure 5.12: Sim. and exp. closed-loop rib angle responses with $\boldsymbol{K}_{p1d}$, $D(13.5\text{Nm}, 2s, x)$.

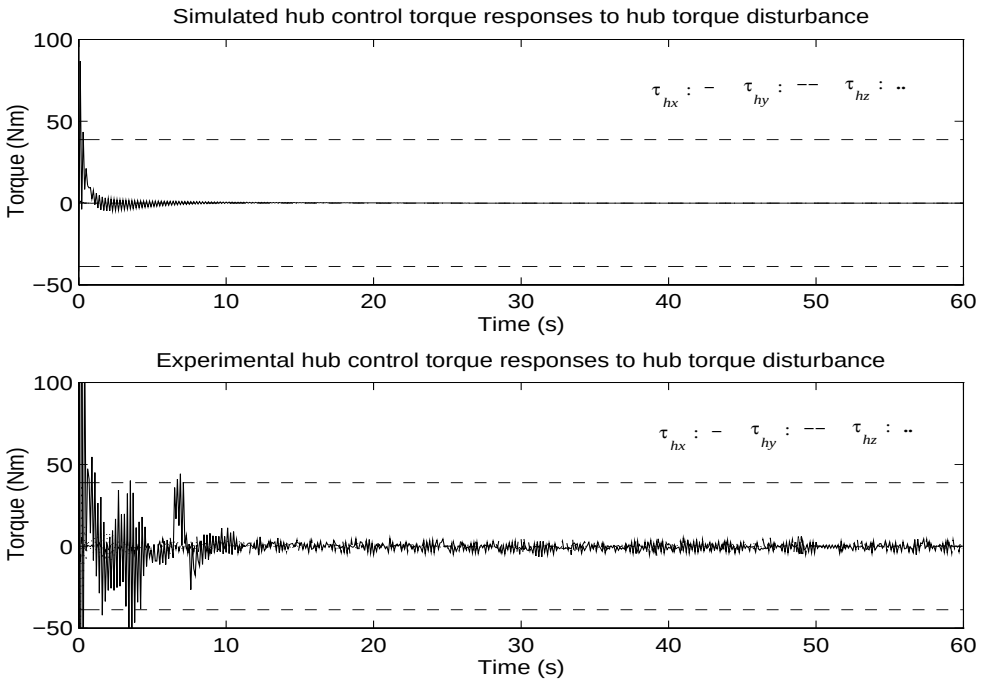

Figure 5.13: Sim. and exp. computed hub control torques for $\boldsymbol{K}_{p1d}$, $D(13.5\text{Nm}, 2s, x)$.

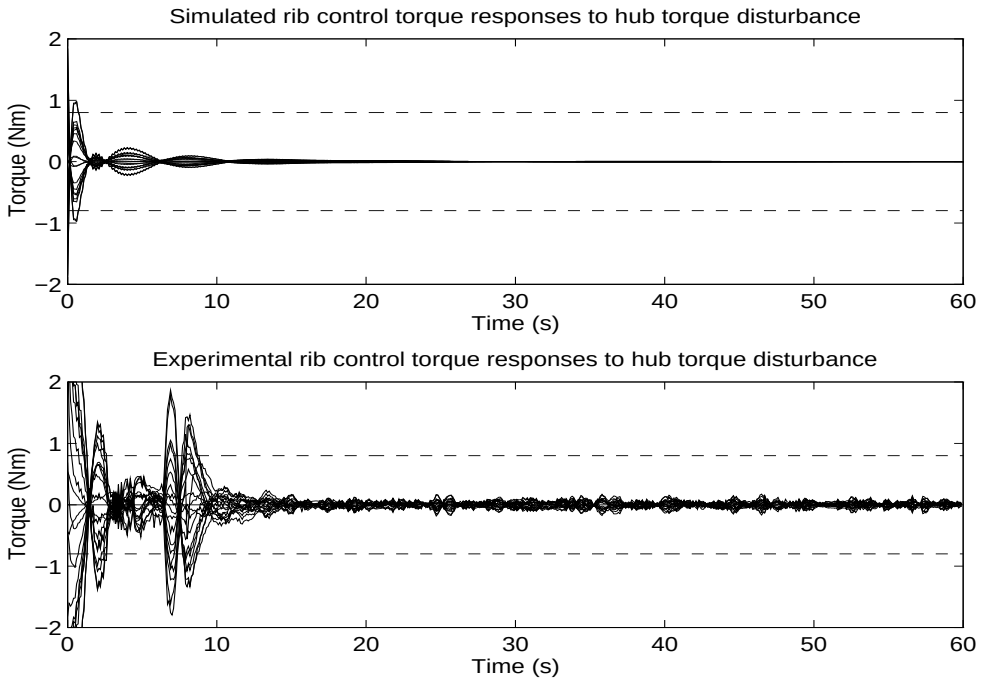

Figure 5.14: Sim. and exp. computed rib control torques for $\boldsymbol{K}_{p1d}$, $D(13.5\text{Nm}, 2s, x)$.

previously given for the x-axis disturbance still applies here. On the other hand, the actual rib responses are quite consistent with the simulated ones, showing actual performance very close to the nominal for $D(13.5\text{Nm}, 2s, y)$. This is in spite of rib torque saturation which occurred for the first two seconds.

For the z-axis disturbance control experiment, the hub and rib angle responses are shown in Figures 5.19 and 5.20, and the hub and rib torques are plotted in Figures 5.21 and 5.22. The experimental and simulated hub angle responses have similar settling times, but the experimental transient is almost twice as large as the simulated one. The rib responses are fairly consistent, and the experimental rib torques are only slightly more oscillatory than in simulation.

In conclusion, the experimental data show that the $\mathcal{H}_\infty$ controller $\boldsymbol{K}_{p1d}$ designed using the coprime factorization method performed quite well except perhaps for the x-axis torque disturbance. No experimental tuning of the controller was necessary, which shows evidence of robustness of the design.

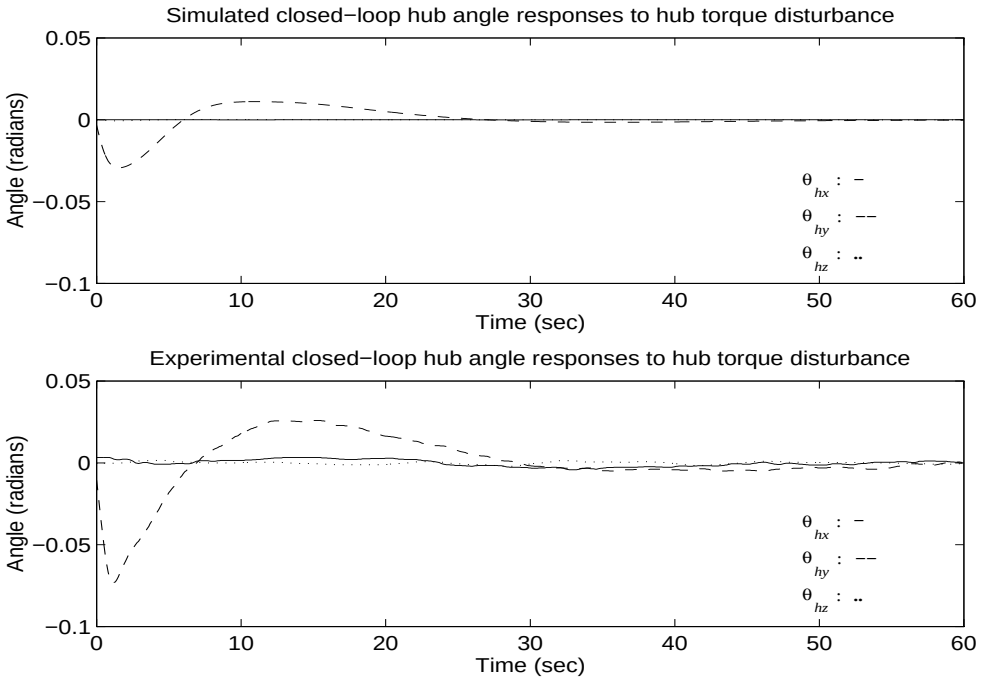

Figure 5.15: Sim. and exp. closed-loop hub angle responses with $\boldsymbol{K}_{p1d}$, $D(13.5\text{Nm}, 2s, y)$.

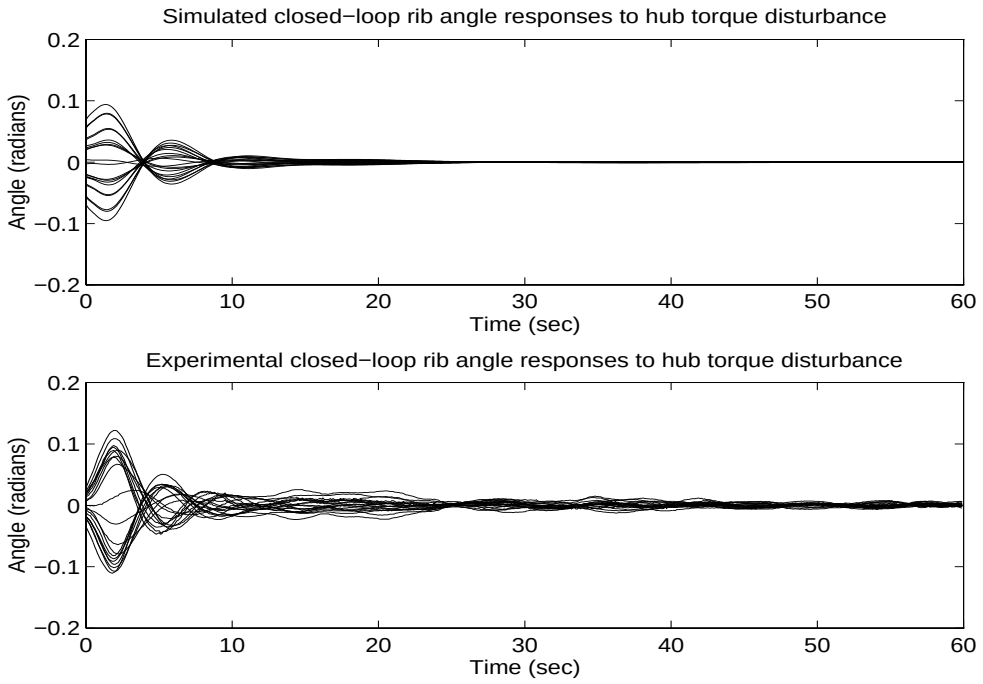

Figure 5.16: Sim. and exp. closed-loop rib angle responses with $\boldsymbol{K}_{p1d}$, $D(13.5\text{Nm}, 2s, y)$.

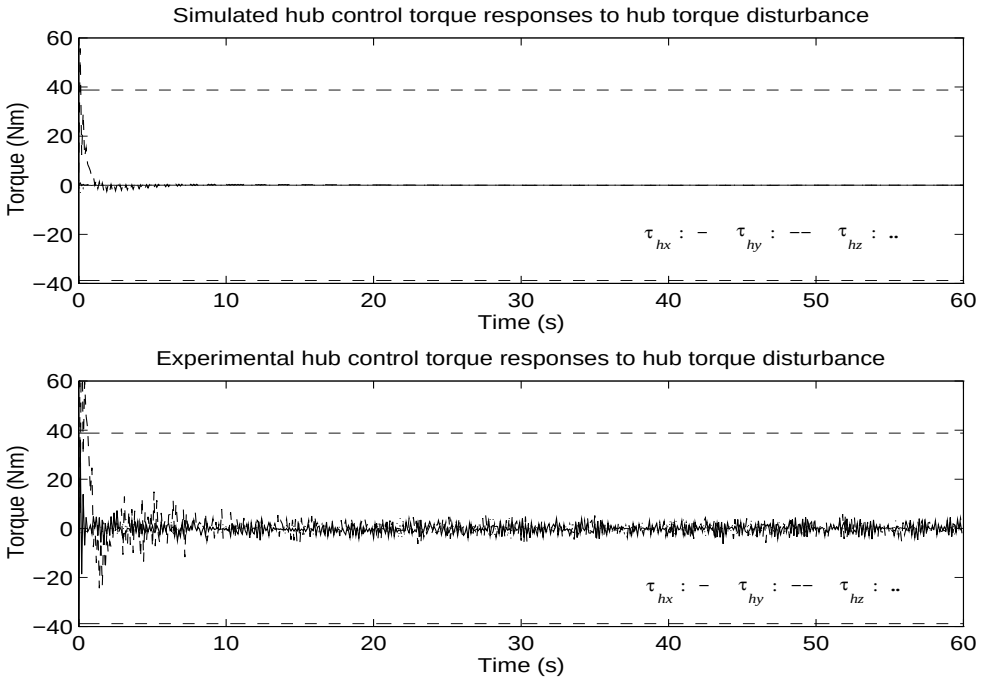

Figure 5.17: Sim. and exp. computed hub control torques for $\boldsymbol{K}_{p1d}$, $D(13.5\text{Nm}, 2s, y)$.

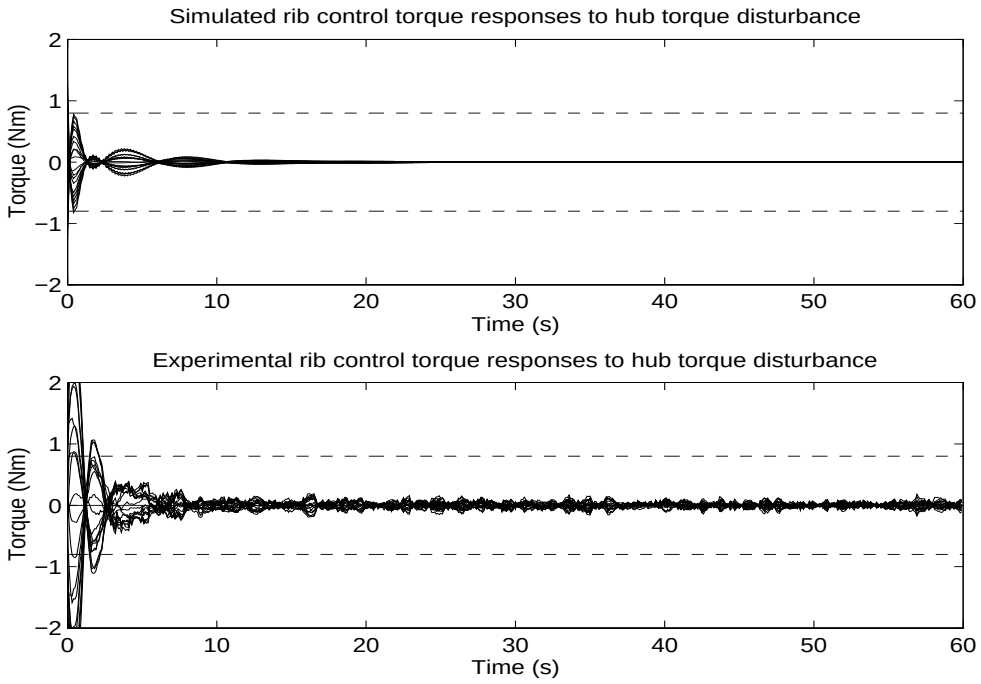

Figure 5.18: Sim. and exp. computed rib control torques for $\boldsymbol{K}_{p1d}$, $D(13.5\text{Nm}, 2s, y)$.

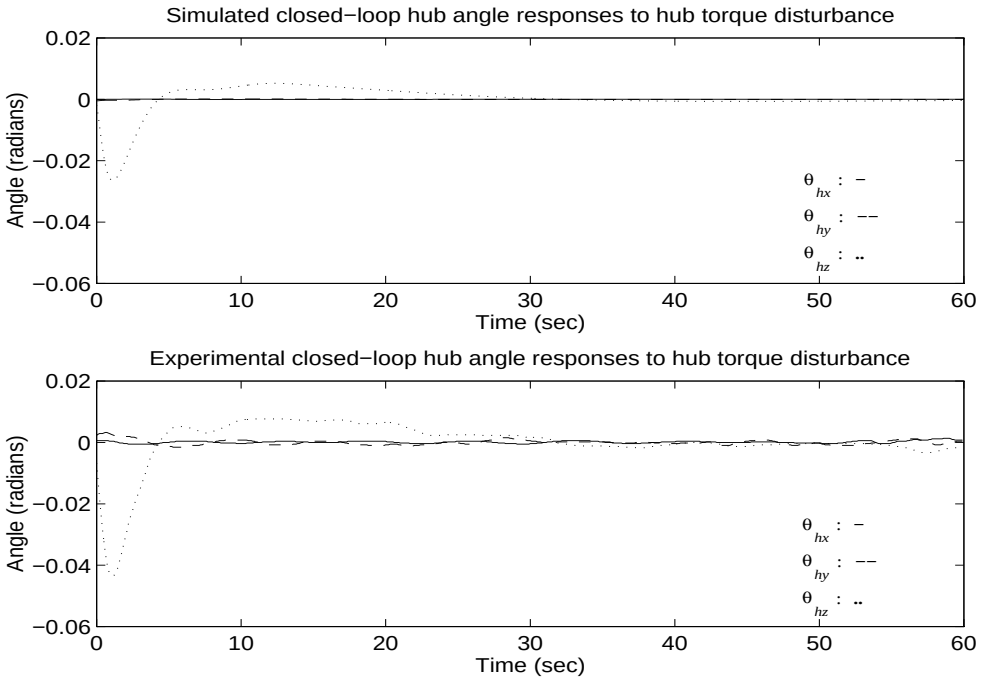

Figure 5.19: Sim. and exp. closed-loop hub angle responses with $\boldsymbol{K}_{p1d}$, $D(13.5\text{Nm}, 2s, z)$.

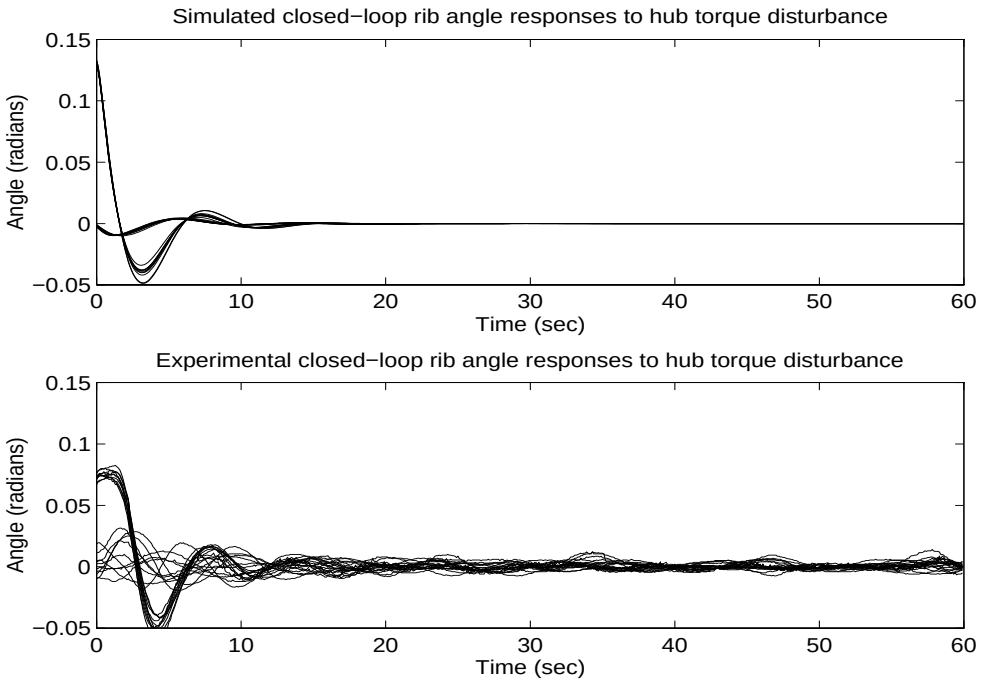

Figure 5.20: Sim. and exp. closed-loop rib angle responses with $\boldsymbol{K}_{p1d}$, $D(13.5\text{Nm}, 2s, z)$.

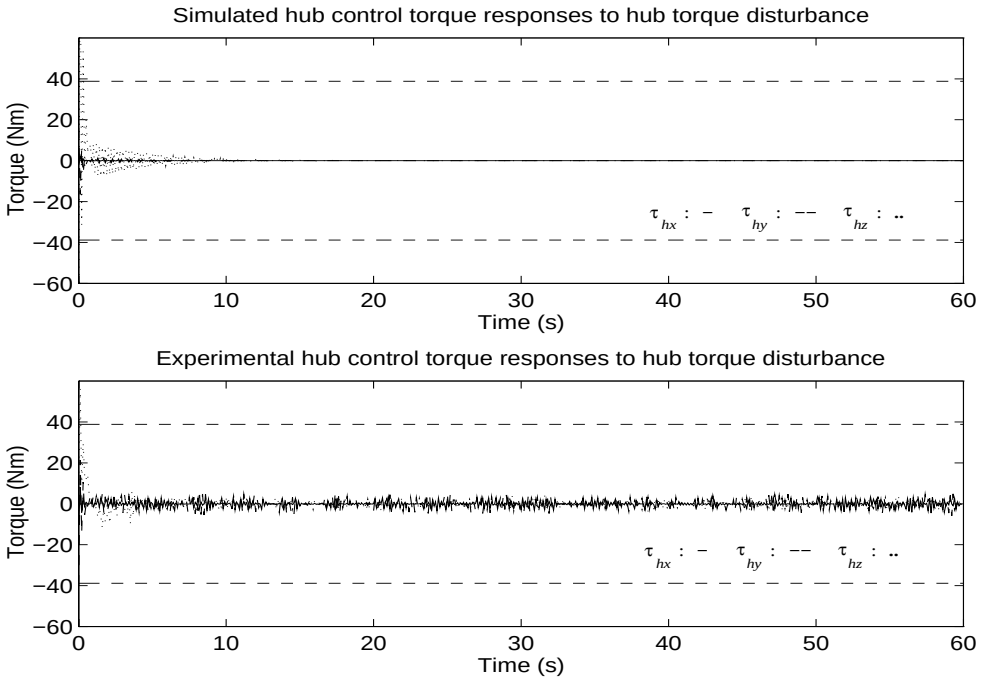

Figure 5.21: Sim. and exp. computed hub control torques for $\boldsymbol{K}_{p1d}$, $D(13.5\text{Nm}, 2s, z)$.

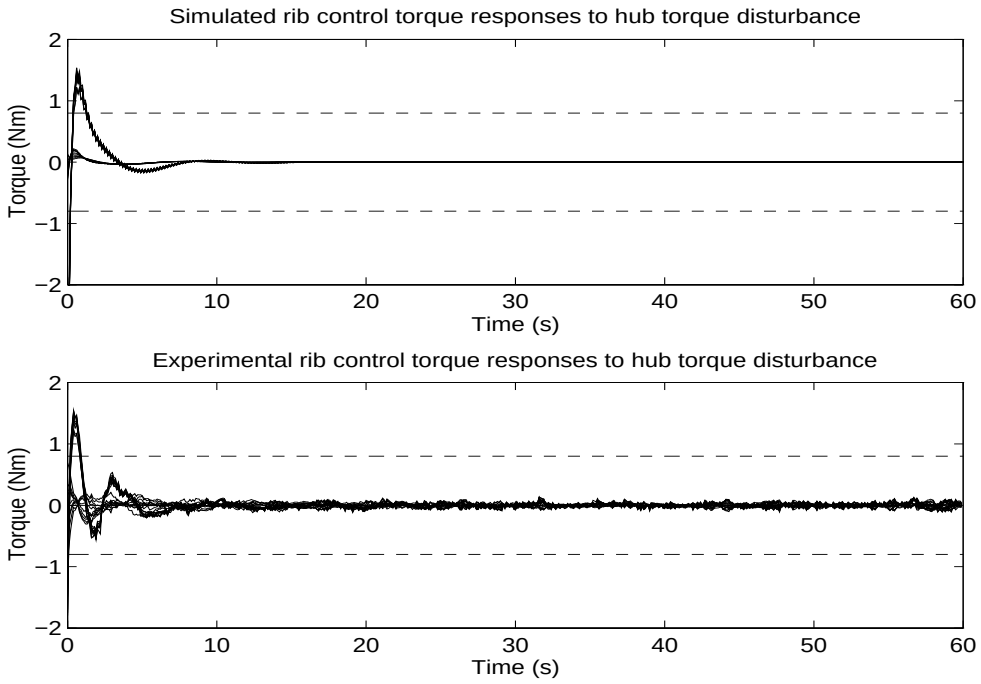

Figure 5.22: Sim. and exp. computed rib control torques for $\boldsymbol{K}_{p1d}$, $D(13.5\text{Nm}, 2s, z)$.

5.1.1.2 Noncollocated Case

Daisy's actuators and sensors can be combined in many different ways, allowing the study of noncollocated control of LFSS. But given that the modes are very close to one another, one has to make a choice of subsets of actuators and sensors based on desired performance and known uncertainty levels. This is due to the observation that even though the nominal noncollocated plant state-space model may be controllable and observable, it may happen that given the bounds on the modal parameter perturbations, some plant models within the corresponding perturbed family of plants lose either controllability or observability of some modes, or both. This means that it may be very difficult in a design to achieve any desired performance level while maintaining robust stability in the face of a reasonable amount of uncertainty. Furthermore, noncollocation may introduce zeros in $\overline{\mathbb{C}}_+$ in the nominal plant model. Finally, nonlinearities and other unmodeled characteristics in Daisy such as centripetal forces, jet thruster deadband and saturation, friction, quantized thruster torques, nonlinear spring stiffness, sampling and computational delays may have greatly amplified effects in such noncollocated configurations.

Thus Daisy can be configured in ways that make the robust control problem extremely difficult if one is to design a finite-dimensional linear time-invariant controller. As an illustration of this, we designed a few controllers based on noncollocated configurations in which some bidirectional out-of-cone jet thrusters were left unused. The designs did not tolerate much uncertainty although nominal performance was acceptable. It turned out that all implementations of these controllers destabilized Daisy. An explanation is that those ribs having only the in-cone thrusters (or none) move around a mechanical singularity which lies right at the rest position. If we see the springs (Figure 5.4) as linear actuators acting along the in-cone thrusters, for small deviations we can see that the out-of-cone direction is nearly singular with respect to the actuators, i.e., very large actuator forces in the in-cone direction translate into very small forces along the out-of-cone direction. This fact added to significant model uncertainty, nonlinearities and imperfections in Daisy have probably caused the system to go unstable.

We chose to use all 23 angle measurements (DEOPS) but only 17 thrusters and the three hub reaction wheels. The three rib actuators not employed are the in-cone jet thrusters of ribs 2, 5 and 7. Past experiments with noncollocated controller designs based on the modal parameters of Table 5.1 always destabilized the closed loop, so it was deemed appropriate to

improve the nominal model using open-loop data in order to reduce the uncertainty in the modal parameters. This exercise resulted in a new set of modal gains and frequencies with associated rough estimates of uncertainties that are displayed in Table 5.2. Notice that the uncertainties are still significant, especially for the damping ratios.

The B_1 matrix of equation (2.3) for this model is a slightly modified version of the one for the previous model with its 7^{th}, 13^{th} and 17^{th} columns removed. It is assumed to have up to 5% uncertainty in its entries. The output matrix $C_1 = E$ is the same as in the previous model. A controllability/observability analysis of all the modes was carried out as explained earlier for the collocated model, and again it was found that they are all almost equally significant and should be kept in the noncollocated nominal design model. There are no transmission zeros in $\overline{\mathbb{C}}_+$ in the nominal plant model.

It is desired to control the noncollocated model so that it remains stable for all bounded perturbations of the modal parameters in Table 5.2 and all perturbations of the entries of B_1 within 5% of their nominal values. We also want good torque/force disturbance rejection in the sense of (5.3) but a few iterations of the design suggested that we have to relax the tracking requirement (5.4) in order to achieve robust stability and (5.3). Hence we will focus only on the disturbance rejection specification. Also, it was found that the uncertainties in the model had to be assumed somewhat smaller than given in Table 5.2 to guarantee closed-loop internal stability, namely 4% in the entries of B_1, 3% in the modal frequencies and 20% in the damping ratios.

Remark 5.3 Note that this does not mean that instability will automatically result if some of the actual modal parameters lie outside those ranges. Indeed inequality (5.2) is only sufficient, and furthermore there is some conservativeness in the choice of $\boldsymbol{r}$ given by Proposition 2. As an illustration of this, the refined model of Table 5.2 shows that all perturbed values for the frequency of mode 16 do not lie in the range of perturbed values in the original model of Table 5.1. Yet a good controller was designed based on the original model and tested successfully on Daisy.

The diagonal scaling matrices J_1 and J_2 are computed as explained in Section 2.3. The generalized plant for the robust $\mathcal{H}_\infty$ design is built according to Figure 5.2, and the different constants and weighting functions are

mode i	frequency ω_i (rad/s)	damping ratio ζ_i
1 (rigid)	0	0
2 (rigid)	$0.31 \pm 5\%$	$0.11 \pm 50\%$
3 (rigid)	$0.31 \pm 5\%$	$0.09 \pm 50\%$
4 (flex.)	$0.60 \pm 5\%$	$0.025 \pm 50\%$
5 (flex.)	$0.59 \pm 5\%$	$0.02 \pm 50\%$
6 (flex.)	$0.59 \pm 5\%$	$0.03 \pm 50\%$
7 (flex.)	$0.59 \pm 5\%$	$0.02 \pm 50\%$
8 (flex.)	$0.62 \pm 5\%$	$0.035 \pm 50\%$
9 (flex.)	$0.61 \pm 5\%$	$0.025 \pm 50\%$
10 (flex.)	$0.70 \pm 5\%$	$0.02 \pm 50\%$
11 (flex.)	$0.76 \pm 5\%$	$0.02 \pm 50\%$
12 (flex.)	$0.61 \pm 5\%$	$0.06 \pm 50\%$
13 (flex.)	$0.60 \pm 5\%$	$0.06 \pm 50\%$
14 (flex.)	$0.78 \pm 5\%$	$0.015 \pm 50\%$
15 (flex.)	$0.77 \pm 5\%$	$0.015 \pm 50\%$
16 (flex.)	$0.79 \pm 5\%$	$0.02 \pm 50\%$
17 (flex.)	$0.70 \pm 5\%$	$0.02 \pm 50\%$
18 (flex.)	$0.59 \pm 5\%$	$0.027 \pm 50\%$
19 (flex.)	$0.63 \pm 5\%$	$0.025 \pm 50\%$
20 (flex.)	$0.61 \pm 5\%$	$0.02 \pm 50\%$
21 (flex.)	$0.75 \pm 5\%$	$0.04 \pm 50\%$
22 (flex.)	$0.75 \pm 5\%$	$0.05 \pm 50\%$
23 (flex.)	$0.79 \pm 5\%$	$0.015 \pm 50\%$

Table 5.2: Modal parameters of Daisy's refined model.

$$d_{max} = 0.038, \qquad c_{max} = 0.018, \qquad k = \frac{c_{max}}{d_{max}} = 0.47, \qquad \gamma = 0.37, \qquad q = 400,$$

$$\boldsymbol{w}(s) = \frac{50}{s^2/(0.01)^2 + 2 \times 0.7s/0.01 + 1}, \tag{5.9}$$

$$\boldsymbol{r}(s) = \frac{0.001s + 1.415}{2.1s + 1}. \tag{5.10}$$

Note that $q = 4 \times 10^4$ when computed using the formula in Proposition 7, but this value was much too large to get the ∞-norm of $w \mapsto z$ down to less than 1. So q was reduced to 400, a satisfactory value obtained after a few iterations of the design procedure.

The $\mathcal{H}_\infty$ design was again carried out in Matlab^{TM} using the μ-Tools [2] command *hinfsyn*. The generalized design plant $\boldsymbol{P}$ is given by (5.1). We used the decentralized fixed-mode method [11] to obtain a minimal realization of $\boldsymbol{P}$, reducing it from 138 to 75 state variables. A stable suboptimal controller achieving $\|w \mapsto z\|_\infty = 0.62$ was obtained. Its order was the same as the order of the minimal realization of the generalized plant, i.e. 75, but a balanced truncation reduced it to the 49^{th} order controller $\boldsymbol{K}_2$ without noticeably affecting the closed-loop ∞-norm.

With this reduced controller $\boldsymbol{K}_2$, Figure 5.23 shows that robust stability was achieved, while Figure 5.24 shows that required performance has been attained, i.e., $\|\boldsymbol{S}_{dh}(j\omega)\|$ is less than $|\boldsymbol{w}^{-1}(j\omega)|$ as desired, although $\|\boldsymbol{S}_{rh}(j\omega)\|$ is not as nice as in the previous collocated design. The least-damped closed-loop mode has a damping ratio of 0.18.

The 49^{th}-order controller $\boldsymbol{K}_2$ was rescaled to $\boldsymbol{K}_{p2} = \frac{d_{max}}{\gamma} J_2^{-1} \boldsymbol{K}_2$. Then $\boldsymbol{K}_{p2}$ was discretized at a sampling rate of 10 Hz using the bilinear transformation; call the resulting controller $\boldsymbol{K}_{p2d}$. Figure 5.25 shows the frequency responses of two entries of $\boldsymbol{K}_{p2}$ and $\boldsymbol{K}_{p2d}$.

The first closed-loop experiment with $\boldsymbol{K}_{p2d}$ is the response to an x-axis hub torque disturbance $D(13.5\text{Nm}, 2s, x)$. The simulated and actual hub angles are shown in Figure 5.26 while Figure 5.27 shows the simulated and actual rib angles. The experimental response of θ_{hx} has a transient about twice as large as in the simulation but the settling times are comparable. However, the experimental rib responses look quite different from the simulated ones. Most noticeable are oscillations of the unactuated ribs in the in-cone direction which die out very slowly. The experimental transients are also larger.

The simulated and experimental computed control torques are shown in Figure 5.28 for the hub and in Figure 5.29 for the ribs. The experimental rib torques saturated for the first two seconds but this might not explain the discrepancy between the experimental and simulated

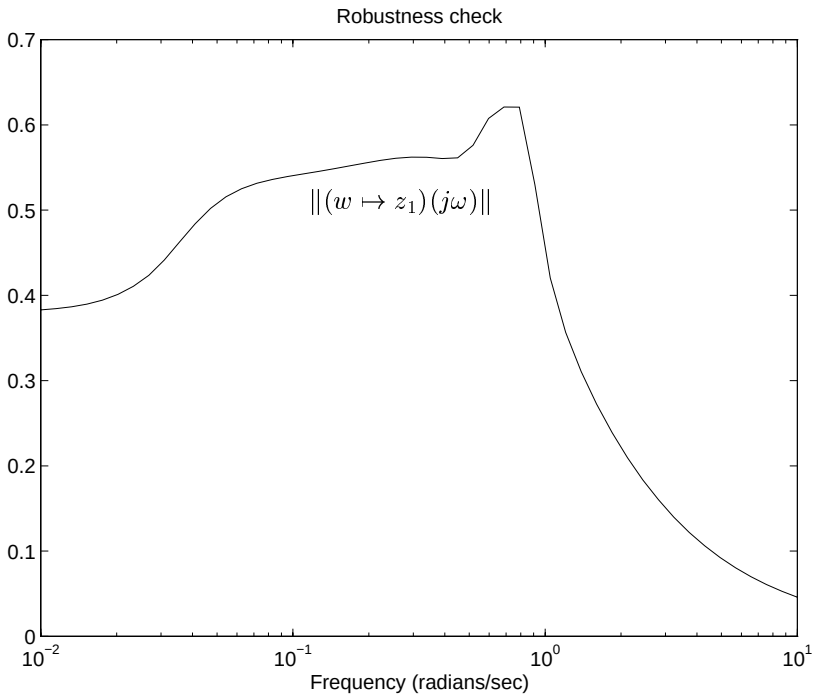

Figure 5.23: Robustness Check: Norm of $w \mapsto z_1$ with $\boldsymbol{K}_2$.

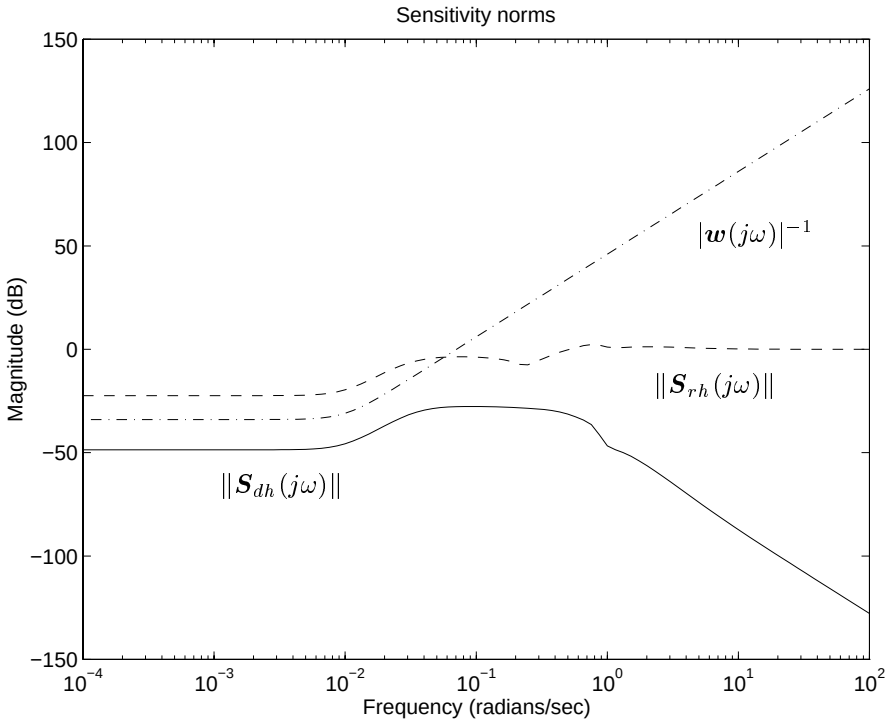

Figure 5.24: Norms of $\boldsymbol{S}_{dh}(j\omega)$ and $\boldsymbol{S}_{rh}(j\omega)$ with $\boldsymbol{K}_2$.

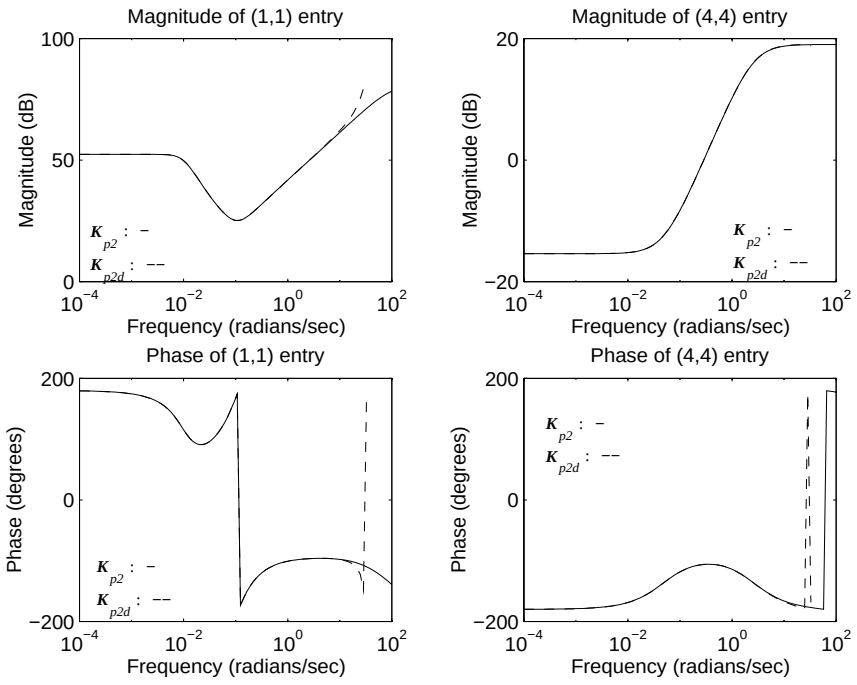

Figure 5.25: Frequency responses of the (1,1) and (4,4) entries of $\boldsymbol{K}_{p2}$ and $\boldsymbol{K}_{p2d}$.

torques. It is more likely that the plant nonlinearities are not well modeled by the family of coprime factorizations. The nonlinearities seem to play a more significant role in this noncollocated configuration because some of the ribs do not have local feedback to reduce their effects. For instance, thruster deadbands and spring nonlinearities appeared to have caused instability in the next two sets of experiments.

The results of two similar control experiments with $\boldsymbol{K}_{p2d}$ and torque disturbances $D(13.5\text{Nm}, 2s, y)$ and $D(6.8\text{Nm}, 2s, z)$ are now discussed. Figures 5.30 and 5.31 show respectively the hub and rib angle responses for the y-axis disturbance, while the hub control torques are plotted in Figure 5.32 and the rib control torques are in Figure 5.33. The experimental hub angle responses are more oscillatory than the simulated ones, but the transients and settling times are comparable. The actual rib responses show somewhat smaller transients than the ones in the x-axis disturbance experiment, but they still look different from the simulated ones. One of the ribs unactuated along the in-cone direction entered a small limit cycle involving only its out-of-cone thruster and in-cone motion. None of the other thrusters was active at that time. It is believed that the thruster deadband, coupling spring nonlinearities and thruster misalignment caused the occurrence of the limit cycle. Note that thruster misalignment is taken

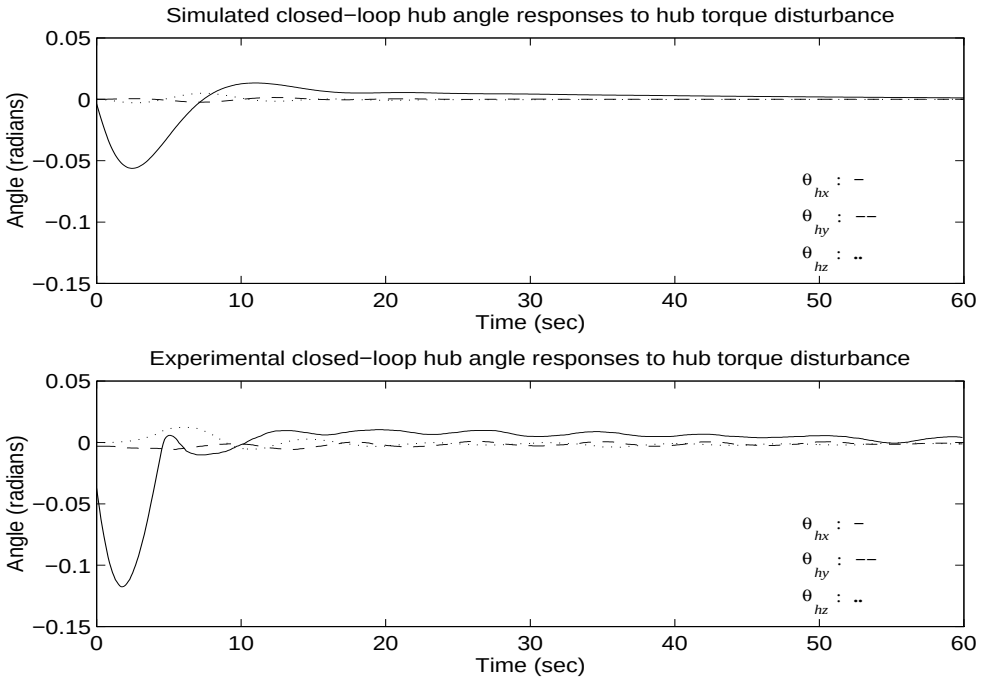

Figure 5.26: Sim. and exp. closed-loop hub angle responses with $\boldsymbol{K}_{p2d}$, $D(13.5\text{Nm}, 2s, x)$.

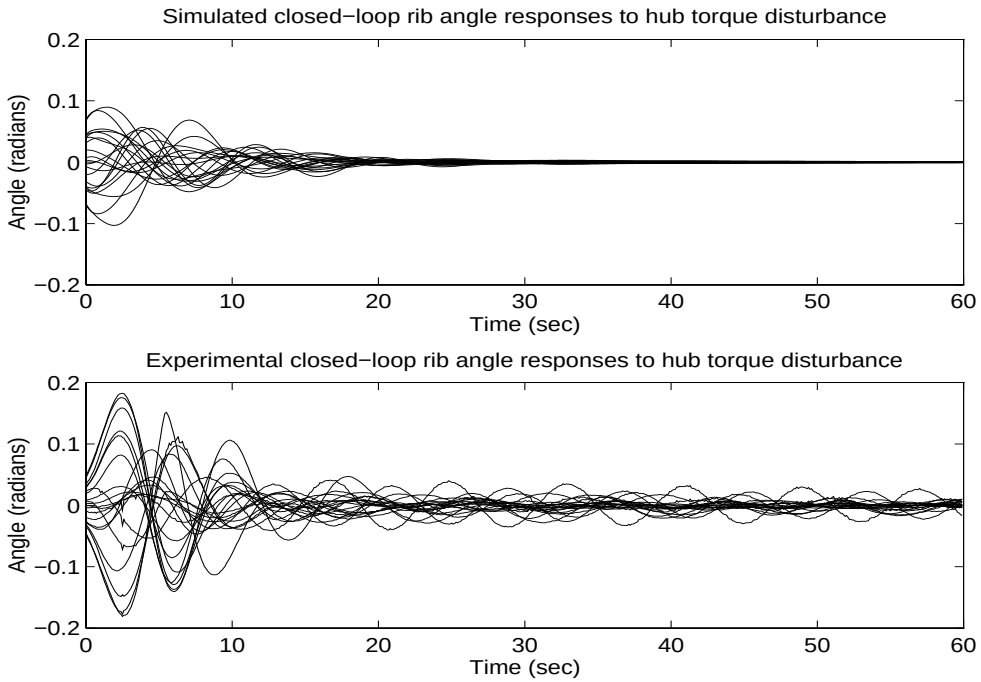

Figure 5.27: Sim. and exp. closed-loop rib angle responses with $\boldsymbol{K}_{p2d}$, $D(13.5\text{Nm}, 2s, x)$.

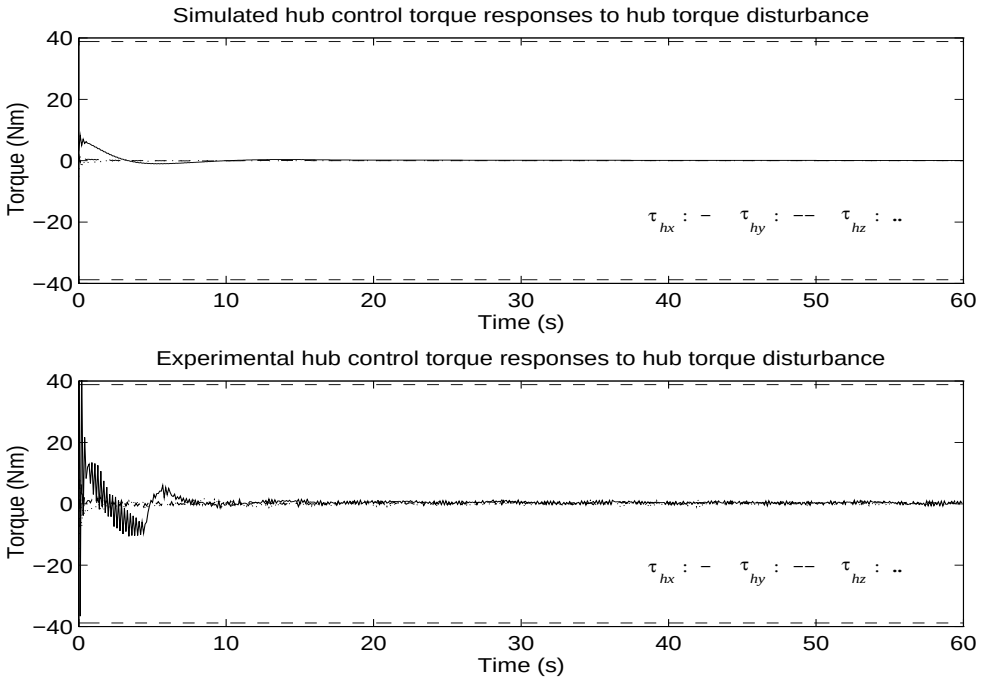

Figure 5.28: Sim. and exp. computed hub control torques for $\boldsymbol{K}_{p2d}$, $D(13.5\text{Nm}, 2s, x)$.

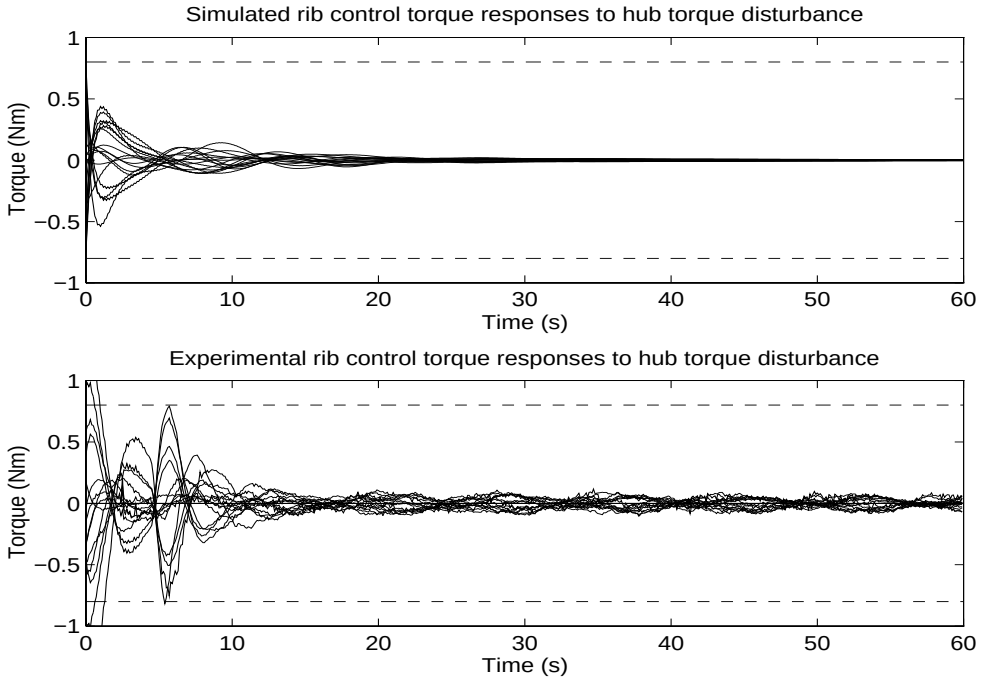

Figure 5.29: Sim. and exp. computed rib control torques for $\boldsymbol{K}_{p2d}$, $D(13.5\text{Nm}, 2s, x)$.

into account as uncertainty in B_1, but not the mentioned nonlinearities. Also note that the rib control torques in Figure 5.33 did not saturate the jet thrusters in this experiment.

For the z-axis disturbance control experiment, the hub and rib angle responses are shown in Figures 5.34 and 5.35, and the hub and rib torques are plotted in Figures 5.36 and 5.37. This last experiment showed that the response to a z-axis torque disturbance is clearly unstable. After noticing this instability for $D(13.5\text{Nm}, 2s, z)$, a smaller torque disturbance $D(6.8\text{Nm}, 2s, z)$ was tried in the hope that nonlinearities would then have a smaller effect. It also led to instability as shown in the figures. The unstable closed-loop mode involved θ_{hx} and θ_{hz} and all the ribs. Interestingly, the hub torques were nearly zero after the first few seconds, but the jet thrusters remained active, pumping energy into Daisy and driving it unstable.

In conclusion, the noncollocated $\mathcal{H}_\infty$ controller $\boldsymbol{K}_{p2d}$ designed using the coprime factorization method stabilized Daisy for the x-axis torque disturbance, but induced a limit cycle for the y-axis disturbance and unequivocally destabilized Daisy for the z-axis disturbance. Those input-dependent stability results hint at what could be significant nonlinear effects for this noncollocated configuration. The linear simulations showed very good nominal performance while the design itself indicated robustness to reasonably large deviations in the modal parameters. Further work on modeling, identification and stability analysis with nonlinearities is needed.

5.2 Summary and Discussion

In this chapter, we have presented an $\mathcal{H}_\infty$ control design technique providing robust stability and nominal performance for LFSS. A compromise $\mathcal{H}_\infty$ problem was formulated and its solution was shown to solve the robust stability and nominal performance problem. The robust performance problem was also discussed and will be solved in Chapter 6. The family of perturbed factorizations of LFSS of Chapter 2 was used to construct a generalized plant whose ∞-norm has to be reduced to a value less than one by a stabilizing feedback controller. This is the compromise $\mathcal{H}_\infty$ problem mentioned above. Note that prior to the design step, the uncertainty bound $\boldsymbol{r}$ in the generalized plant can be improved upon the one given in Proposition 2 by using experimental frequency-response data and the results of Chapters 3 and 4.

Then an LFSS experimental testbed called Daisy and its model were described. Two $\mathcal{H}_\infty$ controllers were designed for collocated and noncollocated configurations of Daisy. These models have significant parameter uncertainty, yet the controllers designed using the coprime factor-

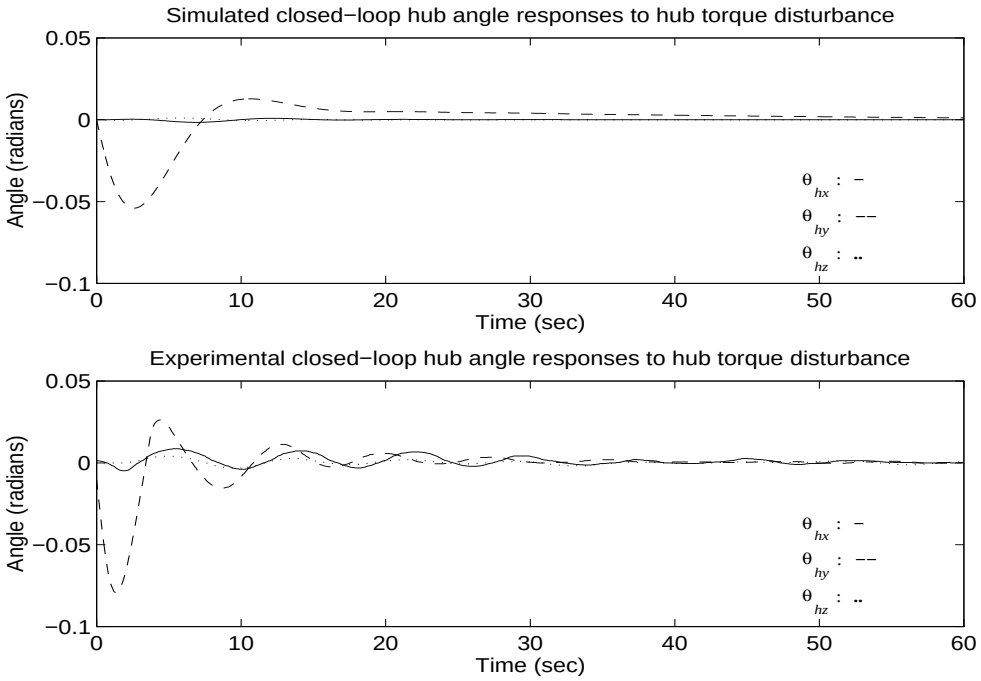

Figure 5.30: Sim. and exp. closed-loop hub angle responses with $\boldsymbol{K}_{p2d}$, $D(13.5\text{Nm}, 2s, y)$.

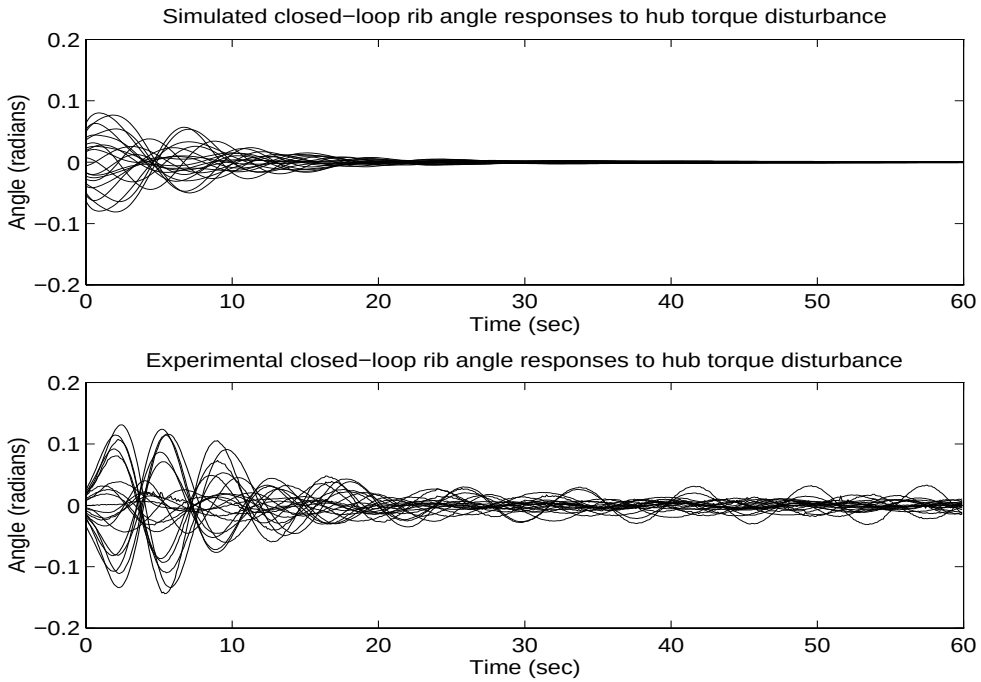

Figure 5.31: Sim. and exp. closed-loop rib angle responses with $\boldsymbol{K}_{p2d}$, $D(13.5\text{Nm}, 2s, y)$.

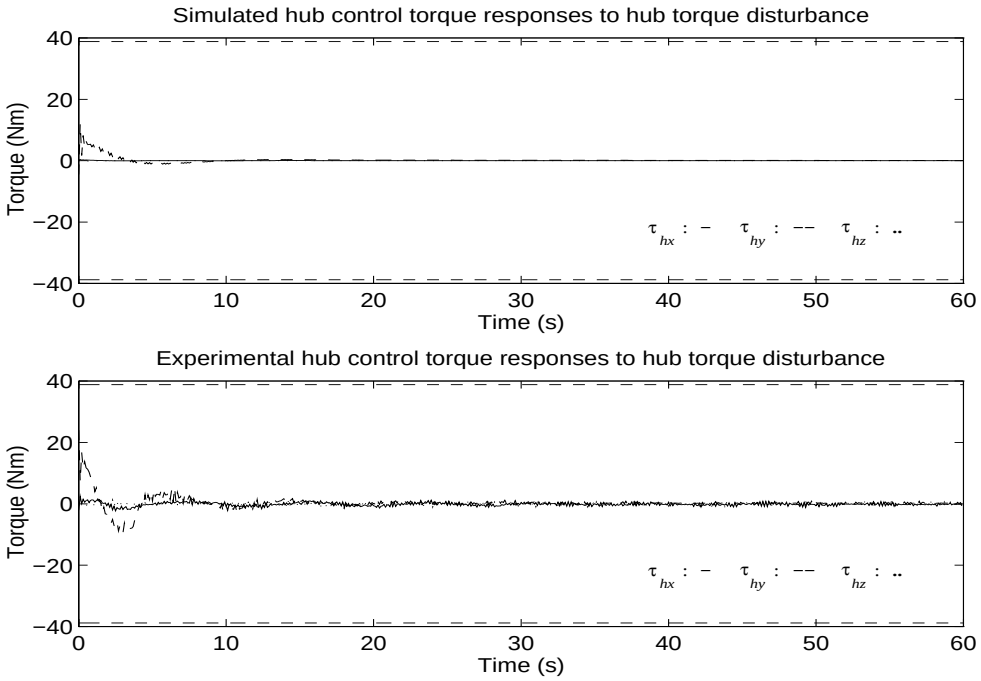

Figure 5.32: Sim. and exp. computed hub control torques for $\boldsymbol{K}_{p2d}$, $D(13.5\text{Nm}, 2s, y)$.

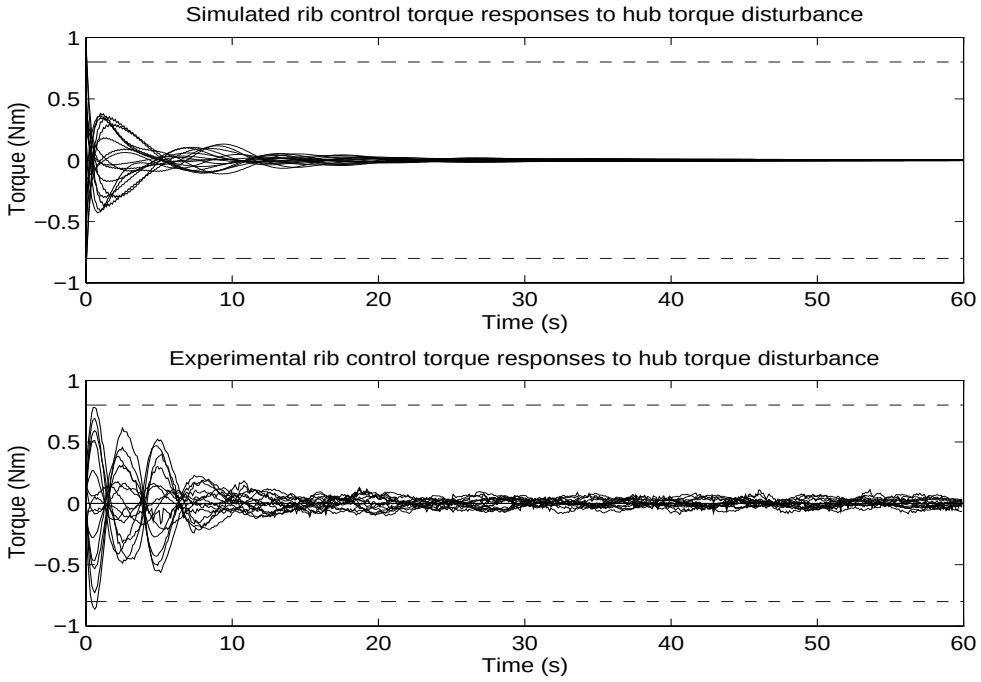

Figure 5.33: Sim. and exp. computed rib control torques for $\boldsymbol{K}_{p2d}$, $D(13.5\text{Nm}, 2s, y)$.

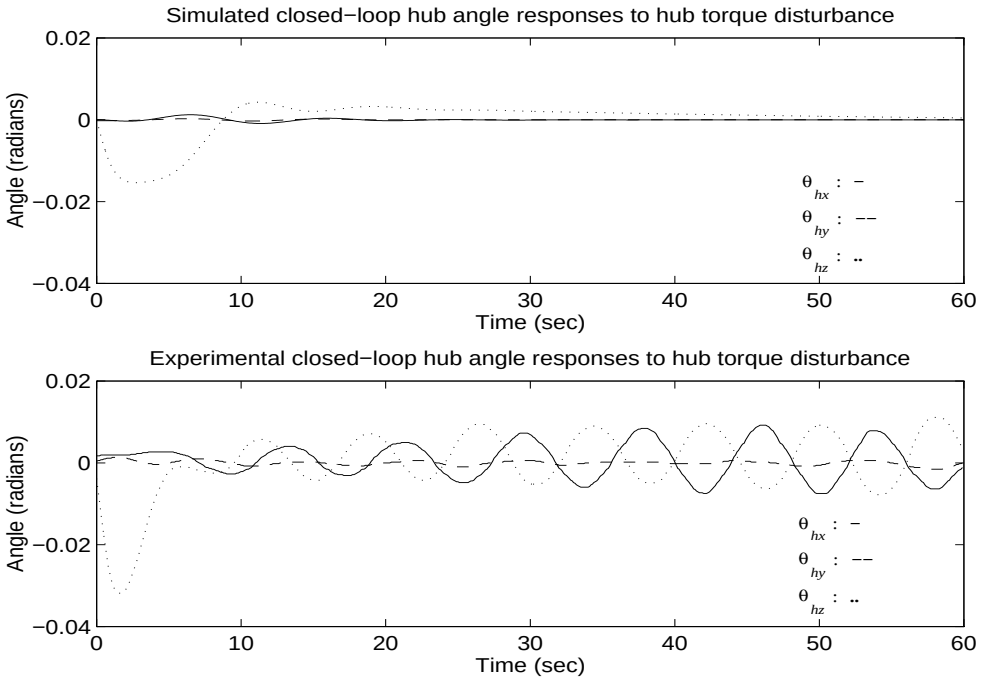

Figure 5.34: Sim. and exp. closed-loop hub angle responses with $\boldsymbol{K}_{p2d}$, $D(6.8\text{Nm}, 2s, z)$.

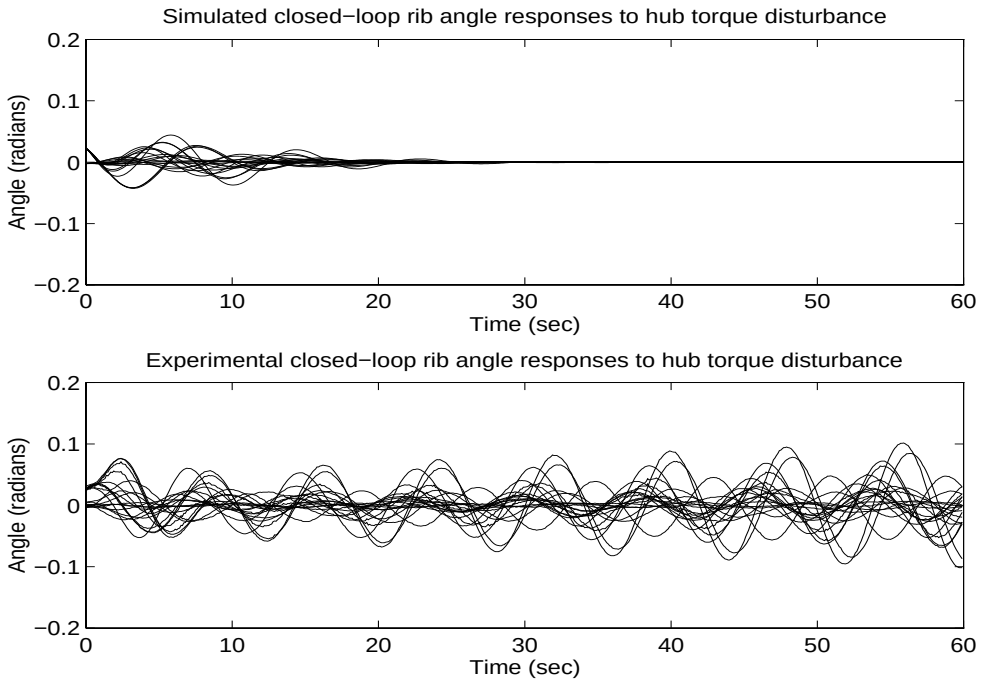

Figure 5.35: Sim. and exp. closed-loop rib angle responses with $\boldsymbol{K}_{p2d}$, $D(6.8\text{Nm}, 2s, z)$.

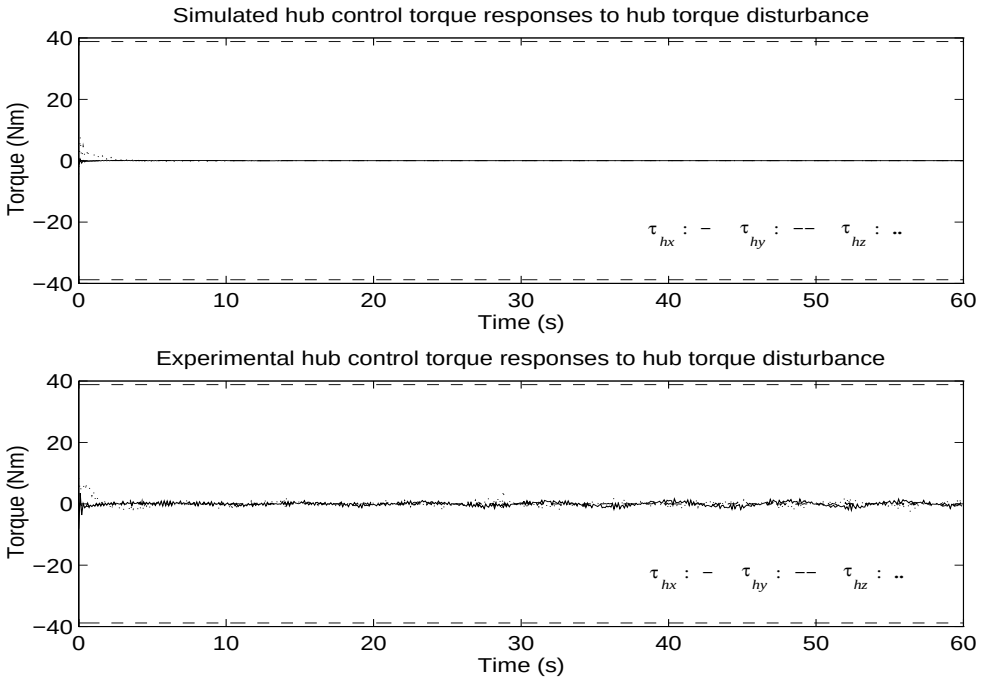

Figure 5.36: Sim. and exp. computed hub control torques for $\boldsymbol{K}_{p2d}$, $D(6.8\text{Nm}, 2s, z)$.

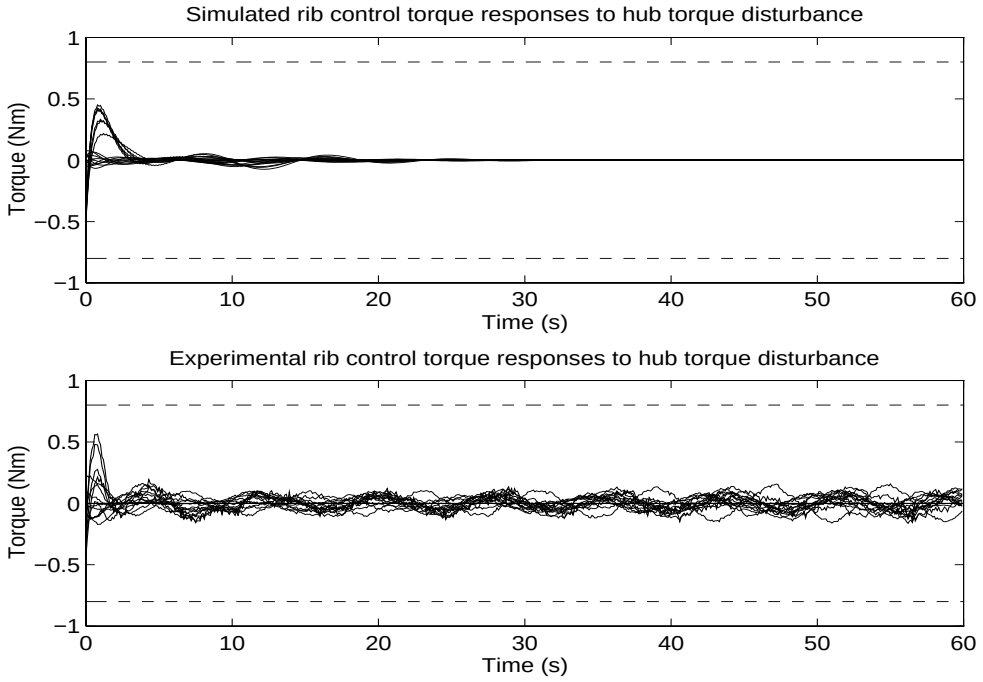

Figure 5.37: Sim. and exp. computed rib control torques for $\boldsymbol{K}_{p2d}$, $D(6.8\text{Nm}, 2s, z)$.

ization technique were quite robust and achieved good performance levels in terms of rejection of hub torque disturbances. Furthermore, both controllers were stable, which is a desirable property. Extensive experimentations showed that the digital implementation of the collocated $\mathcal{H}_\infty$ controller performed very well without the need of any experimental tuning. A digital implementation of the noncollocated $\mathcal{H}_\infty$ controller was less successful at stabilizing Daisy even though the linear simulations showed good performance and robustness levels.

Chapter 6

μ-Synthesis for LFSS Using an LCF Model

In this chapter, we propose a μ-synthesis design approach for robust performance based on the perturbed left-coprime factor model for LFSS introduced in Chapter 2. Our general performance objectives will be attitude regulation and vibration attenuation when the LFSS is subjected to external torque disturbances.

The structured singular value is introduced and a brief account of μ-analysis and synthesis techniques for robust closed-loop stability and performance is given. Two controllers achieving robust performance are designed for collocated and noncollocated configurations of Daisy, and their experimental performance is analyzed.

6.1 μ-Synthesis for Robust Performance

The setup for this problem is illustrated in Figure 6.1. It is basically the same setup as the one in Figure 5.1 for the $\mathcal{H}_\infty$ problem of Section 5.1, except that the torque disturbance channel is included in the design, and $q = 1$ in $\boldsymbol{W}_q$. Thus the disturbance rejection performance requirement is explicitly introduced in the design by the mapping $d \mapsto z_2$ whose ∞-norm is to be reduced to a value no greater than one. More specifically, just as in Section 5.1, we want to shape the closed-loop sensitivity $\boldsymbol{S}_{dh} := d \mapsto y_h$, that is, we want to achieve $\|\boldsymbol{S}_{dh}(j\omega)\| \leq |\boldsymbol{w}^{-1}(j\omega)|$, $\forall\omega$. But now we require that this inequality hold (and internal stability too) for all perturbations of the modal parameters and entries of B_1 within their ranges. Thus we require that for every $\tilde{\boldsymbol{\Delta}}_0 \in \mathcal{BRH}_\infty$, the *perturbed* sensitivity matrix

$\boldsymbol{S}_{dhp} := \mathcal{F}_L\left[\mathcal{F}_U(\boldsymbol{P}, \tilde{\boldsymbol{\Delta}}_0), \boldsymbol{K}\right]$, where the LFTs are constructed according to Figure 6.1, has its ∞-norm less than or equal to one. This is a robust performance requirement well-suited for μ-synthesis.

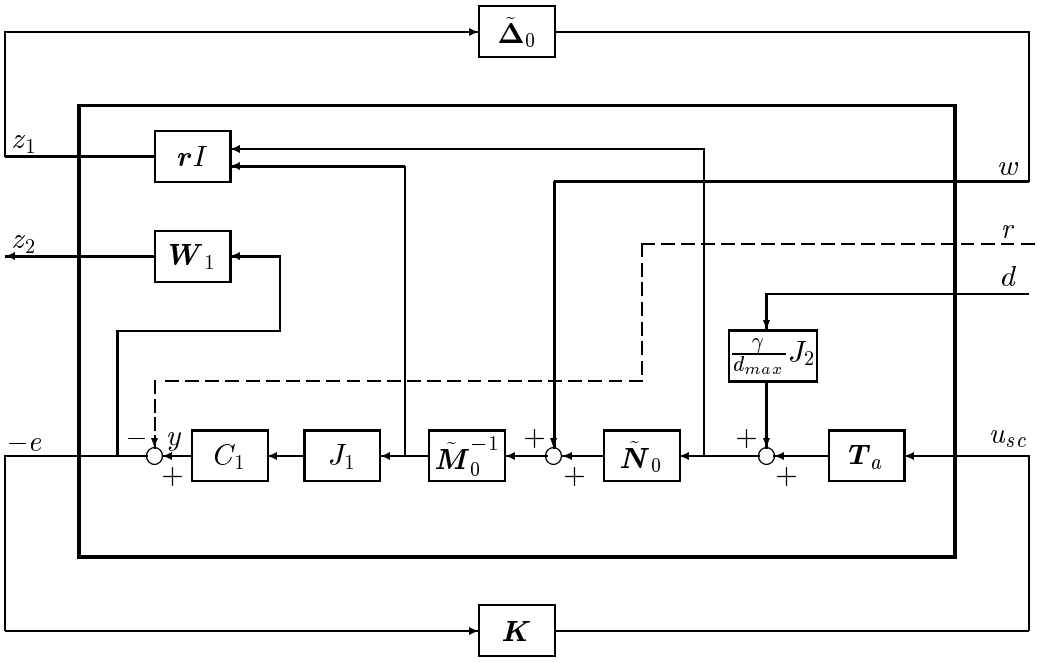

Figure 6.1: Generalized plant with scaled perturbation and controller for μ-synthesis.

For completeness, a brief introduction to the μ-analysis and synthesis technique is given here. For a more detailed introduction to this technique, the reader is referred to [2] and the original paper by Doyle [13]. To keep matters simple, we present the case of structured square perturbations only, although our application involves nonsquare perturbations. The theory covers that case too, and the Matlab^{TM} toolbox μ-Tools [2] can handle it.

Recall that we have already defined μ_Γ in equation (3.28) for a one-full-block, one-scalar-block structured perturbation. Here we redefine μ_Γ for the more general case of a q-scalar-block, l-full-block perturbation, where the scalar blocks may be repeated. Let $M \in \mathbb{C}^{n\times n}$, q and l be two non-negative integers and $r_1, \ldots, r_q$; $m_1, \ldots, m_l$ be positive integers satisfying

$$\sum_{i=1}^{q} r_i + \sum_{j=1}^{l} m_j = n.$$

We define the block structure $\Gamma \subset \mathbb{C}^{n\times n}$ as

$$\Gamma := \left\{ \text{diag}\left[\delta_1 I_{r_1}, \ldots, \delta_q I_{r_q}, \Delta_1, \ldots, \Delta_l\right] : \delta_i \in \mathbb{C}, \Delta_j \in \mathbb{C}^{m_j \times m_j} \right\}.$$

Definition 6.1 For $M \in \mathbb{C}^{n\times n}$, $\mu_\Gamma(M)$ is defined as

$$\mu_\Gamma(M) := \left[\min\left\{\|\Delta_s\| : \Delta_s \in \Gamma, \det(I - M\Delta_s) = 0\right\}\right]^{-1} \tag{6.1}$$

unless no $\Delta_s \in \Gamma$ makes $I - M\Delta_s$ singular, in which case $\mu_\Gamma(M) := 0$.

Suppose $M \in \mathbb{C}^{n\times n}$ and consider the loop shown in Figure 6.2. Here, $\mu_\Gamma(M)$ is the reciprocal

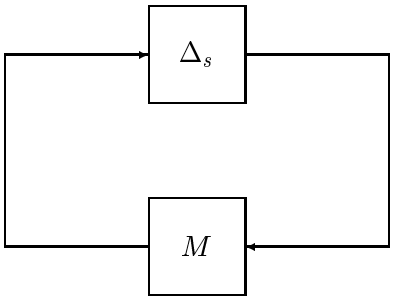

Figure 6.2: Feedback interpretation of $\mu_\Gamma(M)$.

of the norm of the smallest structured perturbation, $\Delta_s \in \Gamma$, that causes "instability" of the feedback loop above, in the sense of singularity of the matrix $I - M\Delta_s$ or well-posedness of the corresponding closed-loop equations.

Now define the set of real-rational, proper, stable structured perturbations:

$$\mathcal{S} := \left\{ \boldsymbol{\Delta}_s \in \mathcal{RH}_\infty \ : \ \boldsymbol{\Delta}_s(s_0) \in \Gamma, \ \forall s_0 \in \overline{\mathbb{C}}_+ \right\}, \tag{6.2}$$

and consider the perturbed feedback loop in Figure 6.3 where $\boldsymbol{\Delta}_s \in \mathcal{S}$. We have the following result, which is the so-called small-μ theorem [2]:

Theorem 14 *Assume* $\boldsymbol{K}$ *is internally stabilizing for the nominal plant* $\boldsymbol{P}$. *Then the closed-loop system in Figure 6.3 is well-posed and internally stable* $\forall \boldsymbol{\Delta}_s \in \mathcal{BS}$ *iff* $\sup_{\omega\in\mathbb{R}} \mu_\Gamma\{\mathcal{F}_L[\boldsymbol{P}(j\omega), \boldsymbol{K}(j\omega)]\} \leq 1$.

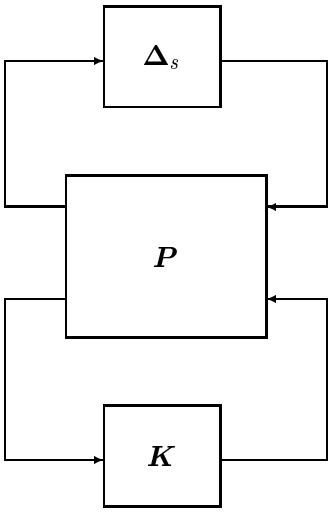

Figure 6.3: Perturbed closed-loop system for μ-analysis of stability.

The following result [2] provides a means to check for robust performance. Consider the perturbed closed-loop system in Figure 6.4 where $z_2(t) \in \mathbb{R}^{n_{z_2}}$ and $d(t) \in \mathbb{R}^{n_d}$, and define the

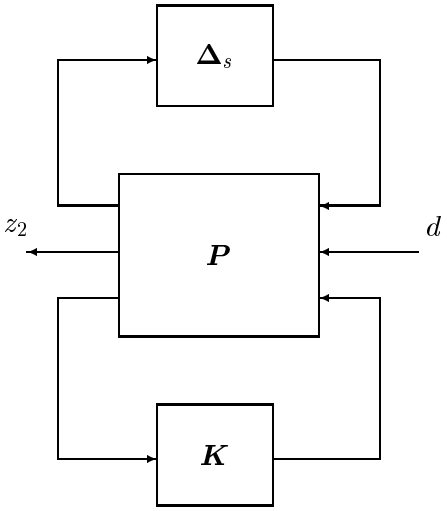

Figure 6.4: Perturbed closed-loop system for μ-analysis of robust performance.

new structure

$$\Omega := \left\{ \begin{bmatrix} \Delta_s & 0 \\ 0 & \Delta_p \end{bmatrix} \; : \; \Delta_s \in \Gamma, \; \Delta_p \in \mathbb{C}^{n_d \times n_{z_2}} \right\} . \tag{6.3}$$

The theorem is:

Theorem 15 *Assume $\boldsymbol{K}$ is internally stabilizing for the nominal plant $\boldsymbol{P}$. Then for the system*

in Figure 6.4, $\forall \boldsymbol{\Delta}_s \in \mathcal{BS}$*, the closed loop is well-posed, internally stable and* $\|d \mapsto z_2\|_\infty \leq 1$ *iff* $\sup_{\omega \in \mathbb{R}} \mu_\Omega\{\mathcal{F}_L[\boldsymbol{P}(j\omega), \boldsymbol{K}(j\omega)]\} \leq 1$.

Let us now turn to the computational and synthesis aspects of μ theory. It is known that if Γ has q scalar blocks (possibly repeated, e.g., $aI_r,\ a \in \mathbb{C}$) and l full blocks, then $\mu_\Gamma(M)$ can be computed to any desired accuracy as long as $2q + l \leq 3$ [13]. However, no algorithm is yet available to compute $\mu_\Gamma(M)$ in the more general case. All algorithms developed so far rely on optimizing upper and lower bounds for $\mu_\Gamma(M)$ and these can be obtained as follows. Define the subsets of $\mathbb{C}^{n\times n}$:

$$\mathcal{Q} := \{Q \in \Gamma \ :\ Q^*Q = I_n\}, \tag{6.4}$$

$$\begin{aligned}\mathcal{A} := \{&\mathrm{diag}\{D_1, \ldots, D_q,\ d_1 I_{m_1}, \ldots, d_l I_{m_l}\} \ : \\ &D_i \in \mathbb{C}^{r_i \times r_i},\ D_i = {D_i}^* > 0,\ d_j \in \mathbb{R},\ d_j > 0,\ d_l = 1\big\},\end{aligned} \tag{6.5}$$

and state the following theorem from [2]:

Theorem 16 *For all* $Q \in \mathcal{Q}$ *and* $D \in \mathcal{A}$

$$\mu_\Gamma(MQ) = \mu_\Gamma(QM) = \mu_\Gamma(M) = \mu_\Gamma(DMD^{-1})$$

Therefore, bounds on $\mu_\Gamma(M)$ may be written as:

$$\max_{Q\in\mathcal{Q}} \rho(QM) \ \leq\ \max_{\Delta_s \in \mathcal{B}\Gamma} \rho(\Delta_s M) \ =\ \mu_\Gamma(M) \ \leq\ \inf_{D\in\mathcal{A}} \|DMD^{-1}\|$$

where ρ denotes the spectral radius. These bounds provide direct estimates of $\mu_\Gamma(M)$ but in general the associated optimization problems are not convex. For instance, it is known that in general the lower bound equals $\mu_\Gamma(M)$, but it is also known that the objective function of the corresponding maximization problem may have local maxima. The upper bound is more important as it provides a sufficient condition for robust stability and performance. Moreover, the associated minimization problem is convex and the upper bound equals μ for the case $2q + l \leq 3$ mentioned above.

We are now in a good position to present the μ-synthesis technique to design optimal controllers. Consider the closed-loop system in Figure 6.3. Using the upper bound, one could

attempt to minimize the supremum of $\mu_\Gamma\{\mathcal{F}_L[\boldsymbol{P}(j\omega), \boldsymbol{K}(j\omega)]\}$ over all frequencies by solving the optimization problem

$$\min_{\boldsymbol{K}, \boldsymbol{D}} \left\| \begin{bmatrix} \boldsymbol{D} & 0 \\ 0 & I \end{bmatrix} \mathcal{F}_L(\boldsymbol{P}, \boldsymbol{K}) \begin{bmatrix} \boldsymbol{D}^{-1} & 0 \\ 0 & I \end{bmatrix} \right\|_\infty$$

where the constraints are that $\boldsymbol{K}$ must stabilize $\boldsymbol{P}$ perturbed by any $\boldsymbol{\Delta}_s \in \mathcal{BS}$, and $\boldsymbol{D} \in \mathcal{RH}_\infty$, $\boldsymbol{D}(s_0) \in \mathcal{A}$ for $s_0 \in \overline{\mathbb{C}}_+$, must be minimum-phase (i.e., no transmission zero in $\overline{\mathbb{C}}_+$). Finding a controller $\boldsymbol{K}$ to achieve this minimum is called μ-synthesis, but unfortunately it is not known how to solve this minimization exactly. However, an approximation to μ-synthesis involves a sequence of minimizations over $\boldsymbol{K}$ (holding $\boldsymbol{D}$ fixed) using the $\mathcal{H}_\infty$ method, and then over $\boldsymbol{D}$ (holding $\boldsymbol{K}$ fixed). This is the so-called D-K iteration algorithm [2] which can be easily implemented in Matlab^{TM}'s μ-Tools.

Now back to our robust performance problem for LFSS. From Theorem 15, we can see that the key idea for designing controllers achieving robust performance is to introduce a fictitious perturbation $\boldsymbol{\Delta}_p$ that wraps as a feedback around the generalized plant, with input z_2 and output d in our current setting (Figure 6.1). Then the robust performance problem is turned into a robust stability problem for the new system with $\boldsymbol{\Delta}_p$. Let us formalize this for our problem. Consider the system in Figure 6.1 and define the following complex structured uncertainty set:

$$\Omega_0 := \left\{ \begin{bmatrix} \tilde{\Delta}_0 & 0 \\ 0 & \Delta_p \end{bmatrix} : \tilde{\Delta}_0 \in \mathbb{C}^{n\times(m+n)}, \Delta_p \in \mathbb{C}^{m\times 3} \right\}. \tag{6.6}$$

Let $\mu_{\Omega_0} : \mathbb{C}^{(m+n+3)\times(m+n)} \to \mathbb{R}_+$ be the structured singular value associated with the structured perturbations in Ω_0. With $\boldsymbol{S}_{dhp} = d \mapsto z_2$ from the figure, Theorem 15 says that a stabilizing controller $\boldsymbol{K}$ achieves robust performance, i.e., $\|(\boldsymbol{W}_1\boldsymbol{S}_{dhp})(j\omega)\| \leq 1, \forall\omega$, $\forall\tilde{\boldsymbol{\Delta}}_0 \in \mathcal{BRH}_\infty$, iff $\mu_{\Omega_0}\{\mathcal{F}_L[\boldsymbol{P}(j\omega), \boldsymbol{K}(j\omega)]\} \leq 1$, $\forall\omega \in \mathbb{R}_+ \cup \{\infty\}$. Thus a μ-synthesis can be performed on the generalized plant $\boldsymbol{P}$ in Figure 6.5, which is just the generalized plant in Figure 6.1 with inputs w, d, u_{sc} and outputs z_1, z_2, y. It is given by

$$\boldsymbol{P} := \begin{bmatrix} \boldsymbol{P}_{11} & \boldsymbol{P}_{12} & \boldsymbol{P}_{13} \\ \boldsymbol{P}_{21} & \boldsymbol{P}_{22} & \boldsymbol{P}_{23} \\ \boldsymbol{P}_{31} & \boldsymbol{P}_{32} & \boldsymbol{P}_{33} \end{bmatrix}, \tag{6.7}$$

where

$$\boldsymbol{P}_{11} := \begin{bmatrix} 0 \\ \boldsymbol{r}\tilde{\boldsymbol{M}}_0^{-1} \end{bmatrix}, \qquad \boldsymbol{P}_{12} := \frac{\gamma}{d_{max}} \begin{bmatrix} \boldsymbol{r}J_2 \\ \boldsymbol{r}\tilde{\boldsymbol{M}}_0^{-1}\tilde{\boldsymbol{N}}_0 J_2 \end{bmatrix}, \qquad \boldsymbol{P}_{13} := \begin{bmatrix} \boldsymbol{r}\boldsymbol{T}_a \\ \boldsymbol{r}\tilde{\boldsymbol{M}}_0^{-1}\tilde{\boldsymbol{N}}_0\boldsymbol{T}_a \end{bmatrix},$$

$$\boldsymbol{P}_{21} := \boldsymbol{W}_1 C_1 J_1 \tilde{\boldsymbol{M}}_0^{-1}, \qquad \boldsymbol{P}_{22} := \frac{\gamma}{d_{max}} \boldsymbol{W}_1 C_1 J_1 \tilde{\boldsymbol{M}}_0^{-1}\tilde{\boldsymbol{N}}_0 J_2, \qquad \boldsymbol{P}_{23} := \boldsymbol{W}_1 C_1 J_1 \tilde{\boldsymbol{M}}_0^{-1}\tilde{\boldsymbol{N}}_0\boldsymbol{T}_a,$$

$$\boldsymbol{P}_{31} := C_1 J_1 \tilde{\boldsymbol{M}}_0^{-1}, \qquad \boldsymbol{P}_{32} := \frac{\gamma}{d_{max}} C_1 J_1 \tilde{\boldsymbol{M}}_0^{-1}\tilde{\boldsymbol{N}}_0 J_2, \qquad \boldsymbol{P}_{33} := C_1 J_1 \tilde{\boldsymbol{M}}_0^{-1}\tilde{\boldsymbol{N}}_0\boldsymbol{T}_a.$$

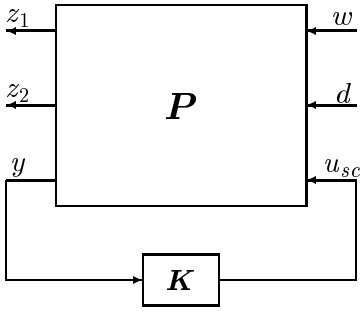

Figure 6.5: Generalized plant for μ-synthesis.

6.1.1 μ-Synthesis for Daisy

The models of Daisy and their uncertainties used in this section are the same collocated and noncollocated models used in Section 5.1.1 for the design of $\mathcal{H}_\infty$ controllers. Figure 6.1 shows the generalized plant in which the disturbance input d is now explicitly included. Recall that in Daisy's collocated model, $m = n = p = 23$, and in its noncollocated model, $m = 20$, $n = 23$, and $p = 23$.

6.1.1.1 Collocated Case

It is desired to control Daisy's model so that it remains stable and achieves the desired torque disturbance rejection level $\|\boldsymbol{S}_{dhp}(j\omega)\| \leq |\boldsymbol{w}^{-1}(j\omega)|$,$\forall\omega$, for all bounded perturbations of the modal parameters in Table 5.1 and all perturbations of the entries of B_1 within 8% of their

nominal values. The diagonal scaling matrices J_1 and J_2 are computed as explained in Section 2.3. The generalized plant for μ-synthesis is built according to Figure 6.5, and the different constants and weighting functions are

$$d_{max} = 0.107, \qquad c_{max} = 0.046, \qquad k = \frac{c_{max}}{d_{max}} = 0.43, \qquad \gamma = 0.79,$$

$$\boldsymbol{w}(s) = \frac{100}{s^2/(0.01)^2 + 2 \times 0.7s/0.01 + 1}, \tag{6.8}$$

$$\boldsymbol{r}(s) = \frac{0.001s + 1.415}{2.33s + 1}. \tag{6.9}$$

The μ-synthesis was carried out using μ-Tools [2] to implement the D-K iteration. Because the plant model is 78^{th}-order, the D-scales were restricted to be constant matrices in order to avoid controller inflation. Thus, we have $\boldsymbol{D} = \begin{bmatrix} dI & 0 \\ 0 & I \end{bmatrix}$ due to the simple structure of Ω_0. One D-K iteration produced a stable, 78^{th}-order controller $\boldsymbol{K}$ achieving $\sup_{\omega \in \mathbb{R}} \mu_{\Omega_0}\{\mathcal{F}_L[\boldsymbol{P}(j\omega), \boldsymbol{K}(j\omega)]\} = 0.91$. A balanced truncation of $\boldsymbol{K}$ yielded the 55^{th}-order controller $\boldsymbol{K}_3$ which basically did not affect the closed-loop plot of μ versus frequency (Figure 6.6). The least-damped closed-loop mode has a damping ratio of 0.38.

The norms of the nominal sensitivity $\boldsymbol{S}_{dh}(j\omega)$ and of five perturbed sensitivities $\{\boldsymbol{S}_{dhp_i}(j\omega)\}_{i=1}^{5}$ for five random sets of perturbations of the modal parameters of the plant model $\boldsymbol{G}$ within their limits are plotted in Figure 6.7. All these curves lie below $|\boldsymbol{w}^{-1}(j\omega)|$ as expected, and furthermore, all five dotted curves corresponding to the perturbed sensitivities are very close to the nominal one.

The 55^{th}-order μ controller $\boldsymbol{K}_3$ was rescaled to $\boldsymbol{K}_{p3} = \frac{d_{max}}{\gamma} J_2^{-1} \boldsymbol{K}_3$. Then $\boldsymbol{K}_{p3}$ was discretized at a sampling rate of 10 Hz using the bilinear transformation to get the controller $\boldsymbol{K}_{p3d}$. Figure 6.8 shows the frequency responses of two entries of $\boldsymbol{K}_{p3}$ and $\boldsymbol{K}_{p3d}$.

The closed-loop experiments with $\boldsymbol{K}_{p3d}$ are the same as those performed with the previous two controllers. First an x-axis hub torque disturbance $D(13.5\text{Nm}, 2s, x)$ was applied to the system. Simulated and recorded hub angles are shown in Figure 6.9, while Figure 6.10 shows the simulated and actual rib angles. The experimental and simulated hub reponses are similar although the experimental transient shows a larger peak. Moreover, the experimental settling time of θ_{hx} is longer than the simulated one. But comparing these results with those obtained with the $\mathcal{H}_\infty$ controller $\boldsymbol{K}_{p1d}$ in Figure 5.11, one can see that the μ controller performed better. This is especially evident for the rib responses. For the μ controller, the experimental rib

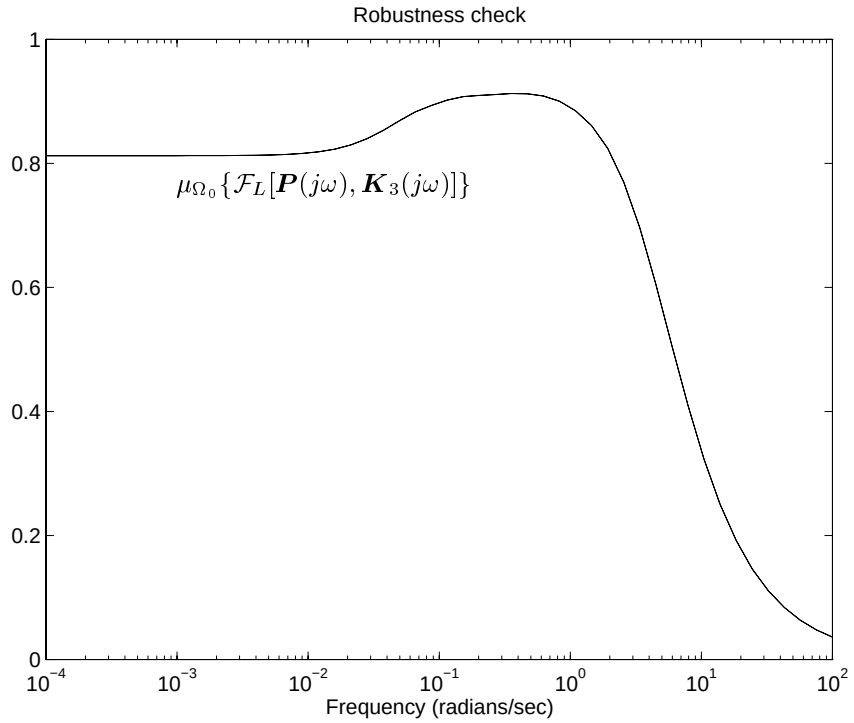

Figure 6.6: Robust performance check: Plot of $\mu_{\Omega_0}\{\mathcal{F}_L[\boldsymbol{P}(j\omega), \boldsymbol{K}_3(j\omega)]\}$.

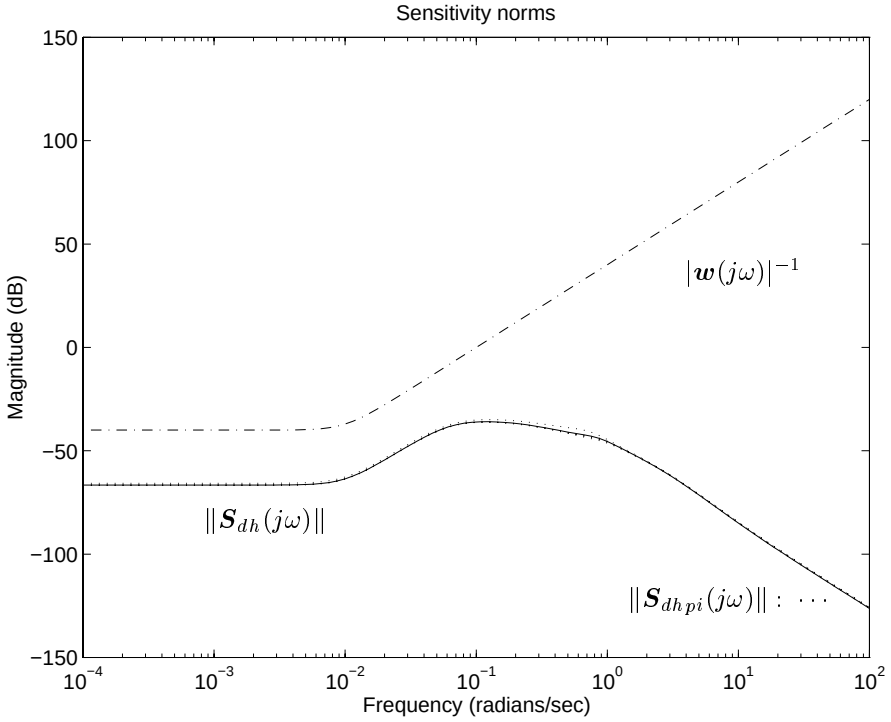

Figure 6.7: Norms of $\boldsymbol{S}_{dh}(j\omega)$ and $\boldsymbol{S}_{dhp_i}(j\omega)$ for $\boldsymbol{K}_3$.

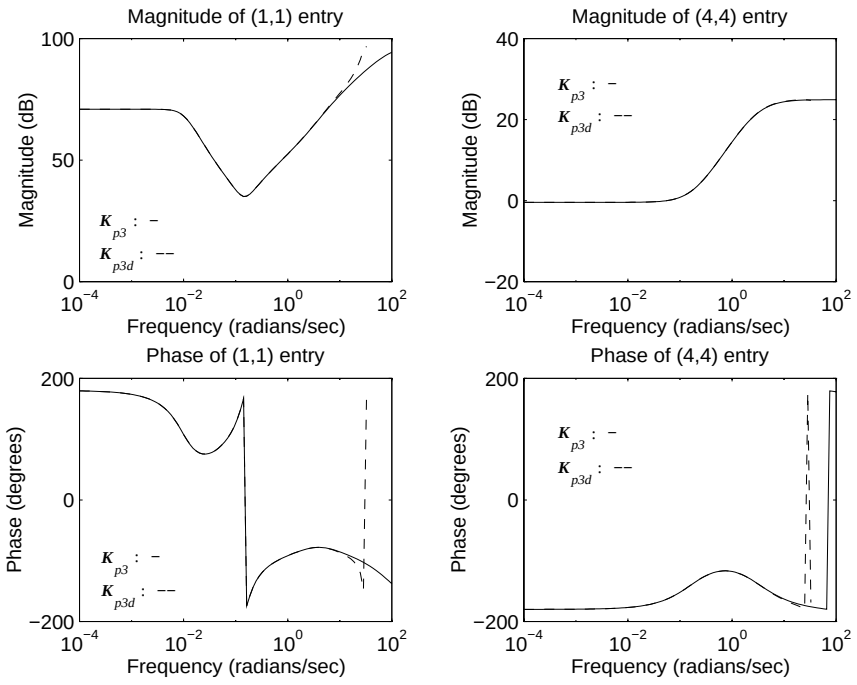

Figure 6.8: Frequency responses of the (1,1) and (4,4) entries of $\boldsymbol{K}_{p3}$ and $\boldsymbol{K}_{p3d}$.

angles are very close to the simulated ones, whereas with the $\mathcal{H}_\infty$ controller, the responses do not match as well. This is a direct consequence of the robust performance property of $\boldsymbol{K}_{p3d}$.

The simulated and experimental computed control torques are shown in Figure 6.11 for the hub and in Figure 6.12 for the ribs. Both of these figures indicate that the actuators saturated during the first few seconds.

The next control experiments with $\boldsymbol{K}_{p3d}$ involve torque disturbances around the y and z-axes: $D(13.5\text{Nm}, 2s, y)$ and $D(13.5\text{Nm}, 2s, z)$. Figures 6.13 and 6.14 show respectively the hub and rib angle responses for the y-axis disturbance, while the hub control torques are plotted in Figure 6.15 and the rib control torques are in Figure 6.16. The transients are again larger in the experimental response of θ_{hy}, but the settling times are comparable. It is interesting to note that the $\mathcal{H}_\infty$ (Figures 5.15, 5.16) and μ controllers produced very similar rib and hub angle responses to $D(13.5\text{Nm}, 2s, y)$. Both sets of data agree well with the simulations. The desired hub torque τ_{hy} saturated the y-axis torque wheel during the first second of the run. Some of the jet thrusters saturated during the first two seconds.

For the z-axis disturbance, the hub and rib angle responses are shown in Figures 6.17 and 6.18. Hub and rib torques are plotted in Figures 6.19 and 6.20. The experimental response of

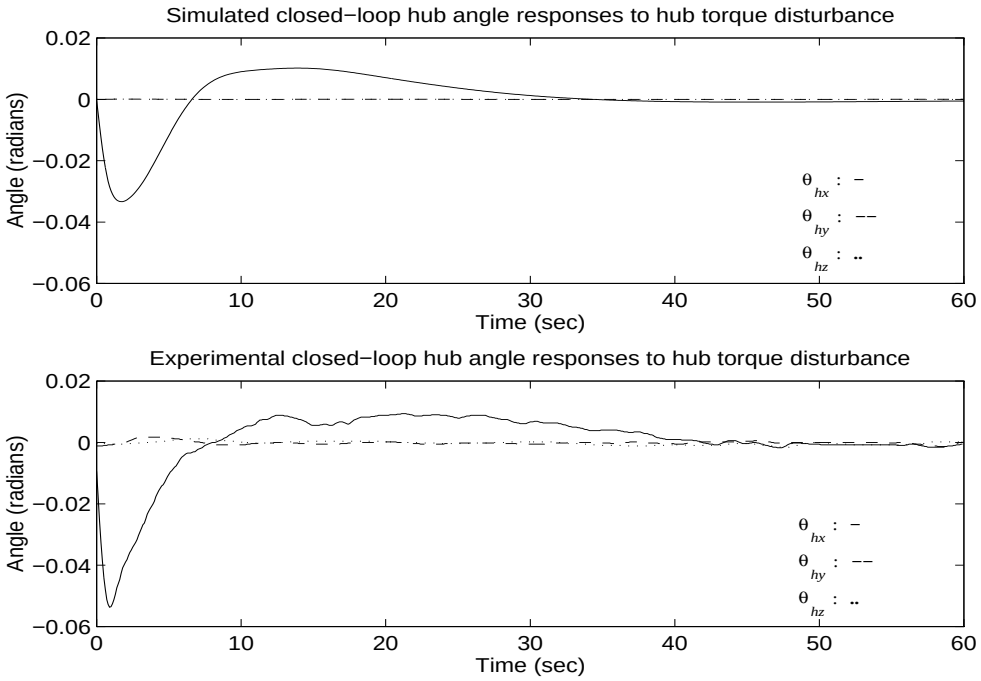

Figure 6.9: Sim. and exp. closed-loop hub angle responses with $\boldsymbol{K}_{p3d}$, $D(13.5\text{Nm}, 2s, x)$.

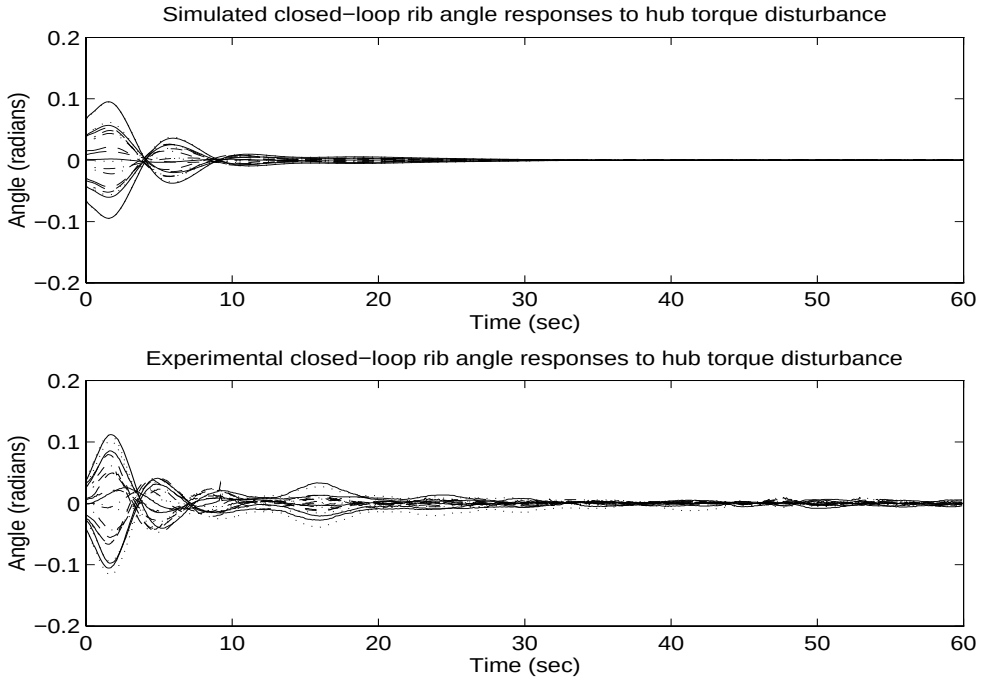

Figure 6.10: Sim. and exp. closed-loop rib angle responses with $\boldsymbol{K}_{p3d}$, $D(13.5\text{Nm}, 2s, x)$.

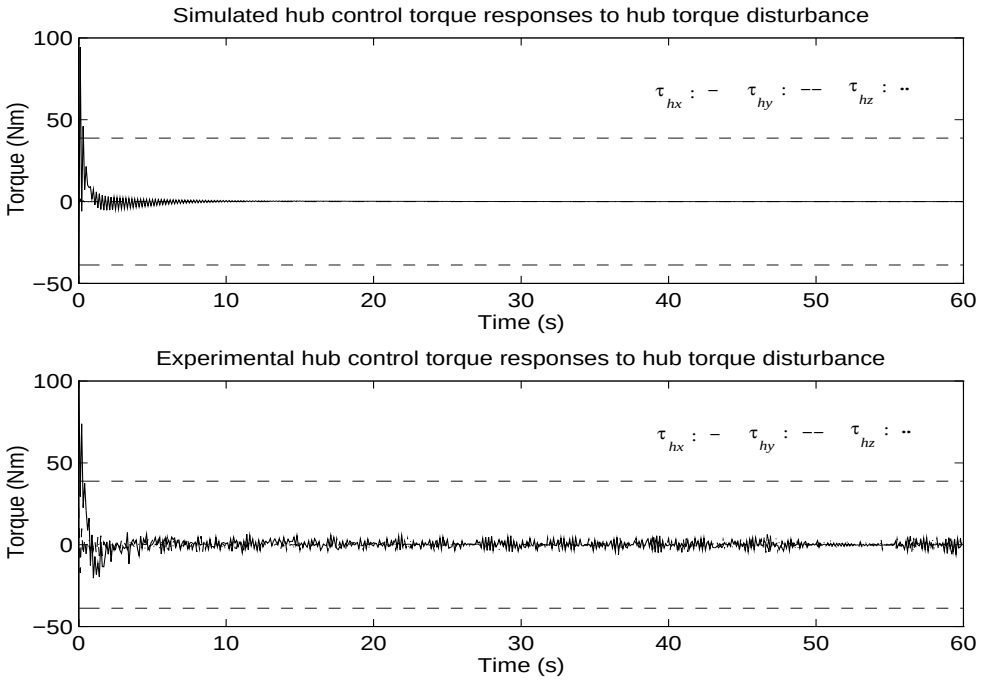

Figure 6.11: Sim. and exp. computed hub control torques for $\boldsymbol{K}_{p3d}$, $D(13.5\text{Nm}, 2s, x)$.

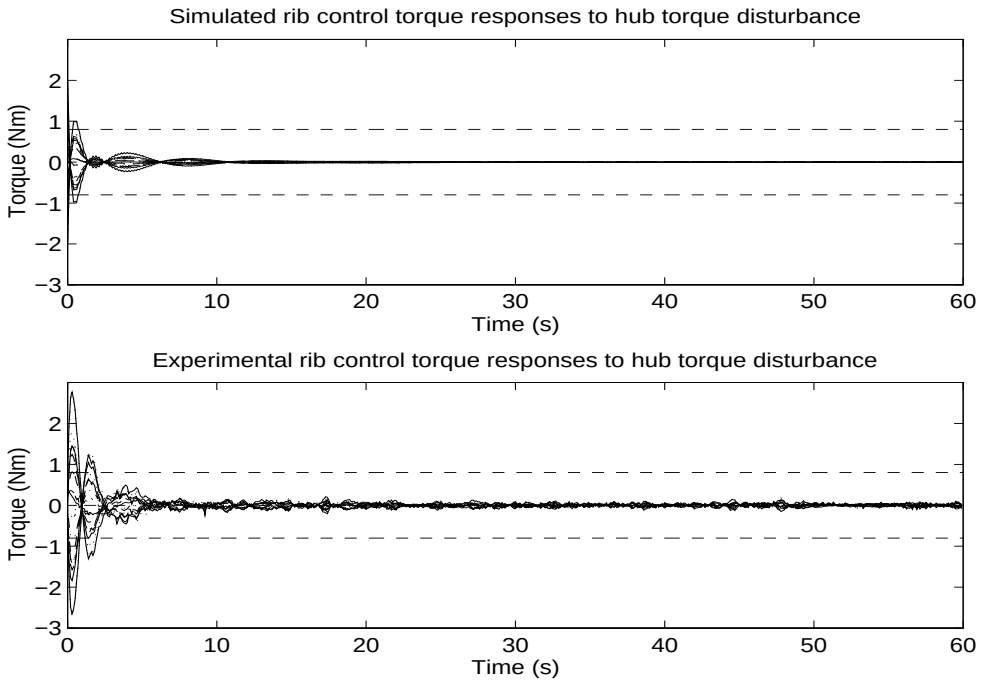

Figure 6.12: Sim. and exp. computed rib control torques for $\boldsymbol{K}_{p3d}$, $D(13.5\text{Nm}, 2s, x)$.

θ_{hz} shows a transient about twice as large as the simulated one. The experimental settling time is also longer but consistent with results obtained for the other axes. When compared to the results obtained with the $\mathcal{H}_\infty$ controller (Figure 5.19), the μ controller's performance is slightly worse, but not significantly. The rib responses are slightly more oscillatory than the simulated ones, but quite similar to those obtained with the $\mathcal{H}_\infty$ controller $\boldsymbol{K}_{p1d}$ (Figure 5.20). Saturation of the z-axis reaction wheel did not occur in this experiment, but some of the thrusters did saturate during the first second. The experimental rib torques were more oscillatory than the simulated ones.

In conclusion, the experimental data show that the μ controller $\boldsymbol{K}_{p3d}$ designed using the coprime factorization method outperformed the $\mathcal{H}_\infty$ controller $\boldsymbol{K}_{p1d}$ overall. Actually, both controllers are comparable for y-axis and z-axis disturbances, but for the x-axis disturbance, the μ controller clearly did a better job rejecting it. These results indicate that the robust performance property obtained using μ-synthesis is highly desirable in order to better predict closed-loop performance for LFSS.

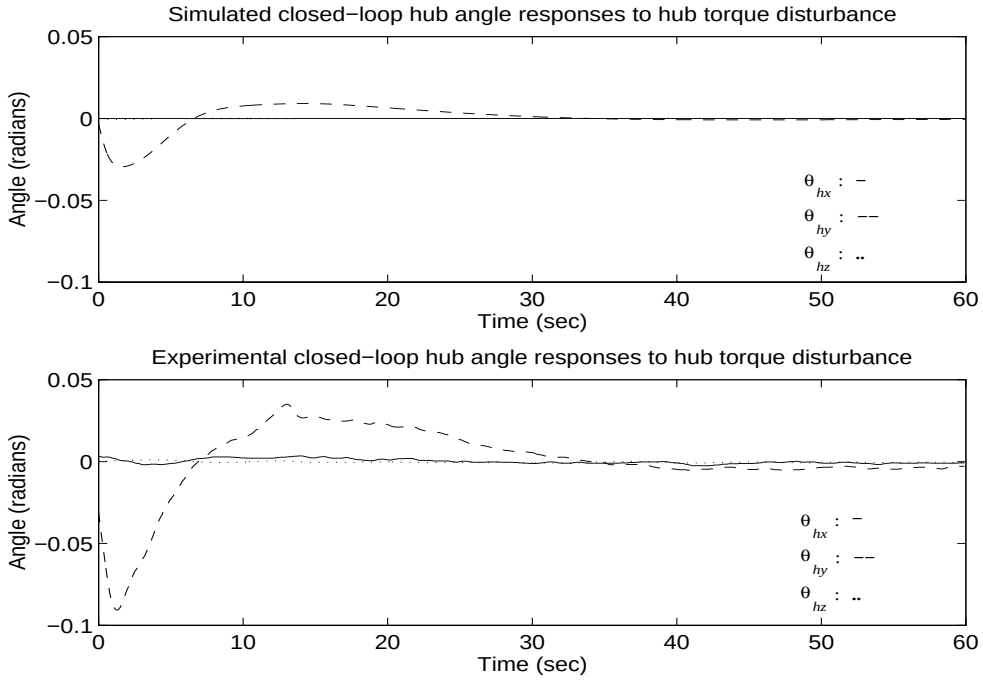

Figure 6.13: Sim. and exp. closed-loop hub angle responses with $\boldsymbol{K}_{p3d}$, $D(13.5\text{Nm}, 2s, y)$.

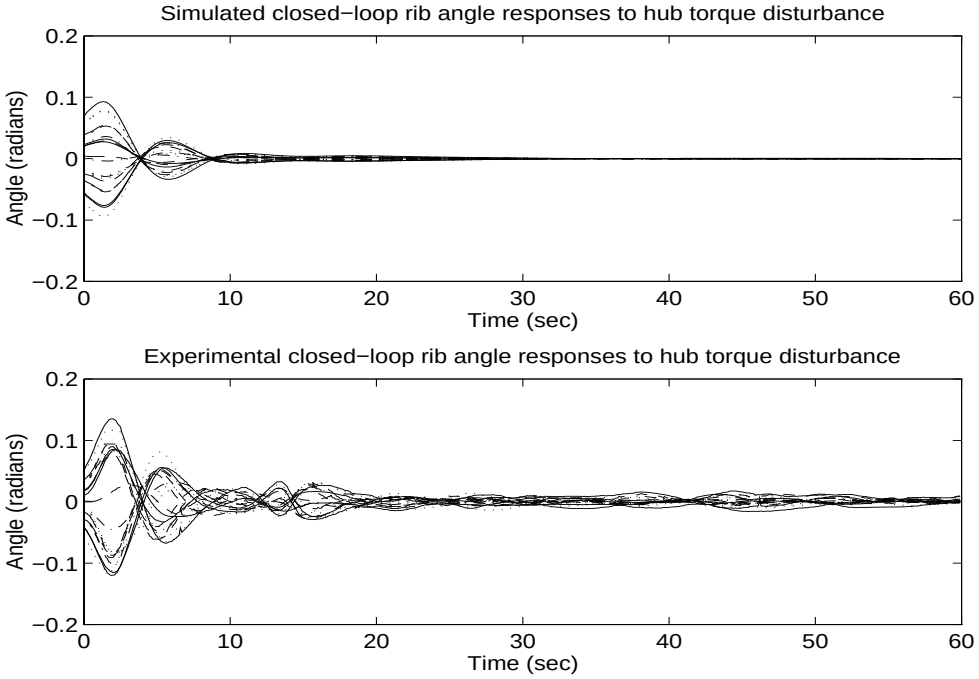

Figure 6.14: Sim. and exp. closed-loop rib angle responses with $\boldsymbol{K}_{p3d}$, $D(13.5\text{Nm}, 2s, y)$.

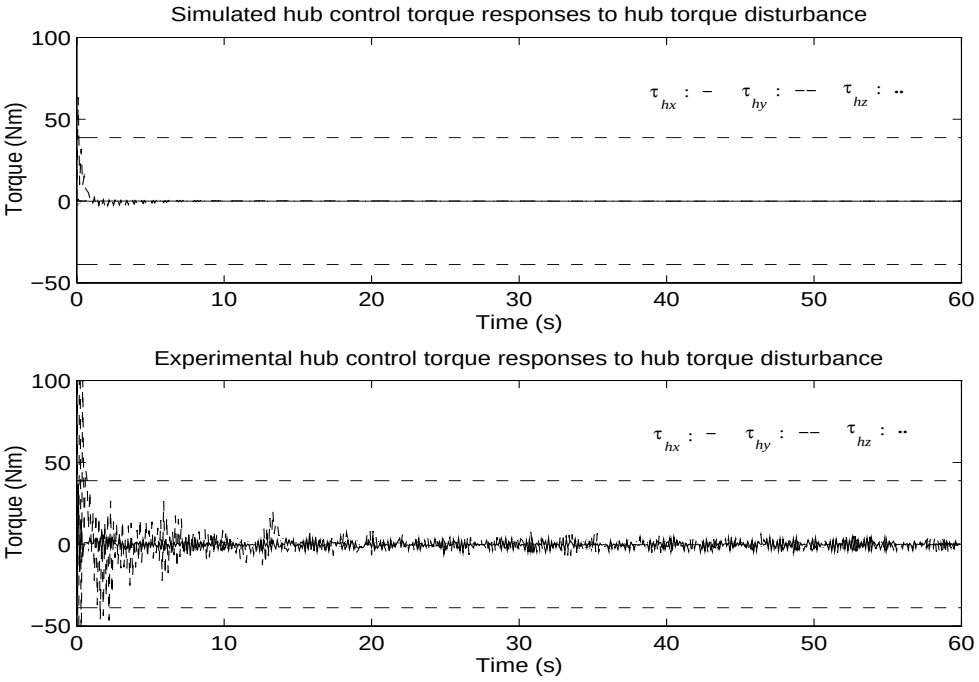

Figure 6.15: Sim. and exp. computed hub control torques for $\boldsymbol{K}_{p3d}$, $D(13.5\text{Nm}, 2s, y)$.

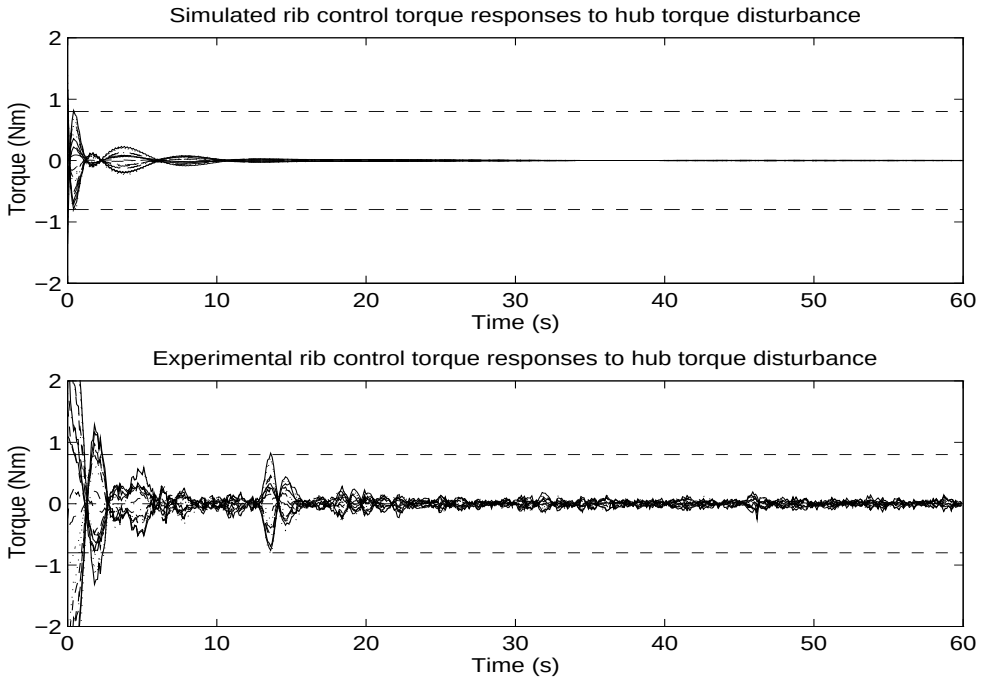

Figure 6.16: Sim. and exp. computed rib control torques for $\boldsymbol{K}_{p3d}$, $D(13.5\text{Nm}, 2s, y)$.

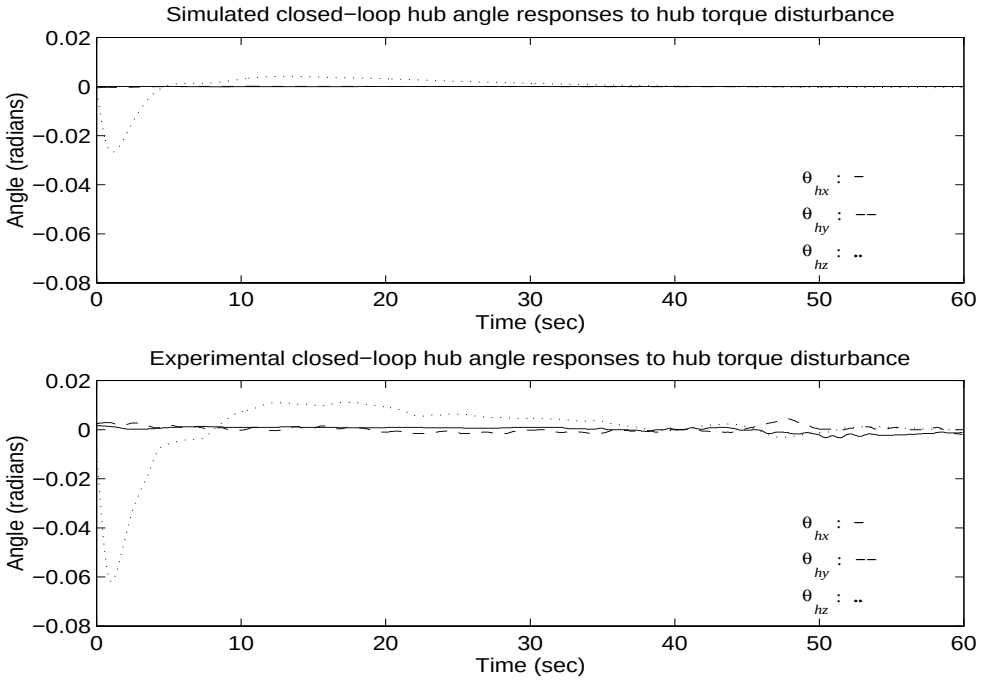

Figure 6.17: Sim. and exp. closed-loop hub angle responses with $\boldsymbol{K}_{p3d}$, $D(13.5\text{Nm}, 2s, z)$.

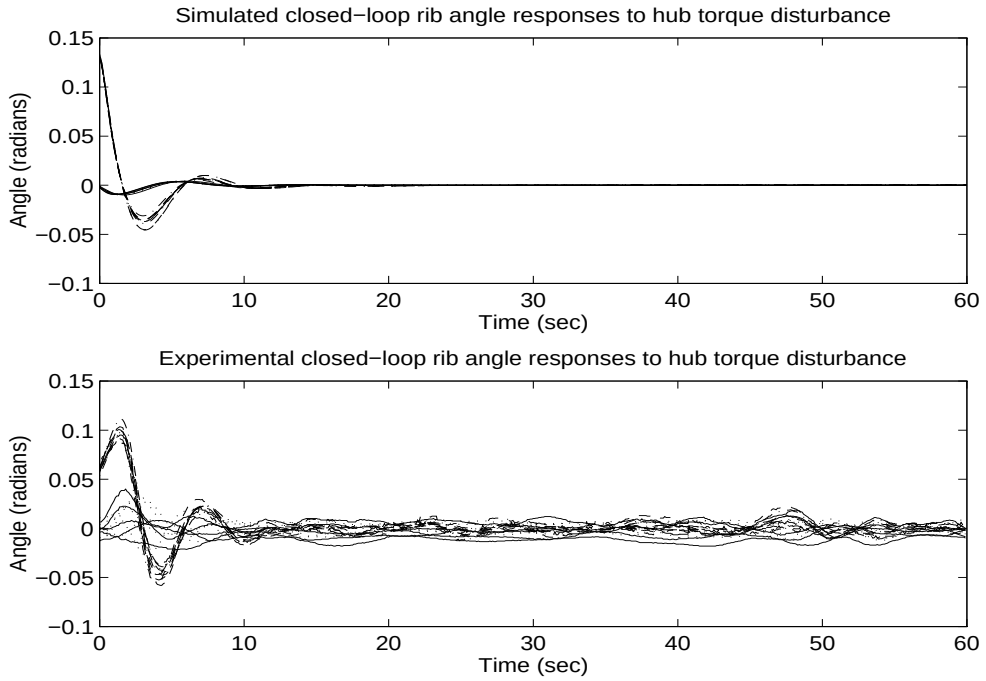

Figure 6.18: Sim. and exp. closed-loop rib angle responses with $\boldsymbol{K}_{p3d}$, $D(13.5\text{Nm}, 2s, z)$.

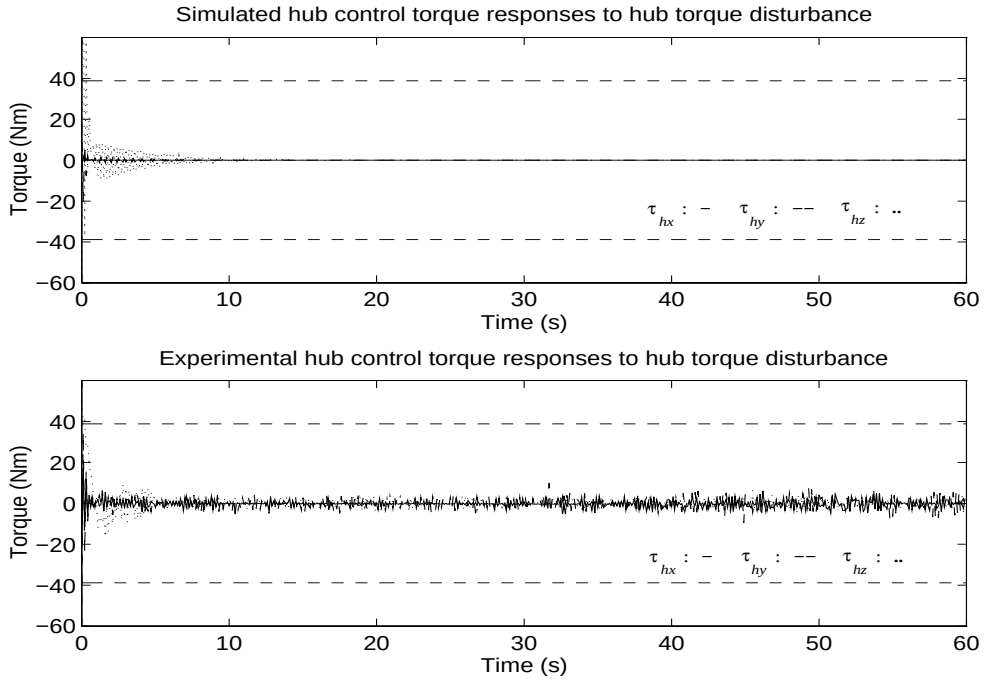

Figure 6.19: Sim. and exp. computed hub control torques for $\boldsymbol{K}_{p3d}$, $D(13.5\text{Nm}, 2s, z)$.

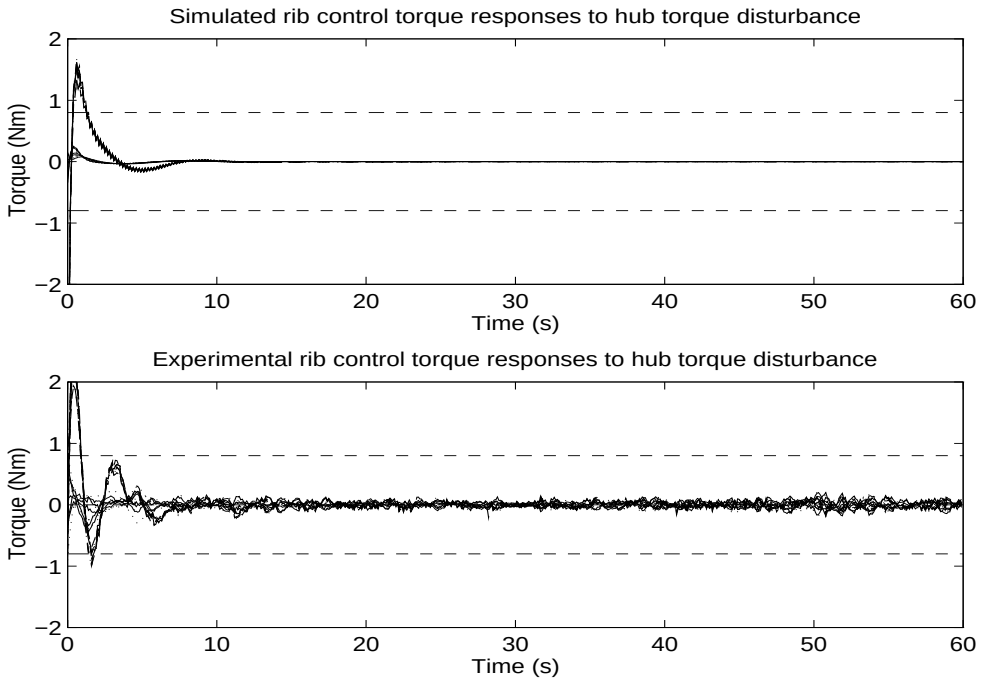

Figure 6.20: Sim. and exp. computed rib control torques for $\boldsymbol{K}_{p3d}$, $D(13.5\text{Nm}, 2s, z)$.

6.1.1.2 Noncollocated Case

Our specifications are still robust stability and robust torque disturbance rejection, that is $\|\boldsymbol{S}_{dhp}(j\omega)\| \leq |\boldsymbol{w}^{-1}(j\omega)|$, $\forall\omega$, for all bounded perturbations of the modal parameters in Table 5.2 and all perturbations of the entries of B_1 within 5% of their nominal values. The noncollocated model is the same that was used in §5.1.1.2. Note that the performance requirement has been relaxed here because the DC gain of $\boldsymbol{w}$ has been decreased to 30. This came about because of the tradeoff between nominal performance and performance robustness accommodating a reasonable amount of uncertainty. A few iterations of the design indicated that the chosen $\boldsymbol{w}$ leads to a seemingly good tradeoff, with robustness to 5% uncertainty in the entries of B_1, 5% uncertainty in the modal frequencies and 30% in the damping ratios. Hence this design could not quite meet the specifications, but it was close. In fact, it guarantees more robustness than the noncollocated $\mathcal{H}_\infty$ design of §5.1.1.2. Note that this noncollocated μ design is different from the one in [4]. The latter destabilized Daisy around all axes, whereas the current design produced stable responses around the x and y axes.

The generalized plant for μ-synthesis is built according to Figure 6.5, and the different

constants and weighting functions are

$$d_{max} = 0.064, \qquad c_{max} = 0.027, \qquad k = \frac{c_{max}}{d_{max}} = 0.43, \qquad \gamma = 0.46,$$

$$\boldsymbol{w}(s) = \frac{30}{s^2/(0.005)^2 + 2 \times 0.7 s/0.005 + 1}, \tag{6.10}$$

$$\boldsymbol{r}(s) = \frac{0.01s + 1.415}{2.33s + 1}. \tag{6.11}$$

The noncollocated plant model is 75^{th}-order. Thus, in the D-K iteration, the D-scales were restricted to be constant in order to avoid controller inflation. One D-K iteration produced a stable, 75^{th}-order controller $\boldsymbol{K}$ achieving $\sup_{\omega \in \mathbb{R}} \mu_{\Omega_0}\{\mathcal{F}_L[\boldsymbol{P}(j\omega), \boldsymbol{K}(j\omega)]\} = 1.01$. A balanced realization of $\boldsymbol{K}$ was truncated to the 49-state controller $\boldsymbol{K}_4$ without noticeably affecting μ versus frequency (Figure 6.21). The least-damped closed-loop mode has a damping ratio of 0.19.

The norms of the nominal sensitivity $\boldsymbol{S}_{dh}(j\omega)$ and of five perturbed sensitivities $\{\boldsymbol{S}_{dhp_i}(j\omega)\}_{i=1}^{5}$ for five random sets of perturbations of modal parameters (within their limits) in the plant model $\boldsymbol{G}$ are plotted in Figure 6.22. These five curves lie below $|\boldsymbol{w}^{-1}(j\omega)|$ as expected, and furthermore they are all very close to the nominal curve.

The 49^{th}-order controller $\boldsymbol{K}_4$ was rescaled to $\boldsymbol{K}_{p4} = \frac{d_{max}}{\gamma} J_2^{-1} \boldsymbol{K}_4$. Then $\boldsymbol{K}_{p4}$ was discretized at a sampling rate of 10 Hz to get $\boldsymbol{K}_{p4d}$ using the bilinear transformation. Figure 6.23 shows the frequency responses of two entries of $\boldsymbol{K}_{p4}$ and $\boldsymbol{K}_{p4d}$.

We will see that responses to x-axis and y-axis torque disturbances were stable in the closed-loop experiments with $\boldsymbol{K}_{p4d}$, but not the response to a z-axis disturbance. First an x-axis hub torque disturbance $D(6.8\text{Nm}, 2s, x)$ was applied to the system. Simulated and recorded hub angles are shown in Figure 6.24 while Figure 6.25 shows the simulated and actual rib angles. The hub angle responses were stable and the transients were satisfactory. The experimental settling time of θ_{hx} is close to the one obtained by simulation. The transients in the experimental rib angle responses are seen to be a bit larger than in the simulation, and lasted roughly twice as long. The simulated and experimental computed control torques are shown in Figure 6.26 for the hub and in Figure 6.27 for the ribs. It can be seen that the hub and rib control torques stayed well within their saturation limits.

Overall, this μ controller seems to have outperformed the $\mathcal{H}_\infty$ controller of §5.1.1.2 for an x-axis disturbance applied on the hub. But one must keep in mind that the torque disturbance was twice as large in the experiment with the $\mathcal{H}_\infty$ controller.

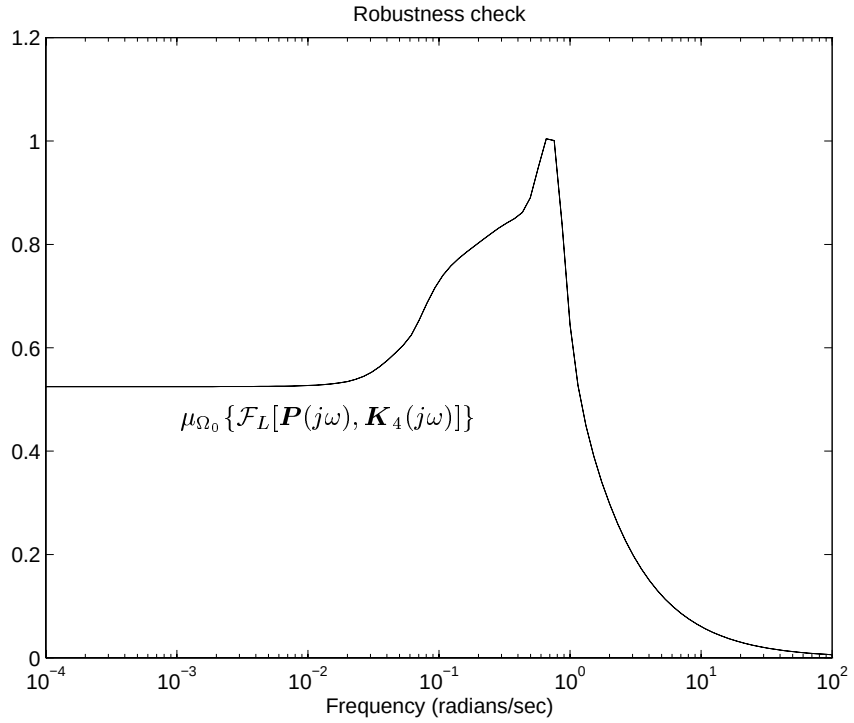

Figure 6.21: Robust performance check: Plot of $\mu_{\Omega_0}\{\mathcal{F}_L[\boldsymbol{P}(j\omega), \boldsymbol{K}_4(j\omega)]\}$.

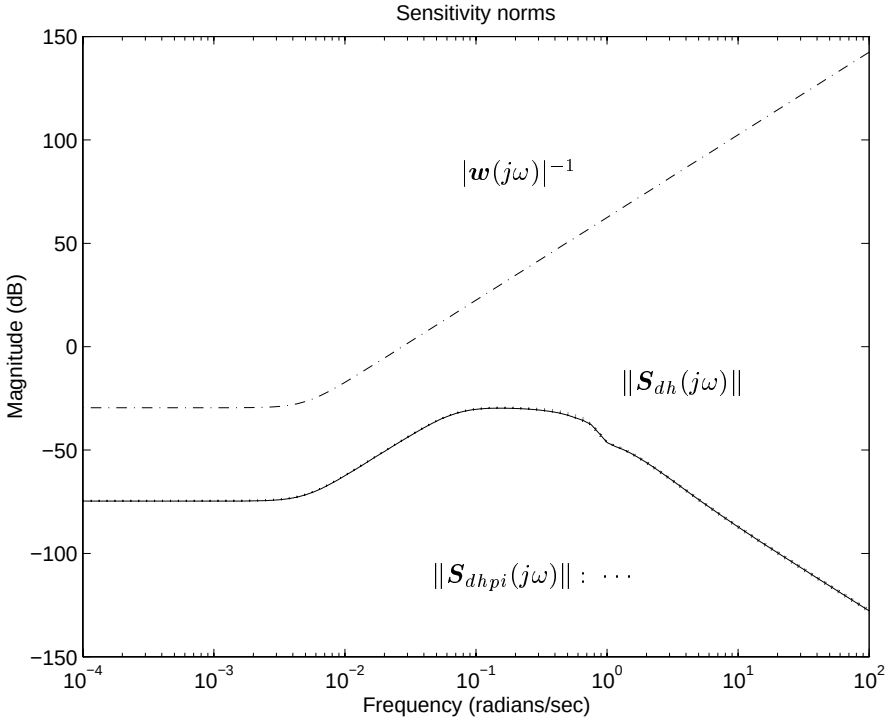

Figure 6.22: Norms of $\boldsymbol{S}_{dh}(j\omega)$ and $\boldsymbol{S}_{dhp_i}(j\omega)$ for $\boldsymbol{K}_4$.

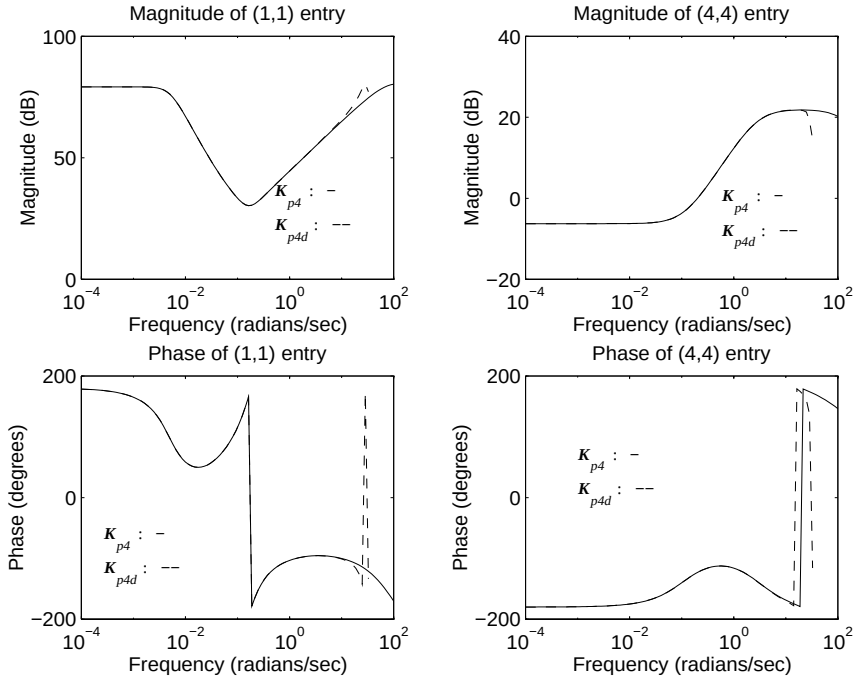

Figure 6.23: Frequency responses of the (1,1) and (4,4) entries of $\boldsymbol{K}_{p4}$ and $\boldsymbol{K}_{p4d}$.

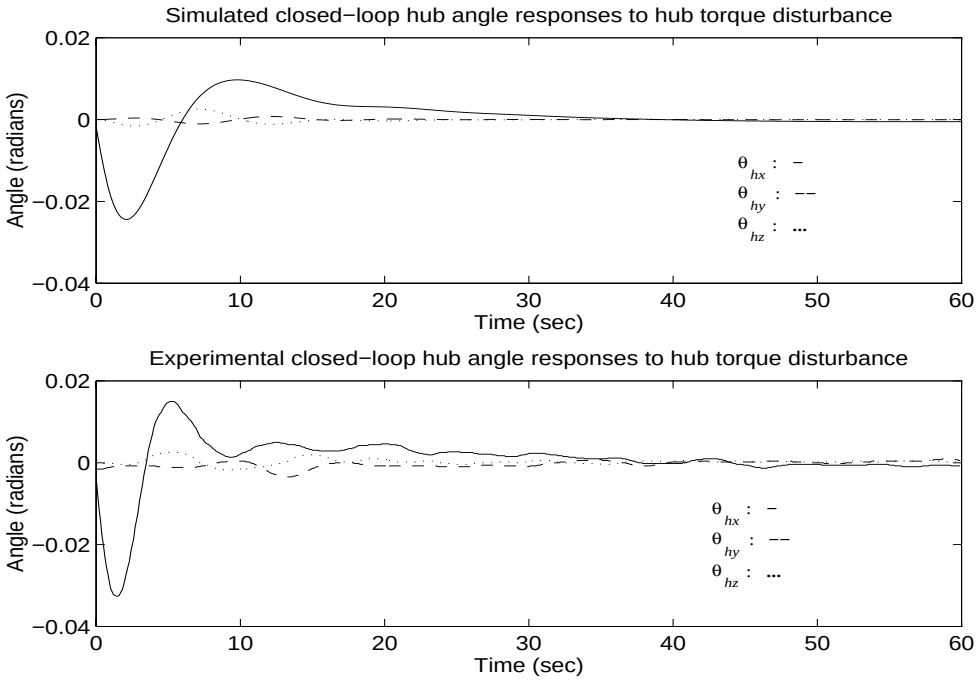

Figure 6.24: Sim. and exp. closed-loop hub angle responses with $\boldsymbol{K}_{p4d}$, $D(6.8\text{Nm}, 2s, x)$.

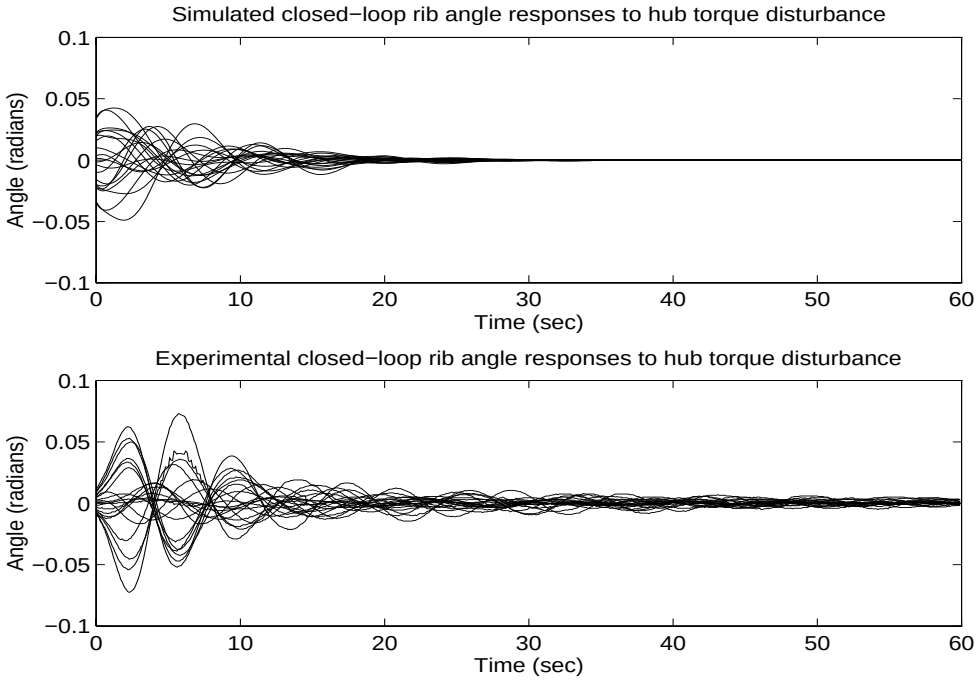

Figure 6.25: Sim. and exp. closed-loop rib angle responses with $\boldsymbol{K}_{p4d}$, $D(6.8\text{Nm}, 2s, x)$.

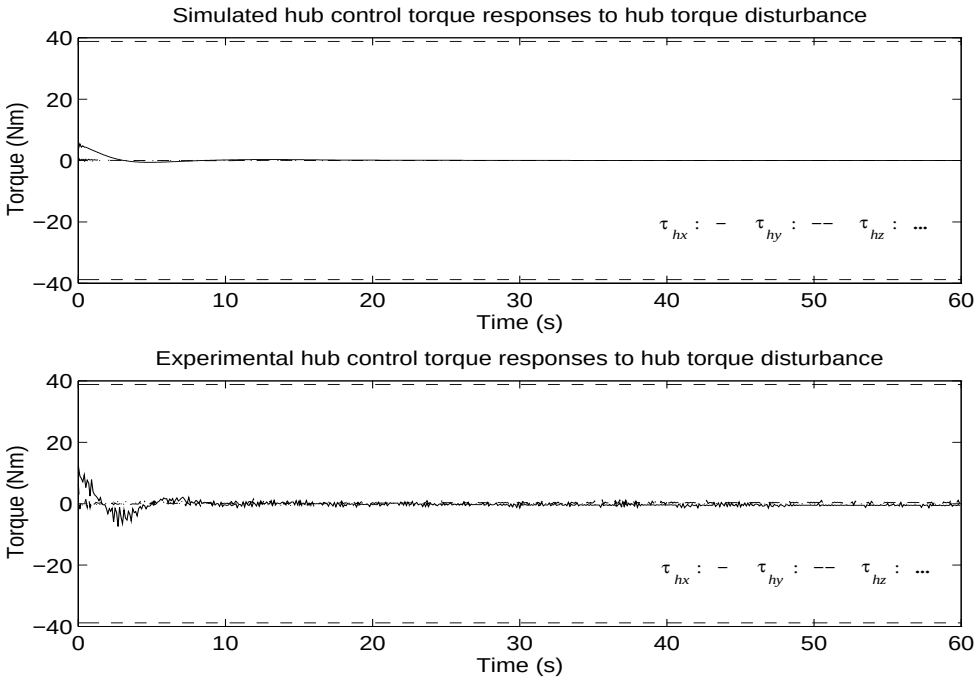

Figure 6.26: Sim. and exp. computed hub control torques for $\boldsymbol{K}_{p4d}$, $D(6.8\text{Nm}, 2s, x)$.

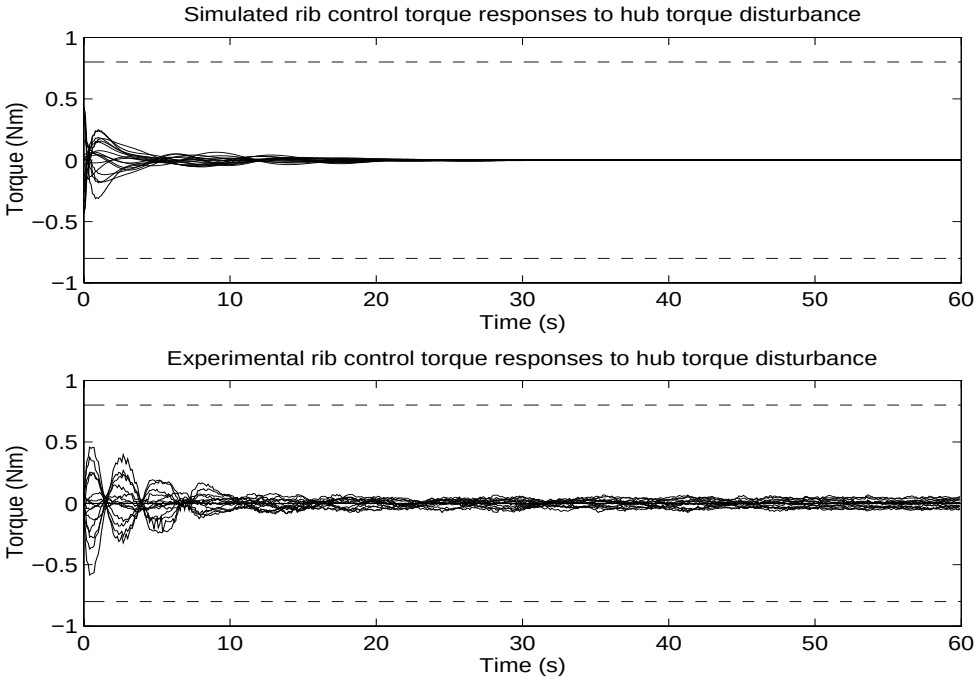

Figure 6.27: Sim. and exp. computed rib control torques for $\boldsymbol{K}_{p4d}$, $D(6.8\text{Nm}, 2s, x)$.

The next control experiments with $\boldsymbol{K}_{p4d}$ involved torque disturbances around the y-axis and the z-axis: $D(6.8\text{Nm}, 2s, y)$ and $D(6.8\text{Nm}, 2s, z)$. Figures 6.28 and 6.29 show respectively the hub and rib angle responses for the y-axis disturbance, while the hub control torques are plotted in Figure 6.30 and the rib control torques are in Figure 6.31. The experimental response of θ_{hy} has a first overshoot about 1.5 times the size of the overshoot of the simulated response, similar to what occurred in the previous experiment for $D(6.8\text{Nm}, 2s, x)$. The settling times of the experimental and simulated responses are comparable, although the experimental θ_{hy} was more oscillatory. The transients in the experimental rib angle responses are slightly larger than in the simulation, lasted a bit longer, but are otherwise satisfactory.

Recall that the response of the noncollocated $\mathcal{H}_\infty$ controller $\boldsymbol{K}_{p2d}$ to $D(13.5\text{Nm}, 2s, y)$ entered a limit cycle, so it appears that the noncollocated μ controller performed better for x-axis and y-axis torque disturbances. Unfortunately, a better comparison of the results is difficult to carry out as a torque disturbance of 13.5 Nm could not be used for the experiments with $\boldsymbol{K}_{p4d}$ because it caused DEOPS to crash after a few seconds. The reason is that the images of some of the infra-red diodes were not centered in the cameras' fields of view when Daisy was at rest. Hence the associated ribs could not move much before the diodes' images were lost, causing the DEOPS software to crash. A careful realignment of the lenses would have had to be done to alleviate this problem. Thus smaller torque disturbances of 6.8 Nm were used in the experiments.

For the z-axis disturbance, the hub and rib angle responses are shown in Figures 6.32 and 6.33. Hub and rib torques are plotted in Figures 6.34 and 6.35. Clearly this run was unstable. Only 40 seconds of data could be recorded before rib angles went out of range, causing DEOPS to crash.

In conclusion, the noncollocated μ controller $\boldsymbol{K}_{p4d}$, being more robust than $\boldsymbol{K}_{p2d}$ on paper, appears to have performed better by stabilizing Daisy for x-axis and y-axis torque disturbances of 6.8 Nm. Although further experiments with 13.5 Nm disturbances would have to be carried out before a stronger conclusion could be reached. The linear simulations showed very good nominal performance while the design itself indicated performance robustness to reasonably large deviations in the modal parameters. A z-axis torque disturbance unequivocally destabilized Daisy, showing input-dependent stability properties of the closed-loop system. This suggests that nonlinearities play a significant role in the noncollocated configuration. As previously stated, further research on LFSS modeling, identification and stability analysis with

nonlinearities will have to be done before we can hope to obtain better experimental results in noncollocated control of Daisy.

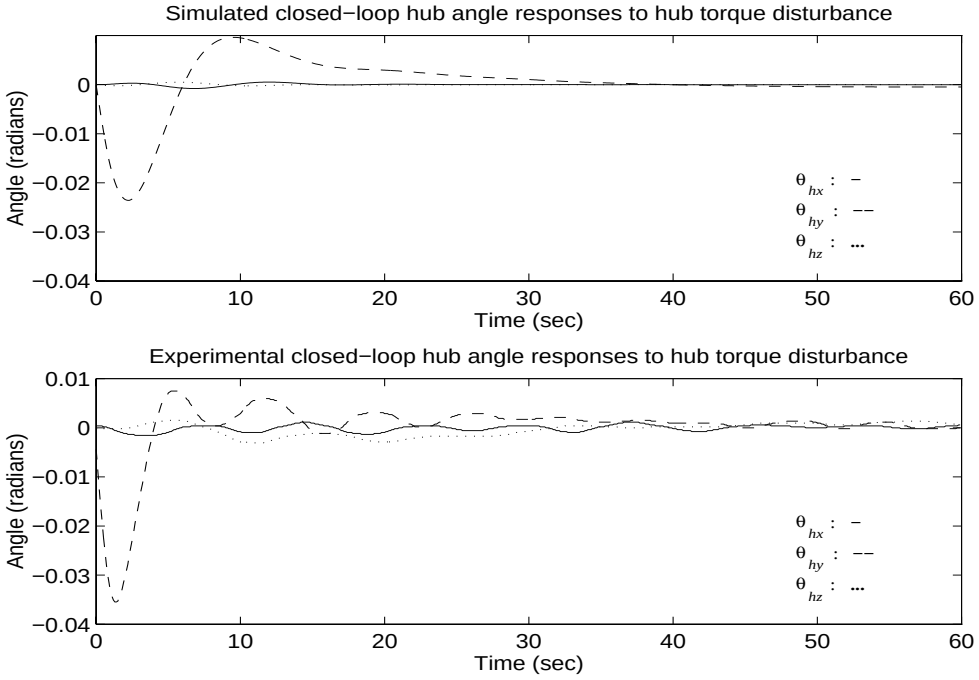

Figure 6.28: Sim. and exp. closed-loop hub angle responses with $\boldsymbol{K}_{p4d}$, $D(6.8\text{Nm}, 2s, y)$.

6.2 Summary and Discussion

In this chapter, we introduced a controller design technique based on μ-synthesis that provides robust performance for LFSS. This design technique uses the perturbed LCF model of LFSS dynamics introduced in Chapter 2. The unit $\boldsymbol{r}$ bounding the factor uncertainty is computed from the expression given in Proposition 2. It can be improved prior to the design step by using experimental frequency-response data obtained on the LFSS. The setup, shown in Figure 6.1, is basically the same as the one in Figure 5.1 for the $\mathcal{H}_\infty$ problem of Section 5.1, except that the torque disturbance channel is included in the design. Thus, the disturbance rejection performance specification is explicitly introduced in the design problem.

The structured singular value μ was introduced, and the standard D-K iteration approach to μ-synthesis was described. This approach was used to design collocated and noncollocated controllers for Daisy, with the D-scales constrained to be constant matrices to avoid controller

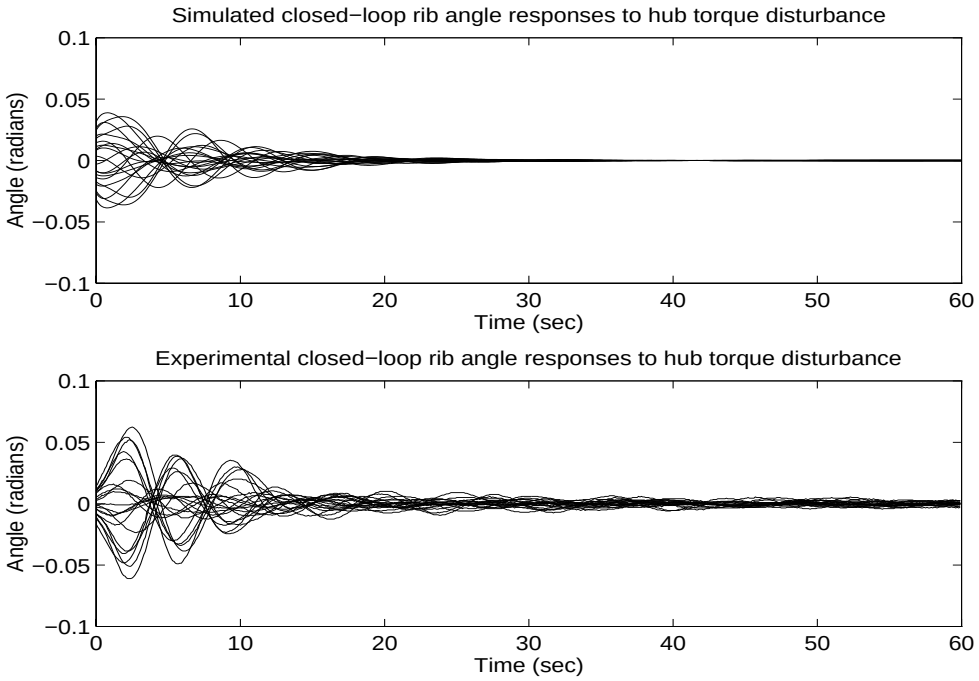

Figure 6.29: Sim. and exp. closed-loop rib angle responses with $\boldsymbol{K}_{p4d}$, $D(6.8\text{Nm}, 2s, y)$.

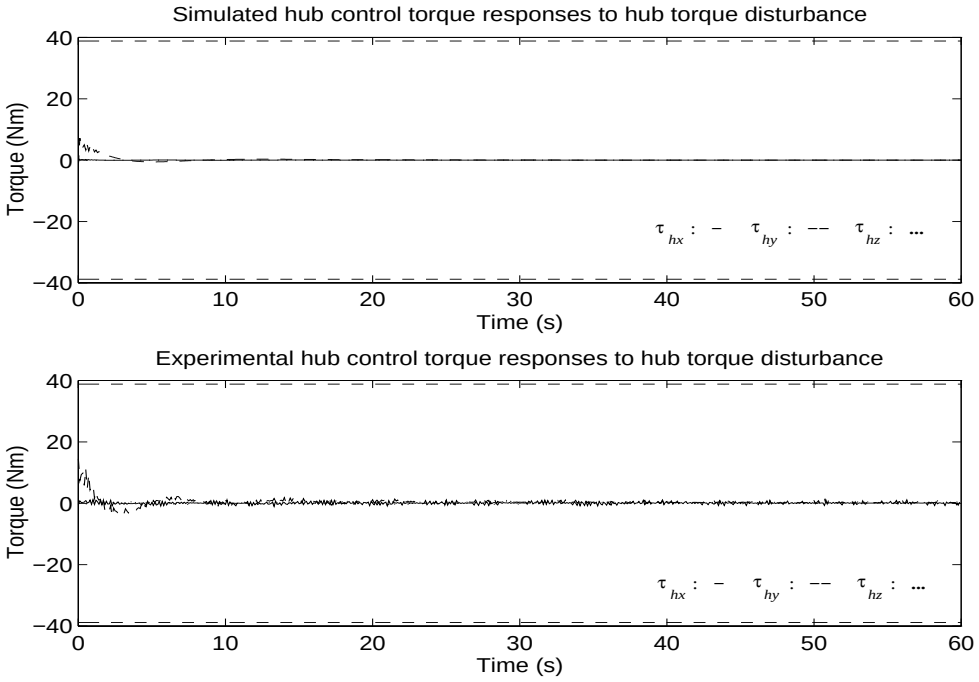

Figure 6.30: Sim. and exp. computed hub control torques for $\boldsymbol{K}_{p4d}$, $D(6.8\text{Nm}, 2s, y)$.

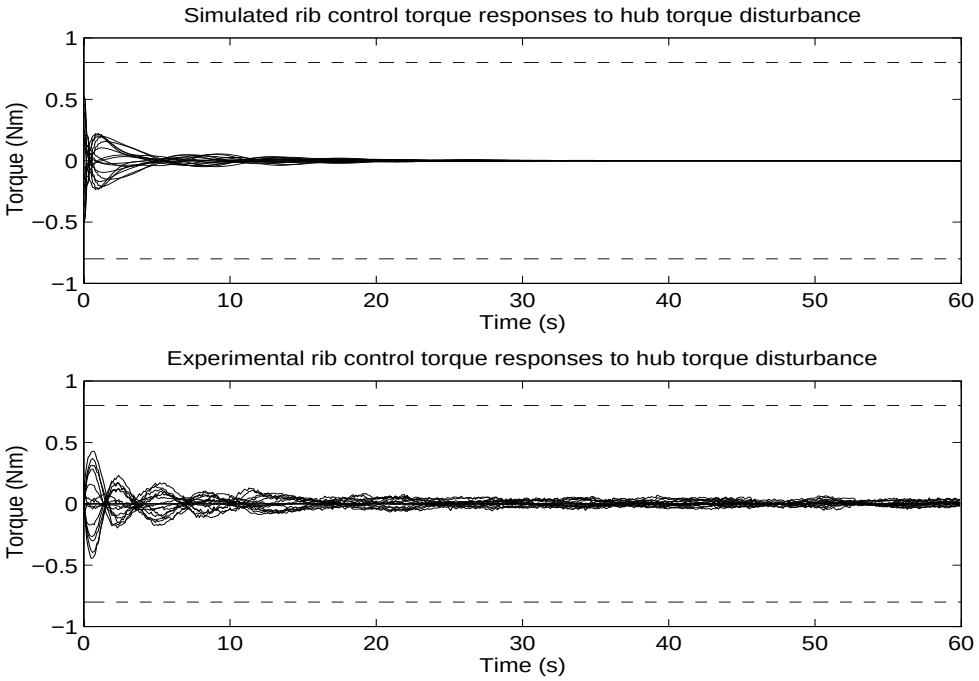

Figure 6.31: Sim. and exp. computed rib control torques for $\boldsymbol{K}_{p4d}$, $D(6.8\text{Nm}, 2s, y)$.

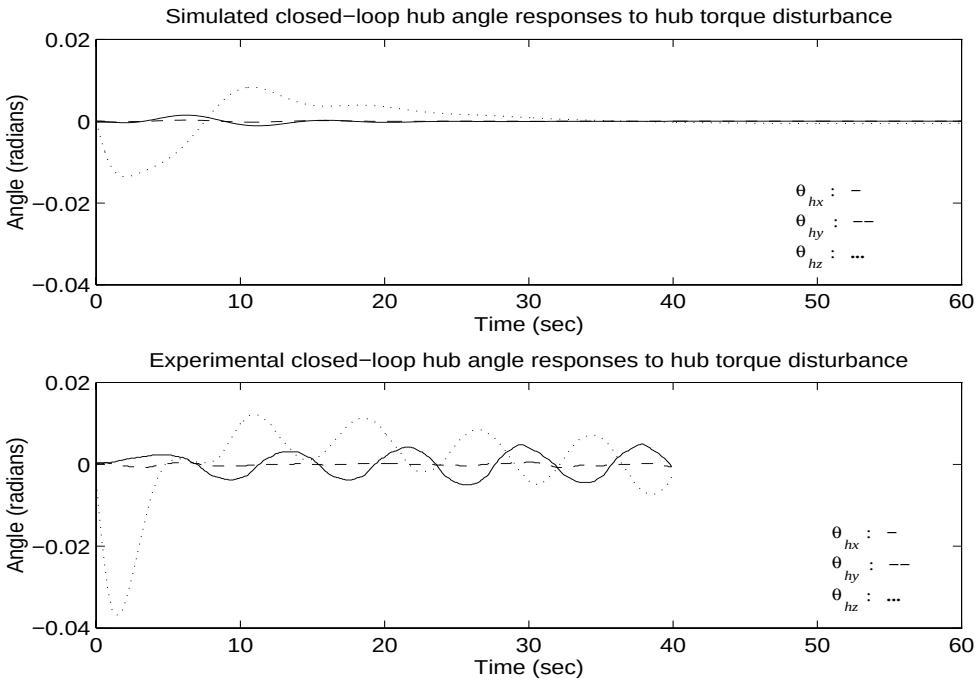

Figure 6.32: Sim. and exp. closed-loop hub angle responses with $\boldsymbol{K}_{p4d}$, $D(6.8\text{Nm}, 2s, z)$.

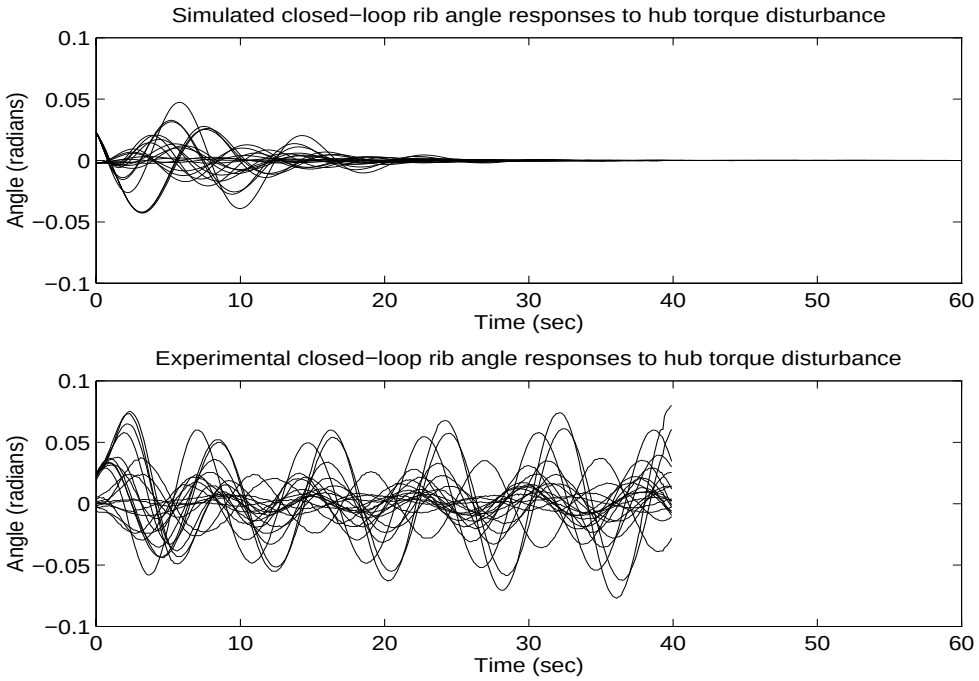

Figure 6.33: Sim. and exp. closed-loop rib angle responses with $\boldsymbol{K}_{p4d}$, $D(6.8\text{Nm}, 2s, z)$.

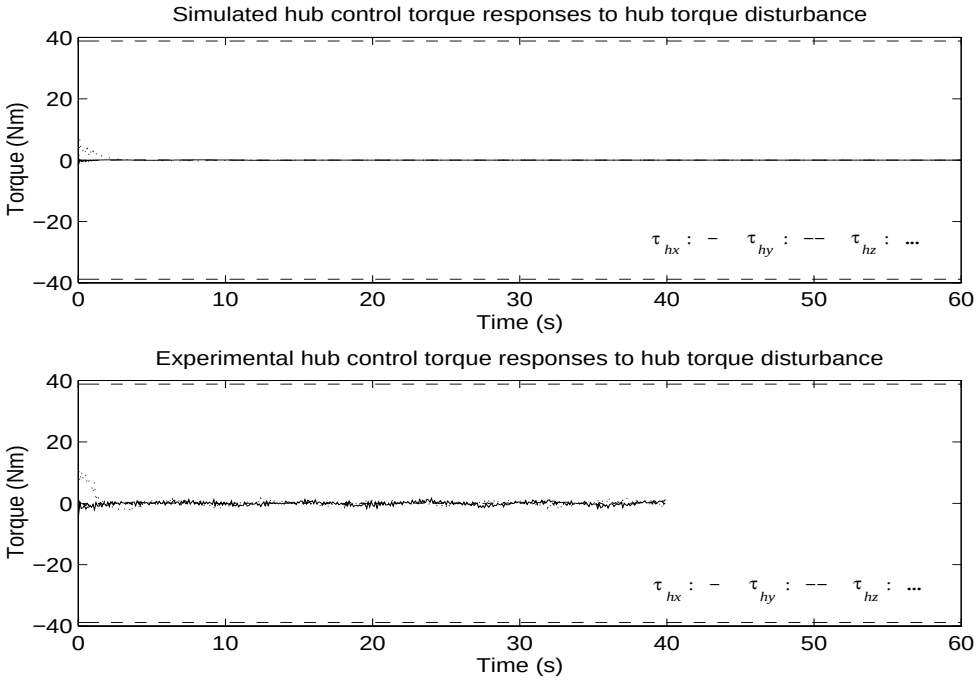

Figure 6.34: Sim. and exp. computed hub control torques for $\boldsymbol{K}_{p4d}$, $D(6.8\text{Nm}, 2s, z)$.

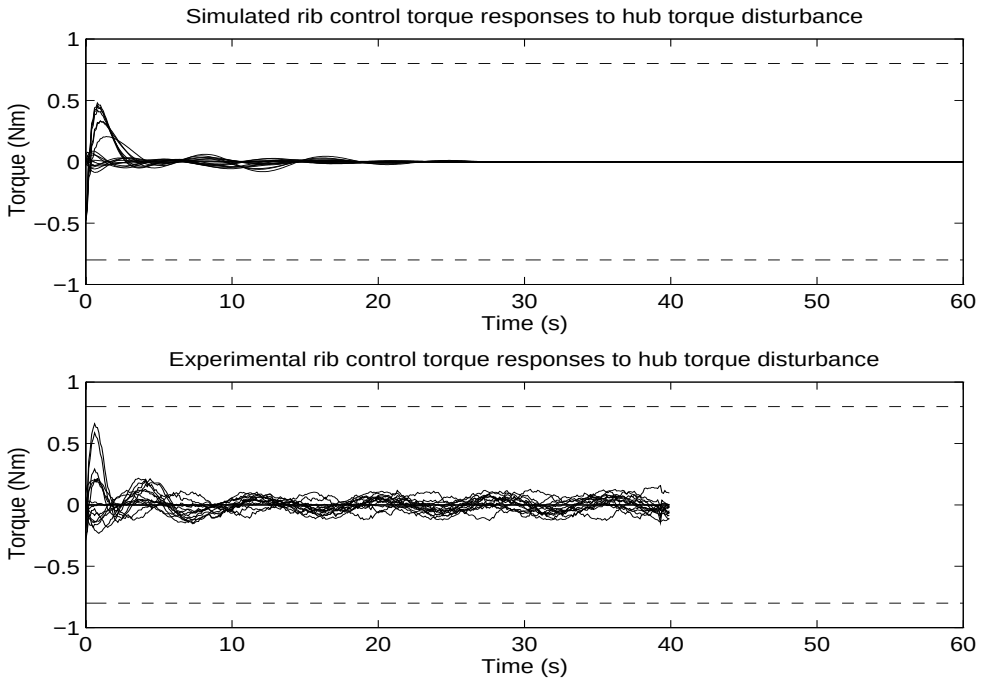

Figure 6.35: Sim. and exp. computed rib control torques for $\boldsymbol{K}_{p4d}$, $D(6.8\text{Nm}, 2s, z)$.

inflation. Implementation of these controllers was discussed and experimental responses to hub torque disturbances were presented. Some conclusions were drawn from these results. First, the collocated μ controller performed better than the $\mathcal{H}_\infty$ controller of §5.1.1.1 (as one would expect) since the results were more consistent with the simulations for all input disturbances used. Second, the noncollocated μ controller also appeared to have outperformed the $\mathcal{H}_\infty$ controller of §5.1.1.2 for x-axis and y-axis hub torque disturbances. But both controllers destabilized Daisy for z-axis disturbances, and it was pointed out that such input-dependent stability results were due to significant nonlinear effects in the noncollocated configuration. Further research on LFSS modeling, identification and nonlinear stability analysis will have to be undertaken before we can hope to obtain better experimental results in the noncollocated control of Daisy.

Chapter 7

Conclusion

7.1 Summary and Discussion

In Chapter 1, it was argued that perturbed coprime factor models of LFSS dynamics can capture most uncertainties present in FE models. Carrying this idea further in Chapter 2, we have introduced a left-coprime factorization in $\mathcal{H}_\infty$ of LFSS dynamics, together with a factor uncertainty bound $\boldsymbol{r}$. This bound has the property that the corresponding family of perturbed factorizations contains all LFSS plant models induced by variations in the modal parameters within some a priori known bounds — an interesting property for robust control design. It is also not too conservative in the sense that it tightly covers the worst-case factor perturbations induced by variations in the modal parameters. The factor uncertainty model can account for unmodeled dynamics as well, such as unmodeled modes or modeled modes not present in the plant, or uncertainty in actuator dynamics. Furthermore, this model has only one full perturbation in $\mathcal{RH}_\infty$ (one full complex block in the frequency domain) which makes the controller design a more tractable problem than a design for a model with real structured uncertainty.

We argued in Chapter 1 that the possibility of checking that a perturbed family of plant models can account for possibly noisy experimental data obtained on the actual plant may help the engineer improve the uncertainty model. Based on these consistency checks, the engineer can modify the uncertainty set (without making it too large) until all data are consistent with the model.

Chapter 3 introduces a general model/data consistency problem and specializes it to coprime factorizations and frequency-response data. For noisy data, it was shown that a good frequency-

domain approximation to the effect of $\mathcal{L}_\infty$ output noise corrupting the recorded signal in a frequency-response experiment is a complex additive perturbation of the noise-free frequency-response.

Consistency of perturbed coprime factor models with open-loop frequency-response measurements was studied in Chapter 3. The following cases were treated: (i) noise-free MIMO with standard coprime factorization; (ii) noise-free MIMO with special factorization for square LFSS model; (iii) general noisy SISO; (iv) noisy MIMO with standard coprime factorization of square plant. Necessary and sufficient conditions for model/data consistency were given for all these cases, except (iv) which is quite difficult. A practical sufficient condition was nonetheless provided for this case. Three numerical examples were presented to illustrate the results, two of which were using experimental frequency-response data obtained on a two-link flexible robot.

Frequency responses are very difficult or even impossible to obtain on lightly-damped systems such as LFSS, unless a feedback controller is implemented to add enough damping for the experiments to be carried out. Consistency of perturbed coprime factor models with closed-loop frequency-response measurements was studied in Chapter 4. It was pointed out that the main difficulty over the open-loop case is that a potential stable factor perturbation providing consistency must not only interpolate a set of matrices, but it must also stabilize the nominal closed-loop system. This is akin to a strong stabilization problem with norm and interpolation constraints, an unsolved problem. Hence, separate necessary and sufficient conditions were given for the following three cases: noise-free MIMO with standard coprime factorization; noise-free MIMO with special factorization for square LFSS model; general noisy SISO. A general sufficient condition applicable to all cases treated and based on a theorem of robust performance involving the structured singular value μ was given. Two numerical examples were worked out for the collocated model of Daisy to illustrate the separate necessary and sufficient conditions.

In Chapter 5, an $\mathcal{H}_\infty$ control design technique providing robust stability and nominal performance for LFSS was proposed. This technique is based on a nominal left-coprime factorization of LFSS dynamics as derived in Chapter 2, and requires a bound $\boldsymbol{r}$ on the factor uncertainty, and a weighting function $\boldsymbol{w}$ for performance. Given an FE model of the LFSS with bounds on the modal parameter uncertainties, an expression for a bound $\boldsymbol{r}$ covering this uncertainty was derived in Chapter 2. But this bound may be modified and improved upon by using frequency-response data as suggested in Chapters 3 and 4.

The general performance requirements for LFSS considered in Chapter 5 were: attitude

regulation, vibration attenuation, and tracking for accurate slewing maneuvers. Then an LFSS experimental testbed called Daisy and its model were described. Two $\mathcal{H}_\infty$ controllers were designed for collocated and noncollocated configurations of Daisy. These models have significant parameter uncertainty, yet the controllers designed using the coprime factorization technique were quite robust and achieved good performance levels in terms of rejection of hub torque disturbances in simulations.

Extensive experimentations with these controllers showed that the digital implementation of the collocated $\mathcal{H}_\infty$ controller performed very well without the need of any experimental tuning. A digital implementation of the noncollocated $\mathcal{H}_\infty$ controller was less successful at stabilizing Daisy even though the linear simulations showed good performance and robustness levels. Interestingly, the closed-loop stability of Daisy was input-dependent for this configuration: The experimental response to an x-axis hub torque disturbance was stable, but not the responses to y-axis and z-axis hub torque disturbances. Only nonlinearities such as the springs' force versus displacement characteristics and PWM thrusters in Daisy could explain this behaviour. These nonlinearities seemed to have greatly amplified effects in the noncollocated configuration, which is not really surprising since local feedback loops were missing on some of the ribs. At the risk of oversimplifying the problem, we can say that one of the basic properties of local feedback is that, in some cases, it can reduce the effect of localized nonlinearities [54].

In Chapter 6, we proposed a μ-synthesis design approach for robust performance based on the perturbed left-coprime factor model for LFSS introduced in Chapter 2. Our general performance objectives were attitude regulation and vibration attenuation when the LFSS is subjected to external torque disturbances. The torque disturbance rejection performance specification was explicitly introduced in the design problem.

The structured singular value was introduced and a brief account of μ-analysis and synthesis techniques for robust closed-loop stability and performance was given. The proposed μ-synthesis approach was used to design collocated and noncollocated controllers for Daisy, with the D-scales constrained to be constant matrices to avoid controller inflation. Implementation of these controllers was discussed and experimental responses to hub torque disturbances were presented.

Some conclusions were drawn from these results. First, as one would expect, the collocated μ controller performed better than the collocated $\mathcal{H}_\infty$ controller since the results were more consistent with the simulations for all input disturbances used. This shows evidence of robust

performance of the design: The closed-loop behaviour of the plant is heuristically close to the closed-loop behaviour of its nominal model in spite of significant model uncertainty. Second, the noncollocated μ controller also appeared to have outperformed the noncollocated $\mathcal{H}_\infty$ controller for x-axis and y-axis hub torque disturbances. But both controllers destabilized Daisy for z-axis disturbances, and it was pointed out that such input-dependent stability results were due to significant nonlinear effects in the noncollocated configuration.

7.2 Some Directions for Future Research

7.2.1 Coprime Factor Uncertainty Models

The bound $\boldsymbol{r}$ on the factor uncertainty in an LCF of LFSS dynamics introduced in Chapter 2 is guaranteed to cover the uncertainty in all plant models induced by variations in the modal parameters within some a priori known bounds. But it is not known to what extent this bound can cover unmodeled modes or modeled modes not present in the plant. It would be desirable to get a handle on how much undermodeling or overmodeling a bound $\boldsymbol{r}$ can cover.

One idea that comes to mind is to use the result on open-loop noise-free MIMO model/data consistency problem given in Chapter 3 as follows. Suppose that we want to test if a full-order LFSS plant model $\boldsymbol{G}_f$ lies in the family of perturbed plants $\mathcal{P}$ defined by a nominal reduced-order LCF and a bound on the factor uncertainty $\boldsymbol{r}$. Then we could use a fine grid of points over a large range of frequencies and evaluate $\boldsymbol{G}_f(j\omega)$ at each of these points. The resulting complex matrices are now our measurements used in a noise-free test of consistency with the family $\mathcal{P}$ as given by Theorem 2. If the data are consistent with $\mathcal{P}$, our intuition tells us that $\boldsymbol{G}_f$ is probably a member of $\mathcal{P}$.

Many things remain to be done for more complete solutions to the CF model/data consistency problems formulated in Chapters 3 and 4. For example, we only gave a sufficient condition for the noisy open-loop MIMO consistency problem (Problem 11). In view of Problem 12 and Lemma 9 which says that consistency is equivalent to a rank condition on some return difference matrix, we can see that what is needed is a structured Schmidt-Mirsky Theorem to get better sufficient conditions, and perhaps even a necessary and sufficient condition. But such a theorem would provide a natural generalization of the structured singular value μ, making this problem even more interesting.

The strong stabilization problem (Problem 22) with norm and interpolation constraints

introduced in Section 4.4 is a difficult one worth investigating. A complete solution to this problem, say in the form of conditions on the Q_i's, combined with the necessary conditions given for the different cases treated would yield necessary and sufficient conditions for the closed-loop consistency problems considered. Note that a necessary condition for the CF noisy closed-loop MIMO consistency problem is not yet available and will be the subject of further investigation.

7.2.2 Robust Control Design for LFSS

The experimental results obtained with the noncollocated controllers designed in Chapters 5 and 6 are interesting in that they reveal significant nonlinear effects in Daisy. It is believed that the most significant nonlinearities that have probably caused instability in the experiments are the thrusters' deadband and the nonlinear coupling springs. It would be worthwhile to carefully model these nonlinearities and develop tools for closed-loop stability analysis. Another step forward would be to enhance the $\mathcal{H}_\infty$ and μ control design techniques in order to get robustness to these types of nonlinearities.

Another interesting problem would be to try to adapt the perturbed LCF model of Chapter 2 to flexible systems with modes far apart such as flexible beams and flexible robots.

7.2.3 Controller Implementation on Daisy: PWM and Sampling Issues

Here we discuss two research problems arising on Daisy that are worth investigating. These problems are in fact generic for LFSS with PWM thrusters. The first problem is the modeling of the nonlinear PWM jet thrusters actuating the ribs. The second problem is performance degradation resulting from a sampled-data implementation of the controller at a low sampling rate.

7.2.3.1 PWM Jet Thrusters

Although Daisy was designed to have approximately linear dynamics, some of its components are nonlinear in nature, the main ones being the gas jet thrusters actuating the ribs. Such thrusters are difficult and expensive to design to be continuous devices because a force sensor and a feedback controller must then be implemented to control the forces they impart to the structure. However, the valves being easier to operate in an on-off fashion, it is often more convenient to use PWM of the thrust to obtain the desired force. This mode of operation can

be justified when the LFSS modal frequencies are much lower than the base pulse frequency. Then it is possible to assume that the structure acts as a low-pass filter on the pulsing forces such that the change in momentum is an average of the force signals and corresponds to desired forces. But when the fastest modes of the structure are close to the base pulse frequency, the linear assumption breaks down and a more detailed analysis must be performed.

It should be recognized that PWM embeds a sampling operation sometimes followed by a quantization operation before the modulation takes place. One particularly interesting recent paper [15] presents a way to model the effect of PWM actuators on LFSS dynamics as nonlinear input-dependent block perturbations at the inputs of the discretized LFSS dynamic model. This block perturbation model seems promising and should be investigated even though the perturbations are nonlinear and input-dependent. Another interesting reference is [46] that develops sufficient conditions for the asymptotic stability in the large of pulse-modulated feedback systems from the operator theoretic viewpoint.

7.2.3.2 Sampled-Data Controller Design

An LFSS controller is implemented using a computer and hence the closed-loop system can be modeled as a sampled-data system. Of course, the sampling frequency can be made high enough such that the controller behaves almost like a continuous-time one when compared to the slow LFSS dynamics. But there are two major motivations arising from slow sampling to look at optimal sampled-data control design methods (see e.g. [8]) instead of using discretized (sub)optimal continuous-time controllers. For a low sampling frequency, the performance of a discretized (sub)optimal continuous-time controller may degrade significantly.

The first motivation is the need to reduce power consumption on an LFSS to a minimum. The on-board computer's power consumption is roughly proportional to its clock frequency, hence a slow clock is desirable. Current space-qualified processors are relatively slow anyway. This in turn means that the sampling frequency should be kept as low as possible to allow enough time for the controller to perform the computations. Another side benefit of slow sampling is the possibility of letting the computer perform other tasks between sampling instants.

Further motivation to use a low sampling frequency is given by the PWM thrusters. It is important to use a pulse base frequency that is fast enough to make the thruster's effect seem approximately linear to the structure. However, the valves must have time to fully open and close during one pulse cycle, which sets an upper limit on the base pulse frequency. Given that

constraint, reducing the controller's sampling frequency will make the thrusters appear more linear because the number of pulse cycles per sampling period increases and hence the linear actuator assumption becomes more valid. Some PWM thruster systems might use a base pulse frequency equal to the sampling frequency, but it is not the case for Daisy which uses two different frequencies.

Appendix A

Coprime Factorizations in $\mathcal{RH}_\infty$

Consider the matrices $\tilde{\boldsymbol{M}} \in \mathcal{RH}_\infty^{n\times r}$ and $\tilde{\boldsymbol{N}} \in \mathcal{RH}_\infty^{n\times m}$. A square matrix $\boldsymbol{D} \in \mathcal{RH}_\infty^{n\times n}$ is said to be a *common left-divisor* of $\tilde{\boldsymbol{M}}$, $\tilde{\boldsymbol{N}}$ if $\tilde{\boldsymbol{M}} = \boldsymbol{D}\tilde{\boldsymbol{M}}_1$ and $\tilde{\boldsymbol{N}} = \boldsymbol{D}\tilde{\boldsymbol{N}}_1$ for some $\tilde{\boldsymbol{M}}_1$, $\tilde{\boldsymbol{N}}_1$ in $\mathcal{RH}_\infty$. A matrix $\boldsymbol{Q} \in \mathcal{RH}_\infty^{n\times l}$ is a *right-multiple* of $\boldsymbol{D}$ if $\boldsymbol{Q} = \boldsymbol{D}\boldsymbol{P}$ for some matrix $\boldsymbol{P} \in \mathcal{RH}_\infty^{n\times l}$. A matrix $\boldsymbol{D}_1$ is a *greatest common left-divisor* (GCLD) of $\tilde{\boldsymbol{M}}$ and $\tilde{\boldsymbol{N}}$ if it is also a right-multiple of all common left-divisors of $\tilde{\boldsymbol{M}}$, $\tilde{\boldsymbol{N}}$. Then, left-coprimeness of $\tilde{\boldsymbol{M}}$, $\tilde{\boldsymbol{N}}$ can be defined as follows [51]:

Definition A.1 The matrices $\tilde{\boldsymbol{M}} \in \mathcal{RH}_\infty^{n\times r}$ and $\tilde{\boldsymbol{N}} \in \mathcal{RH}_\infty^{n\times m}$ are *left-coprime* if every GCLD of $\tilde{\boldsymbol{M}}$ and $\tilde{\boldsymbol{N}}$ is a unit.

We now define a left-coprime factorization of a proper $n \times m$ real-rational transfer matrix $\boldsymbol{G}$.

Definition A.2 The matrices $\tilde{\boldsymbol{M}} \in \mathcal{RH}_\infty^{n\times n}$ and $\tilde{\boldsymbol{N}} \in \mathcal{RH}_\infty^{n\times m}$ form a *left-coprime factorization* of $\boldsymbol{G}$ if

1. $\det\left(\tilde{\boldsymbol{M}}\right) \neq 0$,
2. $\boldsymbol{G} = \tilde{\boldsymbol{M}}^{-1}\tilde{\boldsymbol{N}}$,
3. $\tilde{\boldsymbol{M}}$ and $\tilde{\boldsymbol{N}}$ are left-coprime.

From this definition, we can see that the pair $\left(\tilde{\boldsymbol{M}},\ \tilde{\boldsymbol{N}}\right)$ is left-coprime essentially iff no pole-zero cancellation occurs in $\overline{\mathbb{C}}_+ \cup \{\infty\}$ when the product $\tilde{\boldsymbol{M}}^{-1}\tilde{\boldsymbol{N}}$ is formed. That is, if a GCLD of $\left(\tilde{\boldsymbol{M}},\ \tilde{\boldsymbol{N}}\right)$ is not a unit, then pole-zero cancellations occur in $\overline{\mathbb{C}}_+ \cup \{\infty\}$ when the product

$\tilde{\boldsymbol{M}}^{-1}\tilde{\boldsymbol{N}}$ is formed. Conversely, if a pole-zero cancellation occurs when forming this product, then any GCLD of $\left(\tilde{\boldsymbol{M}},\ \tilde{\boldsymbol{N}}\right)$ is not a unit.

Two useful equivalent conditions for left-coprimeness in $\mathcal{RH}_\infty$ are given next.

Proposition 8 *The matrices $\tilde{\boldsymbol{M}} \in \mathcal{RH}_\infty^{n\times r}$ and $\tilde{\boldsymbol{N}} \in \mathcal{RH}_\infty^{n\times m}$ are* left-coprime *iff there exists a right-inverse of $\left[\begin{array}{cc} \tilde{\boldsymbol{M}} & \tilde{\boldsymbol{N}} \end{array}\right]$ in $\mathcal{RH}_\infty$, i.e. there exist $\boldsymbol{X}$, $\boldsymbol{Y}$ in $\mathcal{RH}_\infty$ of compatible dimensions such that*

$$\tilde{\boldsymbol{M}}\boldsymbol{X} + \tilde{\boldsymbol{N}}\boldsymbol{Y} = \left[\begin{array}{cc} \tilde{\boldsymbol{M}} & \tilde{\boldsymbol{N}} \end{array}\right] \left[\begin{array}{c} \boldsymbol{X} \\ \boldsymbol{Y} \end{array}\right] = I.$$

Equations of this form are known as *Bezout identities* or *Diophantine equations*.

Proposition 9 *The pair $\left(\tilde{\boldsymbol{M}},\ \tilde{\boldsymbol{N}}\right)$ is left-coprime iff $\left[\begin{array}{cc} \tilde{\boldsymbol{M}} & \tilde{\boldsymbol{N}} \end{array}\right]$ has full row rank in $\overline{\mathbb{C}}_+ \cup \{\infty\}$.*

See, e.g., [51] for a proof of Proposition 8. Proposition 9 is given as an exercise in [20, Probl. A.2].

Appendix B

Proof of Lemma 12

For convenience, the lemma is restated here.

Lemma 12 *Suppose that for* $\tilde{\Delta} \in \mathcal{B}\mathbb{C}^{n\times(n+p)}$, $\operatorname{rank}\left\{I - \mathcal{F}_L(H,\Phi^{-1})\tilde{\Delta}\right\} = n$ *and* $I - H_{11}\tilde{\Delta}$ *is singular. Then for* $\epsilon > 0$, *there exists a* $\tilde{\Delta}_0$ *with* $\|\tilde{\Delta}_0 - \tilde{\Delta}\| < \epsilon$ *such that* $\operatorname{rank}\left\{I - \mathcal{F}_L(H,\Phi^{-1})\tilde{\Delta}_0\right\} \leq n$ *and* $I - H_{11}\tilde{\Delta}_0$ *is nonsingular.*

Proof Since $\operatorname{rank}\left\{I - \mathcal{F}_L(H,\Phi^{-1})\tilde{\Delta}\right\} = n$, there exist p orthonormal vectors $z_1,\ldots,z_p$ in $\mathbb{C}^{p+n}$ such that

$$z_i = H_{11}\tilde{\Delta}z_i + H_{12}(I - \Phi^{-1}H_{22})^{-1}\Phi^{-1}H_{21}\tilde{\Delta}z_i,\quad i = 1,\ldots,p\,.$$

Let $Z := [z_1 \cdots z_p] \in \mathbb{C}^{(n+p)\times p}$. Then we can write the equivalent matrix equation

$$Z = H_{11}\tilde{\Delta}Z + H_{12}(\Phi - H_{22})^{-1}H_{21}\tilde{\Delta}Z. \tag{B.1}$$

Note that H_{11} has full column rank, and so does H_{12}. We first show that the square matrix $[H_{11}\ H_{12}]$ has full rank and hence forms a basis for $\mathbb{C}^{n+p}$. Factorize $[H_{11}\ H_{12}]$ as follows:

$$\begin{bmatrix} H_{11} & H_{12} \end{bmatrix} = \begin{bmatrix} r(I + K_2K_1C\tilde{M}^{-1}\tilde{N})^{-1} & 0 \\ 0 & r(I + \tilde{M}^{-1}\tilde{N}K_2K_1C)^{-1} \end{bmatrix} \cdot \begin{bmatrix} -K_2K_1C & I \\ I & \tilde{M}^{-1}\tilde{N} \end{bmatrix} \cdot \begin{bmatrix} \tilde{M}^{-1} & 0 \\ 0 & K_2 \end{bmatrix}.$$

Obviously the matrices premultiplying and postmultiplying $\begin{bmatrix} -K_2K_1C & I \\ I & \tilde{M}^{-1}\tilde{N} \end{bmatrix}$ on the right-hand side are nonsingular, so we only have to check that this matrix is itself nonsingular.

Multiplying this matrix by $\begin{bmatrix} I & K_2K_1C \\ 0 & I \end{bmatrix}$ on the left and by $\begin{bmatrix} 0 & I \\ I & 0 \end{bmatrix}$ on the right, we get $\begin{bmatrix} I + K_2K_1C\tilde{M}^{-1}\tilde{N} & 0 \\ \tilde{M}^{-1}\tilde{N} & I \end{bmatrix}$ which is invertible by our assumption of nominal stability. Therefore $[H_{11}\ H_{12}]$ is invertible and hence forms a basis for $\mathbb{C}^{n+p}$.

Let $Q \in \mathbb{C}^{(n+p)\times n}$ be such that $[Z\ Q]$ is a square orthonormal matrix. Consider the perturbation

$$\tilde{\Delta}_0 := \tilde{\Delta} + \epsilon_0 \epsilon Q^*,$$

where $0 < \epsilon_0 < 1$. Obviously, (B.1) still holds with $\tilde{\Delta}_0$, so $\operatorname{rank}\left\{ I - \mathcal{F}_L(H, \Phi^{-1})\tilde{\Delta}_0 \right\} = n$. Moreover, $\|\tilde{\Delta}_0 - \tilde{\Delta}\| = \epsilon_0 \epsilon \|Q^*\| = \epsilon_0 \epsilon < \epsilon$.

Finally, consider $I - H_{11}\tilde{\Delta}_0$. Multiply this matrix on the right by the nonsingular matrix $[Z\ Q]$ to get

$$(I - H_{11}\tilde{\Delta}_0) \begin{bmatrix} Z & Q \end{bmatrix} = \begin{bmatrix} Z - H_{11}\tilde{\Delta}Z & (I - H_{11}\tilde{\Delta})Q - \epsilon_0 \epsilon H_{11} \end{bmatrix}. \tag{B.2}$$

But from (B.1), $Z - H_{11}\tilde{\Delta}Z = H_{12}(\Phi - H_{22})^{-1}H_{21}\tilde{\Delta}Z$, and this matrix has full column rank as we now show. Assume $H_{12}(\Phi - H_{22})^{-1}H_{21}\tilde{\Delta}Zw = 0$. We must show that $w = 0$. Let $y := Zw$; then we must have

$$y - H_{11}\tilde{\Delta}y = 0 \quad \text{and} \quad H_{21}\tilde{\Delta}y = 0.$$

From the definition of H_{21}, the latter equation implies that $C\tilde{M}^{-1}\tilde{\Delta}y = 0$. This means that there is an *open-loop* internal unstable mode (the modal vector being y) unobservable through C. But this contradicts our assumption that for $\mathbf{\Delta} \in \mathcal{D}_r$, the pair $(C,\ \tilde{\boldsymbol{M}}_p)$ is right-coprime, which implies observability of all open-loop unstable modes. Hence $y = 0$, and since Z has full column rank, it follows that $w = 0$.

Thus $H_{12}(\Phi - H_{22})^{-1}H_{21}\tilde{\Delta}Z$ has full column rank, and it follows that the $p \times p$ matrix $R := (\Phi - H_{22})^{-1}H_{21}\tilde{\Delta}Z$ is invertible. Now (B.2) can be rewritten as:

$$(I - H_{11}\tilde{\Delta}_0) \begin{bmatrix} Z & Q \end{bmatrix} = \begin{bmatrix} H_{12}R & (I - H_{11}\tilde{\Delta})Q - \epsilon_0 \epsilon H_{11} \end{bmatrix}.$$

Since $[H_{11}\ H_{12}]$ is invertible, we can define two matrices U_1 and U_2 by

$$\begin{bmatrix} U_1 \\ U_2 \end{bmatrix} := \begin{bmatrix} H_{11} & H_{12} \end{bmatrix}^{-1} (I - H_{11}\tilde{\Delta})Q$$

so that

$$(I - H_{11}\tilde{\Delta})Q = H_{11}U_1 + H_{12}U_2,$$

where $U_1 \in \mathbb{C}^{n\times n}$ and $U_2 \in \mathbb{C}^{p\times n}$. Thus

$$(I - H_{11}\tilde{\Delta}_0)\begin{bmatrix} Z & Q \end{bmatrix} = \begin{bmatrix} H_{12} & H_{11} \end{bmatrix}\begin{bmatrix} R & U_2 \\ 0 & U_1 - \epsilon_0\epsilon I \end{bmatrix} =: T,$$

and $\epsilon_0 < 1$ is chosen so that $(U_1 - \epsilon_0\epsilon I)$ is nonsingular. Then T has full rank $n+p$, and it follows that $(I - H_{11}\tilde{\Delta}_0)$ also has full rank $n+p$. ■

Appendix C

Proof of Lemma 14

We will need the following simple result in the proof of Lemma 14.

Lemma 16 *Let U, $S \in \mathbb{C}^{(n+1)\times n}$ with the columns of U orthogonal, and the columns of S linearly independent. Let $z \in \mathbb{C}^{n+1}$ be orthogonal to the columns of U and assume that $z \notin span\{S\}$. Then U^*S is nonsingular.*

Proof For a contradiction, suppose U^*S is singular. Then there exists a nonzero $w \in \mathbb{C}^n$ such that $U^*Sw = 0$. That is, the columns of U are all orthogonal to Sw. But since z is also orthogonal to all columns of U, there must exist a nonzero $c \in \mathbb{C}$ such that $Sw = cz$, a contradiction. Hence, U^*S must be nonsingular. ■

For convenience, Lemma 14 is restated here.

Lemma 14 *For $\tilde{\Delta}_s \in \mathcal{B}\Gamma$ with $I - V_{11}\tilde{\Delta}_s$ and $I - \mathcal{F}_L(V, \phi^{-1})\tilde{\Delta}_s$ singular, and for $\epsilon > 0$, $\exists\, \tilde{\Delta}_{s0} \in \Gamma$, $\|\tilde{\Delta}_{s0} - \tilde{\Delta}_s\| < \epsilon$ such that $I - \mathcal{F}_L(V, \phi^{-1})\tilde{\Delta}_{s0}$ is singular and $I - V_{11}\tilde{\Delta}_{s0}$ is nonsingular.*

Proof By the singularity of $I - \mathcal{F}_L(V, \phi^{-1})\tilde{\Delta}_s$, $\exists\, 0 \neq z \in \mathbb{C}^{n+2}$ such that

$$z = V_{11}\tilde{\Delta}_s z + qV_{12}V_{21}\tilde{\Delta}_s z \tag{C.1}$$

Let $\begin{bmatrix} z_1 \\ \vdots \\ z_{n+2} \end{bmatrix} := z$. We first show that $\begin{bmatrix} z_1 \\ \vdots \\ z_{n+1} \end{bmatrix} \neq 0$. Suppose not. Then (C.1) yields

$$z = qV_{12}V_{21}\begin{bmatrix} 0 \\ z_{n+2}\tilde{\delta}_a \end{bmatrix} = qL_a z_{n+2}\tilde{\delta}_a V_{12}.$$

But $q \neq 0$, $L_a \neq 0$, and $z_{n+2}\tilde{\delta}_a \neq 0$ otherwise we would have $z = 0$. Hence,

$$z = qL_a z_{n+2}\tilde{\delta}_a \begin{bmatrix} rd^{-1}k_2 \\ rd^{-1}k_2\tilde{M}^{-1}\tilde{N} \\ 1 \end{bmatrix},$$

and since $rd^{-1}k_2 \neq 0$, $\begin{bmatrix} z_1 \\ \vdots \\ z_{n+1} \end{bmatrix} \neq 0$, a contradiction. Thus, $\begin{bmatrix} z_1 \\ \vdots \\ z_{n+1} \end{bmatrix} \neq 0$ and its left-nullspace $\mathcal{N}_L\left\{\begin{bmatrix} z_1 \\ \vdots \\ z_{n+1} \end{bmatrix}\right\}$ has dimension n.

Let us now rewrite (C.1) with $v := \tilde{\Delta}\begin{bmatrix} z_1 \\ \vdots \\ z_{n+1} \end{bmatrix}$.

$$\begin{aligned} z &= V_{11}\begin{bmatrix} v \\ 0 \end{bmatrix} + qV_{12}\begin{bmatrix} d^{-1}C\tilde{M}^{-1} & L_a \end{bmatrix}\begin{bmatrix} v \\ z_{n+2}\tilde{\delta}_a \end{bmatrix} \\ &= \begin{bmatrix} -d^{-1}rk_1k_2C\tilde{M}^{-1} \\ r(I + \tilde{M}^{-1}\tilde{N}k_1k_2C)^{-1}\tilde{M}^{-1} \\ 0 \end{bmatrix} v + (qd^{-1}C\tilde{M}^{-1}v + qz_{n+2}L_a\tilde{\delta}_a)\begin{bmatrix} rd^{-1}k_2 \\ rd^{-1}k_2\tilde{M}^{-1}\tilde{N} \\ 1 \end{bmatrix} \end{aligned} \quad \text{(C.2)}$$

Given $\epsilon > 0$, we will construct a perturbation $\tilde{\Delta}_{s0}$ as follows.

$$\tilde{\Delta}_{s0} = \begin{bmatrix} \tilde{\Delta} + \epsilon Q^* & 0 \\ 0 & \tilde{\delta}_a \end{bmatrix},$$

where $Q^* \in \mathcal{N}_L\left\{\begin{bmatrix} z_1 \\ \vdots \\ z_{n+1} \end{bmatrix}\right\}$ has linearly independent rows and $\|Q\| < 1$. From (C.1), it is easily seen that $I - \mathcal{F}_L(V, \phi^{-1})\tilde{\Delta}_{s0}$ is still singular. Now consider $I - V_{11}\tilde{\Delta}_s$ which is singular,

that is,

$$\det(I - V_{11}\tilde{\Delta}_s) = \det(I - \tilde{\Delta}_s V_{11}) = 0.$$

An equivalent condition is that there exists a nonzero $y \in \mathbb{C}^{n+1}$ such that $y = \tilde{\Delta}_s V_{11} y$, which expands to

$$\begin{bmatrix} y_1 \\ y_2 \end{bmatrix} = \begin{bmatrix} -d^{-1}rk_1k_2\tilde{\Delta}NC\tilde{M}^{-1} + r(I + \tilde{M}^{-1}\tilde{N}k_1k_2C)^{-1}\tilde{M}^{-1} & 0 \\ 0 & 0 \end{bmatrix} \begin{bmatrix} y_1 \\ y_2 \end{bmatrix},$$

where $\begin{bmatrix} y_1 \\ y_2 \end{bmatrix} := y,\ y_1 \in \mathbb{C}^n,\ y_2 \in \mathbb{C}$. This is equivalent to: $\exists 0 \neq y_1 \in \mathbb{C}^n$ such that

$$y_1 = \begin{bmatrix} \tilde{\Delta}N & -\tilde{\Delta}M \end{bmatrix} \begin{bmatrix} -d^{-1}rk_1k_2C\tilde{M}^{-1} \\ r(I + \tilde{M}^{-1}\tilde{N}k_1k_2C)^{-1}\tilde{M}^{-1} \end{bmatrix} y_1. \tag{C.3}$$

Let $H := \begin{bmatrix} -d^{-1}rk_1k_2C\tilde{M}^{-1} \\ r(I + \tilde{M}^{-1}\tilde{N}k_1k_2C)^{-1}\tilde{M}^{-1} \end{bmatrix}$. Then for $I - V_{11}\tilde{\Delta}_{s0}$, this singularity condition simply goes as follows. There exists a nonzero $y_1 \in \mathbb{C}^n$ such that

$$y_1 = \left(\begin{bmatrix} \tilde{\Delta}N & -\tilde{\Delta}M \end{bmatrix} + \epsilon Q^* \right) H y_1.$$

Equivalently, the matrix $\left(\begin{bmatrix} \tilde{\Delta}N & -\tilde{\Delta}M \end{bmatrix} + \epsilon Q^* \right) H$ has at least one eigenvalue equal to 1. Thus the idea here is to decompose $Q^* = WQ_0^*$ where $W \in \mathbb{C}^{n \times n}$ is invertible and Q_0^* has orthonormal rows, and to show that $Q_0^* H$ is invertible using Lemma 16. In this case, the extra degrees of freedom provided by W allows us to perturb all eigenvalues of $\begin{bmatrix} \tilde{\Delta}N & -\tilde{\Delta}M \end{bmatrix} H$ equal to one, thereby making $I - V_{11}\tilde{\Delta}_{s0}$ nonsingular. In order to show that $Q_0^* H$ is invertible, we have to analyze equation (C.2) to find out whether or not $\begin{bmatrix} z_1 \\ \vdots \\ z_{n+1} \end{bmatrix}$ is a linear combination of the columns of H. For convenience, we rewrite the upper part of (C.2);

$$\begin{bmatrix} z_1 \\ \begin{bmatrix} z_2 \\ \vdots \\ z_{n+1} \end{bmatrix} \end{bmatrix} = \begin{bmatrix} -d^{-1}rk_1k_2C\tilde{M}^{-1}v \\ r(I + \tilde{M}^{-1}\tilde{N}k_1k_2C)^{-1}\tilde{M}^{-1}v \end{bmatrix} + (qd^{-1}C\tilde{M}^{-1}v + qz_{n+2}L_a\tilde{\delta}_a) \begin{bmatrix} rd^{-1}k_2 \\ rd^{-1}k_2\tilde{M}^{-1}\tilde{N} \end{bmatrix}. \tag{C.4}$$

Obviously, the first term on the right-hand side lies in span$\{H\}$. We now show that the second term on the right-hand side does not lie in this subspace, i.e. $\begin{bmatrix} 1 \\ \tilde{M}^{-1}\tilde{N} \end{bmatrix} \notin \text{span}\{H\}$. Suppose

for a contradiction that $\exists\, w \neq 0$ such that

$$\begin{bmatrix} -d^{-1}rk_1k_2C\tilde{M}^{-1} \\ r(I+\tilde{M}^{-1}\tilde{N}k_1k_2C)^{-1}\tilde{M}^{-1} \end{bmatrix} w = \begin{bmatrix} 1 \\ \tilde{M}^{-1}\tilde{N} \end{bmatrix}. \tag{C.5}$$

Then,

$$r(I+\tilde{M}^{-1}\tilde{N}k_1k_2C)^{-1}\tilde{M}^{-1}w = r\tilde{M}^{-1}(I+\tilde{N}k_1k_2C\tilde{M}^{-1})^{-1}w = \tilde{M}^{-1}\tilde{N}.$$

Solving for w, we get

$$w = r^{-1}(I+\tilde{N}k_1k_2C\tilde{M}^{-1})\tilde{N} = r^{-1}\tilde{N}(1+k_1k_2C\tilde{M}^{-1}\tilde{N}) = r^{-1}d\tilde{N}.$$

Substituting this expression for w in the upper part of (C.5), we obtain

$$1 + k_1k_2C\tilde{M}^{-1}\tilde{N} = d = 0,$$

a contradiction. Hence, $\begin{bmatrix} z_1 \\ \vdots \\ z_{n+1} \end{bmatrix} \notin \text{span}\{H\}$ if the second term on the right-hand side of (C.4) is nonzero, i.e. if $qd^{-1}C\tilde{M}^{-1}v + qz_{n+2}L_a\tilde{\delta}_a \neq 0$. We now show that this condition always hold. Suppose for a contradiction that it does not hold. From the block diagram of Figure C.1, it is seen that

$$z_{n+2} = \phi^{-1}\left(d^{-1}C\tilde{M}^{-1}v + z_{n+2}L_a\tilde{\delta}_a\right).$$

Thus $qd^{-1}C\tilde{M}^{-1}v + qz_{n+2}L_a\tilde{\delta}_a = 0$ implies $z_{n+2} = 0$, and these imply $C\tilde{M}^{-1}v = 0$, $z_1 = 0$ and $C\begin{bmatrix} z_2 \\ \vdots \\ z_{n+1} \end{bmatrix} = 0$. then (C.2) becomes

$$z = \begin{bmatrix} 0 \\ r(I+\tilde{M}^{-1}\tilde{N}k_1k_2C)^{-1}\tilde{M}^{-1}v \\ 0 \end{bmatrix},$$

which implies

$$\begin{bmatrix} z_2 \\ \vdots \\ z_{n+1} \end{bmatrix} = r(I+\tilde{M}^{-1}\tilde{N}k_1k_2C)^{-1}\tilde{M}^{-1}\begin{bmatrix} \tilde{\Delta}N & -\tilde{\Delta}M \end{bmatrix}\begin{bmatrix} 0 \\ \begin{bmatrix} z_2 \\ \vdots \\ z_{n+1} \end{bmatrix} \end{bmatrix}$$

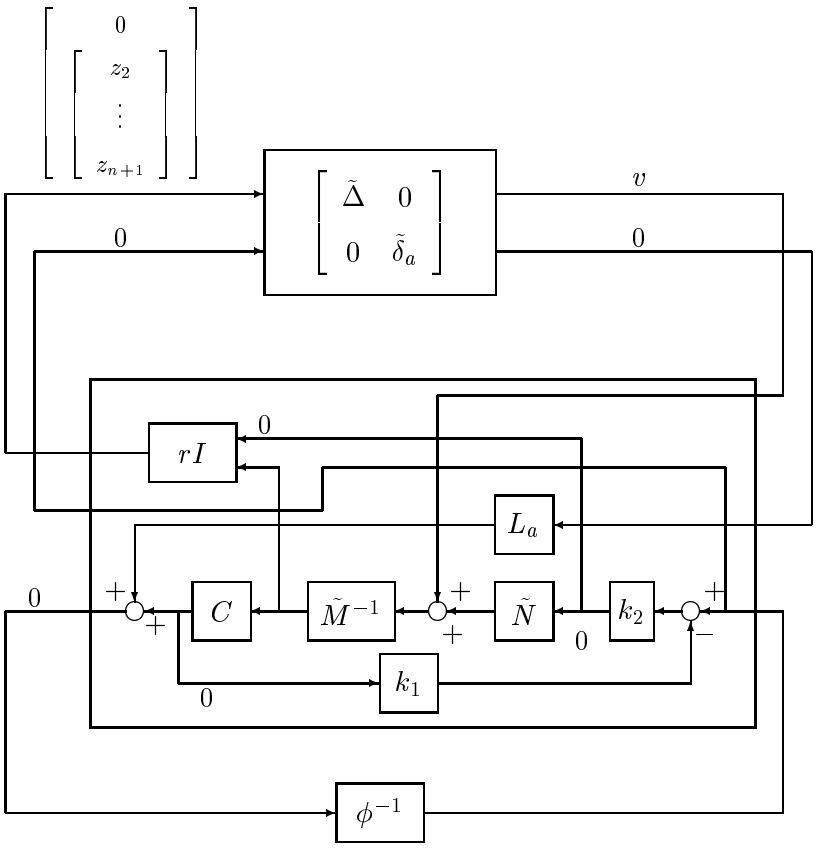

Figure C.1: Feedback diagram showing a solution that leads to a contradiction

$$= \quad r(I + \tilde{M}^{-1}\tilde{N}k_1k_2C)^{-1}\tilde{M}^{-1}\tilde{\Delta}M \begin{bmatrix} z_2 \\ \vdots \\ z_{n+1} \end{bmatrix}.$$

Premultiplying the last equation by $\tilde{M}(I + \tilde{M}^{-1}\tilde{N}k_1k_2C)$ yields

$$\tilde{M} \begin{bmatrix} z_2 \\ \vdots \\ z_{n+1} \end{bmatrix} = r\tilde{\Delta}M \begin{bmatrix} z_2 \\ \vdots \\ z_{n+1} \end{bmatrix},$$

and it follows that $\tilde{M} + r\tilde{\Delta}M$ is singular. This means that the open-loop transfer function matrix $(\tilde{\boldsymbol{M}} + \Delta\boldsymbol{M})(s)$ has a pole at $s = j\omega$, and the corresponding complex modal vector $\begin{bmatrix} z_2 \\ \vdots \\ z_{n+1} \end{bmatrix}$ is unobservable since $C \begin{bmatrix} z_2 \\ \vdots \\ z_{n+1} \end{bmatrix} = 0$. But since $\|\tilde{\Delta}\| < 1$, this contradicts our assumption that all unstable modes in the perturbed model be observable when $\|\tilde{\boldsymbol{\Delta}}\|_\infty < 1$, and hence $d^{-1}C\tilde{M}^{-1}v + z_{n+2}L_a\tilde{\delta}_a \neq 0$.

To recap, the second term on the right-hand side of (C.4) is always nonzero and therefore $\begin{bmatrix} z_1 \\ \vdots \\ z_{n+1} \end{bmatrix} \notin \text{span}\{H\}$. Now H has linearly independent columns, and Q_0 has orthonormal columns, all orthogonal to $\begin{bmatrix} z_1 \\ \vdots \\ z_{n+1} \end{bmatrix}$. Thus Lemma 16 applies and Q_0^*H is invertible. From (C.3), the matrix $\begin{bmatrix} \tilde{\Delta}N & -\tilde{\Delta}M \end{bmatrix} H$ has at least one eigenvalue equal to one, so we have to show that there exists an invertible W that will move those eigenvalues away from 1 in $\begin{bmatrix} \tilde{\Delta}N & -\tilde{\Delta}M \end{bmatrix} H + \epsilon W Q_0^* H$, while keeping $\|\tilde{\Delta}_{s0} - \tilde{\Delta}_s\| < \epsilon$. Let $S := \begin{bmatrix} \tilde{\Delta}N & -\tilde{\Delta}M \end{bmatrix} H$. Pick $W = \epsilon_0 \|S\|^{-1} \underline{\sigma}(Q_0^*H) S (Q_0^*H)^{-1}$, where $\epsilon_0 < 1$. Then,

$$S + \epsilon W Q_0^* H = S + \epsilon\epsilon_0 \|S\|^{-1} \underline{\sigma}(Q_0^*H) S = (1 + \epsilon\epsilon_0 \|S\|^{-1} \underline{\sigma}(Q_0^*H)) S.$$

All the eigenvalues $\{\lambda_i\}_{i=1}^n$ of S are moved to $\{(1 + \epsilon\epsilon_0 \|S\|^{-1} \underline{\sigma}(Q_0^*H))\lambda_i\}_{i=1}^n$, so $\epsilon_0 < 1$ can be adjusted so that they all differ from 1. This choice of $Q^* = WQ_0^*$ for $\tilde{\Delta}_{s0}$ makes $I - V_{11}\tilde{\Delta}_{s0}$ nonsingular and

$$\|\tilde{\Delta}_{s0} - \tilde{\Delta}_s\| \quad = \quad \left\| \begin{bmatrix} \epsilon\epsilon_0 \|S\|^{-1} \underline{\sigma}(Q_0^*H) S (Q_0^*H)^{-1} Q_0 & 0 \\ 0 & 0 \end{bmatrix} \right\|$$

$$
\begin{aligned}
&= \epsilon\epsilon_0 \|S\|^{-1} \underline{\sigma}(Q_0^* H) \left\| S(Q_0^* H)^{-1} Q_0 \right\| \\
&\leq \epsilon\epsilon_0 \|S\|^{-1} \underline{\sigma}(Q_0^* H) \|S\| \underline{\sigma}(Q_0^* H)^{-1} \|Q_0\| \\
&\leq \epsilon.
\end{aligned}
$$

Moreover, $I - \mathcal{F}_L(V, \phi^{-1})\tilde{\Delta}_{s0}$ is still singular because $z = \mathcal{F}_L(V, \phi^{-1})\tilde{\Delta}_{s0} z$ readily reduces to (C.1). ■

Bibliography

[1] G. J. Balas and J. C. Doyle. Robustness and performance tradeoffs in control design for flexible structures. In *Proceedings of the American Control Conference*, 1991.

[2] G. J. Balas, J. C. Doyle, K. Glover, A. Packard, and R. S. R. Smith. *μ-Analysis and Synthesis Toolbox: User's Guide.* The Mathworks Inc., 1991.

[3] D. S. Bayard, Y. Yam, and E. Mettler. A criterion for joint optimization of identification and robust control. *IEEE Transactions on Automatic Control*, AC-37(7):986–991, July 1992.

[4] B. Boulet, B. A. Francis, P. C. Hughes, and T. Hong. Robust $\mathcal{H}_\infty$ control of large flexible space structures using a coprime factor plant description. Technical Report 9401, Department of Electrical and Computer Engineering, University of Toronto, January 1994.

[5] R. P. Braatz, P. M. Young, J. C. Doyle, and M. Morari. Computational complexity of μ calculation. *IEEE Transactions on Automatic Control*, AC-39(5):1000–1002, May 1994.

[6] S. A. Buddie, T. T. Georgiou, Ü. Özgüner, and M. C. Smith. Flexible structure experiment at JPL and WPAFB: $\mathcal{H}_\infty$ controller designs. *International Journal of Control*, 58(1):1–19, 1993.

[7] J. Chen, C. N. Nett, and M. K. H. Fan. Worst-case system identification in $\mathcal{H}_\infty$: validation of a priori information, essentially optimal algorithms, and error bounds. In *Proceedings of the American Control Conference*, pages 251–257, 1992.

[8] T. Chen and B. A. Francis. *Sampled-Data Control Systems.* Lecture Notes in Control and Information Sciences. Springer-Verlag, 1995.

[9] E. G. Collins, Jr., D. J. Phillips, and D. C. Hyland. Robust decentralized control laws for the ACES structure. *IEEE Control Systems Magazine*, 11(3):62–70, April 1991.

[10] G. W. Crocker, P. C. Hughes, and T. Hong. Real-time computer control of a flexible spacecraft emulator. *IEEE Control Systems Magazine*, 10(1):3–8, January 1990.

[11] E. J. Davison, W. Gesing, and S. H. Wang. An algorithm for obtaining the minimal realization of a linear time-invariant system and determining if a system is stabilizable-detectable. *IEEE Transactions on Automatic Control*, AC-23(6):1048–1054, December 1978.

[12] P. H. Delsarte, Y. Genin, and Y. Kamp. The Nevanlinna-Pick problem for matrix-valued functions. *SIAM Journal of Applied Mathematics*, 36(1):47–61, February 1979.

[13] J. C. Doyle. Analysis of feedback systems with structured uncertainties. *IEE Proceedings Part D*, 129(6):242–250, November 1982.

[14] J. C. Doyle, K. Glover, P. P. Khargonekar, and B. A. Francis. State-space solutions to standard $\mathcal{H}_2$ and $\mathcal{H}_\infty$ control problems. *IEEE Transactions on Automatic Control*, AC-34(8):831–847, August 1989.

[15] M. Elgersma, G. Stein, M. Jackson, R. Matulenko, and B. Caldwell. Space station attitude control using reaction control jets. In *Proceedings of the IEEE Conference on Decision and Control*, 1992.

[16] M. K. H. Fan, A. L. Tits, and J. C. Doyle. Robustness in the presence of mixed parametric uncertainty and unmodeled dynamics. *IEEE Transactions on Automatic Control*, AC-36(1):25–38, January 1991.

[17] I. P. Fedčina. A criterion for the solvability of the Nevanlinna-Pick tangent problem. *Mat. Issled.*, 7(vyp.4(26)):213–227, 1972.

[18] B. A. Francis. *A Course in $\mathcal{H}_\infty$ Control Theory.* Lecture Notes in Control and Information Sciences. Springer-Verlag, 1987.

[19] M. R. Garey and D. S. Johnson. *Computers and Intractability: A Guide to NP-Completeness.* Freeman, San Francisco, 1979.

[20] M. Green and D. J. N. Limebeer. *Linear Robust Control.* Information and System Sciences Series. Prentice Hall, 1995.

[21] C. Z. Gregory Jr. Reduction of large flexible spacecraft models using internal balancing theory. *AIAA Journal of Guidance, Control and Dynamics*, 7(6):725–732, Nov.-Dec. 1984.

[22] G. Gu, D. Xiong, and K. Zhou. Identification in $\mathcal{H}_\infty$ using Pick's interpolation. *Systems and Control Letters*, 20:263–272, November 1993.

[23] R. A. Horn and C. R. Johnson. *Matrix Analysis.* Cambridge University Press, 1990.

[24] J. P. How, W. M. Haddad, and S. R. Hall. Robust control synthesis examples with real parameter uncertainty using the Popov criterion. In *Proceedings of the American Control Conference*, San Francisco, June 1993.

[25] J. P. How, S. R. Hall, and W. M. Haddad. Robust controllers for the middeck active control experiment using Popov controller synthesis. *IEEE Transactions on Control Systems Technology*, 2(2):73–87, June 1994.

[26] S. M. Joshi. *Control of Large Flexible Space Structures.* Springer-Verlag, New-York, 1989.

[27] P. P. Khargonekar and A. Tannenbaum. Non-euclidean metrics and the robust stabilization of systems with parameter uncertainty. *IEEE Transactions on Automatic Control*, AC-30(10):1005–1013, October 1985.

[28] R. L. Kosut, M. K. Lau, and S. P. Boyd. Set-membership identification of systems with parametric and nonparametric uncertainty. *IEEE Transactions on Automatic Control*, AC-37(7):929–941, July 1992.

[29] D. G. Laurin. *Development of an Optical Imaging System for Shape Monitoring of Large Flexible Structures.* PhD thesis, Department of Aerospace Engineering, University of Toronto, 1992.

[30] F. C. Lee, H. Flashner, and M. G. Safonov. Positivity embedding for noncolocated and non-square flexible structures. In *Proceedings of the American Control Conference*, Baltimore, Maryland, June 1994.

[31] K. B. Lim and G. J. Balas. Line-of-sight control of the CSI evolutionary model: μ control. In *Proceedings of the American Control Conference*, 1992.

[32] K. B. Lim, P. G. Maghami, and S. M. Joshi. Comparison of controller designs for an experimental flexible structure. *IEEE Control Systems Magazine*, 12(3):108–118, June 1992.

[33] A. P. Low, G. O. Corrêa, and I. Postlethwaite. Estimation of uncertainty bounds for robustness analysis. *IEE Proceedings Part D*, 134, 1987.

[34] D. C. McFarlane and K. Glover. *Robust Controller Design Using Normalized Coprime Factor Plant Descriptions.* Lecture Notes in Control and Information Sciences. Springer-Verlag, 1990.

[35] D. G. Meyer. A fractional approach to model reduction. In *Proceedings of the American Control Conference*, Atlanta, 1988.

[36] M. R. Michez. Identification of a single and dual link flexible system. Master's thesis, Department of Electrical and Computer Engineering, University of Toronto, 1995.

[37] B. C. Moore. Principal component analysis in linear systems: Controllability, observability, and model reduction. *IEEE Transactions on Automatic Control*, AC-26(1):17–32, February 1981.

[38] Yu. Nesterov and A. Nemirovsky. *Interior-Point Polynomial Methods in Convex Programming.* Studies in Applied Mathematics, Vol. 13. SIAM, Philadelphia, PA, 1994.

[39] K. Poolla, P. P. Khargonekar, A. Tikku, J. Krause, and K. Nagpal. A time-domain approach to model validation. *IEEE Transactions on Automatic Control*, AC-39(5):951–959, May 1994.

[40] K. R. Popper. *The Logic of Scientific Discovery.* Basic books, New-York, 1959.

[41] R. Redheffer. Inequalities for a matrix Riccati equation. *Journal of Mathematics and Mechanics*, 8(3):349–367, 1959.

[42] I. W. Sandberg. On the $\mathcal{L}_2$-boundedness of solutions of nonlinear functional equations. *Bell System Technical Journal*, 43:1581–1599, 1964.

[43] G. B. Sincarsin. Laboratory demonstration of control techniques for third generation spacecraft: Detailed design. Technical Report Daisy-9, Dynacon, March 1984.

[44] G. B. Sincarsin and W. G. Sincarsin. Development of flexible spacecraft control systems: Qualification tests. Technical Report Daisy-19, Dynacon, September 1985.

[45] R. E. Skelton and P. C. Hughes. Modal cost analysis for linear matrix-second-order systems. *ASME Journal of Dynamic Systems, Measurement, and Control*, 102:151–158, September 1980.

[46] R. A. Skoog and G. L. Blankenship. Generalized pulse-modulated feedback systems: Norms, gains, Lipschitz constants, and stability. *IEEE Transactions on Automatic Control*, AC-15(3):300–315, June 1970.

[47] R. S. Smith, C.-C. Chu, and J. L. Fanson. The design of $\mathcal{H}_\infty$ controllers for an experimental non-collocated flexible structure problem. *IEEE Transactions on Control Systems Technology*, 2(2):101–109, June 1994.

[48] R. S. R. Smith. *Model Validation for Uncertain Systems.* PhD thesis, California Institute of Technology, 1990.

[49] D. W. Sparks Jr. and J.-N. Juang. Survey of experiments and experimental facilities for control of flexible structures. *AIAA Journal of Guidance, Control and Dynamics*, 15(4):801–816, July-August 1992.

[50] G. W. Stewart and J. G. Sun. *Matrix Perturbation Theory.* Academic Press, San Diego, 1990.

[51] M. Vidyasagar. *Control System Synthesis: a Coprime Factorization Approach.* MIT Press, 1985.

[52] M. Vidyasagar and N. Viswanadham. Algebraic design techniques for reliable stabilization. *IEEE Transactions on Automatic Control*, AC-27(5):1085–1095, October 1982.

[53] D. C. Youla, J. J. Bongiorno, Jr., and C. N. Lu. Single-loop feedback stabilization of linear multivariable plants. *Automatica*, 10:159–173, 1974.

[54] G. Zames. Functional analysis applied to nonlinear feedback systems. *IEEE Transactions on Circuit Theory*, pages 392–404, September 1963.

[55] G. Zames. On the input-output stability of time-varying nonlinear feedback systems, part I: Conditions derived using concepts of loop gain, conicity and positivity. *IEEE Transactions on Automatic Control*, AC-11:228–238, 1966.

[56] G. Zames. Feedback and optimal sensitivity: Model reference transformations, multiplicative seminorms, and approximate inverses. *IEEE Transactions on Automatic Control*, AC-26(2):301–320, 1981.